The determinants and consequences of longitudinal changes in brain structure in later life: insights into preclinical Alzheimer's disease from the 1946 British birth cohort

---

Dr Sarah Elisabeth Keuss

Dementia Research Centre

Department of Neurodegenerative Disease

Queen Square Institute of Neurology

University College London

A thesis submitted to University College London

for the Degree of Doctor of Philosophy

2022

Declaration

I, Sarah Elisabeth Keuss, confirm that the work presented in this thesis is my own. Where information has been derived from other sources, or generated in collaboration with other researchers, this has been appropriately referenced or indicated in the thesis.

Abstract

Alzheimer's disease (AD) has a long preclinical phase, beginning decades prior to the onset of dementia, during which treatments may have greater benefit. There is therefore considerable interest in understanding the changes that occur in this phase. Using data from Insight 46, a sub-study of the National Survey of Health and Development (NSHD; the 1946 British birth cohort), the primary aim of this thesis was to investigate the determinants and consequences of longitudinal changes in brain structure quantified from magnetic resonance imaging (MRI) in cognitively normal older adults. It particularly focuses on the effects of cerebral β-amyloid (Aβ) deposition, one of the pathological hallmarks of AD, and white matter hyperintensity volume (WMHV), a marker of presumed cerebrovascular disease (CVD), which commonly co-exists with AD in later life.

A key finding was that being Aβ positive (measured using florbetapir positron emission tomography (PET) imaging) and having greater WMHV on MRI at baseline were both associated with faster subsequent rates of global and hippocampal volume loss, and these effects were independent and not interactive. Other important results were that: having a higher WMHV at baseline was associated with greater subsequent rates of cortical thinning, including within regions known to be vulnerable in early AD (so-called AD signature regions), whereas baseline Aβ deposition was not; faster progression of structural brain changes was related to faster concurrent rates of cognitive decline (or relatively less improvement) and poorer subsequent cognitive performance in Aβ positive individuals; and use of global atrophy rates as an outcome provided lower sample size estimates for hypothetical preclinical AD trials than hippocampal atrophy rates.

Collectively, these results emphasise the importance of early interventions and risk management targeting both Aβ and CVD, and have implications for the utility of structural MRI measures as biomarkers of neurodegeneration in the preclinical phase of AD.

Impact statement

The work undertaken in this thesis was primary motivated by the recent shift towards secondary prevention of dementia which requires better understanding of the processes that occur in early Alzheimer's disease (AD) and identification of biomarkers for tracking disease progression and response to therapies in the preclinical phase.

Analyses were based on data from Insight 46, a sub-study of 502 individuals recruited from the National Survey of Health Development (NSHD; also known as the 1946 British birth cohort), which involved detailed cognitive and neurological phenotyping and multi-modal brain imaging at two time-points around two years apart. Participants underwent imaging on a single scanner, allowing simultaneous acquisition of dynamic β-amyloid (Aβ) positron emission tomography (PET) and magnetic resonance imaging (MRI) data, at an almost identical age, virtually eliminating these factors as potential confounders.

The results provide useful information regarding the recruitment of a large elderly cohort to a longitudinal study and the detection and management of incidental MRI findings using a pre-specified standardised protocol. They also help to clarify uncertainties regarding the nature of Aβ-related changes in brain structure on MRI in cognitively normal older adults, and the contribution of other pathologies and risk factors, such as cerebrovascular disease (CVD). In addition, data on the cognitive consequences of changes in brain structure on MRI and estimated sample size requirements for preclinical AD trials using structural MRI measures as outcomes are provided.

The findings have the potential to inform future therapeutic strategies and trials aimed at preventing or delaying the onset of dementia in later life. Furthermore, they may be useful

in clinical practice, where they could facilitate discussion with patients about the significance of imaging findings. This is likely to become increasingly relevant as we move towards treating individuals before they develop symptoms, and as elderly but cognitively normal individuals undergo imaging for other reasons more often.

Dissemination of the results in this thesis is currently underway: two data chapters have resulted in publications already and I am in the process of writing up the remaining data chapters for submission; findings have and will continue to be presented at international conferences and local meetings; and key results will be shared with study participants through newsletters and more generally via public engagement activities.

Contents

Declaration 2

Abstract 3

Impact statement 5

List of figures 14

Abbreviations 16

1. INTRODUCTION 18

1.1. Background 18

1.2. Alzheimer's disease 20

1.2.1. Epidemiology and risk factors 20

1.2.2. Pathology 22

1.2.3. Pathogenesis 26

1.2.4. Clinical presentation 28

1.2.5. Diagnosis 29

1.2.6. Recent diagnostic developments and prospects 33

1.2.7. Treatments 37

1.3. Structural magnetic resonance imaging 39

1.3.1. Key principles 39

1.3.2. Detection and management of incidental findings 42

1.3.3. Measuring changes in brain structure 42

1.3.4. Suitability as a biomarker in Alzheimer's disease 48

1.3.5. Age-related structural brain changes 49

1.3.6. Structural brain changes in preclinical Alzheimer's disease 52

1.4. Key limitations and challenges of studies to date 57

1.5. Thesis approach 58

1.5.1. Rationale 58

1.5.2. Insight 46 59

1.5.3. Data chapters 60

2. METHODS 62

2.1. Insight 46 protocol 62

2.1.1. Participants 62

2.1.2. Study design 64

2.1.3. Clinical and neurological assessments 66

2.1.4. Neuropsychological tests 67

2.1.5. Imaging acquisition 69
2.2. Quantification of imaging measures 71
2.2.1. Pre-processing and quality control of structural imaging data 71
2.2.2. Baseline brain volumes 72
2.2.3. Baseline white matter hyperintensity volume 73
2.2.4. Baseline β-amyloid status and standardised uptake value ratios 74
2.2.5. Longitudinal whole brain, ventricular and hippocampal volumes 76
2.2.6. Longitudinal cortical thickness 78
2.3. Classification of participant clinical status 81
2.4. Determination of genetic, life-course and blood measures 82
2.4.1. *APOE* ε4 status 82
2.4.2. Vascular risk factors 82
2.4.3. Childhood cognition, education, and socioeconomic position 83
2.5. Analytical approach 84
2.5.1. Analysis of longitudinal data 84
2.5.2. Adjustment for age 85
2.5.3. Choice of reference region for β-amyloid quantification 86
2.5.4. Correction for multiple comparisons 87
2.6. Statement of contributions 88
2.6.1. Study design 88
2.6.2. Data collection 88
2.6.3. Data processing and variable derivation 89
2.6.4. Data analysis 90
3. RECRUITMENT AND CHARACTERISATION OF STUDY PARTICIPANTS 91
3.1. Statement of contributions 91
3.2. Introduction 91
3.3. Methods 92
3.3.1. Determining variables 92
3.3.2. Statistical analysis 93
3.4. Results 93
3.5. Discussion 102
3.6. Conclusion 105
4. DETECTION AND MANAGEMENT OF INCIDENTAL FINDINGS 106
4.1. Publication statement 106

4.2. Statement of contributions 106
4.3. Introduction 106
4.4. Methods 107
4.4.1. Scan review process 107
4.4.2. Statistical analysis 109
4.5. Results 110
4.5.1. Number and type of incidental findings 110
4.5.2. Subsequent action and follow-up 110
4.6. Discussion 116
4.7. Conclusion 118
5. LONGITUDINAL BRAIN VOLUME CHANGES 120
5.1. Publication statement 120
5.2. Statement of contributions 120
5.3. Introduction 121
5.4. Methods 122
5.4.1. Determining variables 122
5.4.2. Statistical analysis 122
5.5. Results 125
5.5.1. Baseline variables 125
5.5.2. Rates of change in whole brain, ventricular and hippocampal volume 125
5.5.3. Effects of baseline β-amyloid deposition 128
5.5.4. Effects of baseline vascular burden 129
5.5.5. Independent and interactive effects of β-amyloid and vascular burden 129
5.5.6. Disproportionate hippocampal atrophy 133
5.5.7. Effects of APOE ε4 status 134
5.5.8. Effects of exposure to vascular risk at ages 36, 53 and 69 years 134
5.5.9. Sensitivity analyses 137
5.6. Discussion 139
5.7. Conclusion 145
6. LONGITUDINAL CORTICAL THICKNESS CHANGES 146
6.1. Publication statement 146
6.2. Statement of contributions 146
6.3. Introduction 146

6.4. Methods 147
6.4.1. Determining variables 147
6.4.2. Statistical analysis 148
6.5. Results 150
6.5.1. Rates of change in cortical thickness in AD signature regions 150
6.5.2. Effects of baseline β-amyloid deposition 152
6.5.3. Effects of baseline vascular burden 153
6.5.4. Independent and interactive effects of β-amyloid and vascular burden 153
6.5.5. Effects of APOE ε4 status 156
6.5.6. Effects of vascular risk at ages 36, 53 and 69 157
6.5.7. An unbiased analysis of β-amyloid-related cortical thickness changes 159
6.5.8. Sensitivity analyses 160
6.6. Discussion 162
6.7. Conclusion 167
7. ASSOCIATIONS WITH PERFORMANCE ON COGNITIVE TESTING 168
7.1. Publication statement 168
7.2. Statement of contributions 168
7.3. Introduction 168
7.4. Methods 169
7.4.1. Determining variables 169
7.4.2. Statistical analysis 170
7.5. Results 171
7.5.1. Cross-sectional and longitudinal cognitive data 171
7.5.2. Predictors of rates of change in cognition between time-points 174
7.5.3. Predictors of cognitive performance at phase two 178
7.5.4. Sensitivity analyses 182
7.6. Discussion 183
7.7. Conclusion 187
8. SAMPLE SIZE REQUIREMENTS FOR PRECLINICAL TRIALS 188
8.1. Statement of contributions 188
8.2. Introduction 188
8.3. Methods 190
8.3.1. Determining variables 190

8.3.2. Sample size calculations 190
8.4. Results 192
8.5. Discussion 194
8.6. Conclusion 197
9. GENERAL DISCUSSION 198
9.1. Overview 198
9.2. Summary of key findings 198
9.3. Implications 200
9.3.1. Pathophysiological processes underlying progression to dementia 200
9.3.2. Trials targeting the preclinical phase of Alzheimer's disease 202
9.4. Strengths and limitations 204
9.5. Directions for future research 205
9.6. Concluding statement 207
Acknowledgements 208
Declaration Form 1 209
Declaration Form 2 210
Publications 211
References 217
Appendix 1 266
Appendix 2 267
Appendix 3 270
Appendix 4 273
Appendix 5 274

List of tables

Table 1.1. IWG-2 diagnostic criteria for AD 35
Table 1.2. NIA-AA framework for defining stages of AD 35
Table 1.3. Effect sizes based on mean comparison of preclinical AD versus controls .. 55
Table 2.1. Required life course data for recruitment to Insight 46 64
Table 2.2. Typical day one plan for visits in second phase of the study 65
Table 3.1. Number of participants with a major brain disorder in full Insight 46 sample 94
Table 3.2. Number of participants with complete longitudinal T1 data with a disorder that causes progressive neurodegeneration or non-vascular white matter disease 95
Table 3.3. Characteristics across whole sample and of cognitively normal participants with and without complete longitudinal T1 MRI data 97
Table 3.4. Characteristics of cognitively normal participants with complete longitudinal T1 MRI data by baseline Aβ status 100
Table 4.1. List of reportable and non-reportable MRI abnormalities 109
Table 4.2. Number and percentage of reportable abnormalities by type and sex 111
Table 4.3. A more detailed summary of the incidental findings detected during the first phase of data collection and how they were managed 113
Table 5.1. Rates of volume change in cognitively normal participants 126
Table 5.2. Interactive associations of predictors with rates of change in whole brain, ventricular and total hippocampal volume in cognitively normal participants 133
Table 5.3. Associations of APOE ε4 with rates of change in whole brain, ventricular and hippocampal volume in cognitively normal participants 135
Table 5.4. Associations of FHS-CVS at ages 36, 53 and 69 with rates of change in whole brain, ventricular and hippocampal volume in cognitively normal participants .. 136
Table 5.5. Effects of systolic BP at ages 36, 53 and 69 on rates of change in whole brain, ventricular and hippocampal volume in cognitively normal participants 137
Table 5.6. Sensitivity analyses using SUVR with a whole cerebellum reference: effects of Aβ and WMHV on rates of whole brain, ventricular and hippocampal volume change in cognitively normal participants 138
Table 5.7. Sensitivity analyses using SUVR with a whole cerebellum reference: interactive associations of predictors with rates of change in whole brain, ventricular and hippocampal volume in cognitively normal participants 139
Table 6.1. Rates of cortical thickness change in cognitively normal participants 151

Table 6.2. Interactive associations of predictors with rates of change in cortical thickness in AD signature regions in cognitively normal participants 156
Table 6.3. Associations of APOE ε4 with rates of change in AD signature cortical thickness in cognitively normal participants 157
Table 6.4. Associations of the FHS-CVS at ages 36, 53 and 69 with rates of change in cortical thickness in AD signature regions in cognitively normal participants 158
Table 6.5. Associations of systolic BP at ages 36, 53 and 69 with rates of change in cortical thickness in AD signature regions in cognitively normal participants 159
Table 6.6. Sensitivity analyses using SUVR with a whole cerebellum reference: effects of Aβ and WMHV on rates of change in AD signature cortical thickness in cognitively normal participants..... 161
Table 6.7. Sensitivity analyses using SUVR with a whole cerebellum reference: interactive associations of predictors with rates of change in cortical thickness in AD signature regions in cognitively normal participants 162
Table 7.1. Cognitive performance in cognitively normal participants 172
Table 7.2. Raw scores for each PACC component in cognitively normal participants 172
Table 7.3. Predictors of rates of change in performance on the PACC components between time-points in cognitively normal participants 176
Table 7.4. Predictors of performance on the PACC components at phase two in cognitively normal participants 180
Table 7.5. Sensitivity analyses using SUVR with a whole cerebellum reference:..... 182
Table 7.6. Sensitivity analyses using SUVR with a whole cerebellum reference: differential associations of rates of change in structural MRI measures with rates of change in PACC and PACC performance at phase two by baseline Aβ status 183
Table 8.1. Sample sizes for a relative reduction in rate of change in the outcome..... 193
Table 8.2. Sample sizes for an absolute reduction in rate of change in the outcome . 193

List of figures

Figure 1.1. The annual incidence rate of AD at different ages. 21
Figure 1.2. AD brain section with Aβ plaques (green arrows) and NFTs (blue arrows). 23
Figure 1.3. Phases of Aβ deposition in AD. 24
Figure 1.4. Braak staging of tau spread in AD. 25
Figure 1.5. Simplified overview of amyloid precursor protein processing. 27
Figure 1.6. Progressive medial temporal lobe atrophy on MRI in cognitively normal (CN), amnestic mild cognitive impairment (aMCI) and Alzheimer's disease (AD) subjects. 30
Figure 1.7. MRI findings associated with small vessel disease. 31
Figure 1.8. Aβ-negative (left) and Aβ-positive (right) 18F-florbetapir PET scans. 33
Figure 1.9. Hypothetical model of biomarkers in AD pathophysiology 34
Figure 1.10. The NMV forms when protons are exposed to a magnetic field (B0). 40
Figure 1.11. (Left) T1-weighted, (Middle) T2-weighted and (Right) FLAIR MRI brain 41
Figure 1.12. Linear registration involves a series of transformations including translations, rotations, zooms +/- shears to match two images to one another. 44
Figure 1.13. A one-dimensional representation of a boundary shift (Δw) 45
Figure 1.14. Stages of the Freesurfer cortical thickness pipeline 47
Figure 1.15. MRIs with voxel-compression-mapping overlay in an Alzheimer's disease patient showing areas of contraction (blue/green) and expansion (red/yellow). 48
Figure 1.16. Meta-regression results of hippocampal atrophy rate in relation to age in studies using manual (magenta line) and automated segmentation (blue line) 50
Figure 1.17. The prevalence of β-amyloid positivity in cognitively normal adults (blue line) and the prevalence of AD-type dementia (orange line). The blue arrow indicates the age of Insight 46 participants at baseline. 60
Figure 2.1. Summary of available life course data from the NSHD 63
Figure 2.2. Magnetic resonance imaging sequence parameters 70
Figure 2.3. Original T1 scan (left), pre-processed T1 scan (after gradient non-linearity and bias correction) (middle) and T1 scan with overlaid GIF parcellation (right). 72
Figure 2.4. Examples of T1 scan that failed cross-sectional quality control. 73
Figure 2.5. Axial (left), coronal (middle) and sagital (right) FLAIR MRI with segmentation (bright green) of white matter hyperintensities. 74
Figure 2.6. Histogram and mixture models of baseline global SUVRs generated with an eroded subcortical white matter reference region. 75
Figure 2.7. Left: baseline (red) and follow-up (blue) T1 images overlaid before registration illustrating positional difference in the scanner. Right: baseline image with BSI overlay after image registration; apparent volume loss (red) and gain (green) either side of gyri due to geometric distortion (stretch) caused by positional differences. 77
Figure 2.8. Plot of indirect (difference between MAPS-derived volume at each time-point) versus direct (BSI) values in millilitres 78
Figure 2.9. Example of modified Freesurfer pipeline (red) underestimating the pial surface compared to standard (blue) pipeline 79
Figure 2.10. Two AD signature composite regions. 80

Figure 2.11. Histogram showing age distribution of Insight 46 participants 86
Figure 3.1. Flowchart of study recruitment and reasons for missing T1 MRI data. 96
Figure 3.2. Maps showing population density of mainland Britain (left) and where Insight 46 participants were recruited from (right) 103
Figure 4.1. The radiological read report completed by radiologists in XNAT (www.xnat.org). 108
Figure 4.2. Examples of incidental findings detected on brain MRI in phase one 112
Figure 5.1. Histograms showing distribution and mean (red dashed line) of BSI data 127
Figure 5.2. Forest plot showing coefficients and 95% confidence intervals for associations of baseline Aβ and WMHV with rates of change in whole brain, ventricular and hippocampal volume in cognitively normal participants 130
Figure 5.3. Scatter plots for associations of baseline Aβ (status and SUVR) with rates of change in whole brain, ventricular and hippocampal volume in cognitively normal 131
Figure 5.4. Scatter plots for associations of baseline WMHV with rates of change in whole brain, ventricular and hippocampal volume in cognitively normal participants.. 132
Figure 5.5. Scatter plots highlighting outlier (circled in red) in analyses of effects of FHS-CVS and systolic BP at age 53 on rates of hippocampal atrophy in later life 136
Figure 6.1. Histograms showing distribution and mean (red dashed line) of cortical thickness change values 151
Figure 6.2. Forest plots showing coefficients and 95% confidence intervals for associations of baseline Aβ and WMHV with rates of change in AD signature cortical thickness in cognitively normal participants 154
Figure 6.3. Scatter plot showing associations of baseline Aβ and WMHV with rates of change in cortical thickness in ADsig Harvard (top) and ADsig Mayo (bottom) regions in cognitively normal participants 155
Figure 6.4. Vertex-wise analysis of Aβ-related cortical thickness changes 160
Figure 7.1. Histograms showing the distribution and mean (red dashed line) of cognitive change scores 173
Figure 7.2. Predictors of rates of change in performance on the PACC between time-points in cognitively normal participants 175
Figure 7.3. Differential associations between rates of change in structural MRI measures and rates of change in PACC by baseline Aβ status 177
Figure 7.4. Predictors of PACC performance at phase two in cognitively normal participants 179
Figure 7.5. Differential associations between rates of change in structural MRI measures and PACC at phase two by baseline Aβ status 181
Figure 8.1. Diagram showing the difference between an absolute and relative reduction in rate of outcome change 189

Abbreviations

Aβ – β-amyloid

AChEI – acetylcholinesterase inhibitor

AD – Alzheimer's Disease

APOE – apolipoprotein E

ADNI – Alzheimer's Disease Neuroimaging Initiative

ADsig – Alzheimer's disease signature region

AIBL – Australian Imaging, Biomarker and Lifestyle Flagship Study of Ageing

APP – amyloid precursor protein

ARIA – amyloid-related imaging abnormalities

AT(N) – amyloid tau neurodegeneration framework

BaMoS – Bayesian Model Selection

BP – blood pressure

BSI – boundary shift integral

CAA – cerebral amyloid angiopathy

CSF – cerebrospinal fluid

CT – computed tomography

CVD – cerebrovascular disease

DBC – differential bias correction

DSST – digit symbol substitution test

FDG – fluorodeoxyglucose

FHS-CVS – Framingham Heart Study cardiovascular risk score

FLAIR – fluid attenuated inversion recovery

FNAME – face-name associative memory exam

GIF – geodesic information flow

GP – general practitioner

IWG – International Working Group

LMDR – logical memory delayed recall

LPA – logopenic aphasia

MCI – mild cognitive impairment

MMSE – mini-mental state examination

MRI – magnetic resonance imaging

MRC – Medical Research Council

NIA-AA – National Institute on Aging – Alzheimer's Association

NFT – neurofibrillary tangle

NMV – net magnetisation vector

NODDI – neurite orientation dispersion and density imaging

NSHD – National Survey of Health and Development

PACC – preclinical Alzheimer's cognitive composite

PCA – posterior cortical atrophy

PD – Parkinson's disease

PVC – partial volume correction

PVC – partial volume effect

PET – positron emission tomography

PSEN-1 – presenilin-1

PSEN-2 – presenilin-2

QC – quality control

RF – radiofrequency

ROI – region of interest

SCD – subjective cognitive decline

SPM – Statistical Parametric Mapping

SUVR – standardised uptake value ratio

SVD – small vessel disease

TDP-43 – TAR DNA-binding protein-43

TIV – total intracranial volume

TE – echo time

TR – repetition time

WMH – white matter hyperintensity

WMHV – white matter hyperintensity volume

WML – white matter lesion

1. INTRODUCTION

1.1. Background

Dementia is a clinical syndrome, characterised by progressive loss of cognitive function and impaired ability to carry out activities of daily living. It has a devastating impact on patients, their families and the wider community, costing the UK £26 billion/year (Prince, Knapp, *et al.*, 2014). It typically affects the elderly, roughly doubling in prevalence with every five-year increase in age (Lobo *et al.*, 2000), and as the ageing population grows, its prevalence is predicted to triple worldwide by 2050 (Prince, Albanese, *et al.*, 2014).

Dementia has multiple causes, the commonest of which is Alzheimer's disease (AD) (Van Der Flier and Scheltens, 2005). Despite significant advances in basic science and drug development, clinical trials of disease-modifying therapies for AD have repeatedly yielded disappointing results, possibly because they have been given too late in the disease course to symptomatic patients with already widespread, irreversible neuronal damage. Indeed, it is now well recognised that the pathophysiological processes underlying AD begin as early as twenty years before the onset of clinical symptoms (Dubois *et al.*, 2016).

Current efforts are focussed on understanding the changes that occur in this preclinical phase, so that therapies can be targeted earlier with the aim of preventing or delaying progression to dementia. A major issue is how best to assess the efficacy of these treatments since cognitive outcomes show considerable variability within subjects and between examiners, and are subject to practice and ceiling effects in the early stages of

AD, meaning large sample sizes and extended follow-up are needed to detect a meaningful effect (Doraiswamy *et al.*, 2001; Cano *et al.*, 2010; Hobart *et al.*, 2013).

One solution is to use a surrogate marker of disease progression (i.e., a biomarker). AD is characterised by excess neurodegeneration, even in the predementia stages (Schott *et al.*, 2010; Andrews *et al.*, 2013), which can be quantified from structural magnetic resonance imaging (MRI). Its measurement is more precise than cognitive testing, meaning less variability and greater statistical power, which should allow smaller sample sizes in trials (Jack *et al.*, 2004; Ridha *et al.*, 2008); for example, it has been estimated that detection of a 25% slowing in annual rate of change among patients with mild cognitive impairment would require a sample size of 130 per treatment arm using MRI-derived whole brain atrophy as an outcome versus 2628 per treatment arm using the mini-mental state examination – a widely used cognitive test – as an outcome (Jack *et al.*, 2004). Another advantage of MRI is that it can be performed repeatedly and safely in most individuals and analysed using automated techniques, which makes it ideally suited for implementation on a large scale in a clinical trial setting. Additionally, it can be used to assess the safety of treatments and so may serve more than one purpose.

To inform the utility of structural MRI measures as biomarkers of neurodegeneration in the preclinical phase of AD and to better understand the processes that might underlie progression to dementia in later life, the primary aim of this thesis was to investigate the determinants and consequences of longitudinal changes in brain structure quantified from serial MRI in cognitively normal older adults. It particularly focusses on the effects of cerebral β-amyloid (Aβ) deposition, one of pathological hallmarks of AD (De Strooper and Karran, 2016), and white matter hyperintensities, a marker of presumed

cerebrovascular disease, which commonly co-exists with AD in later life and may be involved in its pathogenesis (Brickman, 2013; Deture and Dickson, 2019).

In this introductory chapter, I begin by providing an overview of AD and structural MRI, before discussing existing literature relevant to this work and its limitations. I then outline the approach taken in this thesis, including the rationale for analyses performed, the unique dataset on which they were based, and subsequent data chapters.

1.2. Alzheimer's disease

1.2.1. Epidemiology and risk factors

AD is responsible for 50-75% of the 24 million cases of dementia worldwide (Mayeux and Stern, 2012; Prince, Albanese, *et al.*, 2014). It is more common in Western Europe and North America, and its incidence rises exponentially with age, with a 15-fold increase between the ages of 60 and 85 years old (Figure 1.1) (Evans *et al.*, 1989; Mayeux and Stern, 2012). Women are also more likely to be affected than men (Lobo *et al.*, 2000).

AD is usually sporadic, most likely driven by a complex interaction between genetic and environmental factors. The apolipoprotein E (*APOE*) gene, which exists in three isoforms (ε2, ε3 and ε4), is by far the strongest known genetic predictor (Yu, Tan and Hardy, 2014; Carmona, Hardy and Guerreiro, 2018). Having one or two ε4 alleles increases the risk of AD dementia by 3- and 12-fold respectively, and is associated with an earlier age of onset, while the ε2 variant is protective (Verghese, Castellano and Holtzman, 2011). Genome-wide association studies and whole-exome/ genome sequencing have revealed a number of other loci that confer increased susceptibility to AD, including

variants involved in immune pathways, cholesterol metabolism and endosomal vesicle recycling (Bertram *et al.*, 2008; Harold *et al.*, 2009; Hollingworth *et al.*, 2011; Naj *et al.*, 2011; Guerreiro *et al.*, 2013; Lambert *et al.*, 2013; Karch and Goate, 2015).

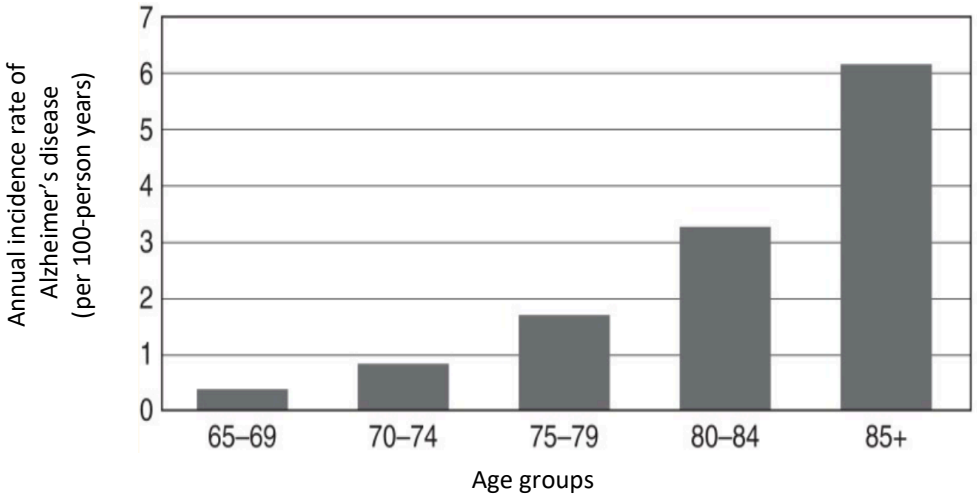

Figure 1.1. The annual incidence rate of AD at different ages.

Reprinted from Cold Spring Harbor Perspectives in Medicine, Vol. 2, Mayeux and Stern, Epidemiology of Alzheimer's disease, 2012, with permission from Cold Spring Harbor Laboratory Press. doi: 10.1101/cshperspect.a006239.

Numerous factors from across the life-course have also been implicated, many of which are potentially modifiable. These include: low childhood education; midlife obesity, alcohol excess, hypertension, head injury and hearing loss; and late life physical inactivity, social isolation, diabetes, smoking, air pollution and depression (Livingston *et al.*, 2020). The underlying mechanisms are not well understood, but several pathways have been proposed. For example, low education might increase vulnerability to cognitive decline because individuals have less cognitive reserve, which is thought to protect against the effects of brain pathology (Valenzuela, 2008; Stern and Barulli, 2019). Specifically, it has been proposed that lifetime exposures, such as education, might influence the adaptability of an individual's cognitive processes and how successfully a

person can cope with age- or disease-related brain changes. Some risk factors, particularly those in late life, might also reflect reversed causation (i.e., individuals with prodromal dementia may be less likely to participate in exercise and social activity).

In less than 1% of cases, AD develops due to an autosomal dominantly inherited mutation in one of three genes – amyloid precursor protein (*APP*), presenilin-1 (*PSEN1*) or presenilin-2 (*PSEN2*). These rare mutations are highly penetrant, meaning that approximately 50% of individuals within affected families are destined to develop dementia. Familial AD shares many features with the more common sporadic form of the disease, but there are some important differences, most notably its earlier age of onset, which is usually between the ages of 30 and 50 years old (Bateman *et al.*, 2011).

1.2.2. Pathology

Macroscopically, AD is characterised by generalised cerebral atrophy, particularly within medial temporal lobe regions, such as the hippocampus and entorhinal cortex (Love, 2005). Microscopically, the pathological hallmarks are extracellular Aβ neuritic plaques and intracellular tau neurofibrillary tangles (NFTs) (Figure 1.2) (Nelson *et al.*, 2012).

Neuritic plaques consist of abnormally aggregated Aβ peptides with 40 or 42 amino acids (Aβ40 and Aβ42), surrounded by dystrophic neurites, activated microglia and reactive astrocytes (Selkoe, 2001). Aβ42 is usually more abundant, likely due to its longer length and greater insolubility (Jarrett, Berger and Lansbury, 1993). Aβ is also found within diffuse plaques, which lack the surrounding neurites and compacted fibrillar structure of neuritic plaques (Selkoe, 2001). These plaques are commonly observed in elderly persons without cognitive impairment and possibly represent immature precursors to

neuritic plaque development (Knopman *et al.*, 2003). Aβ deposition starts in the neocortex, then spreads to the allocortex, followed by the basal ganglia and diencephalon, before eventually involving the brainstem and cerebellum (Figure 1.3) (Thal, Attems and Ewers, 2014).

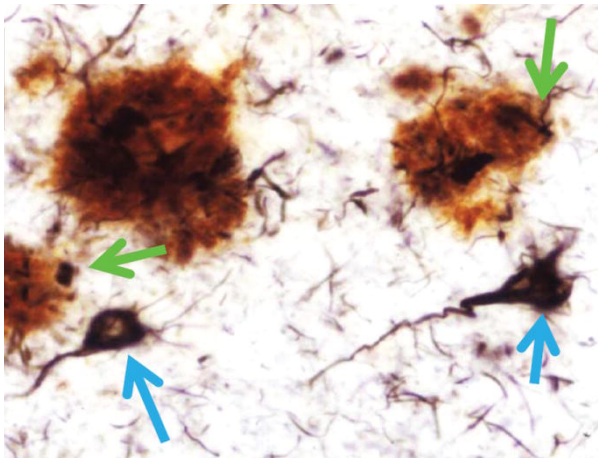

Figure 1.2. AD brain section with Aβ plaques (green arrows) and NFTs (blue arrows). Reprinted from the Journal of Neuropathology and Experimental Neurology, Vol. 7, 362-381, Nelson *et al.*, Correlation of Alzheimer Disease Neuropathologic Changes with Cognitive Status: A Review of the Literature, 2012, with permission from Oxford University Press. doi: 10.1097/NEN.0b013e31825018f7.

NFTs are composed of hyperphosphorylated tau proteins, which aggregate into insoluble paired helical filaments and occupy the neuronal cytoplasm (Calderon-Garcidueñas and Duyckaerts, 2018). NFTs have been shown to correlate better with dementia severity and neuronal loss than Aβ plaques (Berg *et al.*, 1998; Giannakopoulos *et al.*, 2003; Ingelsson *et al.*, 2004). In addition to forming NFTs, tau also accumulates in the dendrites as neuropil threads and in the axons of neuritic plaques (Duyckaerts, Delatour and Potier, 2009). Deposition of tau follows a characteristic pattern of spread, starting in the transentorhinal region, followed by limbic structures such as the hippocampus, before

ultimately leading to marked deposition throughout the neocortex (Figure 1.4) (Braak and Braak, 1991).

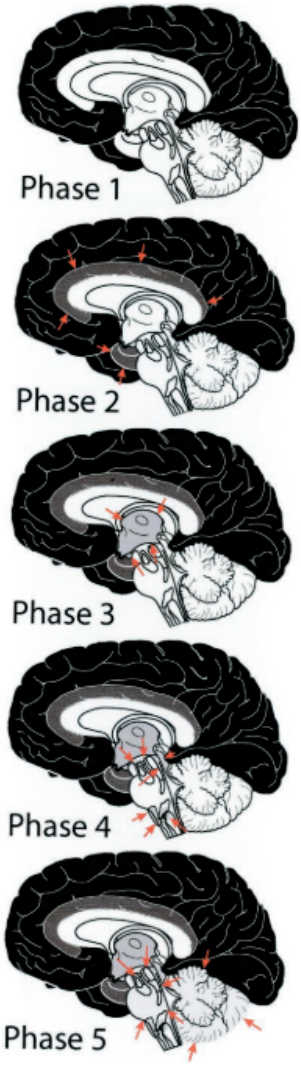

Figure 1.3. Phases of Aβ deposition in AD.

Phase 1 involves neocortical deposits (black region), phase 2 has allocortical deposits, phase 3 involves the diencephalic nuclei and striatum, phase 4 spreads to the brainstem and phase 5 includes the cerebellum.

Reprinted from Neurology, Vol. 58, 1791-1800, Thal *et al.*, Phases of Aβ-deposition in the human brain and its relevance for the development of AD, 2002, with permission from Wolters Kluwer Health, Inc. doi: 10.1212/WNL.58.12.1791.

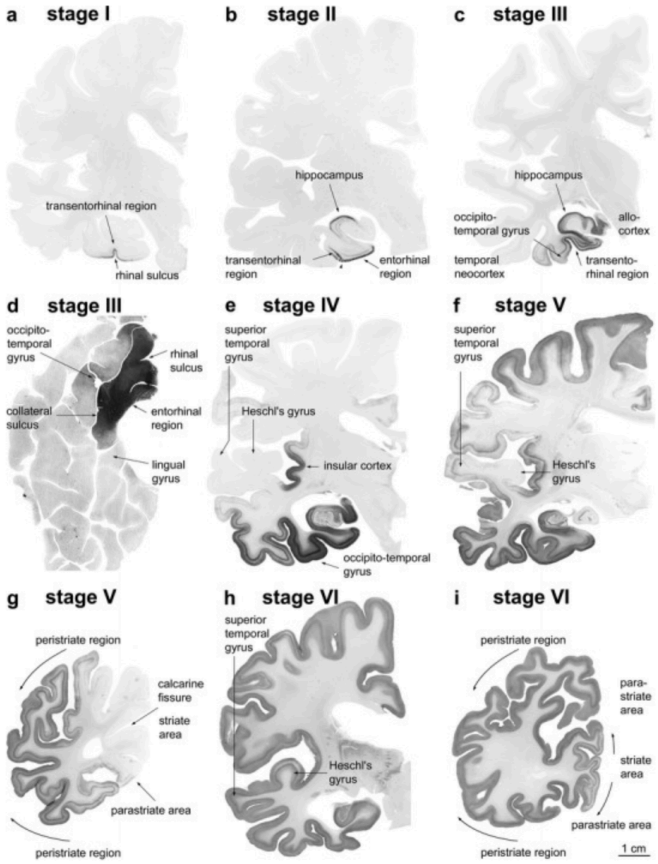

Figure 1.4. Braak staging of tau spread in AD.

Stages I-II involve transentorhinal and entorhinal regions; III-IV include limbic allocortex and adjoining neocortex; and V-VI is spread to other neocortical areas.

Reprinted from Acta Neuropathologica, Vol. 112, 389-404, Braak *et al.*, Staging of Alzheimer's disease-associated neurofibrillary pathology using paraffin sections and immunocytochemistry, 2006, under the terms of the Creative Commons Attribution Non-commercial License. doi: 10.1007/s00401-006-0127-z.

Other pathologies often co-exist, including Lewy body disease, TDP-43 pathology and cerebrovascular disease (Calderon-Garcidueñas and Duyckaerts, 2018), and the presence of mixed pathologies has been linked to earlier onset of AD-type dementia (Snowdon *et al.*, 1997; James *et al.*, 2016; Kapasi, DeCarli and Schneider, 2017).

White matter lesions (WMLs) are particularly common and are presumed to occur mostly as a consequence of chronic ischaemia due to arteriolosclerosis-related small vessel disease (SVD). Arteriosclerosis refers to endothelial alteration, thickening, fibrosis and plaque formation in perforant and small arterioles, with periventricular and subcortical brain regions especially vulnerable to its effects (Ferrer and Vidal, 2018). In addition to increasing age, hypertension is consistently recognised as a risk factor for its development (de Leeuw *et al.*, 2002; Gottesman *et al.*, 2010; Verhaaren *et al.*, 2013).

WMLs also occur in association with cerebral amyloid angiopathy (CAA), another type of SVD, seen frequently with AD. CAA involves deposition of congophilic Aβ in blood vessel walls, leading to necrosis, leakage of blood, perivascular macrophages and haemorrhages, with a predilection for posterior brain regions (Vinters and Gilbert, 1983; Ferrer and Vidal, 2018). There is also evidence linking WMLs to Wallerian degeneration in AD, again in posterior brain regions (McAleese *et al.*, 2017). Thus, it may be that their underlying pathology varies to some extent depending on their location.

1.2.3. Pathogenesis

The Aβ cascade hypothesis proposes that cerebral Aβ deposition is the initiating factor in AD, and that subsequent NFTs, neuronal loss and dementia are downstream consequences (Hardy and Higgins, 1992). Supporting this hypothesis, mutations in familial AD result in increased Aβ production by modifying the amyloid precursor protein (APP) and key enzymes involved in its proteolytic processing (Scheuner *et al.*, 1996). Normally, cleavage of APP by α-secretase leads to formation of secreted APP (sAPPα), which is non-pathogenic. Mutations in familial AD, however, result in sequential cleavage of APP by β- and γ-secretase, which favours Aβ production (Figure 1.5).

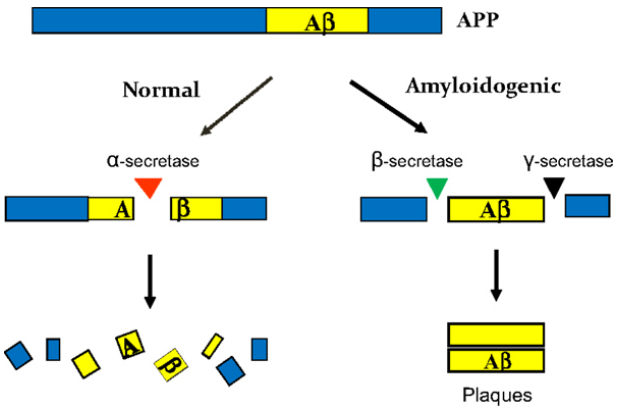

Figure 1.5. Simplified overview of amyloid precursor protein processing. Reprinted from Frontiers in Cellular Neuroscience, Vol.9, Chen, The Maze of APP Processing in Alzheimer's Disease: Where Did We Go Wrong in Reasoning, 2015, under the terms of the Creative Commons Attribution License (CC BY). doi: 10.3389/fncel.2015.00186.

Further evidence for the Aβ hypothesis comes from the observation that individuals with Down syndrome, who possess an extra copy of the *APP* gene, develop early onset Aβ plaques and dementia (Wiseman *et al.*, 2015). Conversely, individuals with an *APP* missense mutation that decreases production of Aβ have life-long protection against AD (Jonsson *et al.*, 2012). In sporadic AD, the exact mechanism of Aβ accumulation is unknown, but it is thought to be related to an imbalance between Aβ production and clearance, and is likely multifactorial (Selkoe and Hardy, 2016). The APOE ε4 allele, for example, has been linked to impaired clearance of Aβ in mice (Castellano *et al.*, 2011).

The mechanism via which Aβ interacts with NFTs to cause neurodegeneration is also uncertain, but the immune system is thought to be important (Calsolaro and Edison, 2016). Several genes involved in immune pathways and inflammation, including *TREM2*, *CD33* and *CR1*, have been associated with increased risk of AD (Lambert *et al.*, 2009; Guerreiro *et al.*, 2013). Moreover, immune-related cells, such as activated microglia, co-

localise with Aβ plaques in AD brains at post-mortem (Hopperton *et al.*, 2018), a finding that has also been confirmed *in vivo* using positron emission tomography (Hamelin *et al.*, 2016). While the immune system has clearly evolved to have a protective function against disease, many pathologies are due to aberrant functioning immunity, and it is possible that excessive inflammation over time might cause or contribute to development of pathology or deleterious neuronal loss in AD (McGeer and McGeer, 2001).

It has also been proposed that cerebrovascular disease (CVD) may be involved in AD pathogenesis and that it might even precede Aβ accumulation (de la Torre, 2004; Zlokovic, 2011). Central to this hypothesis is the idea that disrupted cerebral blood flow and neurovascular unit dysfunction might lead to increased Aβ production or impaired clearance, as has been demonstrated in mouse models (Zlokovic, 2011; Scheffer *et al.*, 2021). Evidence from neuropathological and imaging studies in humans, however, has been mixed (Chui *et al.*, 2011; Roseborough *et al.*, 2017), which has led to considerable debate in the field. One possibility is that, rather than being directly involved in AD pathogenesis, CVD might independently influence neurodegeneration and cognition, thereby lowering the threshold for onset of dementia (Attems and Jellinger, 2014).

1.2.4. Clinical presentation

AD typically presents with progressive episodic memory impairment, characterised by difficulty recalling recent events and conversations, forgetting appointments, repetitive questions and misplacing belongings (Rabinovici, 2019). There may be varying degrees of other problems, including executive dysfunction, visuospatial impairment, and language disturbance, but these are usually not prominent in early disease.

Rarely, AD can present with a non-amnestic phenotype, of which there are three canonical variants: logopenic aphasia (LPA); posterior cortical atrophy (PCA); and 'frontal' or executive AD (Mendez, 2019). These presentations are most often seen in patients with early onset AD, which is somewhat arbitrarily defined as symptom onset before the age of 65 years old (Koedam *et al.*, 2010). LPA is characterised by word-retrieval difficulties, which manifest as hesitant speech with prolonged pauses (Marshall *et al.*, 2018). PCA is associated with higher order visual symptoms, difficulties with spelling and arithmetic, and apraxia (Crutch *et al.*, 2012), while the rare 'frontal' AD variant presents with marked behavioural change and impairment of executive functions (Ossenkoppele *et al.*, 2015).

Recently, there has been growing interest in the concept of subjective cognitive decline (SCD), which refers to a self-perceived decline in cognition relative to baseline, with normal performance on objective neuropsychological tests (Jessen *et al.*, 2020). SCD is increasingly recognised as a risk factor for the development of cognitive impairment and AD dementia, although it can also occur in the context of other disorders, including depression, anxiety and sleep disturbance (Rabin, Smart and Amariglio, 2017). SCD features that have been proposed to increase the likelihood of underlying AD (so-called SCD-plus criteria) include: subjective decline in memory rather than other cognitive domains; onset within the last 5 years; onset ≥ 60 years old; associated concerns and worries; and perception of being worse than others of the same age (Jessen *et al.*, 2014).

1.2.5. Diagnosis

Clinical assessment is the mainstay of diagnosis in symptomatic patients. A detailed history should be obtained, ideally from both the patient and an informant, as well as a

focussed physical exam and cognitive assessment. The Mini-Mental State Examination (MMSE) is commonly used as a screening test (Folstein, Folstein and McHugh, 1975), but it has several limitations, including low sensitivity in early dementia and confounding by language fluency, literacy ability and cultural factors (Devenney and Hodges, 2017). Other screening tests include the Montreal Cognitive Assessment (MOCA) and the Addenbrooke's Cognitive Examination (ACE) (Nasreddine *et al.*, 2005; Mioshi *et al.*, 2006). Where available, a standardised battery of neuropsychological tests to quantify cognitive function in different domains using age-matched normative data is also helpful.

Blood tests and structural brain imaging (computed tomography or MRI) should then be performed to rule out potentially treatable causes of cognitive impairment (NICE, 2018). MRI also allows assessment for characteristic patterns of atrophy (Figure 1.6), which help to differentiate AD from other neurodegenerative disorders. These changes are a major focus of this thesis and will be discussed in detail in section 1.3.6.

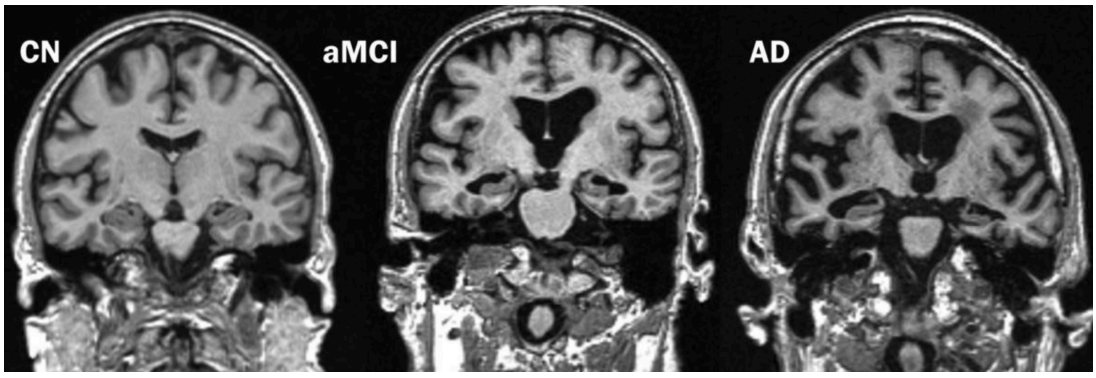

Figure 1.6. Progressive medial temporal lobe atrophy on MRI in cognitively normal (CN), amnestic mild cognitive impairment (aMCI) and Alzheimer's disease (AD) subjects.

Reprinted from Alzheimer's Research and Therapy, Vol. 2, Vemuri and Jack, Role of Structural MRI in Alzheimer's disease, 2010, with permission from Springer Nature. doi: 10.1186/alzrt47.

Markers of cerebrovascular disease can also be visualised on MRI and include large-vessel strokes and changes related to small vessel disease (Figure 1.7). White matter lesions are best seen as areas of increased brightness, referred to as white matter hyperintensities (WMHs), on T2 or FLAIR (fluid-attenuated inversion recovery) MRI.

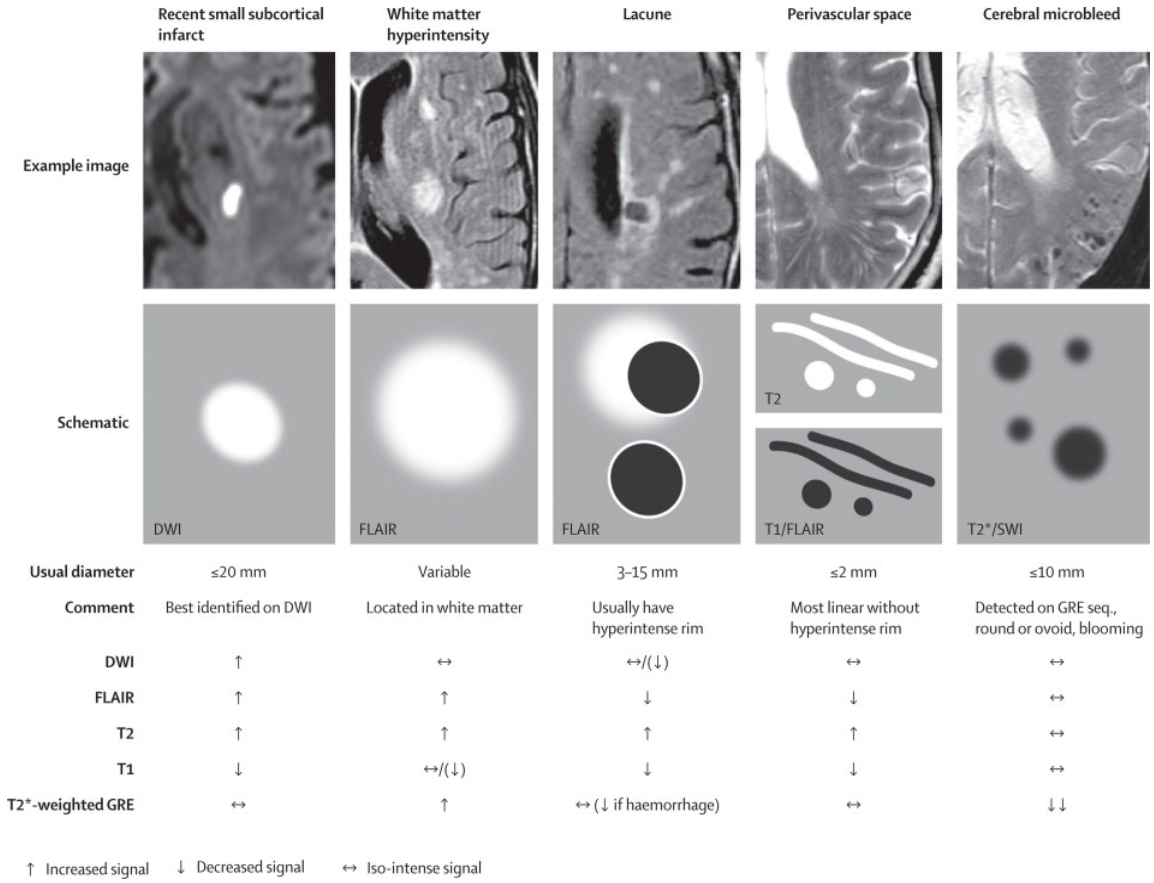

Figure 1.7. MRI findings associated with small vessel disease.

Reprinted from the Lancet Neurology, Vol. 12, 822-838, Wardlaw *et al.*, Neuroimaging standards for research into small vessel disease and its contribution to ageing and neurodegeneration, 2013, with permission from Elsevier. doi: 10.1016/S1474-4422(13)70124-8.

In situations where the MRI is normal or shows non-specific changes, positron emission tomography (PET) with 2-[fluorine-18]fluoro-2-deoxy-D-glucose (FDG) may be useful. FDG is an analogue of glucose, the brain's energy substrate, and its accumulation is a

marker of metabolic activity. Hypometabolism on FDG-PET is supportive of neurodegeneration and its pattern may help to distinguish between disorders. For example, parieto-temporal including posterior cingulate and precuneus hypometabolism is characteristic of AD, while frontal and anterior temporal hypometabolism is typical of the behavioural variant of frontotemporal dementia (Tripathi *et al.*, 2014).

Clinicians also sometimes have access to cerebrospinal fluid (CSF) studies. CSF is collected via lumbar puncture and analysed for markers of AD pathology, including Aβ42, total tau (t-tau), and phosphorylated tau (p-tau). A CSF profile with a reduced Aβ42 concentration or Aβ42/40 ratio, and elevated t-tau and p-tau concentrations, is highly sensitive and specific for AD (Olsson *et al.*, 2016). The neuronal injury marker neurofilament light can also be quantified in the CSF and may be useful as marker of disease severity, but it is not specific for AD (Bacioglu *et al.*, 2016).

Aβ-PET is an alternative to CSF when lumbar puncture is contraindicated, but it is more expensive and much less available or accessible. Patients are injected with a radioactive tracer that binds to Aβ neuritic plaques. The signal produced by the tracer is then detected by the PET scanner to generate an image of cerebral Aβ uptake (Figure 1.8), which can be read using a quantitative method or assessed qualitatively.

Use of these tests has resulted in improved diagnostic accuracy for patients. For example, in one study, Aβ-PET altered the diagnosis in almost a third of individuals with clinically suspected AD, with a negative scan resulting in a change to a non-AD diagnosis in most cases (Fantoni *et al.*, 2018). Tau-PET tracers have also been developed (Yet et al 2021), but they are not yet available for use in clinical practice, at least in the UK.

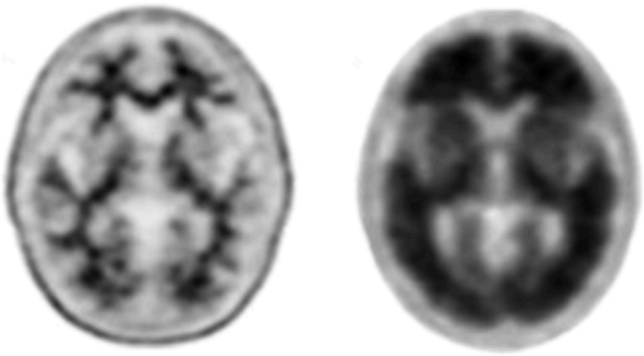

Figure 1.8. Aβ-negative (left) and Aβ-positive (right) 18F-florbetapir PET scans. Darker colours reflect binding of tracer; on the left, there is non-specific binding to white matter; on the right, intense cortical binding to fibrillary Aβ plaques is seen. Reprinted from Journal of Nuclear Medicine Technology, Vol. 43, 175-184, Trembath, Newell and Devous, Technical Considerations in Brain Amyloid PET Imaging with 18F-Florbetapir, 2015, according to the permissions policy of the Society of Nuclear Medicine and Molecular Imaging (SNMMI). doi: 10.2967/jnmt.115.156679

1.2.6. Recent diagnostic developments and prospects

Historically, AD has been viewed as a clinicopathological diagnosis, meaning that clinicians made a diagnosis of 'probable' AD based on clinical presentation during life, with a definitive diagnosis only being reached at post-mortem. However, the development of CSF and PET biomarkers to detect AD pathology *in vivo* has led to a major shift in the diagnosis and conceptualisation of AD. Firstly, AD is increasingly recognised as a clinicobiological diagnosis, supported by compatible clinical phenotype and the presence of AD biomarkers (Dubois *et al.*, 2007). Secondly, it is now appreciated that AD has a long preclinical phase with Aβ deposition beginning decades prior to dementia, and before the development of tau pathology and neurodegeneration (Figure 1.9) (Jack *et al.*, 2010).

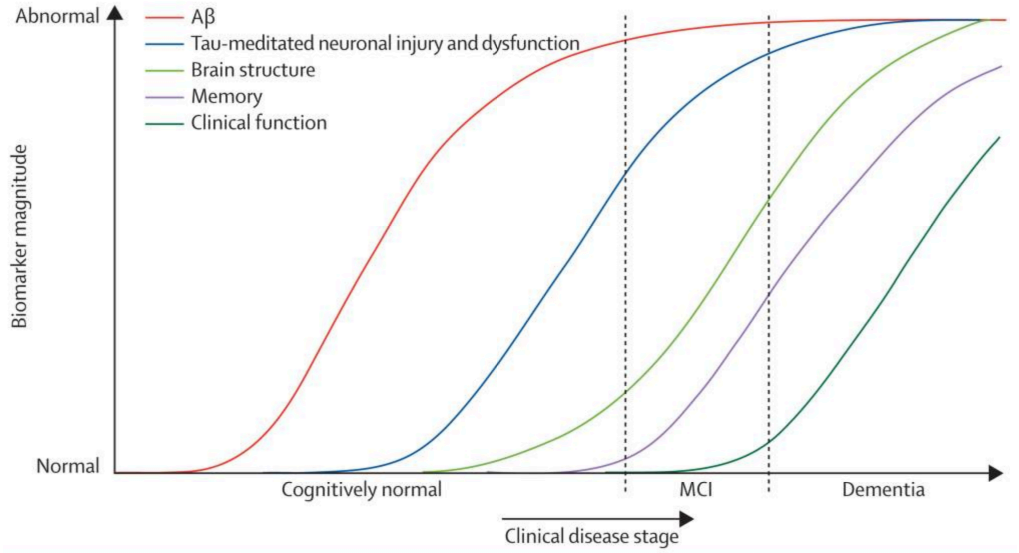

Figure 1.9. Hypothetical model of biomarkers in AD pathophysiology. Reprinted from The Lancet Neurology, Vol. 9, 119-128, Jack *et al.*, Hypothetical model of dynamic biomarkers of the Azlehimer's pathological cascade, 2010, with permission from Elsevier. doi: 10.1016/S1474-4422(09)70299-6

The International Working Group (IWG) and National Institute of Ageing and Alzheimer's Association (NIA-AA) criteria have now been adapted to incorporate biomarker evidence of AD and to allow a diagnosis of AD prior to dementia (Tables 1.1 and 1.2) (Dubois *et al.*, 2014; Jack *et al.*, 2018). It is important to note that these criteria were developed for research purposes, rather than for use in clinical practice. Due to the diagnostic and prognostic uncertainties of biomarker results in cognitively normal individuals, and the current lack of effective disease-modifying treatments for preclinical AD, use of these criteria in the clinical setting is not yet recommended.

Table 1.1. IWG-2 diagnostic criteria for AD

(Dubois *et al.*, 2014, 2016)

Disease stage		**Cognitive profile**	**Biomarker profile**
Symptomatic AD	Typical	Amnestic syndrome	Consistent CSF (low Aβ42 and high tau or p-tau) OR high retention of tracer on Aβ PET
	Atypical	Logopenic, posterior cortical atrophy or frontal variant	
Preclinical (sporadic) or presymptomatic (familial) AD		No phenotype	Consistent CSF (low Aβ42 and high tau or p-tau) OR high retention of tracer Aβ **and** tau PET OR pathogenic AD mutation
Asymptomatic at risk of AD		No phenotype	High retention of tracer on Aβ OR tau PET

AD = Alzheimer's disease; CSF = cerebrospinal fluid; Aβ = β-amyloid; PET = positron emission tomography

Table 1.2. NIA-AA framework for defining stages of AD

(Jack *et al.*, 2018)

		Cognitive stage		
		Cognitively unimpaired	MCI	Dementia
Biomarker Profile	A- T- (N)-	Normal AD biomarkers, cognitively unimpaired	Normal AD biomarkers with MCI	Normal AD biomarkers with dementia
	A+ T- (N)-	Preclinical Alzheimer's pathologic change	Alzheimer's pathologic change with MCI	Alzheimer's pathologic change with dementia
	A+ T+ (N)- A+ T+ (N)+	Preclinical AD	AD with MCI (Prodromal AD)	AD with dementia

A = β-amyloid; T = tau; (N) = neurodegeneration; '+' = positive; '-' = negative; AD = Alzheimer's disease; MCI = mild cognitive impairment

While similar, the IWG and NIA-AA criteria differ in their approach to classification, which has implications when comparing findings across research studies that have defined individuals according to different criteria. They also continue to evolve over time as new information becomes available and biomarkers are developed.

A notable difference between the 2014 and 2016 IWG criteria (Dubois *et al.*, 2014, 2016), which is relevant to the work undertaken in this thesis, is the definition of preclinical AD. Whereas the 2014 criteria required abnormal Aβ biomarkers only, the updated 2016 criteria necessitate evidence of abnormal Aβ and tau, referring to those with abnormal Aβ alone as being "asymptomatic at risk." This change was made due to insufficient data regarding the fate of cognitively normal individuals harbouring only Aβ, in contrast to the strong evidence that accumulation of both Aβ and tau leads to faster onset of cognitive decline (Vos *et al.*, 2013). The latest NIA-AA criteria are similar in this regard, reserving the term preclinical AD for those with abnormal Aβ and tau, while those with only Aβ are defined as "preclinical Alzheimer's pathologic change" (Jack *et al.*, 2018).

A disadvantage of this change is that it limits application of these criteria to centres with sufficient resources to quantify both biomarkers. However, since it is generally agreed that Aβ deposition is necessary for the development of AD and, while it is not yet possible to say definitively that Aβ positive individuals will develop dementia if they live long enough, many studies have and continue to draw conclusions about preclinical AD from differences between cognitively normal Aβ positive and negative individuals.

Another consideration is that both criteria involve dichotomising individuals by biomarker status (i.e., positive/negative). While necessary, this is unlikely to reflect the pathological processes in AD, which develop along a continuum. There is also considerable variability

between studies with regard to how thresholds for positivity are determined, which is further complicated by the availability of different methods of biomarker quantification. Methods of standardisation have recently been proposed to address this heterogeneity, including the 'centiloid' technique, which scales the outcome of a particular PET tracer or analysis method from 0 to 100 (Klunk *et al.*, 2015), and internationally accepted reference standards and reference methods for the assessment of CSF biomarkers (Carrillo *et al.*, 2013; Kuhlmann *et al.*, 2017).

Several blood-based biomarkers are also in development, including measures of Aβ, t-tau, p-tau and neurofilament light (Keshavan *et al.*, 2017). Use of blood biomarkers would offer several advantages over CSF or PET, including being less invasive and more cost-effective and accessible (Hampel *et al.*, 2018). There are multiple challenges that need to be overcome, however, before accurate and standardised blood biomarkers are available for incorporation into diagnostic criteria. The low concentration of biomarkers in the blood, together with the presence of other proteins that interfere with assays, and proteases that degrade the biomarker of interest, have been the main difficulties to date (Zetterberg, 2019). The recent development of sensitive and specific immunological- and mass spectrometry- based assays show some promise and current research is focused on validating these techniques in large independent cohorts (Alawode *et al.*, 2021).

1.2.7. Treatments

Acetylcholinesterase inhibitors (AChEIs) have remained the first line treatment for AD since their introduction to clinical practice in 1993. They work by inhibiting breakdown of acetylcholine at the neuronal synapse, thereby enhancing cholinergic transmission. Clinical trials have demonstrated symptomatic improvement (Aisen, Cummings and

Schneider, 2012), but the benefits are modest and often difficult to discern in clinical practice. Memantine is an alternative option for patients intolerant of AChEIs or as an adjunct in patients with moderate to severe AD (NICE, 2018). It acts as a non-competitive *N*-methyl-D-aspartate receptor antagonist and is thought to work by restoring normal neurotransmission (Wilcock, 2003). Similar to AChEIs, the effects of Memantine are symptomatic and patients inevitably continue to deteriorate as the disease progresses.

Despite substantial progress in basic science research and drug development, trials of disease-modifying therapies for AD have repeatedly delivered disappointing results. Most strategies to date have targeted the Aβ hypothesis, either using antibodies to clear Aβ from the brain or enzyme inhibitors to prevent its accumulation (Hardy and De Strooper, 2017). Several explanations have been proposed for their repeated failure in trials including: inclusion of patients without AD pathology; inadequate study recruitment and retention; use of subtherapeutic doses; administration too late in the disease course; insufficient understanding of AD pathogenesis; and use of inappropriate outcomes (Gauthier *et al.*, 2016). A number of trials are currently trying to address these issues, including the A4 study, which aims to recruit 1000 cognitively normal individuals with evidence of significant Aβ pathology on PET imaging, and will test whether an anti-Aβ therapy slows down rate of cognitive decline using a composite measure of neuropsychological tests sensitive to change in early AD (Sperling *et al.*, 2014).

On 7th June 2021, the United States Food and Drug Administration (FDA) approved aducanumab, the first ever disease-modifying drug for AD dementia, via its accelerated approval program. This decision has been hugely controversial, particularly since results from two phase III randomised clinical trials in patients with mild AD dementia showed conflicting evidence with regards to efficacy and clinical benefit. Recruitment took place

between August 2015 and July 2018, and both trials were terminated early (March 2019) based on a futility analysis. Subsequent FDA approval was justified on the basis that aducanumab led to a reduction in Aβ burden on PET, which might reasonably be expected to result in downstream cognitive benefits. However, in the one successful trial, the difference in MMSE change was minimal and of questionable clinical benefit to patients. Moreover, a significant number of patients – 41% receiving the highest dose (10mg/kg) – developed amyloid-related imaging abnormalities (ARIA) such as oedema or new microhaemorrhages, sometimes leading to serious symptoms. These issues, together with its high cost, mean that clinicians in the US are faced with difficult decisions regarding its use. Despite these problems, experts in the field are hopeful that the approval of aducanumab will have a positive impact on research and drug development going forward, which may be beneficial in the longer term (Lalli *et al.*, 2021).

1.3. Structural magnetic resonance imaging

1.3.1. Key principles

As a non-invasive and widely accessible means of creating high-resolution images of the brain, MRI has revolutionised the study of AD-related changes in life. The physics of MRI have been comprehensively reviewed elsewhere (Pooley, 2005; Bitar *et al.*, 2006), but, in brief, it relies on the electromagnetic properties of hydrogen nuclei, which are ubiquitous in the body due to their presence in water. Each hydrogen nucleus consists of a single positively charged proton, which rotates around its own axis in a random direction. On entering the scanner, subjects are exposed to a magnetic field (B_0), usually along the z-axis (head-to-foot direction). Protons try to align in the direction of B_0, which causes them to spin in a particular way, known as precession. The frequency of

precession (ω_0) is defined by the Larmor equation: $\omega_0 = \gamma B_0$; where γ is a constant for a particular nucleus (the gyromagnetic ratio) and B_0 is the magnetic field strength in Tesla.

Most protons align parallel to B_0, but some align in the opposite direction, cancelling out some protons. The result is longitudinal magnetisation. The force created by excess protons in the B_0 direction is called the net magnetisation vector (NMV) (Figure 1.10).

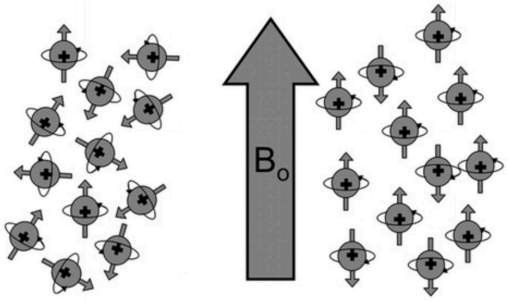

Figure 1.10. The NMV forms when protons are exposed to a magnetic field (B0). Reprinted from Radiographics, Vol. 25, 1087-1099, Pooley, AAPM/RSNA Physics Tutorial for Residents Fundamental Physics, 2005), with permission from The Radiological Society of North America (RSNA). doi: 10.1148/rg.254055027

The next step is to deliver radiofrequency (RF) pulses at the same rate as the precessional frequency of hydrogen protons. RF pulses are formed by passing electrical currents through a head coil in short bursts. When an RF pulse is applied to B_0, hydrogen protons are excited and the NMV rotates away from B_0 towards the x- and y-axes, a process known as transverse magnetisation. The amount of rotation (the flip angle) is related to the strength and duration of the RF pulse. As the NMV rotates into the transverse plane, it induces an electrical current which forms the basis of the MRI signal. When the RF pulse is switched off, protons release energy and the NMV returns to its resting state along B_0. This happens in two ways: loss of transverse magnetisation (T2 relaxation) and restoration of longitudinal magnetisation (T1 relaxation). T1 relaxation – also referred to as spin-lattice relaxation – involves a transfer of energy between protons

and surrounding tissues which return protons to their lower energy state, while T2 relaxation – also termed spin-spin relaxation – refers to the process by which protons lose phase coherence due to the effects of small magnetic fields from neighbouring nuclei (Currie *et al*., 2013). T1 and T2 relaxation rates vary by tissue type.

Two important acquisition parameters are repetition time (TR) and echo time (TE). These represent the interval between RF pulses and the interval between the RF pulse and reception of the MR signal, respectively. A short TR maximises the effects of T1 relaxation, and a short TE minimises the effects of T2 relaxation, creating a T1-weighted image, in which CSF appears dark, white matter appears light, and grey matter is an intermediate shade (Figure 1.11). A long TE maximises the effects of T2 relaxation, and a long TR limits the effects of T1 relaxation, creating a T2-weighted image, in which CSF appears bright and white matter is dark (Figure 1.11). T1 images are ideally suited for assessing brain structure, while T2 images are useful for detecting diseases, which usually appear bright due to the high water content of most pathologies.

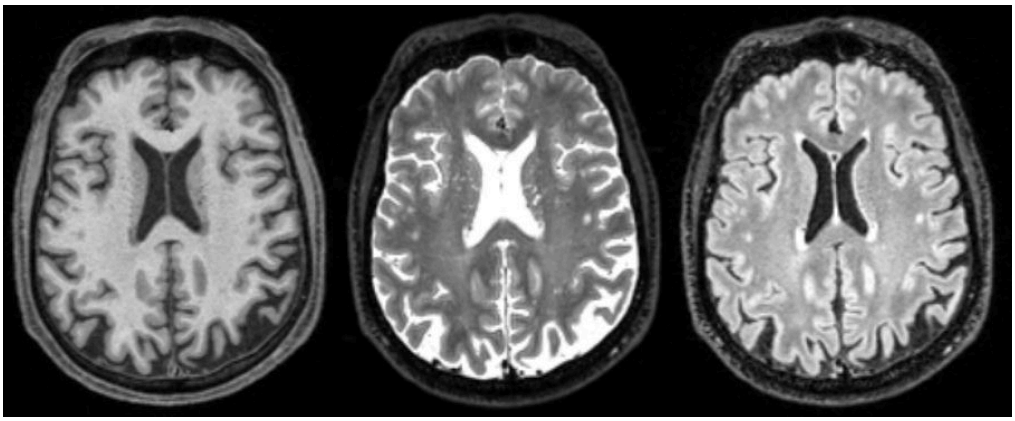

Figure 1.11. (Left) T1-weighted, (Middle) T2-weighted and (Right) FLAIR MRI brain

An inversion recovery sequence can also be performed to null the CSF signal. It involves application of a 180^{o} RF pulse to bring about inversion of longitudinal magnetisation. As

the NMV grows back towards B_0, a further 90° RF pulse is applied when the CSF signal crosses the transverse plane (the null point for any tissue). The resulting fluid-attenuated inversion recovery (FLAIR) image looks like a T2 image, except that the signal from CSF has been suppressed and therefore appears dark (Figure 1.11). FLAIR images are helpful for making subtle abnormalities in regions bordering the CSF more apparent.

1.3.2. Detection and management of incidental findings

An important consideration for research studies involving MRI is the detection and management of incidental findings. An incidental finding is an abnormality "concerning an individual research participant that has potential health or reproductive importance…but is beyond the aims of the study" (Wolf *et al.*, 2008). While the primary aim of most research is to generate data and advance knowledge, rather than to diagnose health problems in participants, there are important ethical reasons for disclosing incidental findings in appropriate circumstances, particularly when they relate to serious and potentially treatable conditions (Wolf *et al.*, 2008). There is no consensus on how this should be done, but it is generally recommended that researchers weigh up the potential benefits and harms of being informed, as well as considering the associated time and cost to the study and publicly funded health services (Medical Research Council, 2014). The practicalities of detecting and managing incidental findings will be discussed further in Chapter Four.

1.3.3. Measuring changes in brain structure

The key features of MRI which are important for the measurement of structural brain changes are image resolution and contrast. High resolution 3D images reduce partial

volume errors and allow more accurate alignment of serial scans than 2D images, while T1 images, with or without CSF suppression, offer better contrast between brain and CSF than T2 images (Miller *et al.*, 2002). For these reasons, 3D T1 MRI is generally preferred for measurement of structural brain changes.

Measurement techniques have progressed over the years from simple visual inspection, to manual volumetry, to complex automated algorithms that quantify changes in brain structure with high precision (Ashburner *et al.*, 2003). Manual delineation by experienced operators is considered the gold standard but is time-consuming and prone to bias and operator error. Automated algorithms that have been validated against manual techniques or pathological findings offer an alternative approach. These can be performed cross-sectionally to assess for differences between groups, or longitudinally to detect changes within individuals over time. Longitudinal approaches, where individuals act as their own control, reduce inter-subject variability, and increase statistical sensitivity to detect subtle changes in brain structure. In this thesis, I use two well-validated automated longitudinal techniques, which are described briefly below.

1.3.3.1. The boundary shift integral

The boundary shift integral (BSI) provides a direct measure of the total volume by which the brain's boundaries have shifted between two scans from the same person by comparing differences in MRI signal intensities (Freeborough and Fox, 1997). Brain tissue is first segmented from each scan and then linear registration is used to align brain tissue across both images using a series of transformations (Figure 1.12).

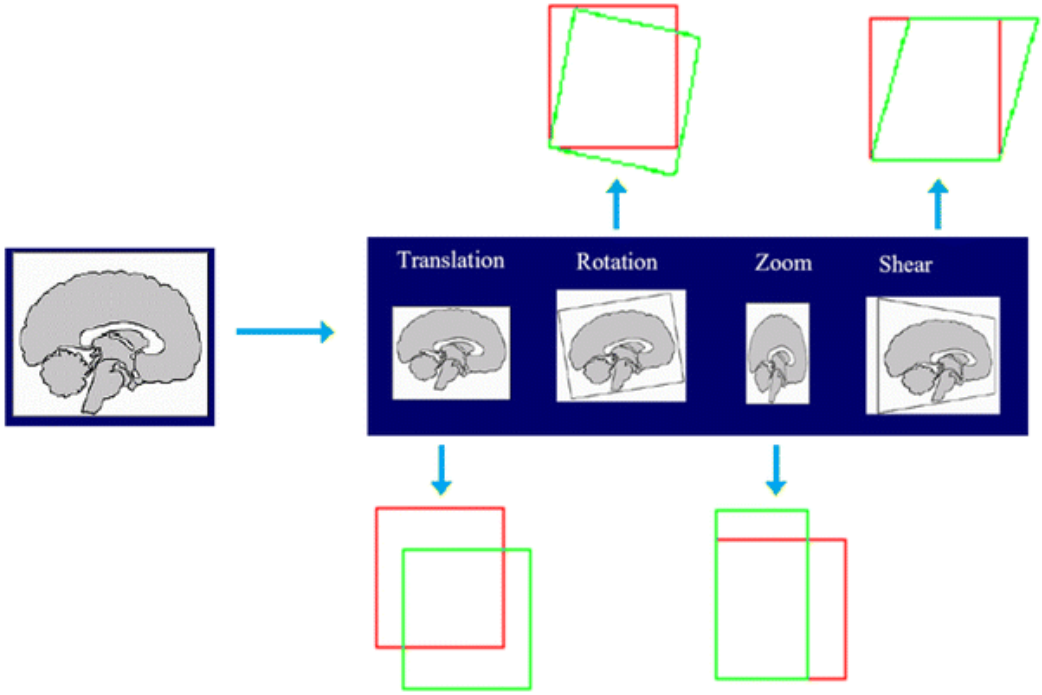

Figure 1.12. Linear registration involves a series of transformations including translations, rotations, zooms +/- shears to match two images to one another. Reprinted from Network Modeling and Analysis in Health Informatics and Bioinformatics, Vol. 4, 191-208, Vizza *et al.*, Methodologies for the analysis and classification of PET images, 2013, with permission from Springer Nature. doi: 10.1007/s13721-013-0035-9.

The distance through which the brain's boundary has shifted between two scans – a one dimensional representation of which is shown in Figure 1.13 – can then be estimated.

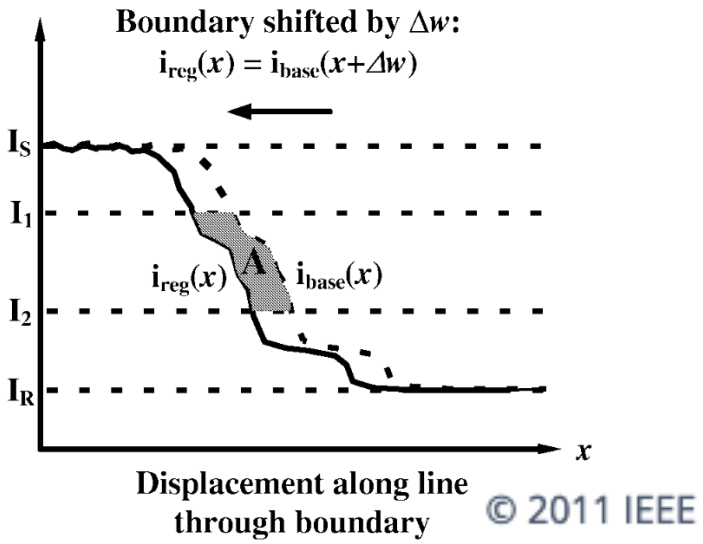

Figure 1.13. A one-dimensional representation of a boundary shift (Δw) between a baseline scan, ibase(x), and a registered repeat scan, ireg(x). Reprinted from IEEE Transactions on Medical Imaging, Vol. 16, 623-629, Freeborough and Fox, The boundary shift integral: an accurate and robust measure of cerebral volume changes from registered repeat MRI, 1997), according to the permissions policy of IEEE. doi: 10.1109/42.640753.

Specifically, the shaded area (A) between boundary intensity profiles from the baseline and repeat scan and the upper and lower intensity limits (I_1, I_2) can be calculated using integration and then divided by the difference between I_1 and I_2:

$$A = \int (\text{clip}(i_{base}(x), I_1, I_2) - \text{clip}(i_{reg}(x), I_1, I_2)$$

where clip $(I, I_1, I_2) = I$ for $I_1 > I > I_2$, I_1 for $I > I_1$, and I_2 for $I < I_2$

$$\text{thus } \Delta w = \int \left((\text{clip}(i_{base}(x), I_1, I_2) - \text{clip}(i_{reg}(x), I_1, I_2) \right) \div (I_1 - I_2)$$

The total volume by which the boundary has shifted can then be estimated as:

$$\Delta v = \int \left((\text{clip}(i_{base}(x, y, z), I_1, I_2) - \text{clip}(i_{repeat}(x, y, z), I_1, I_2) \right) \div (I_1 - I_2)$$

The BSI method provides more precise estimates compared to indirectly calculating the difference in volume between time-points because it reduces the effects of segmentation errors. In addition to change in whole brain volume (BBSI), change within a specific region can be assessed, provided the boundary of the region involves a distinct transition in signal intensity, e.g., the ventricles (VBSI) or hippocampus (HBSI) (Leung *et al.*, 2010).

1.3.3.2. Freesurfer: cortical thickness

Techniques have also been developed to quantify the thickness of cortical grey matter, with Freesurfer (http://surfer.nmr.mgh.harvard.edu/) being one of the most commonly used and accessible methods. The technical steps of Freesurfer's processing pipeline have been described in detail in previous publications (Dale, Fischl and Sereno, 1999; Fischl, Sereno and Dale, 1999; Fischl and Dale, 2000; Fischl, Liu and Dale, 2001), and include motion correction and averaging of volumetric T1 MRI data, removal of the skull and non-brain tissue, tessellation of the grey/white matter boundary, and surface deformation to optimally place the grey/white matter and grey/CSF matter borders (Figure 1.14). Additional procedures can then be performed depending on whether a vertex-wise whole brain or region of interest analysis is desired.

For longitudinal studies, it is recommended that data is processed using Freesurfer's longitudinal stream (Reuter *et al.*, 2012), which is designed to be unbiased with respect to any time-point. It uses robust inverse consistent registration to create a within-subject template (Reuter, Rosas and Fischl, 2010), and then repeats several of the processing steps above using information from this common template, thereby increasing reliability and statistical power (Reuter *et al.*, 2012). In contrast to the BSI, an indirect measure of

longitudinal change is obtained by calculating the difference in cortical thickness between time-points (i.e., subtracting the value at timepoint one from timepoint two).

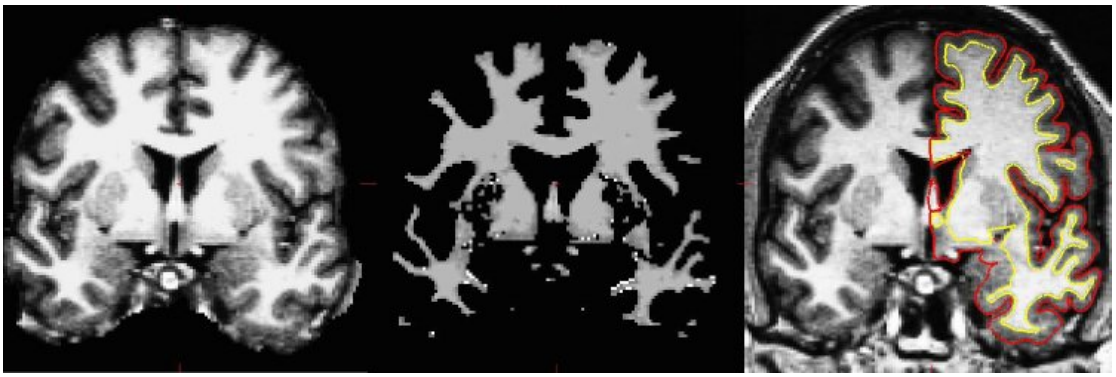

Figure 1.14. Stages of the Freesurfer cortical thickness pipeline
from left to right: removal of the skull; segmentation of white matter; and delineation of the grey/white matter (yellow line) and grey/CSF surfaces (red line).
Reprinted from the Freesurfer Wiki page "Freesurfer Analysis Pipeline Overview" http://surfer.nmr.mgh.harvard.edu/fswiki/FreeSurferAnalysisPipelineOverview, with permission from the developers.

1.3.3.3. Other approaches

Various other approaches have been developed, which are beyond the scope of the work in this thesis. One of these is voxel-compression mapping, which allows assessment of regional volume in an unbiased manner, essentially at each voxel within an image (Freeborough and Fox, 1998). After linear registration globally across both images, a non-linear warping technique, based on the physical model of a viscous fluid, is applied to determine the deformation field required to match a repeat scan onto a baseline scan at each voxel by generating three-dimensional displacement vectors (Crum, Scahill and Fox, 2001). The amount of expansion or contraction required to match the scans at each

voxel is referred to as the Jacobian value. These values can then be colour-coded and overlaid onto the original image to produce a voxel-compression map (Figure 1.15), and differences can be assessed using statistical parametric mapping (Friston *et al.*, 1991).

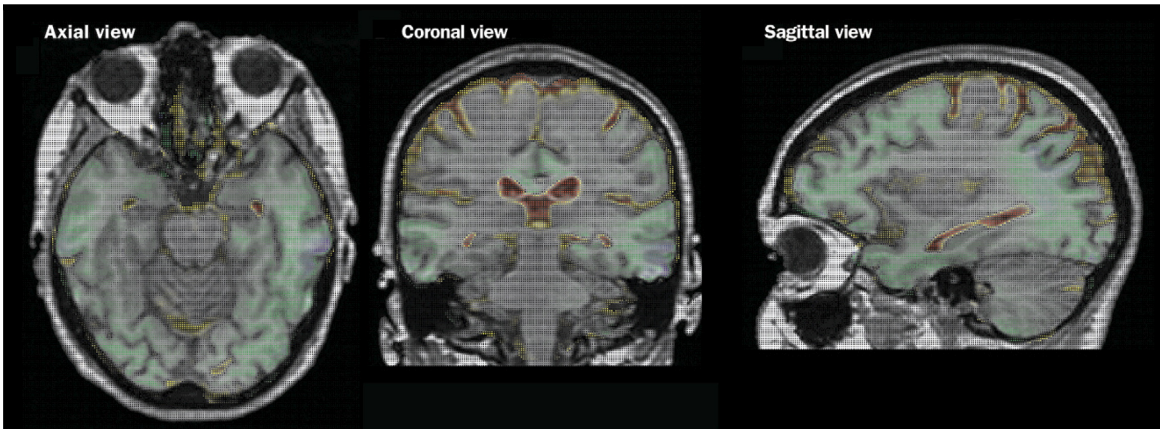

Figure 1.15. MRIs with voxel-compression-mapping overlay in an Alzheimer's disease patient showing areas of contraction (blue/green) and expansion (red/yellow). Reprinted from The Lancet, Vol. 358, 201-205, Fox *et al.*, Imaging of onset and progression of Alzheimer's disease with voxel-compression mapping of serial magnetic resonance images, 2001, with permission from Elsevier. doi: 10.1016/S0140-6736(01)05408-3.

1.3.4. Suitability as a biomarker in Alzheimer's disease

The suitability of structural MRI as an AD biomarker can be evaluated according to whether it has the following key characteristics: (1) applicability, meaning widely available and non-invasive; (2) reliability on repeated testing and between centres; and (3) validity with respect to the disease and clinical presentation (Hampel *et al.*, 2010). For the most part, MRI is readily accessible and generally considered low burden for patients. Since it does not involve ionising radiation, subjects can be safely scanned multiple times. The exception is those in whom its use is contraindicated due to the

presence of electronic or metallic implants (e.g., pacemakers or aneurysm clips), and some people cannot to tolerate it due to claustrophobia. With regards to reliability, automated techniques have been shown to yield reproducible quantitative measures, provided similar MRI scanners and protocols are used (Giedd *et al.*, 1995; Byrum *et al.*, 1996). This is important for clinical trials which are often conducted across multiple centres. Structural MRI changes have also been corroborated with findings at post-mortem (Bobinski *et al.*, 1999), and have been shown to correlate with cognition in AD (Ridha *et al.*, 2008; Schott *et al.*, 2008; Jack *et al.*, 2009), even in the pre-dementia stages (Vyhnalek *et al.*, 2014), thus supporting their validity as biological markers of disease progression.

1.3.5. Age-related structural brain changes

When using MRI as a tool to study AD, it is important to understand the changes that might be expected with normal ageing (although defining what is normal is not straightforward). Diagnostically, this knowledge helps to distinguish pathological from age-related findings, whereas from a therapeutic perspective, it is essential to consider the effects of ageing when designing clinical trials, since it may be unrealistic to expect a disease-modifying drug for AD (e.g., an Aβ-targeted therapy) to slow their progression.

Rates of whole brain atrophy have been shown to gradually increase with age from around 0.2% per year at age 30-50 to 0.3-0.5% per year at age 70-80 (Mueller *et al.*, 1998; Fox *et al.*, 1999; Resnick *et al.*, 2003; Scahill *et al.*, 2003; Schott *et al.*, 2003). Rates of hippocampal atrophy have been reported to increase from 0.38% per year in young adults (<55 years) to 0.98% per year in midlife (55-70 years) to 1.12% per year in older age (70+ years) (Figure 1.16), with no difference between the left and right

hippocampus (Fraser, Shaw and Cherbuin, 2015). The presence of asymmetry might therefore be useful as a marker of underlying pathology (Cherbuin *et al.*, 2010).

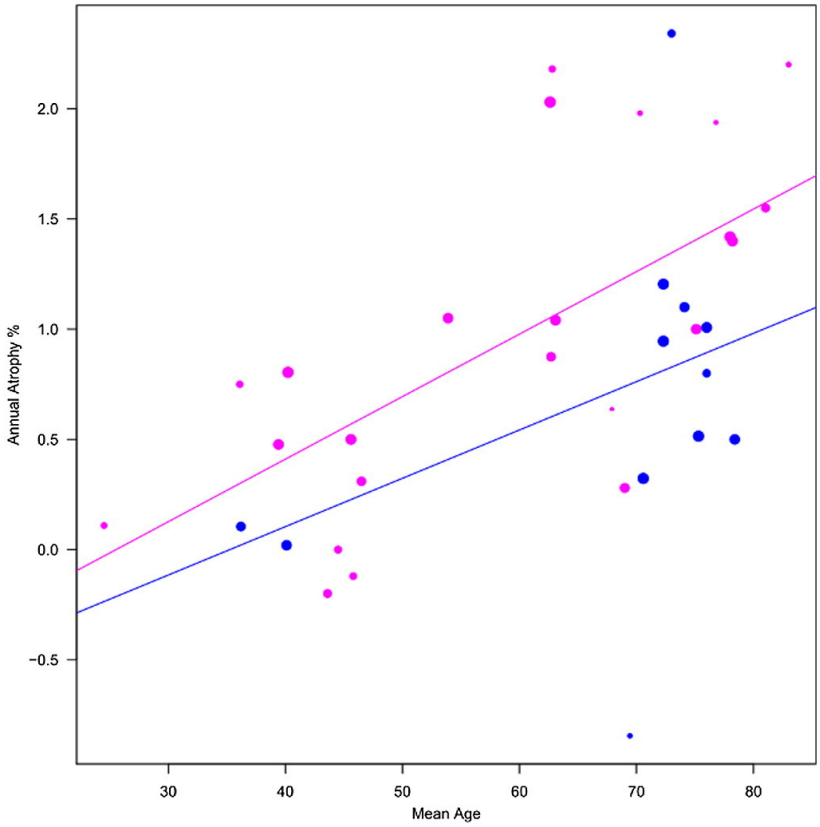

Figure 1.16. Meta-regression results of hippocampal atrophy rate in relation to age in studies using manual (magenta line) and automated segmentation (blue line) Reprinted from Neuroimage, Vol 112, 364-274, Fraser, Shaw and Cherbuin, A systematic review and meta-analysis of longitudinal hippocampal atrophy in healthy human ageing, 2015, with permission of Elsevier.

doi: 10.1016/j.neuroimage.2015.03.035.

Rates of entorhinal cortex atrophy have been reported as 1.4% per year in older adults in their seventies, accelerating by approximately 0.04% per year between 60 and 85 years old (Du *et al.*, 2003, 2006), while rates of ventricular expansion are relatively stable

at around one ml/year before the age of 70 years, accelerating to approximately four ml/year towards the age of 80 years (Resnick *et al.*, 2003; Scahill *et al.*, 2003).

Examination of patterns of changes across the whole brain, either by analysis of lobar regions or using voxel-based comparisons, has shown greater volume loss in frontal and parietal, compared to temporal and occipital areas, with loss of grey matter in orbital and inferior frontal, cingulate, insular and inferior parietal regions, while white matter volume loss was diffuse (Resnick *et al.*, 2003). Assessment of cortical thickness has shown similar findings, in particular confirming greater reductions in anterior structures, such as the prefrontal cortex, compared to posterior regions (Thambisetty *et al.*, 2010). This is consistent with the observation that executive functions, which are subserved by the frontal lobe, are particularly vulnerable to decline with advancing age (Schretlen *et al.*, 2000).

While the studies described above have provided insight into age-related changes, many were performed before the advent of pathological biomarkers and it is now recognised that a significant proportion of apparently healthy elderly are accumulating AD or other neurodegenerative pathologies (Jansen et al., 2015). This highlights the challenge faced by researchers trying to disentangle the effects of ageing and disease, and has led to questions regarding the definition of so-called normal ageing (Schott, 2017). The implications of this issue are discussed further in Chapter Eight.

1.3.6. Structural brain changes in preclinical Alzheimer's disease

The feasibility of using structural MRI measures as biomarkers of neurodegeneration in preclinical AD is dependent on differences being detectable on MRI during this phase. Their magnitude and timing are also important.

1.3.6.1. Studies of cognitively normal elderly

Studies in cognitively normal elderly who later developed mild cognitive impairment or AD dementia have detected smaller brain volumes, relative to controls, particularly in medial temporal lobe structures, such as the hippocampus, amygdala and entorhinal cortex (Kaye *et al.*, 1997; Den Heijer *et al.*, 2006; Smith *et al.*, 2007; Martin *et al.*, 2010; Tondelli *et al.*, 2012). Most have observed changes around four to six years before symptoms (Den Heijer *et al.*, 2006; Smith *et al.*, 2007; Martin *et al.*, 2010), although one study detected reductions as early as ten years prior to cognitive decline (Tondelli *et al.*, 2012). This might reflect the high education level of participants in the latter study (they were recruited based on whether they perceived their memory and thinking to be superior to peers), since greater cognitive reserve may allow individuals to continue performing well on cognitive tasks despite structural brain changes.

Smaller medial temporal lobe volumes have also been reported in relation to Aβ deposition in cognitively normal elderly (Fagan *et al.*, 2009; Storandt *et al.*, 2009; Bourgeat *et al.*, 2010; Bos *et al.*, 2017), as has reduced cortical thickness in the precuneus, posterior cingulate and parietal areas (Becker *et al.*, 2011). Other studies have identified fairly consistent patterns of cortical thinning in early AD (so-called AD

signature regions) which predict cognitive decline and dementia in asymptomatic Aβ positive elderly (Dickerson *et al.*, 2011; Dickerson and Wolk, 2012; Schwarz *et al.*, 2016).

Some cross-sectional studies, however, have not detected Aβ-related differences in brain structure in cognitively normal elderly (Schott *et al.*, 2010; Wirth *et al.*, 2013; Mattsson *et al.*, 2015; Armstrong *et al.*, 2019; Parker *et al.*, 2020), while others have reported larger temporal lobe volumes (Chételat *et al.*, 2010), or greater cortical thickness in temporo-parietal regions and the precuneus (Fortea *et al.*, 2011). It has been suggested that this might reflect a transient response to Aβ, possibly involving inflammation or neuronal hypertrophy. Longitudinal studies have shown more consistent results, with most reporting faster rates of atrophy or cortical thinning in relation to Aβ (Schott *et al.*, 2010; Chételat *et al.*, 2012; Ewers *et al.*, 2012; Andrews *et al.*, 2013; Doré *et al.*, 2013; Mattsson *et al.*, 2014; Petersen *et al.*, 2016), although some have not (Josephs *et al.*, 2008; Driscoll *et al.*, 2011).

These discrepancies might relate to methodological differences between studies (e.g., techniques for quantifying Aβ or neurodegeneration) or the limitations of many studies to date (see section 1.4 for discussion). Alternatively, it may be that Aβ deposition is "necessary but not sufficient in isolation" to cause decline, i.e., that other factors may be required (Sperling, Mormino and Johnson, 2014). Consistent with this possibility, post-mortem studies have shown that tau deposition correlates more closely with synaptic and neuronal loss than Aβ (Arriagada *et al.*, 1992; Gómez-Isla *et al.*, 1997), as has more recent data from CSF and imaging biomarker studies (Tarawneh *et al.*, 2015; La Joie *et al.*, 2020). Thus, perhaps changes in brain structure can only be reliably detected in the preclinical phase of AD once Aβ has triggered downstream tau accumulation.

1.3.6.2. Studies of presymptomatic mutation carriers

Studies of presymptomatic AD mutation carriers have also provided insight into structural brain changes, although the extent to which these are translatable to the more common sporadic form of AD, which has a much later age at onset, is debatable. Most have detected reductions in cortical thickness or brain volumes, including in the hippocampus, entorhinal cortex, precuneus, cingulate and subcortical areas, such as the caudate and thalamus (Fox *et al.*, 1996, 2001; Schott *et al.*, 2003; Ridha *et al.*, 2006; Knight *et al.*, 2011; Cash *et al.*, 2013; Ryan *et al.*, 2013; Weston *et al.*, 2016).

One study detected smaller hippocampal and whole brain volumes at three and one year prior to dementia diagnosis, while even earlier changes were observed using longitudinal MRI measures, with greater rates of whole brain and hippocampal atrophy preceding dementia diagnosis by 3.5 and 5.5 years (Ridha *et al.*, 2006). Another study detected lower cortical thickness in the precuneus and posterior cingulate around four and two years prior to estimated symptom onset (Knight *et al.*, 2011), while a larger study has since reported increased rates of AD signature and precuneus thinning at five and eight years prior to predicted symptom onset (Weston *et al.*, 2016).

1.3.6.3. Effect sizes and sample size estimates

Calculation of effect sizes (in studies with the necessary raw data) highlights that there is considerable variability with regards to the magnitude of preclinical changes in brain structure, even between studies assessing the same brain region (Table 1.3).

Table 1.3. Effect sizes based on mean comparison of preclinical AD versus controls

Author (year)	No.	MRI measure examined	Cohen's d [95% CI]
Cross-sectional, cognitively normal elderly (biomarker positive or future diagnosis)			
Kaye (1997)	30	Hippocampal volume Parahippocampal volume Temporal lobe volume	-0.85 [-1.61, -0.08]* -0.43 [-1.16, 0.31] -0.64 [-1.39, 0.11]
Fagan (2009)	58	Hippocampal volume	-0.73 [-1.26, -0.19]*
Martin (2010)	71	Whole brain volume Entorhinal cortex volume Hippocampal volume	-0.33 [-0.87, 0.22] -0.01 [-0.55, 0.54] -1.18 [-1.76. -0.60]*
Schott (2010)	105	Whole brain volume Ventricular volume Hippocampal volume	0.22 [-0.17, 0.62] 0.27 [-0.12, 0.67] -0.13 [-0.53, 0.26]
Andrews (2013)	66	Whole brain volume Ventricular volume Hippocampal volume	-0.31 [-0.82, 0.21] -0.01 [-0.53, 0.50] -0.29 [-0.80, 0.22]
Cross-sectional, presymptomatic AD mutation carriers			
Ridha (2006)	33	Whole brain volume Hippocampal volume	-0.16 [-0.96, 0.63] -0.88 [-1.70, -0.04]
Longitudinal, cognitively normal elderly (biomarker positive or future diagnosis)			
Kaye(1997)	30	Rate of change in hippocampal volume Rate of change in parahippocampal volume Rate of change in temporal lobe volume	0.03 [-0.71, 0.76] -0.26 [-0.99, 0.48] -0.78 [-1.53, -0.01]*
Schott (2010)	105	Rate of change in whole brain volume Rate of change in ventricular volume Rate of change in hippocampal volume	-0.82 [-1.23, -0.41]* 0.73 [0.32, 1.14]* -0.45 [-0.85, -0.05]*
Andrews (2013)	66	Rate of change in whole brain volume Rate of change in ventricular volume Rate of change in hippocampal volume	-0.34 [-0.86, 0.17] 0.50 [-0.02, 1.02] -0.76 [-1.29, -0.23]*
Longitudinal, presymptomatic AD mutation carriers			

Ridha (2006)	31	Rate of change in whole brain volume Rate of change in hippocampal volume	-0.95 [-1.87, -0.02]* -1.16 [-2.09, -0.22]*

*Effect sizes were based on mean in preclinical AD compared to controls and were calculated using the esizei command in Stata version 16; *reported as statistically significant difference in study*

Some studies have used this data to estimate sample size requirements for hypothetical preclinical trials. Using data from the Australian Imaging Biomarker and Lifestyle (AIBL) study (Andrews *et al.*, 2013), the number of subjects needed per treatment arm to power an 18-month trial to detect a 25% slowing in outcome change in Aβ positive individuals was estimated to be 442 (95% CI, 180–1650) for whole brain atrophy, 542 (180–1649) for ventricular expansion and 384 (195–1080) for hippocampal atrophy, while using data from the Alzheimer's Disease Neuroimaging Initiative (ADNI) (Schott *et al.*, 2010), the number of participants required per treatment arm to show the same effect over one year was estimated to be 141 (95% CI, 86–287) for whole brain atrophy, 225 (95% CI, 147–442) for ventricular expansion and 467 (95% CI, 197–2675) for hippocampal atrophy.

The number of Aβ positive participants in these studies was small, and calculations did not account for the effects of ageing. Nonetheless, these estimates support the potential feasibility of including structural MRI measures as outcomes in preclinical AD trials. Since both ADNI and AIBL used the same BSI technique to quantify volume changes from MRI, differences in sample size estimates between the two studies most likely reflect differences in participant characteristics. For example, there was preferential recruitment of APOE ε4 carriers and individuals with subjective memory complaints to AIBL.

1.4. Key limitations and challenges of studies to date

A significant limitation of many studies to date has been the representativeness of their participants. One particular issue is recruitment from convenience samples, including volunteers who seek out research opportunities or patients presenting to memory clinics with cognitive concerns (Brodaty *et al.*, 2014; Parnetti *et al.*, 2019). These individuals are generally better educated than those recruited from the general population and are more likely to have a family history of dementia or to be an APOE ε4 carrier (Brodaty *et al.*, 2014). As such, their findings may not be generalisable to the wider population. For example, greater rates of hippocampal atrophy have been reported in convenience samples compared to those that are population-based (Whitwell *et al.*, 2012).

Many studies have also been limited by small participant numbers and there has been considerable heterogeneity within studies with regards to scanner properties and imaging protocols, which has the potential to influence detection of disease-related differences (Kruggel, Turner and Muftuler, 2010). Moreover, knowledge regarding the progression of changes over time has often been inferred from cross-sectional MRI data, which is difficult to interpret due to inter-individual variability in premorbid brain size.

Another challenge is the variation in neurodegeneration that exists between individuals, particularly that related to age – the effects of which are difficult to disentangle – and other pathologies that often co-exist with AD in later life. As discussed previously, white matter hyperintensities (WMHs) – a marker of presumed cerebrovascular disease (CVD) – are common with increasing age, detectable on MRI in greater than 90% of adults over 60 years old (De Leeuw *et al.*, 2001). Higher WMH volume has been linked to lower brain volumes and cortical thickness (Habes *et al.*, 2016; Petersen *et al.*, 2016; Rizvi *et al.*,

2018; Vipin *et al.*, 2018; Parker *et al.*, 2020), and faster rates of atrophy, including within the hippocampus (Barnes, Carmichael, *et al.*, 2013; Fiford *et al.*, 2017). Thus, the presence of WMHs could confound detection of Aβ-related neurodegeneration, particularly in the preclinical phase when findings are likely to be subtle. As previously discussed, the relationship between CVD and Aβ, and the extent to which they act separately or together to influence downstream processes such as neurodegeneration, is also poorly understood.

1.5. Thesis approach

1.5.1. Rationale

Overall, the evidence described thus far suggests that differences in brain structure can be detected on MRI before the onset of AD dementia and that structural MRI measures may be useful as biomarkers of neurodegeneration during this preclinical phase. However, there remain some uncertainties regarding the magnitude of these changes, the nature of their relationship with Aβ, and the contribution of other brain pathologies such as CVD. This knowledge is essential to inform the appropriate use of structural MRI measures as biomarkers and for the design of efficient preclinical AD trials. Furthermore, studying these relationships could provide insight into the processes that underlie progression to dementia in later life, which may inform strategies for preventing or delaying its onset. These are the overarching reasons for the analyses in this thesis.

1.5.2. Insight 46

Insight 46 is a longitudinal study of 502 participants involving detailed clinical testing, neuropsychological assessment, cerebral Aβ PET and multi-modal brain MRI at two time-points, around two years apart (Lane *et al.*, 2017). Participants were all recruited from the Medical Research Council (MRC) National Survey of Health and Development (NSHD; also known as the 1946 British birth cohort), a representative sample of individuals born in mainland Britain during one week in 1946 (Kuh *et al.*, 2011). As well as being virtually identical in age, NSHD members have been extensively studied since birth, resulting in years of prospectively collected data from across the life-course. Now in their seventies, they are in the decade of their lives during which changes related to preclinical AD would be expected to occur, i.e., young enough to be at risk of having significant AD pathology, but years before significant numbers are likely to get dementia (Stafford *et al.*, 2013; Prince *et al.*, 2014; Jansen *et al.*, 2015) (Figure 1.17).

Another feature of Insight 46 – which makes it unique in comparison to similar cohort studies of ageing populations – is the use of a single hybrid PET/MRI scanner. This relatively new technology, only available at a limited number of sites in the UK, allows simultaneous acquisition of dynamic Aβ PET and MRI data whilst minimising scanning time and radiation exposure to study participants (compared to PET/CT). Of relevance to this thesis, it provides an invaluable opportunity to study relationships between concurrent imaging measures of Aβ, CVD and neurodegeneration in a well-characterised and closely age-matched sample of older adults.

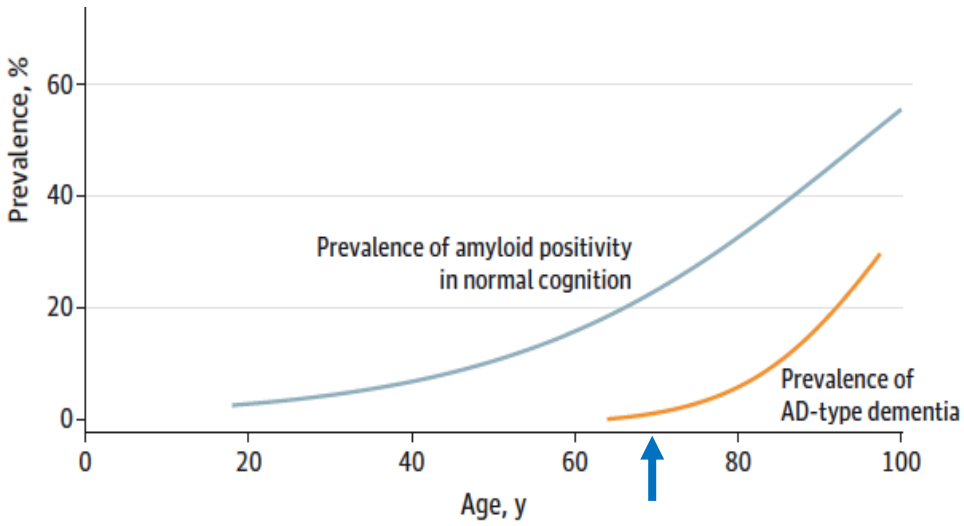

Figure 1.17. The prevalence of β-amyloid positivity in cognitively normal adults (blue line) and the prevalence of AD-type dementia (orange line). The blue arrow indicates the age of Insight 46 participants at baseline.

Reprinted from JAMA, Vol 313, 1924-1938, Jansen et al., Prevalence of Cerebral Amyloid Pathology in Persons Without Dementia: A Meta-analysis, 2015, with permission from the American Medical Association. doi: 10.1001/jama.2015.4668.

1.5.3. Data chapters

Using the Insight 46 dataset, I aimed to investigate the following areas:

- The feasibility of recruiting a large elderly cohort to an MRI study **(Chapter Three).**
- The detection and management of incidental MRI brain findings **(Chapter Four).**
- The longitudinal changes in brain structure – volume **(Chapter Five)** and cortical thickness **(Chapter Six)** – that can be detected on MRI in cognitively normal older adults and how they relate to Aβ, WMHs and other risk factors.
- The relationship between longitudinal structural MRI changes and performance on cognitive testing in cognitively normal older adults **(Chapter Seven).**

- The number of participants needed to power hypothetical preclinical AD trials using structural MRI measures as outcomes **(Chapter Eight).**

The rationale for these specific studies will be discussed in detail in the relevant data chapters, but the main research questions I hoped to address were:

- What is the relationship of Aβ and vascular burden with longitudinal changes in brain structure quantified from MRI in cognitively normal older adults?
- Are associations of Aβ and vascular burden with longitudinal changes in brain structure in cognitively normal older adults independent or interactive?
- Do longitudinal changes in brain structure quantified from MRI represent clinically meaningful and feasible outcome measures for preclinical AD trials?

2. METHODS

2.1. Insight 46 protocol

The full Insight 46 protocol has been published (Lane *et al.*, 2017). An overview of methods relevant to this thesis and a statement of contributions will be provided here.

2.1.1. Participants

The NSHD is the oldest of the British birth cohort studies, and many of its findings have been pivotal to the development of UK healthcare, education and social policies (Wadsworth, 2010). It started with a maternity survey of all 13,687 babies born in mainland Britain in one week in March 1946, from which a representative sample of 5,362 babies were selected for follow up. Since then, members have been studied 24 times (Figure 2.1), with 2,638 remaining in active follow-up at the latest whole cohort visit (Kuh *et al.*, 2016).

The Insight 46 study involved a sample of NSHD participants who attended a study visit at age 60-64, who had previously indicated they would be willing to consider a study visit in London, and for whom relevant life course data were available (Table 2.1). NSHD members meeting criteria for inclusion were sent an information booklet about the study and then recruited by myself or another study doctor over the telephone. Those with known contraindications to PET or MRI were excluded. To achieve the study's recruitment target of 500 participants, eligibility criteria were relaxed slightly towards the end of the study to allow inclusion of a small number of individuals with a few missing data points.

			Time point (ages)						
			1946 (birth)	1947–50 (1–4 yrs)	1951–61 (5–15 yrs)	1962–77 (16–31 yrs)	1978–2003 (32–57 yrs)	2006–10 (60–64 yrs)	2014–15 (68–69 yrs)
Number of data collections			1	2	8	8	3	1	1
Measure	Social factors	Socioeconomic position	✓	✓	✓	✓	✓	✓	✓
		Social function (contacts, support, participation)	-	-	-	-	✓	✓	✓
		Occupation	-	-	-	✓	✓	✓	✓
		Educational Qualifications			✓	✓			
	Psychological measures	Behaviour and mental health	-	✓	✓	✓	✓	✓	✓
	Physical and health measures	Survival and morbidity	✓	✓	✓	✓	✓	✓	✓
		Anthropometric measures	✓	✓	✓	✓	✓	✓	✓
		Smoking status	-	-	-	✓	✓	✓	✓
		Exercise and physical health	-	-	✓	-	✓	✓	✓
		Diet	-	✓	-	-	✓	✓	✓
		Respiratory function	-	-	-	-	✓(36, 43, 53)	✓	✓
		Cardiovascular function	-	-	-	-	✓(36, 43, 53)	✓	✓
		Musculoskeletal measures	-	-	-	-	✓ (53)	✓	✓
		Blood sample	-	-	-	-	✓ (53)	✓	✓
		Urine sample	-	-	-	-	-	✓	-
	Cognition	Cognitive function (verbal/non-verbal)	-	-	✓ (8, 11, 15)	✓ (26)	✓ (43, 53)	✓	✓

Figure 2.1. Summary of available life course data from the NSHD

Table 2.1. Required life course data for recruitment to Insight 46

1. Attendance at a clinic visit at age 60-64
2. Parental socioeconomic position: either occupational social class or education
3. Cognition: at 60-64 clinic visit AND at least one set of measures ages 8, 11 or 15
4. Early physical growth: birth weight and at least one height and weight at ages 4-15
5. Educational attainment: highest qualification by age 26
6. Mental health: teacher ratings of behaviour and temperament at ages 13 or 15, and at least one measure of affective symptoms at ages 36, 43, 53 or 60-64
7. Blood pressure, lung health, height, weight: at least one from age 36, 43, 53, 60-64
8. Health behaviours (smoking and exercise): at least from age 36, 43, 53, 60-64
9. Blood: either age 53 or 60-64 samples

2.1.2. Study design

Assessments were performed at University College London in the UK at two-time points approximately two years apart. Data collection for the first phase was completed between May 2015 and January 2018. I joined the study in August 2017 and mostly recruited and assessed participants for the second phase of the study. This initially ran from January 2018 until March 2020, at which point the study was unfortunately interrupted by the coronavirus pandemic. Study visits resumed with a combination of in-person and virtual assessments in August 2020 and were completed by January 2021.

In the first phase, study participants attended for a single day, during which they underwent: a detailed clinical interview; neuropsychological testing; structured neurological and physical examinations; sensory assessments; blood and urine collection; and Aβ PET and multi-modal MRI brain imaging. In the second phase, most

of these assessments were repeated and participants were offered the option of completing an additional half-day visit involving cardiovascular tests and a lumbar puncture. A typical day plan for visits carried out in the second phase of the study is provided in Table 2.2.

Table 2.2. Typical day one plan for visits in second phase of the study

Time	**Assessment**	**Assessor**
08.30	Greet and consent	Research assistant
08.50	Neuropsychology battery (with 10-minute break): • Logical memory (immediate and delayed) • Matrix reasoning • Circle tracing • Face-name associative memory exam • Task Set shifting • Digit symbol substitution • Visual binding • Graded naming	Research assistant
10.35	Break	
10.45	Physical tests: • Blood and urine collection • Height and weight measurement	Doctor
11.00	Detailed clinical assessment: • Cognitive and neurological history • Subjective cognitive decline questions • Delirium questions • Medication history • Family history • Mini-mental state examination • Clinical dementia rating	Doctor
12.00	Lunch	
13.00	Physical tests • Cardiopulmonary exercise testing • Blood pressure (sitting, lying, and standing) • Unified Parkinson's Disease Rating Scale (UPDRS) • Brain-Tap test • Gait assessment with cognitive task	Doctor
14.50	Break	
15.00	PET/MRI scan	Doctor

A duty of care protocol was developed to feedback specific health-related findings to the participant and their general practitioner. Reportable findings included: significant cognitive concerns; evidence of Parkinson's disease; abnormally low or high blood pressure; deranged clinical blood results; and potentially serious or treatable MRI brain abnormalities. The protocol for detecting and managing incidental MRI findings is discussed further in Chapter Four.

All study members provided written informed consent prior to participation (Appendix 1). Ethical approval was granted by the National Research Ethics Service Committee London (REC reference 14/LO/1173, PI Schott).

2.1.3. Clinical and neurological assessments

As one of the study doctors, I performed a detailed clinical interview of participants which consisted of questions about their personal and family history of neurological illness and cognitive impairment, and their current medications. I assessed for subjective cognitive decline by asking them whether they perceived difficulties with their memory or thinking, and whether they felt there had been a decline with regards to their memory or thinking in the last two years. If they responded yes to either of these questions, I then asked further questions to probe whether they felt that their difficulties were worse than people of the same age and whether they were concerned enough to seek medical help. I also used the MyCog tool was used to enquire about the presence or absence of difficulties in relation to 24 cognitive activities (Rami *et al.*, 2014), and participants completed the state and trait anxiety inventory, a 40-item questionnaire, to assess anxiety levels at the time of testing and in general (Spielberger *et al.*, 1983). An informant history was also

obtained using the AD8 tool, which contains eight items relating to memory, orientation, judgement and function (Galvin *et al.*, 2005).

As part of their physical examination, I measured their height and weight, and lying and standing blood pressure (using an OMRON HEM-905 machine). I also administered a self-paced gait assessment both with and without a cognitive task, as well as the Movement Disorder Society Unified Parkinson's Disease Rating Scale Part III (Motor) (Goetz *et al.*, 2008) which quantifies the presence of tremor, bradykinesia, rigidity, gait disturbance and postural instability, and the Bradykinesia Akinesia Incoordination tap test which assesses for emerging motor dysfunction (Noyce *et al.*, 2014). Lastly, I performed venepuncture to collect blood samples for genetic analysis and biomarker exploration, and lumbar puncture (if participant willing and able) to obtain cerebrospinal fluid for biomarker testing.

2.1.4. Neuropsychological tests

The neuropsychology battery included:

- The mini-mental state examination (MMSE) (Folstein, Folstein and McHugh, 1975) – a widely used 30-point screening tool for cognitive impairment, which assesses several cognitive domains: including orientation (ten points); registration (three points); attention and calculation (five points); recall (three points); language (two points); repetition (one point); following a three stage command (three points); reading (one point); writing (one point); and visuospatial function (one point).

- The Logical Memory test, from the Wechsler Memory Scale-Revised (WMS-R) (Wechsler, 1987), which assesses immediate and delayed (after 20 minutes) free recall of a short story comprised of 25 details.

- The Digit-Symbol substitution test (DSST), from the Wechsler Adult Intelligence Scale-Revised (WAIS-R) (Wechsler and De Lemos, 1981), which is a test of attention and psychomotor speed; participants were asked to match digits to their corresponding symbols as quickly and accurately as possible; the score was the number of substitutions correctly completed within 90 seconds.

- The 12-item Face-Name Associative Memory Exam (FNAME-12A) (Papp *et al.*, 2014) – a test of associative memory which requires participants to learn 12 unfamiliar face-name and face-occupation pairs; participants were exposed to each pair twice, then after each exposure and following a ten minute delay, they were asked to recall the name and occupation associated with each face; after a 35 minute delay, they were presented with three faces and asked to identify the face they recognised and the associated name and occupation; the total score was the number of correct responses across all recall tests.

Other tests – not relevant to the analyses in this thesis – were: a visual short-term memory binding task (Pertzov *et al.*, 2012); a task-set switching/ response inhibition test (Aron *et al.*, 2004); an irrelevant distractor paradigm (Forster and Lavie, 2011); a circle tracing task (Say *et al.*, 2011); the matrix-reasoning test from the Wechsler Abbreviated Scale of Intelligence (WASI) (Wechsler, 2011); and a test of learning and recall of a complex visual figure (phase two only) (Coughlan and Hollows, 1985).

The Preclinical Alzheimer's Cognitive Composite (PACC) was derived using the scores of four tests: MMSE; Logical Memory delayed recall; DSST; and FNAME. This is similar to the original PACC that has been proposed elsewhere (Donohue *et al.*, 2017), except that FNAME was used instead of the Free and Cue Selective Reminding Test due to concerns that it resembled another test given to NSHD participants previously. To derive the PACC, scores from each component were first converted into z-scores, based on the mean and standard deviation of the full Insight 46 sample, using the formula: z-score = (score – mean) / standard deviation. The four z-scores were then averaged. Means and standard deviations at baseline were used to derive z-scores at both time-points so that it was possible to evaluate change over time.

Some participants did not have all four scores available. For participants with missing data, PACC scores were generated if they had scores for at least two of the four components. Missing data in phase two was primarily due to tests not being administered during virtual assessments (when it was not possible to review participants in-person due to the coronavirus pandemic). Since these participants were also unable to undergo brain imaging, they are not included in most of the analyses in this thesis.

2.1.5. Imaging acquisition

Participants underwent brain imaging on a single Biograph mMR 3 Tesla PET/MRI scanner (Siemens Healthcare). They were injected intravenously with 370 MBq of the ^{18}F Aβ PET ligand florbetapir at the start of the imaging session, and dynamic Aβ data was obtained over 60 minutes. MRI data was acquired simultaneously including volumetric T1-weighted, T2-weighted and FLAIR sequences; resting state functional MRI; multi-shell diffusion-weighted imaging; three-dimensional gradient echo sequence

for T2*-weighted/ susceptibility-weighted imaging; and arterial spin labelling (non-invasive perfusion imaging). An overview of the MRI parameters relevant to this thesis is given in Figure 2.2.

	MPRAGE (3D T1)	SPACE (3D T2)	IR-SPACE (3D FLAIR)
Voxel resolution (mm^3)	1.1 × 1.1 × 1.1	1.1 × 1.1 × 1.1	1.1 × 1.1 × 1.1
Matrix size	256 × 256 × 208	256 × 256 × 176	256 × 256 × 176
FoV (read x PE) (mm)	282 × 282	282 × 282	282 × 282
Slice coverage (mm)	229	194	194
Orientation	Sagittal	Sagittal	Sagittal
PE direction	A > > P	A > > P	A > > P
TE (ms)	2.92	409	402
TR (ms)	2000	3200	5000
Flip angle (°)	8	Variable	Variable
Acq bandwidth (Hz/pix)	240	751	751
Parallel imaging	×2	×2	×2
Total scan time	5 min 06 s	4 min 43 s	6 min 27 s
Other sequence-specific parameters	Water selective excitation pulse TI = 870 ms	Water selective excitation pulse Turbo factor 141 Slice TF 2	Water selective excitation pulse Turbo factor 141 Slice TF 2 T2 sel IR TI = 1800 ms

Figure 2.2. Magnetic resonance imaging sequence parameters

Reprinted from BMC Neurology, Vol 17, Lane *et al.*, Study protocol: Insight 46 - a neuroscience sub-study of the MRC National Survey of Health and Development, 2017, under the Creative Commons Attribution License (CC BY). doi: 10.1186/s12883-017-0846-x

All T1, T2 and FLAIR MRI sequences were reviewed by myself or another team member while the participant was on the scanner table and, if we had concerns about motion or other artefacts, sequences were repeated (up to a maximum of three times).

A shortened protocol was occasionally performed if it was suspected that the participant would not be able to tolerate the full scan or if there were delays at the scanner. In these instances (affecting 2-3% of scans), florbetapir was injected at least 40 minutes prior to scan and static PET data was obtained instead (i.e., from 40-60 minutes post injection only, rather than continuously during injection and for up to 60 minutes post injection),. A minimum of T1, T2 and FLAIR MRI sequences were also acquired.

2.2. Quantification of imaging measures

2.2.1. Pre-processing and quality control of structural imaging data

A grad-warp correction was performed on T1, T2 and FLAIR MRI images to minimise geometric image distortions due to gradient non-linearity (Jovicich *et al.*, 2006), followed by brain-masked (by registration of Montreal Neurological Institute [MNI] space template to the scan) N4-bias correction to reduce signal intensity non-uniformity (Tustison *et al.*, 2010). T1 images then underwent automated anatomical parcellation using geodesic information flow (GIF) (Cardoso *et al.*, 2015). These steps are shown in Figure 2.3

All T1, T2 and FLAIR images were manually checked by a trained team, in line with quality control protocols developed for clinical trials, who assessed motion, coverage, and other issues (Figure 2.4). T1 images were specifically examined for blurring, image wrap-around and contrast problems, and FLAIR images for adequate CSF suppression.

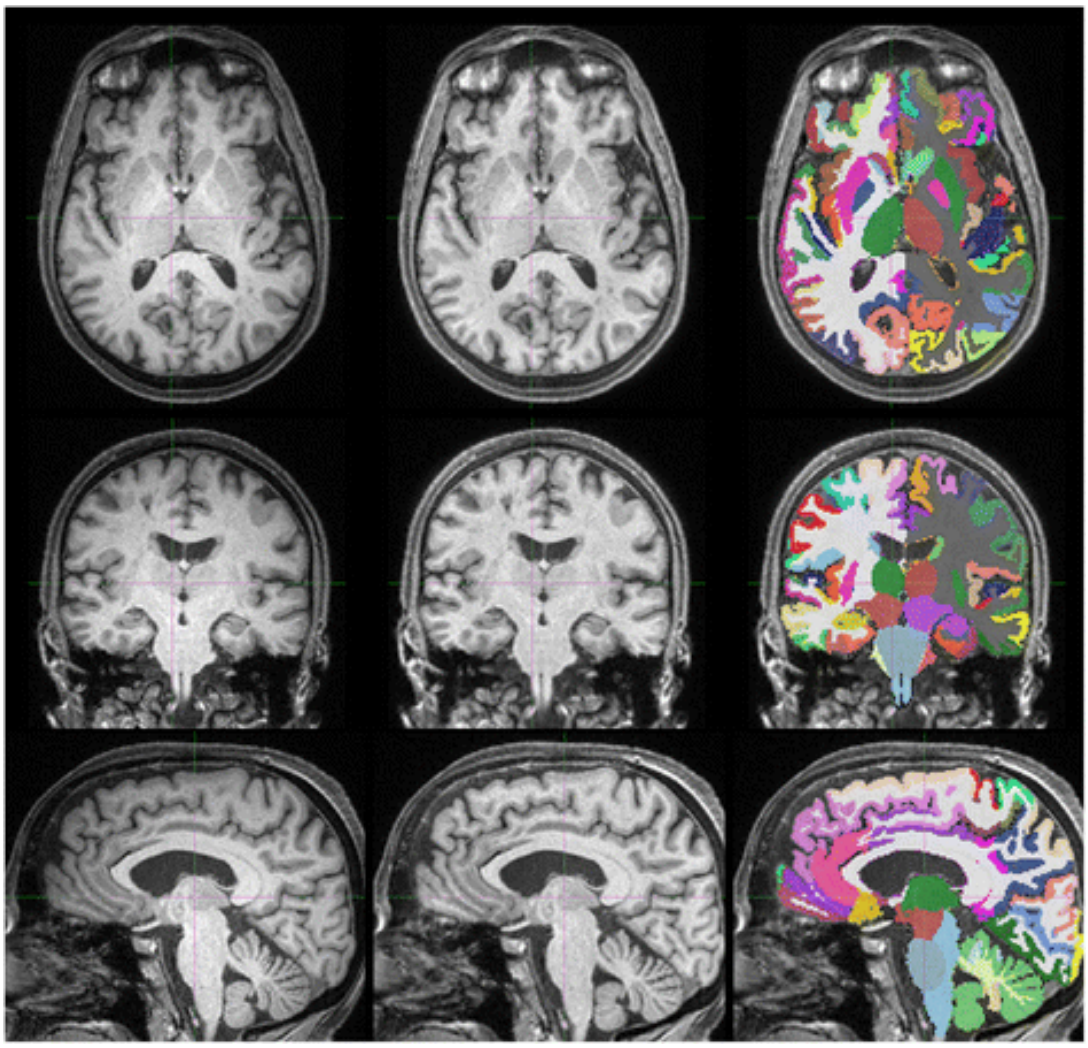

Figure 2.3. Original T1 scan (left), pre-processed T1 scan (after gradient non-linearity and bias correction) (middle) and T1 scan with overlaid GIF parcellation (right). Reprinted from BMC Neurology, Vol 17, Lane *et al.*, Study protocol: Insight 46 - a neuroscience sub-study of the MRC National Survey of Health and Development, 2017, under the Creative Commons Attribution License (CC BY). doi: 10.1186/s12883-017-0846-x

2.2.2. Baseline brain volumes

Baseline whole brain and hippocampal volumes were automatically segmented from T1 images using Multi-Atlas Propagation and Segmentation (MAPS) and Similarity and

Truth Estimation for Propagated Segmentation (STEPS) respectively (Leung *et al.*, 2011; Cardoso *et al.*, 2013). Images were visually checked for segmentation errors and manually edited if needed. Baseline ventricular volumes were determined from T1 images using a semi-automated technique (Freeborough, Fox and Kitney, 1997). Baseline total intracranial volumes were calculated from T1 images using the tissue utility in Statistical Parametric Mapping (SPM) version 12 (Malone *et al.*, 2015).

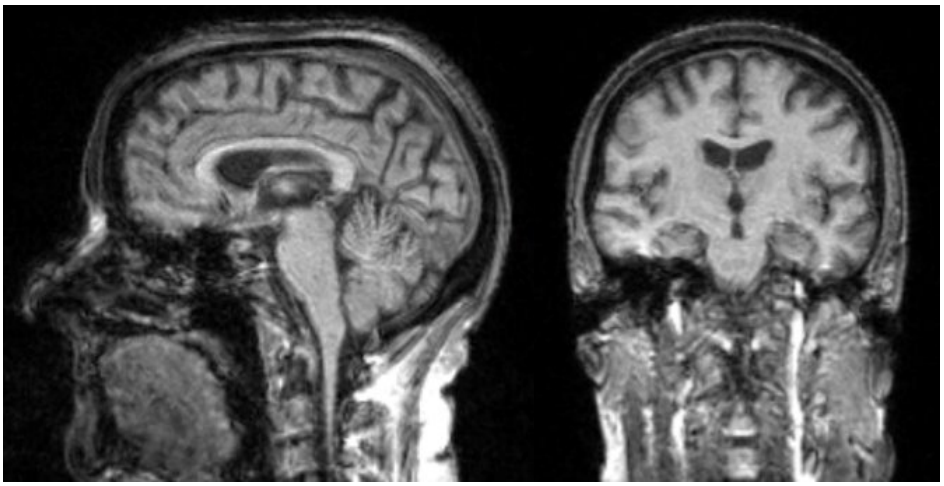

Figure 2.4. Examples of T1 scan that failed cross-sectional quality control. Images show blurring of sulci and ringing, indicative of motion.

2.2.3. Baseline white matter hyperintensity volume

White matter hyperintensity volume (WMHV) was quantified using Bayesian Model Selection (BaMoS), an automated algorithm that uses multivariate Gaussian mixture modelling to segment WMHs from T1 and FLAIR MRI sequences (Figure 2.5) (Sudre *et al.*, 2015). Segmentations were visually checked and edited if required. A global WMHV was generated that included subcortical grey matter and excluded infratentorial regions.

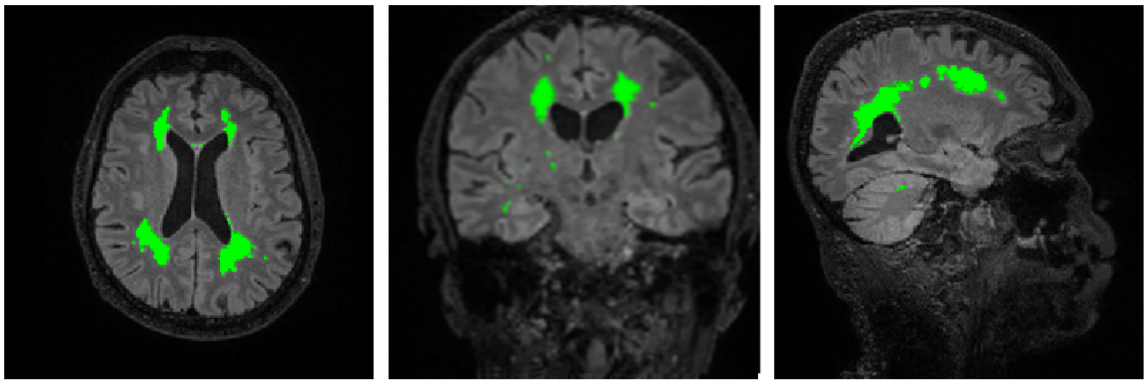

Figure 2.5. Axial (left), coronal (middle) and sagital (right) FLAIR MRI with segmentation (bright green) of white matter hyperintensities

2.2.4. Baseline β-amyloid status and standardised uptake value ratios

Aβ PET data from the 10-minute period, approximately 50 minutes post-injection, were reconstructed including correction for signal attenuation from the skull. In the absence of a computed tomography (CT) scan to delineate the skull, attenuation maps were computed from T1 and T2 MRI using a multi-atlas CT (pseudo-CT) synthesis method, which has been shown to improve reconstruction accuracy (Burgos *et al.*, 2014, 2015).

The T1 image was then rigidly registered to the PET and GIF parcellation was resampled to native PET-space. Mean uptake values in subcortical white matter (with an erosion of one PET voxel to avoid partial volume effects) were used to normalise cerebral uptake, producing standardised uptake value ratios (SUVRs). A global SUVR was then calculated using an average SUVR from a volume-weighted composite of several GIF-parcellated regions (lateral and medial frontal, anterior and posterior cingulate, lateral parietal, and lateral temporal), based on work published elsewhere (Landau *et al.*, 2013). Participants were dichotomised as being Aβ positive or negative by using a mixture model to define two Gaussians and then taking the 99th percentile of the lower Gaussian (0.6104) as the cut-point for positivity (Figure 2.6).

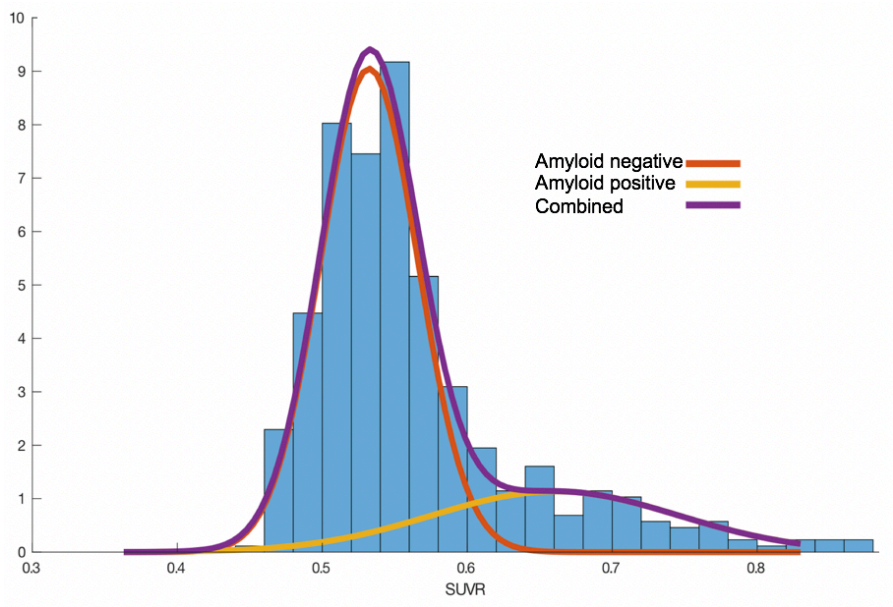

Figure 2.6. Histogram and mixture models of baseline global SUVRs generated with an eroded subcortical white matter reference region.

Figure produced by Dr David Cash, Dementia Research Centre, UCL

Processing PET data with or without partial volume correction (PVC) (iterative Yang method) made little difference to the results (Yang *et al.*, 1996; Erlandsson *et al.*, 2012). Specifically, PVC and non-PVC SUVR values were highly correlated (R^2=0.94), and rates of amyloid positivity were almost identical (18.2 versus 18.6%). Non-PVC SUVRs have therefore been used as standard in all Insight 46 analyses to date.

It was not possible to perform reconstruction using pseudo-CT attenuation correction maps for some participants (n=26) due to missing or corrupted list-mode PET data or unusable T1 or T2 MRI data. In these instances, a pseudo-CT SUVR was imputed based on SUVR values obtained using attenuation maps computed from ultra-short echo time (UTE) sequences from the console. Comparison of SUVRs (global and regional) in participants with both methods available showed a strong correlation (all R^2>0.97).

For use in sensitivity analyses, baseline global Aβ SUVRs and Aβ status were also generated using a whole cerebellum reference region (see section 2.5.3).

2.2.5. Longitudinal whole brain, ventricular and hippocampal volumes

For subjects with T1 MRI data that passed cross-sectional quality control at both time-points, longitudinal changes in whole brain, ventricular and hippocampal volume were measured using the boundary shift integral (BSI) (Freeborough and Fox, 1997).

Each segmented scan-pair underwent affine registration (12 degrees of freedom, i.e., translations, rotations, scaling and shearing in x, y, and z directions) to align the two images globally, followed by differential bias correction (DBC) to reduce intensity inhomogeneities between the two images, and calculation of whole brain atrophy using the k-means normalised BSI (Leung *et al.*, 2010b). Ventricular expansion was calculated using an affine whole-brain registration, followed by an additional rigid registration (6 degrees of freedom, i.e., translations and rotations in x, y, and z directions) using the ventricle regions, and calculation of BSI without DBC (Freeborough and Fox, 1997). Hippocampal atrophy was derived using an affine whole-brain registration, followed by an additional rigid registration focusing on the hippocampus and surrounding regions, with DBC and calculation of BSI using a double intensity window approach (Leung *et al.*, 2010a). Total hippocampal BSI was calculated as the sum of the left and right.

All scan pairs were reviewed to ensure longitudinal continuity. If concerns were raised regarding differences in quality between time-points, I re-reviewed the scan-pair, together with the imaging team, and a decision was made regarding whether it should be excluded. Examples of encountered problems were differences in motion or contrast,

or registration issues such as stretch caused by positional differences between time-points (Figure 2.7). When positional differences were detected, I worked closely with the radiographers to ensure that they were correctly positioning participants in the scanner.

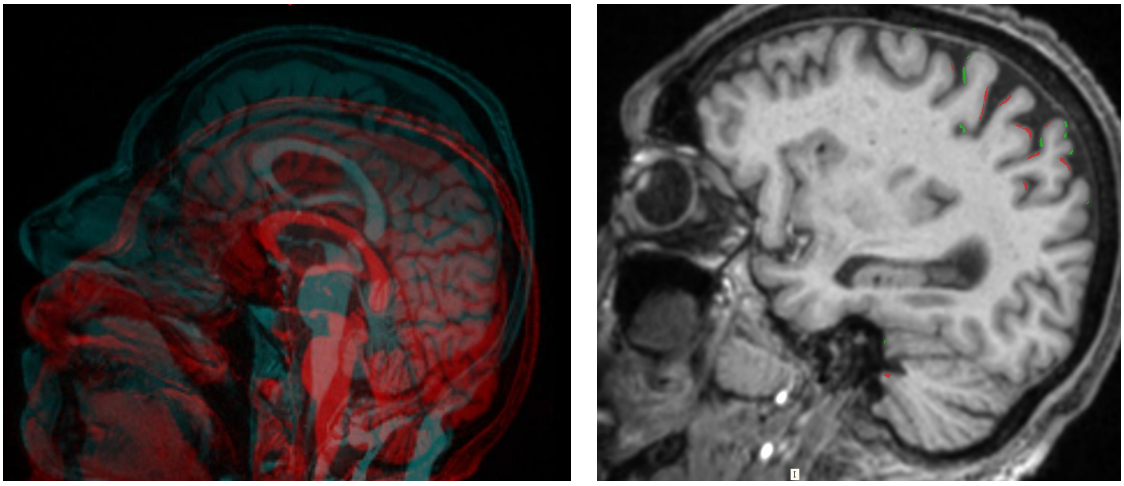

Figure 2.7. Left: baseline (red) and follow-up (blue) T1 images overlaid before registration illustrating positional difference in the scanner. Right: baseline image with BSI overlay after image registration; apparent volume loss (red) and gain (green) either side of gyri due to geometric distortion (stretch) caused by positional differences.

Range checks were also performed on the complete dataset to ensure that any outliers were consistent with accepted protocols. Together with the imaging team, I helped to re-review scan-pairs of the top 2%, bottom 2% and a random 1% of BSI data, as well as any scan-pairs that showed significant discrepancies in direct (BSI) and indirect (difference between MAPS-derived volume at each time-point) values (Figure 2.8).

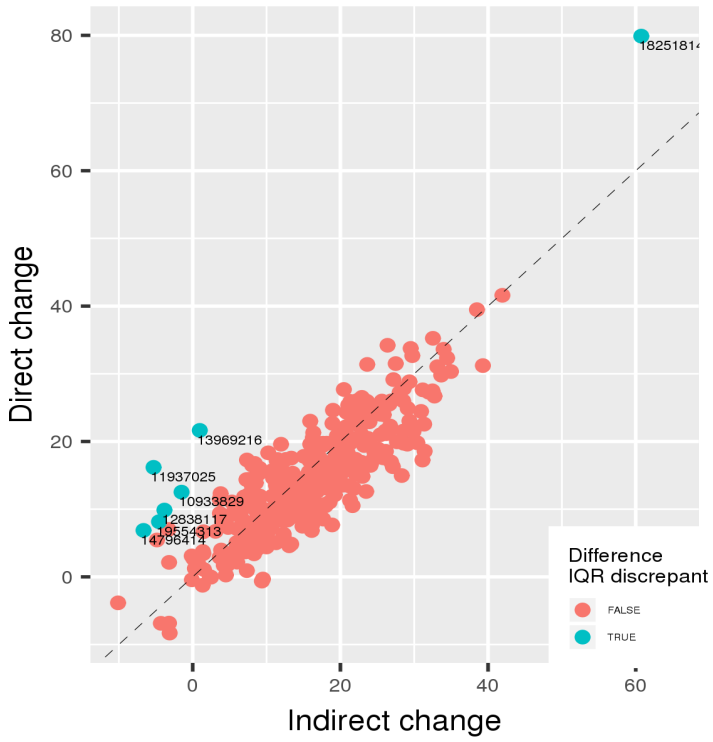

Figure 2.8. Plot of indirect (difference between MAPS-derived volume at each time-point) versus direct (BSI) values in millilitres

2.2.6. Longitudinal cortical thickness

For participants with T1 MRI data that passed cross-sectional and longitudinal quality control, I used Freesurfer version 7.1.0 (surfer.nmr.mgh.harvard.edu) to assess cortical thickness (Fischl and Dale, 2000). Grad-warp corrected images from both time-points first underwent cross-sectional processing, including motion correction, removal of the skull, spatial transforms, intensity normalisation, cortical surface reconstruction and parcellation (Dale, Fischl and Sereno, 1999; Fischl, Sereno and Dale, 1999; Fischl and Dale, 2000; Desikan *et al.*, 2006). Images were then run through the longitudinal stream in Freesurfer (Reuter *et al.*, 2012). Specifically, an unbiased within-subject template was created based on data from both time-points using robust inverse, consistent registration

(Reuter, Rosas and Fischl, 2010; Reuter and Fischl, 2011), and then several processing steps were initialised using common information from this template (Reuter *et al.*, 2012).

Two modifications – previously validated in-house using an older version of Freesurfer cross-sectional – were initially made to the standard pipeline including: (1) use of a locally generated brain mask; and (2) input of T2 in addition to T1 images. The resulting data, however, was biologically implausible, with a mean *increase* in cortical thickness of around 0.2-0.3% per year. To investigate this further, I re-analysed a small sample of participants (n=15) using the standard pipeline. Visual comparison of segmentations revealed that the modified version tended to underestimate the pial surface and was more prone to segmentation errors (Figure 2.9). Results with the standard version were also more credible – mean decrease in cortical thickness of around 0.3% per year – and were similar to previously reported findings around this age (Fjell *et al.*, 2014). I therefore decided that T1 MRI data should be re-processed using the standard Freesurfer pipeline.

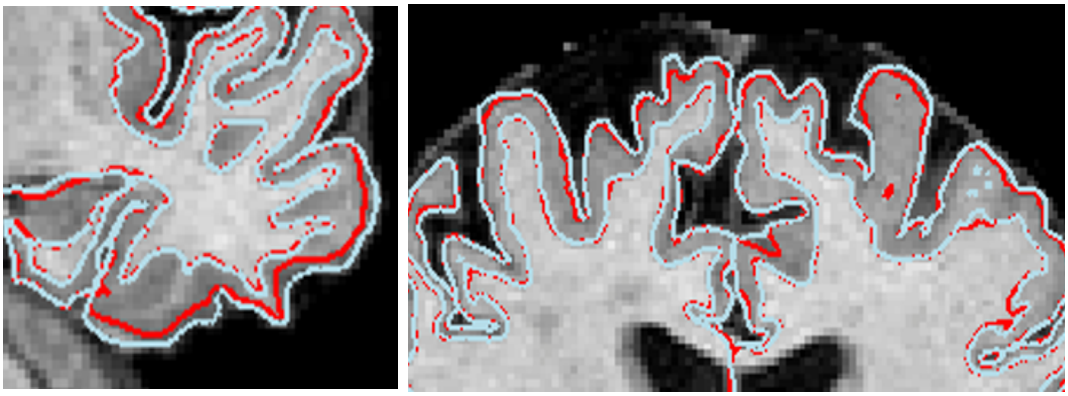

Figure 2.9. Example of modified Freesurfer pipeline (red) underestimating the pial surface compared to standard (blue) pipeline

After visually inspecting segmentations for major errors, I assessed cortical thickness in two composite regions of interest (ROIs) which have previously been shown to be

vulnerable in early AD (Figure 2.10): one comprised of middle temporal, inferior temporal, entorhinal and fusiform areas (ADsig Mayo) (Jack *et al.*, 2015); and one consisting of entorhinal, parahippocampal, inferior temporal, temporal pole, precuneus, supramarginal, superior and inferior parietal, superior frontal, parsopercularis, parstriangularis and parsorbitalis areas (ADsig Harvard) (Dickerson *et al.*, 2009).

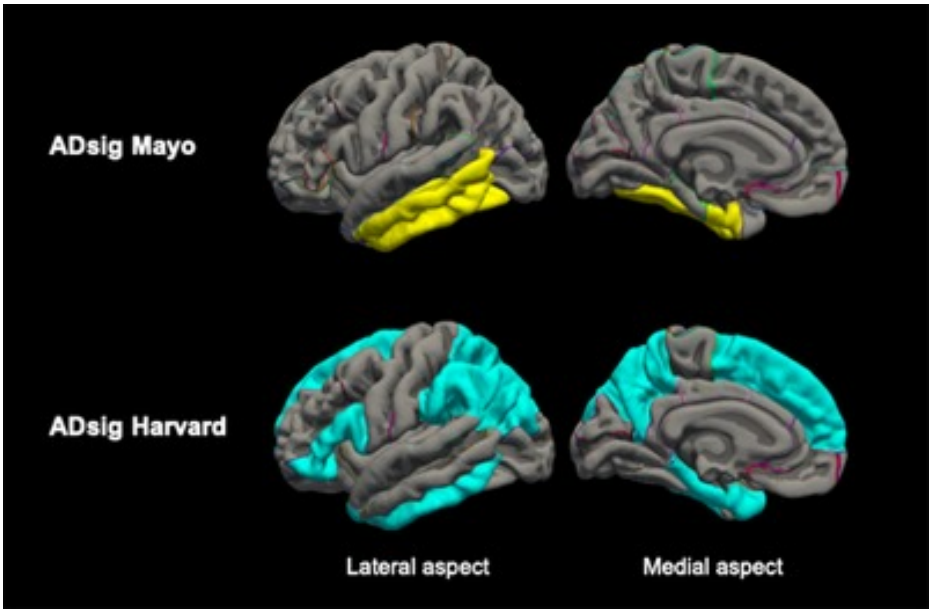

Figure 2.10. Two AD signature composite regions.

ADsig Mayo (entorhinal cortex, fusiform, inferior/middle temporal) and ADsig Harvard (entorhinal cortex, parahippocampus, inferior temporal, temporal pole, precuneus, supramarginal gyrus, superior/inferior parietal, superior/inferior frontal).

Regions were formed using the *mri_mergelabels* command to merge anatomical labels from the Desikan-Killian atlas (Desikan *et al.*, 2006), and the *mris_label2annot* command

to create a single annotation file. I then generated cortical thickness values using the *mris_anatomical_stats* command and extracted them using the *aparcstats2table* command. To calculate surface area weighted averages of left and right hemisphere cortical thickness values, I used the formula: (left surface area ∗ left thickness + right surface area ∗ right thickness) / left + right surface area (Whitwell *et al.*, 2013). I calculated change over time by subtracting time-point one from time-point two.

I also performed an unbiased vertex-wise analysis to test for group differences in rates of change in cortical thickness across the whole brain. Thickness data were first resampled onto an average subject (fsaverage) and smoothed at 15 mm full width half maximum (FWHM). There is no consensus on how much cortical thickness data should be smoothed, but a FWHM of 10-20 is typically used (Dickerson *et al.*, 2009; Fjell *et al.*, 2009; Benzinger *et al.*, 2013; Wirth, Madison, *et al.*, 2013; Weston *et al.*, 2016). I then ran a general linear model using the mri_glmfit command, and a cluster-wise correction for multiple comparisons by using the mri_glmfit-sim command to run a permutation simulation (1000 permutations; cluster-forming threshold $p<0.05$).

2.3. Classification of participant clinical status

Decisions regarding a participant's clinical status were made at an adjudication meeting involving study doctors, psychologists, and other team members.

Dementia was determined based on self-reported diagnosis, clinician assessment, informant history, and participant performance on cognitive testing. Mild cognitive impairment was defined as cognitive concern (from either participant or informant) **and** objective evidence of impairment on the delayed Logical Memory or Digit Symbol

Substitution tests (score > 1.5 standard deviations below the mean), but **no** clinical evidence of dementia (Petersen, 2011). Participant concern referred to self-reported difficulties more than people of the same age or enough that they wanted to seek medical help. Informant concern was defined as an AD8 score ≥ 2.

Participants were defined as having a major brain disorder based on self-report or radiological evidence of a neurological condition that could negatively impact cognition. These included but were not limited to: Alzheimer's disease; Parkinson's disease; radiological (cortical) or clinical stroke; epilepsy requiring active treatment; demyelination; psychiatric disorder requiring hospital admission, electroconvulsive therapy, or anti-psychotic medication; and traumatic brain injury or a history of major neurosurgery.

2.4. Determination of genetic, life-course and blood measures

2.4.1. *APOE* ε4 status

Genotyping was performed on DNA extracted from blood, as previously described (Rawle *et al.*, 2018). Two single nucleotide polymorphisms, rs439358 and rs7412, were used to distinguish between the three *APOE* alleles (ε2, ε3, ε4), and participants were categorised as being APOE ε4 carriers or non-carriers.

2.4.2. Vascular risk factors

Office-based Framingham Heart Study Cardiovascular Risk Scores (FHS-CVS) were derived at ages 36, 53 and 69 years, as previously described (Lane *et al.*, 2020). The

FHS-CVS, which provides a ten-year risk of cardiovascular events, is a weighted sum of age, sex, systolic blood pressure, use of anti-hypertensive medication (yes/no), diabetic status (yes/no), current smoking status (yes/no) and body mass index (D'Agostino *et al.*, 2008). Seated blood pressure was measured in the upper arm twice after 5 minutes rest at ages 36, 53 and 69 years. A Hawksley Random Zero sphygmomanometer was used at age 36 years and an Omron HEM-705 automated digital oscillometric sphygmomanometer was used at ages 53 and 69 years. Conversion equations were applied to ensure compatibility (Stang *et al.*, 2006), and the second blood pressure was used for analyses, unless missing, in which case the first reading was used. Participant use of anti-hypertensive medication was self-reported. Smoking status was determined by questionnaire. For smoking status at age 69 years, data from a postal questionnaire participants completed at age 68 years was used (or if missing, age 60-64 years). At age 36 years, the presence of diabetes was based on self-reported diagnosis, and at ages 53 and 69 years, it was based on either self-reported diagnosis or a haemoglobin A_{1C} level ≥ 6.5%. Body mass index at ages 36, 53 and 69 was calculated as weight in kilograms divided by height in metres squared.

2.4.3. Childhood cognition, education, and socioeconomic position

Childhood cognition at age 8 was assessed using tests of verbal and non-verbal ability from the National Foundation for Education Research. The total score from all tests was standardised into a z score representing global cognition. If data from this age was missing, the equivalent z score from age 11 was used (or from age 15 if age 11 data was missing). Standardised scores were based on the full NSHD cohort. Educational attainment was assessed at age 26 and categorised into three groups: no qualifications; O-level or equivalent or vocational qualifications; or A-level or higher education (e.g.,

degree) or equivalent. Socioeconomic position was derived from occupation at age 53, or earlier if missing, and grouped into manual or non-manual occupations.

2.5. Analytical approach

All analyses in this thesis were performed in Stata (using either version 16 or 17). The specific analyses conducted are described in the relevant data chapters, but the thinking behind certain aspects warrant further explanation here.

2.5.1. Analysis of longitudinal data

Since change between two time-points is a single numeric value, it can be analysed using linear regression. Normally, a multiple linear regression model relating an independent variable (y) to predictor variables (x_1,…, x_p) can be expressed as:

$$y_i = \alpha + \beta_1 x_{1i} + \beta_2 x_{2i} + \cdots + \beta_p x_{pi} + \varepsilon_i \quad (1)$$

where α = the constant; β = the regression co-efficient; and ε = the error term.

In a linear regression model for change in a measure between two time-points (y), all predictors (x_1,…, x_p) act through their effects on rate of change in the measure and so are included as a series of two-way interactions with the interval between time-points (t):

$$y_i = \left(\alpha + \beta_1 x_{1i} + \beta_2 x_{2i} + \cdots + \beta_p x_{pi}\right)t + \varepsilon_i \quad (2)$$

To fit an interaction in this model, a three-way interaction is included between the two predictors of interest and the interval between time-points. For example, the model including an interaction between predictors x_1 and x_2 is:

$$y_i = \left(\alpha + \beta_1 x_{1i} + \beta_2 x_{2i} + \beta_{(1*2)} x_{1i} x_{2i} \ldots + \beta_p x_{pi}\right) t + \varepsilon_i \quad (3)$$

In this thesis, the boundary shift integral provided a direct measure of volume change over time, whereas changes in cortical thickness and cognition were calculated indirectly (i.e., subtracting values at time-point one from values at time-point two).

For all models, I checked that the assumptions of linear regression were met by examining residual plots. If residuals were non-normally distributed, I performed bootstrapping (with 2,000 replications) to obtain bias-corrected and accelerated 95% confidence intervals.

2.5.2. Adjustment for age

Insight 46 participants are virtually identical in age, owing to their recruitment from a birth cohort, but there was a small difference in age at time of visit or scan (see Figure 2.11 for distribution) related to the length of time taken to complete assessments for the study. Due to the possibility of recruitment bias, in which healthier subjects may have been more likely to attend towards the start of the study, correcting for age in analyses could confound the results. While there was no evidence of recruitment bias in a previous study looking at self-reported health and disease burden in Insight 46 (James *et al.*, 2018), it is possible that untested differences may still exist. For this reason, I decided to perform analyses in this thesis both with and without adjustment for age at baseline.

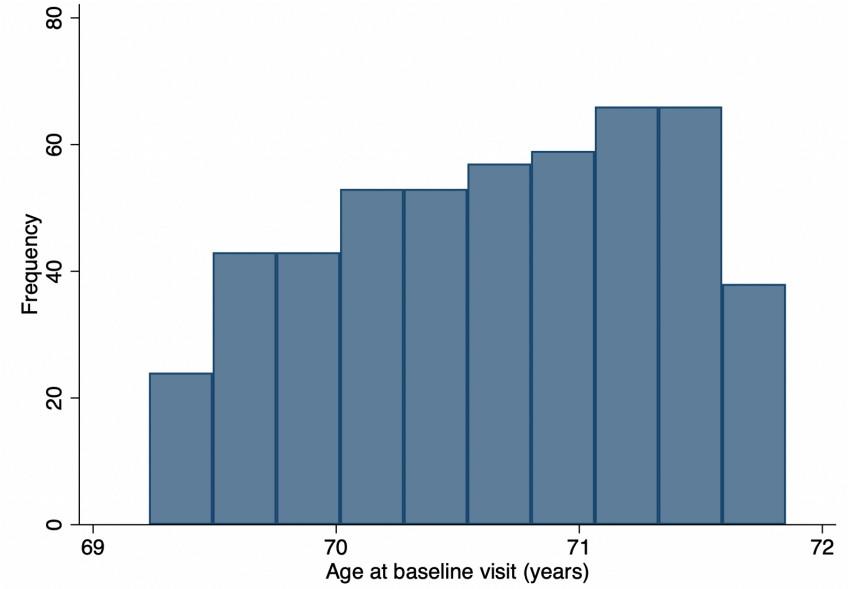

Figure 2.11. Histogram showing age distribution of Insight 46 participants

2.5.3. Choice of reference region for β-amyloid quantification

The cerebellum has often been chosen as a reference region for Aβ quantification, since it is generally spared from Aβ deposition until late in AD (Rowe and Villemagne, 2013). However, concerns have been raised regarding the accuracy of cerebellar normalisation, particularly for assessment of longitudinal change, with several studies suggesting that an eroded subcortical white matter reference region may be superior in this regard (Brendel *et al.*, 2015; Chen *et al.*, 2015; Landau *et al.*, 2015). The cerebellum is also affected by potential confounds. For example, with a PET/MRI system as was used in Insight 46, it can be more prone to attenuation correction artefacts due to its position near the bone, and it is also more susceptible to noise and small registration errors due to its proximity to the edge of the field of view and relatively small size. For these reasons, eroded subcortical white matter was chosen as the primary reference region in all Insight 46 analyses to date. Of particular relevance to the work in this thesis, however, emerging evidence suggests that Aβ PET tracer uptake may be influenced by the presence of

white matter hyperintensities (Glodzik *et al.*, 2015; Goodheart *et al.*, 2015; Lowe *et al.*, 2018; Zeydan *et al.*, 2019). Specifically, some studies have shown that Aβ tracer binding is reduced in areas of white matter hyperintensities. Since this has the potential to affect Aβ quantification using a white matter reference region and may confound the results of analyses in this thesis, I re-ran certain models using SUVRs with a whole cerebellum reference for comparison.

2.5.4. Correction for multiple comparisons

It is commonly stated that multiple comparisons in a study increase the likelihood of observing a statistical result by chance, also known as a type I error or false positive. The example quoted is that when performing 20 statistical tests with a significance level of 0.05, the chance of a type I error is 0.64. However, this is only the case if there are no true associations for any of the 20 tests performed, which is unlikely when researchers are conducting clearly defined hypothesis-driven analyses. A potentially greater concern is that methods of correcting for multiple comparisons increase the risk of type II errors, or false negatives, and some researchers have therefore argued that they should be avoided in exploratory biomedical studies (Perneger, 1998; Althouse, 2016). For most analyses in this thesis, I decided not to correct for multiple comparisons and the results should be evaluated in this context. An exception to this was the vertex-wise cortical thickness analysis in Chapter Six, in which statistical tests were performed at all vertices simultaneously without making any *a priori* anatomical hypotheses (i.e., in an exploratory fashion), thereby necessitating correction for multiple comparisons.

2.6. Statement of contributions

2.6.1. Study design

Insight 46 was conceived by Professors Jonathan Schott, Nick Fox, Marcus Richards, and Diana Kuh, and the protocol was developed with input from many people including Dr Christopher Lane, Dr Thomas Parker, Dr David Cash, Dr Kirsty Lu, Professor Sebastian Crutch, Elizabeth Donnachie, Heidi Murray-Smith, Andrew Wong, Dr Michelle Byford, Dr Ian Malone, Dr Jo Barnes, Dr Marc Modat, Dr Carole Sudre, Dr David Thomas, Dr Gary Zhang, Dr Anna Barnes, Dr John Dickson, Professor Sebastien Ourselin and Suzie Barker.

2.6.2. Data collection

As previously stated, I was primarily involved in data collection for the second phase of the study. My main responsibilities were recruitment of participants by telephone, conducting neurological and physical assessments, attending the scanner to assess the quality of structural MRI sequences, and managing incidental findings. In total, I completed 146 full-day participant assessments. The remaining participants were assessed by other doctors, including Drs Thomas Parker, Christopher Lane, Ashvini Keshavan, Sarah Buchanan, Aaron Wagen, Mathew Storey, Matthew Harris, and John Baker. The neuropsychology assessments were carried out by Dr Kirsty Lu, Dr Sarah-Naomi James, Dr Ivanna Pavisic, Jessica Collins, Hannah Carr, Elizabeth Donnachie, and Rebecca Street. Study visits were coordinated by Heidi Murray-Smith and Tamar Freiberger and scheduled by Molly Cooper. Life-course data including vascular risk

factors, childhood cognition, educational attainment, and adult socioeconomic position were collected by the NSHD team.

2.6.3. Data processing and variable derivation

Imaging data was processed at the Dementia Research Centre. Jana Kilmova, William Coath, Lloyd Prosser, Maggie Fraser, Dr Hugh Pemberton, Dr Emily Manning, Dr Elizabeth Gordon, and Laila Ahsan performed cross-sectional quality control of T1, T2 and FLAIR MRI sequences. Drs Ian Malone and Casper Nielsen oversaw the pipelines for whole brain, ventricular and hippocampal volume segmentation, and calculation of change in these measures between time-points using the boundary shift integral (BSI). William Coath, Lloyd Prosser, and Maggie Fraser carried out the initial longitudinal quality control of the BSI data. I helped to re-review scan-pairs flagged as having potentially unacceptable differences in quality between time-points or those identified as being outliers on range checks. I oversaw the processing of MRI data using Freesurfer, with input from William Coath who ran computationally demanding steps on UCL's cluster, and senior support from Dr David Cash. I visually inspected most of the cortical thickness segmentations (~300 scan pairs), with assistance from Dr Thomas Parker (~50 scan pairs). The BaMoS pipeline for white matter hyperintensity volume quantification was run by Dr Carole Sudre, and quality control and editing were performed by Dr Christopher Lane. Processing of Aβ PET data, SUVR quantification, and derivation of the cut-point for Aβ positivity was conducted by Dr David Cash. Structural MRI sequences were reviewed for incidental findings by Drs Chandrashekar Hoskote and Sachit Shah.

Dr Kirsty Lu cleaned the neuropsychology data and generated the PACC variable. APOE genotyping was coordinated by Andrew Wong and Heidi Murray-Smith and performed at LGC Hoddesdon. The FHS-CVS was derived by Dr Christopher Lane.

2.6.4. Data analysis

I conducted and planned most of the analyses in this thesis, with statistical support from Dr Jennifer Nicholas and Teresa Poole, and senior guidance from Professor Jonathan Schott, Professor Nick Fox, Dr David Cash and Dr Jo Barnes. An additional statement of contributions regarding the analyses performed is provided in each data chapter.

3. RECRUITMENT AND CHARACTERISATION OF STUDY PARTICIPANTS

3.1. Statement of contributions

I conceived and designed this study. Data collection and variable derivation were performed with assistance, as described in section 2.6. I performed the statistical analyses and interpretation of the results.

3.2. Introduction

As previously discussed, Insight 46 participants were all recruited from the NSHD, which was intended to be a representative sample of 5362 individuals born in mainland Britain during one week in 1946 (Kuh *et al.*, 2016). While participation rates have declined over time, with 2638 remaining in active follow-up at the latest clinic visit, the sample has remained broadly representative of British men and women born during the post-war period (Stafford *et al.*, 2013). Of note, NSHD members who attended the most recent clinic visit at age 60-64 had higher educational attainment than those who did not, but there were no significant differences in previously measured physical performance and health indicators, sex, or other socioeconomic factors (Kuh *et al.*, 2011).

A key challenge in Insight 46 was recruitment of a large sample of NSHD members who were able to tolerate an MRI brain scan and had no contraindications. While MRI is generally considered low burden, claustrophobia is a common issue, and may be more likely in people that are better educated and have a higher socioeconomic position (Sarji *et al.*, 1998). Those with health problems, such as arthritis, heart failure or lung disease, may be unable to lie flat in the scanner or, if they do manage to complete the scan, they

may find it challenging to stay still, leading to motion artefact and poor-quality data. There is also a higher chance of study drop out due to ill health or death in elderly populations (Brilleman, Pachana and Dobson, 2010). All these factors could lead to data that is not missing at random and difficulties maintaining a representative sample. In a previous analysis, Insight 46 participants were found to have slightly higher self-reported health, educational attainment and socioeconomic status than NSHD members who were not recruited, and those who were able to tolerate an MRI scan in phase one were less likely to be obese or to have mental health problems (James *et al.*, 2018).

In this chapter, I give an overview of recruitment to Insight 46, including reasons for missing scan data. I also provide a breakdown of participant cognitive status, followed by a summary of participant characteristics and variables that will be studied in later chapters. I then assess differences in characteristics and variables between cognitively normal participants with and without high quality longitudinal T1 MRI data in order to evaluate the representativeness of the sample used in most analyses in this thesis, before finally comparing characteristics and variables with respect to baseline Aβ status.

3.3. Methods

3.3.1. Determining variables

The presence of dementia, mild cognitive impairment (MCI) or major brain disorder(s) was defined as described in section 2.3, and participant characteristics and variables were derived as outlined in section 2.2 and 2.4.

3.3.2. Statistical analysis

Continuous variables were summarised as means and standard deviations (or medians and interquartile ranges if highly skewed) and categorical variables were summarised as percentages. Group differences were assessed using t-tests for continuous normally distributed variables, Wilcoxon rank-sum tests for continuous non-normally distributed variables, and χ^2 tests for categorical variables.

3.4. Results

The number of participants at each stage of the study, including reasons for non-completion of scan and missing data, are summarised as a flowchart in Figure 3.1.

502 participants (mean [SD] age at baseline visit 70.7 [0.7] years; 49% female) were recruited, of whom 471 (94%) completed a brain scan in phase one. By far, the most common reason for non-completion was claustrophobia (n=25). Of those that did complete a scan, three had T1 MRI data that were severely degraded by motion and failed quality control (QC). Therefore, 468 participants had high quality T1 MRI data.

All participants were invited back to phase two, irrespective of whether they had undergone a brain scan in phase one. There were 47 individuals no longer interested in taking part and 13 had passed away, meaning the attrition rate was 12%. Of the 442 participants that completed a phase two visit, 369 (83%) had a brain scan. Due to restrictions related to the coronavirus pandemic, 29 subjects were assessed remotely and therefore could not have a scan. Otherwise, claustrophobia remained the most

common reason for not having a scan (n=26). All 369 participants with a phase two scan had T1 MRI data that passed QC.

Overall, there were 365 participants with T1 MRI data that passed cross-sectional QC at both time-points. Nine of these had unacceptable differences in quality between scans (discussed in section 2.2.5) and failed longitudinal QC. Therefore, 356 (69%) participants had T1 MRI data from both time-points that passed both cross-sectional and longitudinal QC. They are hereafter referred to as having complete longitudinal T1 data.

Of the 502 participants seen at baseline, three had dementia, 11 had MCI, and 42 had a major brain disorder (Table 3.1). One participant had more than one major brain disorder, and seven participants with a major brain disorder also had dementia or MCI.

Table 3.1. Number of participants with a major brain disorder in full Insight 46 sample

Disorder	**N**
Radiological (cortical) or clinical stroke	18
Epilepsy requiring active treatment	7
Parkinson's disease	3
Demyelination	3
Alzheimer's disease	2
Bipolar disorder requiring anti-psychotic medication	2
Depression requiring electroconvulsive therapy	2
Traumatic brain injury	1
Brain metastasis	1
Dementia not otherwise specified	1
Myotonic dystrophy	1
Subdural haematoma requiring neurosurgical evacuation	1
Hepatic encephalopathy secondary to non-alcoholic steatohepatitis	1

NB. one participant had both Parkinson's disease and epilepsy

Of the 356 participants with complete longitudinal T1 data, two had dementia at baseline, four had MCI, and 30 had a major brain disorder. Of those with a major brain disorder, seven had a condition associated with progressive neurodegeneration or non-vascular white matter disease (Table 3.2), three of which also met criteria for dementia or MCI. Therefore, in total, 346 participants had complete longitudinal T1 data and were free of dementia, MCI, and confounding brain disorders at baseline. They are hereafter referred to as cognitively normal and represent the sample used in most analyses in this thesis.

Table 3.2. Number of participants with complete longitudinal T1 data with a disorder that causes progressive neurodegeneration or non-vascular white matter disease

Disorder	**N**
Alzheimer's disease	1
Parkinson's disease	2
Demyelination	2
Dementia not otherwise specified	1
Myotonic dystrophy	1

Table 3.3 summarises characteristics and key variables of the full Insight 46 sample, and of cognitively normal participants with and without complete longitudinal T1 data. Of note, cognitively normal participants without complete data were slightly older (mean age 71.0 versus 70.5 years; $p<0.001$), more overweight (mean body mass index 28.8 versus 27.3 kg/m^2; $p<0.001$) and had higher white matter hyperintensity volume (WMHV; median 3.9 versus 2.7ml; $p=0.03$) at baseline compared to cognitively normal participants with complete data. However, there were no significant differences with respect to most of the variables examined, including other demographic factors, APOE ε4 status, vascular risk profiles, baseline Aβ status, and other baseline structural MRI measures.

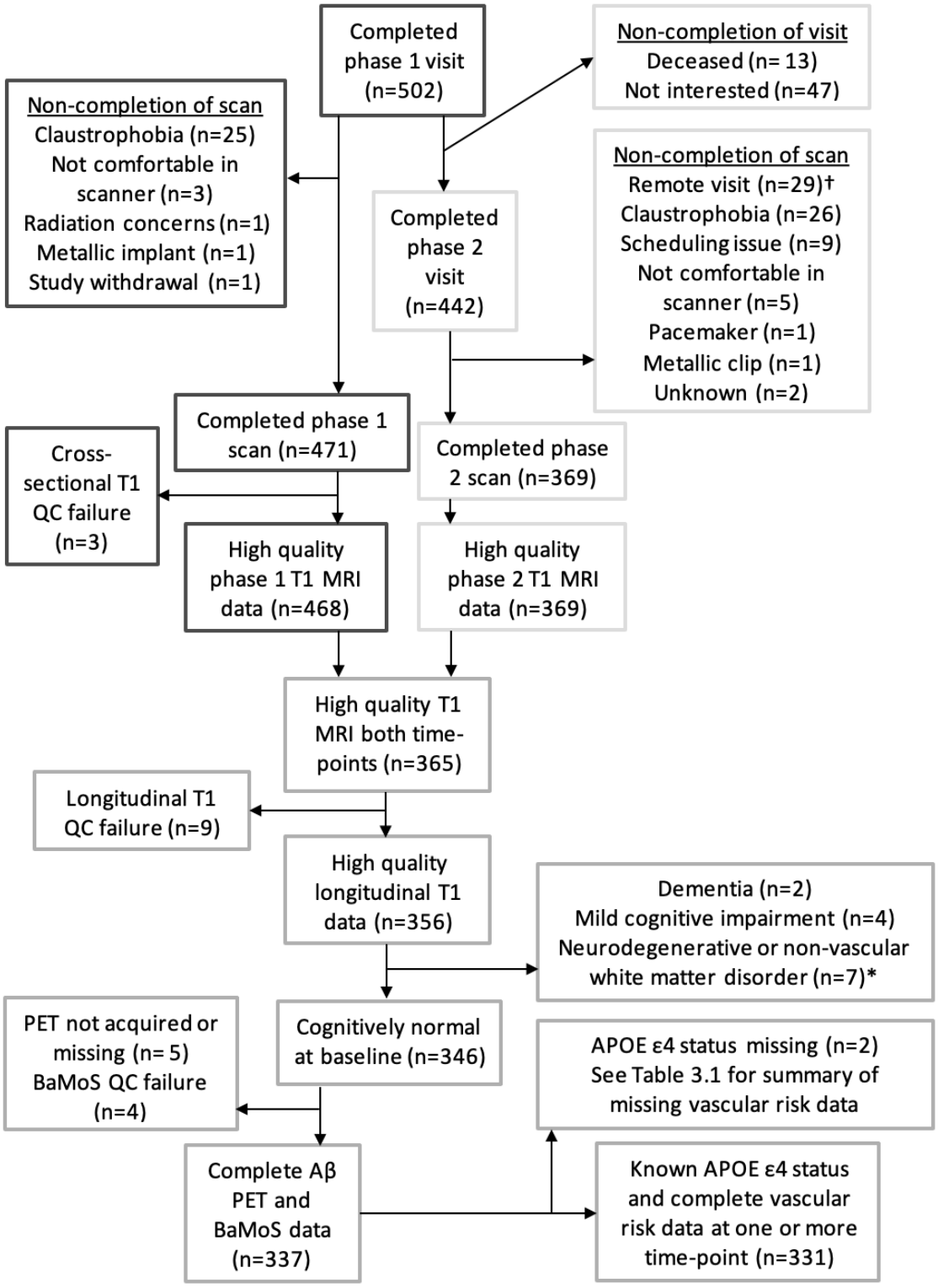

** NB. 2 participants with a neurodegenerative disorder had dementia, and 1 had mild cognitive impairment*
† some participants had remote visits by telephone or video only due to restrictions related to the coronavirus pandemic
Aβ= β-amyloid; PET = positron emission tomography; BaMoS = Bayesian Model Selection; QC = quality control

Figure 3.1. Flowchart of study recruitment and reasons for missing T1 MRI data.

Table 3.3. Characteristics across whole sample and of cognitively normal participants with and without complete longitudinal T1 MRI data

Characteristic		**All (n=502)**	**Cognitively normal participants with complete T1 data (n=346)**	**Cognitively normal participants with incomplete T1 data (n=137)**	**p-value**
Age at baseline visit, years, mean (SD)		70.7 (0.7)	70.5 (0.6)	71.0 (0.7)	<0.001 **
Sex, % female		49	48.3	50.4	0.68
MMSE at baseline, score out of 30, median (IQR)		30 (29-30)	30 (29-30)	30 (29-30)	0.66
PACC at baseline, mean z-score (SD)		-0.00 (0.73)	0.04 (0.66)	0.06 (0.68)	0.72
Childhood cognition, mean z-score (SD)		0.39 (0.74)	0.41 (0.72)	0.38 (0.78)	0.71
Education level	None	15.5	15.3	16.1	0.14
	O-level or equivalent or vocational	30.1	32.4	23.4	
	A-level or equivalent or higher	54.4	52.3	60.6	
Socioeconomic position at age 53, % manual		15.1	15.0	13.9	0.75
APOE ε4 carrier, %		29.6	29.9	29.9	0.99

		(n=500)[a]	(n=344)[a]		
Diabetes at baseline, % yes		11.3 (n=497)[a]	10.8 (n=344)[a]	12.7 (n=134)[a]	0.55
Smoking status at baseline, % ever smoker		65.9	65.3	67.9	0.59
Body mass index at baseline, kg/m^2		27.8 (4.5)	27.3 (4.1)	28.8 (5.1)	<0.001 **
FHS-CVS, %, median (IQR)	Age 36	2.7 (1.5-3.6) (n=455)[a]	2.7 (1.6-3.6) (n=312)[a]	2.6 (1.5-3.7) (n=125)[a]	0.95
	Age 53	10.9 (6.7-15.6) (n=487)[a]	10.9 (6.5-15.6) (n=337)[a]	11.1 (6.7-15.4) (n=131)[a]	0.69
	Age 69	24.2 (15.1-34.9) (n=488)[a]	23.5 (14.9-34.7) (n=341)[a]	25.2 (15.2-35.8) (n=128)[a]	0.39
Systolic blood pressure, mmHg, mean (SD)	Age 36	120.2 (13.7) (n=460)[a]	120.0 (14.1) (n=313)[a]	120.0 (12.3) (n=129)[a]	0.97
	Age 53	133.5 (19.0) (n=488)[a]	133.6 (19.0) (n=338)[a]	132.7 (19.3) (n=131)[a]	0.66
	Age 69	132.3 (16.0) (n=495)[a]	132.5 (15.9) (n=344)[a]	132.0 (16.7) (n=132)[a]	0.78
Global Aβ SUVR at baseline, median (IQR)		0.55 (0.52-0.58) (n=462)[a]	0.54 (0.51-0.58) (n=341)[a]	0.55 (0.52-0.58) (n=103)[a]	0.16

Aβ status at baseline, % positive	18.6 (n=462)[a]	16.7 (n=341)[a]	21.4 (n=103)[a]	0.28
Global WMHV at baseline, ml, median (IQR)	3.1 (1.6-6.8) (n=455)[a]	2.7 (1.5-6.1) (n=342)[a]	3.9 (1.9-7.0) (n=99)[a]	0.03 *
Total intracranial volume, ml, mean (SD)	1433 (133) (n=468)[a]	1434 (131)	1435 (131) (n=104)	0.95
Whole brain volume at baseline, ml, mean (SD)	1100 (99) (n=468)[a]	1104 (97)	1095 (98) (n=104)[a]	0.34
Ventricular volume at baseline, ml, median (IQR)	27.2 (20.0-38.4) (n=468)[a]	27.0 (19.6-37.2)	27.4 (21.1-40.4) (n=104)[a]	0.33
Total hippocampal volume at baseline, ml, mean (SD)	6.27 (0.67) (n=468)[a]	6.30 (0.64)	6.23 (0.71) (n=104)[a]	0.36
ADsig Harvard cortical thickness at baseline, mm, mean (SD)	2.46 (0.08) (n=468)[a]	2.47 (0.07)	2.46 (0.08) (n=104)[a]	0.95
ADsig Mayo cortical thickness at baseline, mm, mean (SD)	2.66 (0.08) (n=468)[a]	2.66 (0.08)	2.66 (0.08) (n=104)[a]	0.86

Aβ = β-amyloid; APOE = apolipoprotein; FHS-CVS = Framingham Heart Study Cardiovascular Risk Score; MMSE = mini-mental state examination; PACC = preclinical Alzheimer's cognitive composite; SUVR = standardised uptake value ratio; WMHV = white matter hyperintensity volume. Differences between cognitively normal subjects with and without complete longitudinal T1 data were assessed using t-tests for continuous normally distributed variables, Wilcoxon rank-sum tests for continuous non-normally distributed variables, and χ^2 tests for categorical variables. [a] number of participants with available data if below maximum possible *$^*p \leq 0.05$; $^{**}p \leq 0.001$*

Table 3.4 summarises characteristics and key variables of cognitively normal participants with complete longitudinal T1 data by baseline Aβ status. Aβ positive (versus negative) participants had a significantly higher percentage of APOE ε4 carriers (59.6% versus 22.7%; p<0.001) and a marginally lower mean body mass index (26.2 versus 27.5 kg/m^2; p=0.03) but they did not differ significant with respect to any other variables examined.

Table 3.4. Characteristics of cognitively normal participants with complete longitudinal T1 MRI data by baseline Aβ status

Characteristic		**Aβ positive (n=57)**	**Aβ negative (n=284)**	**p-value**
Age at baseline visit, years, mean (SD)		70.5 (0.6)	70.5 (0.7)	0.56
Sex, % female		49.3	43.9	0.45
MMSE at baseline, score out of 30, median (IQR)		29 (29-30)	30 (29-30)	0.09
PACC at baseline, mean z-score (SD)		-0.03 (0.69)	0.07 (0.66)	0.28
Childhood cognition, mean z-score (SD)		0.36 (0.71)	0.42 (0.73)	0.54
Education level, %	None	17.5	14.8	0.24
	O-level or equivalent or vocational	40.4	31.1	
	A-level or equivalent or higher	42.1	54.2	
Socioeconomic position at age 53, % manual		14.8	15.8	0.85
APOE ε4 carrier, %		59.6	22.7	<0.001**
Diabetes at baseline, % yes		14.0	10.2 (n=282)[a]	0.41
Smoking status at baseline, % ever smoker		66.7	65.1	0.83

Body mass index at baseline, kg/m^2		26.2 (3.7)	27.5 (4.2)	0.03*
FHS-CVS, %, median (IQR)	Age 36	2.7 (1.6-3.6) (n=51)[a]	2.7 (1.6-3.6) (n=256)[a]	0.77
	Age 53	11.1 (6.9-15.7) (n=56)[a]	10.7 (6.2-15.6) (n=276)[a]	0.92
	Age 69	25.4 (18.0-32.4)	23.3 (14.5-34.8) (n=279)[a]	0.72
Systolic blood pressure, mmHg, mean (SD)	Age 36	120.0 (14.9) (n=51)[a]	120.0 (14.1) (n=257)[a]	0.99
	Age 53	132.4 (17.4) (n=56)[a]	133.8 (19.4) (n=277)[a]	0.61
	Age 69	135.4 (16.7)	131.9 (15.7) (n=281)[a]	0.13
Global WMHV at baseline, ml, median (IQR)		3.3 (1.7-6.2) (n=56)[a]	2.6 (1.5-6.1) (n=281)[a]	0.51
Total intracranial volume, ml, mean (SD)		1451 (114)	1428 (133)	0.23
Whole brain volume at baseline, ml, mean (SD)		1122 (95)	1099 (96)	0.10
Ventricular volume at baseline, ml, median (IQR)		28.6 (22.3-39.7)	26.6 (19.5-36.6)	0.23
Total hippocampal volume at baseline, ml, mean (SD)		6.23 (0.50)	6.31 (0.67)	0.44
ADsig Harvard cortical thickness at baseline, mm, mean (SD)		2.46 (0.08)	2.47 (0.7)	0.88
ADsig Mayo cortical thickness at baseline, mm, mean (SD)		2.66 (0.08)	2.66 (0.08)	0.99

*Aβ = β-amyloid; APOE = apolipoprotein; FHS-CVS = Framingham Heart Study Cardiovascular Risk Score; MMSE = mini-mental state examination; PACC = preclinical Alzheimer's cognitive composite; WMHV = white matter hyperintensity volume. Differences between Aβ positive and negative participants were assessed using t-tests for continuous normally distributed variables, Wilcoxon rank-sum tests for continuous non-normally distributed variables, and χ^2 tests for categorical variables. [a] number of participants with available data if below maximum possible *p ≤0.05; **p ≤0.001*

3.5. Discussion

In summary, most participants recruited to Insight 46 were cognitively normal at baseline, two thirds had high quality T1 MRI data from both time-points, and cognitively normal participants without complete longitudinal T1 data were slightly older, more overweight, and had higher WMHV at baseline than those with complete data.

As expected at their age, most participants were cognitively normal, with a median mini mental state examination (MMSE) score of 30/30. Dementia prevalence was 0.6%, which is somewhat lower than the general population, where it is estimated that around 3% of adults age 70-74 years old are living with dementia (Prince, Knapp, *et al.*, 2014). Rates of stroke were also low at around 3.6%, with previous studies reporting that around 15-20% of the population will have experienced a stroke by the age of 75 years old (Seshadri *et al.*, 2006). This is perhaps not unexpected, given that participation involved travelling to London from across mainland Britain (Figure 3.2) for in-depth clinical assessment, often with at least one overnight stay, meaning individuals with cognitive impairment or comorbidities may have been less able or willing to take part. Importantly, however, the proportion of APOE ε4 carriers was consistent with population estimates, as was the frequency of Aβ positivity at this age (Jansen *et al.*, 2015).

Overall, the attrition rate between phase one and two was 12%. Reported rates of attrition vary in the literature but are higher with increasing age and cognitive impairment (Chatfield, Brayne and Matthews, 2005). The rate in Insight 46 is less than that observed in the 1936 Lothian birth cohort, which had 20% attrition between phase one (mean [SD] age 69.5 [0.8] years) and phase two (mean [SD] age 72.5 [0.7] years) (Taylor, Pattie and Deary, 2018). This possibly reflects that individuals were recruited to Insight 46 based

on their previous participation in NSHD study visits, and prior study engagement has been shown to influence future participation (Kuh *et al.*, 2016). The NSHD has also been running continuously since its onset and has purposefully kept in regular contact with its study members, including annual birthday cards with study updates.

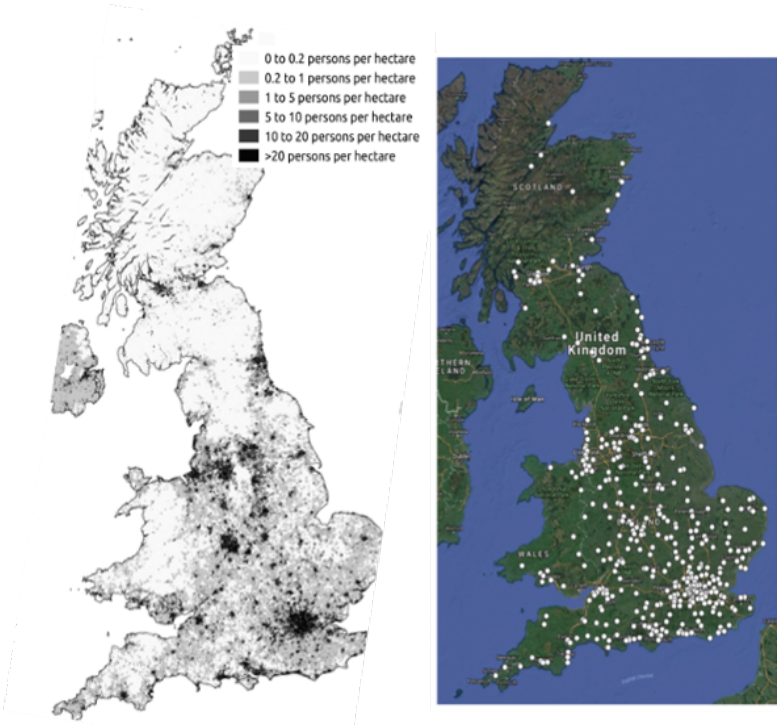

Figure 3.2. Maps showing population density of mainland Britain (left) and where Insight 46 participants were recruited from (right)

Figure produced by Dr Thomas Parker, Dementia Research Centre, UCL

The proportion of participants that completed brain imaging was 94% in phase one and 83% in phase two. The lower completion rate in phase two was mostly related to not being able to see participants in-person due to the coronavirus pandemic. Otherwise, the most common reason for not having a brain scan was claustrophobia, which affected around 5% of participants. A review of previous studies found that 1-15% of individuals (mean, 2.3%; 95% CI 2.0-2.5%) suffer from claustrophobia during MRI and either cannot be imaged or need sedation to complete the scan (Dewey, Schink and Dewey, 2007).

Despite the narrow age range of the Insight 46 sample, there was a significant difference in age at baseline between cognitively normal participants with and without complete longitudinal T1 data, such that those with incomplete data were slightly older. Since age at time of visit was determined by the order participants were seen, this may be partly related to less scans being performed towards the end of phase two due to restrictions related to the coronavirus pandemic. Another possible explanation is that participants seen at the start of the study may have been healthier and potentially more likely to tolerate an MRI. Consistent with this possibility, participants with incomplete longitudinal T1 data had marginally higher body mass index and WMHV at baseline, suggesting that their health may be somewhat poorer. Importantly, however, there were no significant differences between cognitively normal participants with and without complete longitudinal T1 data with respect to most of the measures assessed in the current analysis, including other demographic factors, vascular risk profiles, APOE ε4 status, baseline Aβ burden, and baseline structural MRI measures.

As expected, Aβ positive participants had a higher proportion of APOE ε4 carriers than Aβ negative participants, which is consistent with the important role that APOE is known to play in Aβ metabolism and the association between the ε4 variant and higher Aβ deposition (Liu *et al.*, 2013). On average, they also had a lower body mass index at baseline, as has been reported in previous Insight 46 analyses (Lane *et al.*, 2021), perhaps reflecting that weight loss can precede the onset of AD dementia by a number of years (Buchman *et al.*, 2005; Knopman *et al.*, 2007). Of note, there was no significant difference in baseline WMHV by Aβ status, and no significant Aβ-related differences in any of the other characteristics and variables examined.

3.6. Conclusion

This chapter highlights the feasibility of recruiting a large elderly cohort to a longitudinal MRI study. While Insight 46 participants, particularly those with complete data, may be somewhat healthier than the general population, rates of Aβ positivity and APOE ε4 carriers were consistent with population estimates, which suggests that the study is well placed to investigate the changes that might occur in the preclinical phase of AD.

4. DETECTION AND MANAGEMENT OF INCIDENTAL FINDINGS

4.1. Publication statement

I presented this work as an oral presentation at the virtual American Academy of Neurology (AAN) conference in 2020: Keuss SE, Parker TD, Lane CA, et al., Incidental Findings on Brain Magnetic Resonance Imaging. Neurology 2020;94(15). It has also undergone peer review and been published: Keuss SE, Parker TD, Lane CA, et al. Incidental findings on brain imaging and blood tests: results from the first phase of Insight 46, a prospective observational sub-study of the 1946 British birth cohort. BMJ Open 2019;9:e029502. doi: 10.1136/bmjopen-2019-029502. It has been adapted for inclusion in this thesis, under the terms of the Creative Commons Attribution License (CC BY).

4.2. Statement of contributions

I conceived and designed this study, with advice from Professor Jonathan Schott. Data collection and variable derivation were performed with assistance, as described in section 2.6. I conducted the statistical analyses and interpretation of the results.

4.3. Introduction

A major consideration for MRI studies is the management of incidental findings. While the primary aim of most research is to generate data and advance knowledge, rather than to diagnose health problems in participants, there are important ethical reasons for disclosing certain findings, particularly when they relate to serious and potentially treatable conditions (Wolf *et al.*, 2008). Since the management of incidental findings is

often uncertain, and they have the potential to cause anxiety or lead to further unnecessary or invasive procedures (Schmidt *et al.*, 2013; de Boer *et al.*, 2018; Gibson *et al.*, 2018a), it is essential that researchers weigh up the potential benefits and harms of being informed.

Knowledge of the expected prevalence of incidental findings, based on clearly defined protocols for their determination, is useful since it allows researchers to be better prepared for managing them and participants to be informed of their likelihood as part of the consent process. Several studies have reported rates of incidental findings on brain MRI previously (Gibson *et al.*, 2018b; O'Sullivan *et al.*, 2018), but data from large country-wide birth cohorts is limited. In this chapter, I summarise the incidental findings detected on brain MRI during the first phase of Insight 46 and how they were managed.

4.4. Methods

4.4.1. Scan review process

Given the unique nature of the 1946 British birth cohort, and since participants were all scanned at a single centre with access to neuroradiologists, it was agreed that all MRI scans (T1, T2, FLAIR) would be reviewed for incidental findings. One of two radiologists reviewed each scan within four weeks of the study visit and flagged them as potentially reportable using a prespecified list of reportable and non-reportable abnormalities (Table 4.1). This list was adapted from the UK Biobank study, which classified findings as being reportable if they were life-threatening or likely to have a major impact on quality of life (Bertheau *et al.*, 2016; Gibson *et al.*, 2018a). Radiologists were also encouraged to flag other findings if there was any possibility that further assessment might be required.

The reporting process was performed electronically using the web-based data management tool XNAT (www.xnat.org) (Figure 4.1), thereby creating an audit trail. Reporting radiologists downloaded images from the XNAT server, reviewed them and then completed a radiological read report within XNAT. This took around ten minutes per scan. Radiologists received no clinical information regarding participants, other than knowing that they were all born in 1946. If a scan was flagged as being potentially reportable, a multi-disciplinary meeting between the radiologist, study chief investigator and relevant team members was organised. If the abnormality was agreed to meet criteria for being reportable, the team decided on a clinical action plan (e.g., further imaging or specialist referral). A study doctor then contacted the participant and their general practitioner (GP) to inform them of the finding and recommended clinical action.

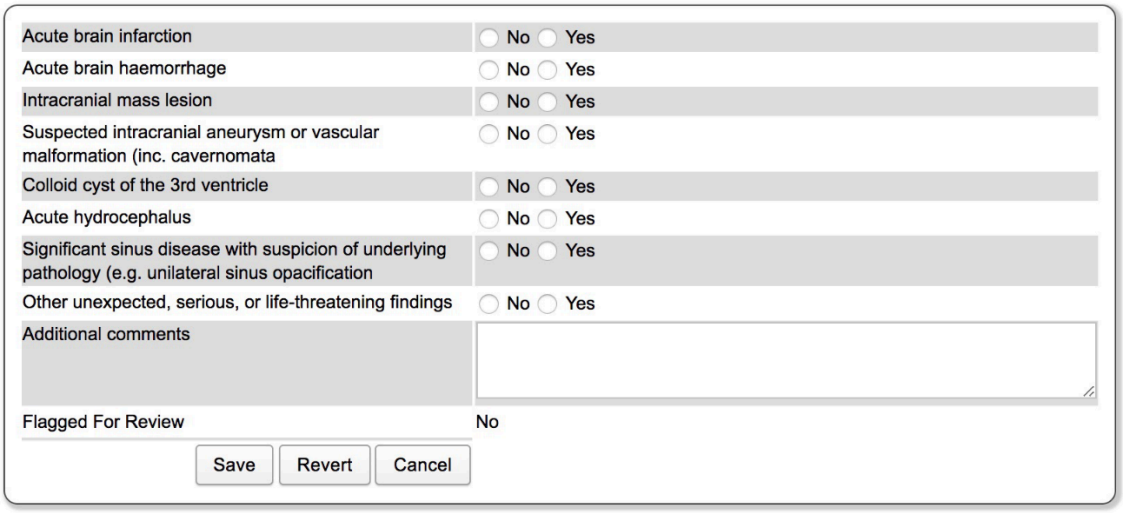

Figure 4.1. The radiological read report completed by radiologists in XNAT (www.xnat.org).

Table 4.1. List of reportable and non-reportable MRI abnormalities

Reportable findings	**Non-reportable findings**
▪ Acute brain infarction ▪ Acute brain haemorrhage (note: not old bleeds) ▪ Intracranial mass lesions (note: not meningiomas in locations unlikely to cause problems) ▪ Suspected intracranial aneurysm or vascular malformation (including cavernomata) (note: not aneurysms <7mm in diameter) ▪ Colloid cyst of the 3rd ventricle ▪ Acute hydrocephalus ▪ Significant sinus disease with suspicion of underlying pathology (e.g. unilateral sinus opacification)	▪ White matter hyperintensities ▪ Suspected demyelination ▪ Non-acute brain infarction ▪ Chronic hydrocephalus ▪ Asymmetric ventricles ▪ Lipoma of the corpus callosum ▪ Developmental abnormalities ▪ Enlarged perivascular spaces ▪ Chiari malformation ▪ Hippocampal or other focal atrophy

4.4.2. Statistical analysis

The number and types of incidental findings, and the actions taken by the study team in response to them, were summarised as counts and percentages, and 95% CIs for proportions were calculated using the exact Clopper-Pearson method. Sex differences were assessed using a two-sample test of proportions.

4.5. Results

7.6% of all scans (36/471) were flagged by neuroradiologists as having a potentially reportable abnormality for review. Following multi-disciplinary discussion, 58.3% (21/36) were deemed to have an abnormality that fulfilled criteria for being reportable. Therefore, in total, 4.5% of all scans had a finding that was fed back to the participant and their GP.

4.5.1. Number and type of incidental findings

The number and percentage of reportable abnormalities are summarised by type and sex in Table 4.2. The most common reportable findings were suspected vascular malformations and suspected intracranial mass lesions, which were detected in 1.9% (n=9) and 1.5% (n=7) of scanned participants respectively. Suspected intracerebral aneurysms were the most common vascular abnormality, affecting 1.1% of scanned participants (n=5; Figure 4.2A), and suspected meningiomas were the most common intracranial lesion, affecting 0.6% of scanned participants (n=3; Figure 4.2B). Women were more likely to have a reportable abnormality than men (6.5% vs 2.5%; p=0.034).

4.5.2. Subsequent action and follow-up

Further imaging was advised in 66.6% of cases (n=14); specialist referral was suggested in 57.1% of cases (n=12); advice regarding medication or management was given in 19% of cases (n=4); and no action was needed in 9.5% of cases (n=2) where the abnormalities were found to be pre-existing and already being managed by the participant's local health services. Data regarding subsequent follow-up is summarised in Table 4.3.

Table 4.2. Number and percentage of reportable abnormalities by type and sex

	All (N = 471)		**Male (N = 241)**		**Female (N = 230)**	
	n	% (95% CI)	n	% (95% CI)	n	% (95% CI)
Any abnormality	21	4.5 (2.8, 6.7)	6	2.5 (0.9, 5.3)	15	6.5 (3.7, 10.5)
Acute brain infarction	-	-	-	-	-	-
Acute brain haemorrhage	-	-	-	-	-	-
Suspected mass lesion	7	1.5 (0.6, 3.0)	2	0.8 (0.1, 3.0)	5	2.2 (0.7, 5.0)
Suspected intracranial aneurysm or vascular malformation	9	1.9 (0.9, 3.6)	2	0.8 (0.1, 3.0)	7	3.0 (1.2, 6.2)
Colloid cyst of the 3rd ventricle	-	-	-	-	-	-
Acute hydrocephalus	-	-	-	-	-	-
Significant sinus pathology	3	0.6 (0.1, 1.9)	1	0.4 (0.0, 2.3)	2	0.9 (0.1, 3.1)
Other*	2	0.4 (0.0, 1.5)	1	0.4 (0.0, 2.3)	1	0.4 (0.0, 2.4)

* possible keratocystic odontogenic right mandible tumour (n=1); hyperintense area suprasellar cistern (dermoid cyst, craniopharyngioma or thrombosed anterior communicating artery aneurysm) (n=1).

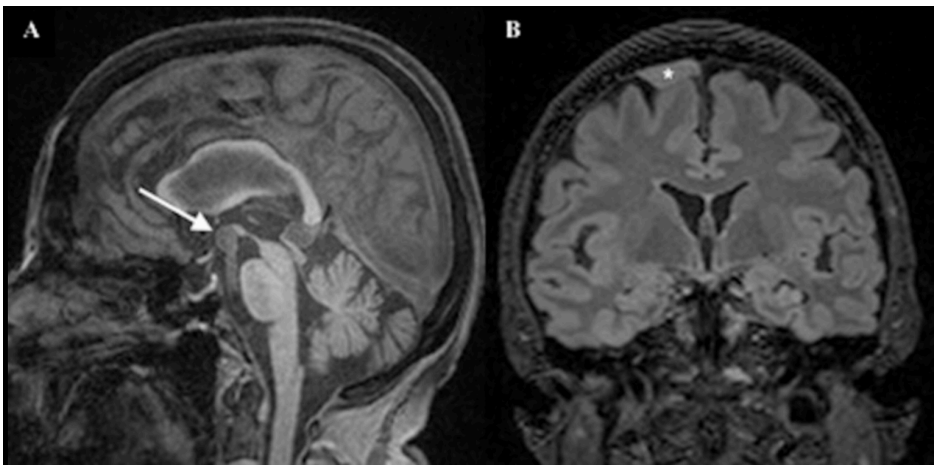

Figure 4.2. Examples of incidental findings detected on brain MRI in phase one (A) Sagittal T1 image showing a 10 mm aneurysm (arrow) arising from the tip of the basilar artery. (B) Coronal FLAIR image showing a broad-based extra-axial lesion (asterisk) overlying the right superior formal gyrus, consistent with a meningioma.

Table 4.3. A more detailed summary of the incidental findings detected during the first phase of data collection and how they were managed

Incidental Finding	**Outcome**	**Source**
Possible aneurysm right internal carotid artery	Known about previously and already being followed up locally.	Participant
Probable right middle cerebral artery bifurcation aneurysm	Seen by neurosurgery. Did not require further imaging or follow-up.	Participant
Possible right posterior communicating artery aneurysm	Seen by neurosurgery. Had angiogram which showed 8mm right internal carotid aneurysm. Subsequently underwent endovascular treatment.	Clinician letter
Left cerebellar cavernoma with previous perinidal haemorrhage	No immediate action. Will have follow-up imaging at phase 2 visit.	Study documents
Anterior communicating artery aneurysm	Seen by neurosurgery and underwent angiogram. Will have follow-up angiogram in 6 months to assess whether any interval change.	Participant
Possible cavernoma left mid cerebellar peduncle	Had contrast CT. Felt to be solitary cavernoma and deemed low risk.	Study documents
Multiple T2 hypointense lesions and possible pontine cavernoma	Given advice regarding blood pressure control and avoidance of blood-thinning medication.	Study documents
Basilar tip artery aneurysm, partially thrombosed	Seen by neurosurgery. Underwent exploratory endovascular surgery, but no intervention performed. Subsequently died of stroke (aetiology unknown) around 17 months post-visit.	Participant/family

Prominent right thalamostriate vein with smaller adjacent connecting vessels	Seen by neurology. Further imaging confirmed developmental venous anomaly right frontal area and cavernomata. Given advice regarding BP control and avoidance of blood-thinning medication.	Clinician letter
Asymmetric configuration of pituitary fossa with T2-hyperintense signal on the left, and mild deviation of pituitary stalk to the right	Seen by neurosurgery. Further imaging confirmed small pituitary adenoma, which is being followed up with interval imaging.	Clinician letter
Signal change and mild swelling within medial aspect of right post-central gyrus	Previous breast cancer. Lung lesion on recent chest xray. GP informed oncology re. brain scan abnormality, which in clinical context was felt likely to be a metastasis. Subsequently died.	GP/family
Small median mass at outlet of 4th ventricle without mass effect or hydrocephalus	Seen by neurology. Underwent contrast MRI brain and c-spine. Lesion thought to be subependyoma and being followed up locally.	Clinician letter
Small well circumscribed extra-axial lesion centred on the pontine cistern on the left	Known meningioma. Already under follow-up, so no action taken.	Participant
Right frontal parasagittal meningeal sessile mass	Seen by neurology. Contrast MRI confirmed meningioma and follow-up MRI at 1 year showed no interval change.	Clinician letter
Bulky pituitary gland with convex superior border	Seen by neurosurgery. Asymptomatic. Normal pituitary function tests. Baseline and repeat imaging at 1 year showed no interval change. No longer under follow-up.	Participant
Meningioma overlying left cerebellar hemisphere	Seen by neurology. Contrast MRI confirmed meningioma and follow-up MRI at 1 year showed no interval change.	Clinician letter

Right maxillary antrum almost completely filled by retained secretions.	Seen by ENT. As asymptomatic, not felt to require further tests.	Participant
Complete filling left maxillary sinus with expansion of the osteomeatal complex, raising possibility of an underlying obstructing lesion	Seen by ENT. Underwent nasoendoscopy which excluded underlying structural lesion. Advised nasal irrigation to decrease congestion. Discharged.	Participant
Complete opacification of the right maxillary sinus and adjacent nasal cavity	Seen by ENT. Had an MRI which did not show evidence of an obstructing lesion. Prescribed antibiotics for sinusitis. Discharged.	Participant
Well circumscribed T1-hyperintense lesion within mandible on right, suggestive of a keratocystic odontogenic tumour	Seen by maxillofacial surgery. Tumour excised.	Participant
T1-hyperintense lesion within suprasellar cistern, differential of which includes dermoid, craniopharyngioma or anterior communicating artery aneurysm	Seen by neurology. Further imaging suggested lipoma or small dermoid cyst. No further action recommended.	Clinician letter

CT= computed tomography; ENT = ear nose and throat specialist: BP = blood pressure; MRI = magnetic resonance imaging; GP = general practitioner

4.6. Discussion

In summary, potentially serious or treatable findings were detected on brain MRI in almost 5% of scanned participants during the first phase of Insight 46, with suspected vascular malformations and intracranial mass lesions present in 1.9% and 1.5% respectively.

Reported rates of incidental findings vary in the literature, likely reflecting differences in the definition of what constitutes an incidental finding, as well as variation in methods for detecting them and participant demographics (Gibson *et al.*, 2018b). Many imaging studies, for example, do not require routine review of all scans by a radiologist, and researchers will only ask for a radiologist opinion if an abnormality is detected incidentally by a radiographer during scanning or by researchers during data analysis (Illes *et al.*, 2004; Booth *et al.*, 2012). Such studies may have lower detection rates but are presumably less likely to publish data on incidental finding prevalence.

A recent systematic review reported an overall prevalence of 1.4% (95% CI 1.0% to 2.1%) for potentially serious brain incidental findings (Gibson *et al.*, 2018). This is somewhat lower than the 4.5% (95% CI 2.8% to 6.7%) detected in Insight 46, perhaps because this review consisted mainly of studies with younger participants using MRI scanners of 1.5 Tesla or less. Another review reported a much higher prevalence of 22% (95% CI 14% to 31%), likely due to their inclusion of all findings, regardless of their clinical seriousness (O'Sullivan *et al.*, 2018). Rates of specific abnormalities in Insight 46, including cerebral aneurysms and intracranial lesions, were similar to those observed in other population-based studies in participants of similar age (Sandeman *et al.*, 2013; Bos *et al.*, 2016).

Previous studies have not shown consistent sex differences in rates of potentially serious brain MRI findings (Gibson *et al.*, 2018). In Insight 46, however, higher rates were observed in females versus males. This was driven by greater vascular abnormalities and intracranial mass lesions in women, possibly reflecting that cerebral aneurysms and meningiomas are more common in women than in men (Bos *et al.*, 2016).

Major strengths of this study include that a large number of participants underwent MRI at an almost identical age and received feedback regarding incidental findings according to a prespecified standardised protocol. MRI sequences were obtained on the same 3 Tesla scanner and all images were reviewed by experienced neuroradiologists. Reflecting on the process for reviewing scans, the user-friendly and automated system allowed neuroradiologists to report scans within a short timeframe, thereby reducing their workload. Scans were sometimes flagged for review, despite not having a reportable finding as defined by the study protocol, usually because the radiologist felt that the abnormality was serious enough to warrant further discussion. This was encouraged to avoid overlooking findings that might be considered actionable in the appropriate clinical context. In practice, however, it did not alter the number of findings reported.

A key limitation of this study is that participant perception regarding the disclosure of incidental findings was not formally assessed, nor was the impact on their longer-term health and psychological well-being. Many participants, however, gave informal feedback on post-visit evaluation forms that they appreciated being told about findings pertinent to their health and saw this as a benefit of being involved in the study. These observations are consistent with the results of a study commissioned by the Wellcome Trust and MRC, which found overwhelming public support for the disclosure of incidental findings in research, particularly in relation to serious and treatable conditions (Medical

Research Council, 2014), and the work of several other studies (Hegenscheid *et al.*, 2013; de Boer *et al.*, 2018; Gibson *et al.*, 2018a; Hegedüs *et al.*, 2019).

While it can be argued that research is generally not meant to benefit participants directly, clearly many participants view medical input as an incentive to take part and there is an expectation from participants that they will be informed of any serious findings. This should be balanced against the potential negative consequences, however, and further work is needed to assess the implications of disclosing incidental findings in research studies, including the psychological effects and long-term clinical consequences. The impact on research integrity should also be considered, particularly in cohort studies where disclosure might lead to a biased sample. Due to the longitudinal nature of Insight 46, it should be possible to collect these outcomes in a more systematic way after a longer interval. This will be helpful to inform debates on the ethics of feeding back incidental findings, adding to the work of several other ongoing studies (Hegenscheid *et al.*, 2013; Schmidt *et al.*, 2013; de Boer *et al.*, 2018; Gibson *et al.*, 2018a; Hegedüs *et al.*, 2019).

4.7. Conclusion

Potentially serious or treatable findings were detected on brain MRI in almost 5% of scanned participants. Awareness of the expected prevalence of incidental findings in this age group, based on predefined protocols for their determination, should allow researchers to be better prepared for managing them and participants to be appropriately informed of their likelihood as part of the consent process. It also has implications for clinical practice, where patients are rarely consented for the risk of discovering an incidental finding, despite the potential negative consequences. Greater awareness

should allow clinicians to counsel patients regarding their probability, and to balance this risk against the potential benefits of undergoing a test when deciding whether it is appropriate.

5. LONGITUDINAL BRAIN VOLUME CHANGES

5.1. Publication statement

I presented this work as a poster at the Alzheimer's Association International Conference in 2020: Keuss SE, Poole T, Cash DM, et al., Cerebral amyloid and white matter hyperintensity volume are independently associated with rates of cerebral atrophy in Insight 46, a sub-study of the 1946 British birth cohort. Alzheimer's and dementia 2020;16(S4). doi.org/10.1002/alz.044924. It has also undergone peer review and been published: Keuss SE, Coath W, Nicholas JM, et al., Associations of β-amyloid and vascular burden with rates of neurodegeneration in cognitively normal members of the 1946 British birth cohort. Neurology 2022;99(2):e129-e141 doi: https://doi.org/10.1212/WNL.0000000000200524. It has been adapted for inclusion in this thesis, under the terms of the Creative Commons Attribution License (CC BY).

5.2. Statement of contributions

I conceived and designed this study, with advice from Professor Jonathan Schott, Professor Nick Fox, and Dr Jo Barnes. Data collection and variable derivation were performed with assistance, as described in section 2.6. Dr Jennifer Nicholas calculated the squared semi-partial correlations. I conducted the remaining analyses and interpreted the results, with statistical support from Dr Nicholas and Teresa Poole.

5.3. Introduction

As discussed in the first chapter, MRI-derived global and regional brain volume measures have transformed the study of AD-related neurodegeneration in life, and are increasingly used as biomarkers for disease staging and monitoring, and assessment of treatment efficacy in trials (Cash *et al.*, 2014). Understanding the factors that influence their progression is therefore important, particularly in cognitively normal older adults who are a key target population for strategies aimed at preventing or delaying dementia.

Studies examining their relationship with Aβ deposition in cognitively normal older adults have produced mixed results, with some reporting lower brain volumes or faster rates of atrophy, while others have observed no association or larger brain volumes (see section 1.3.6.1). A significant challenge faced by these studies – which Insight 46 is uniquely placed to address – is the heterogeneity that exists between individuals, either reflecting premorbid differences in brain volume – a major issue in cross-sectional studies – or the effects of age and other brain pathologies that often co-exist in later life.

White matter hyperintensities (WMHs) – a marked of presumed cerebrovascular disease (CVD) – are particularly common, detectable on MRI in greater than 90% of adults over the age of 60 years (De Leeuw *et al.*, 2001). As well as being associated with faster rates of global and hippocampal atrophy (Barnes, Carmichael, *et al.*, 2013; Fiford *et al.*, 2017), increased WMH volume has been observed in individuals at risk of AD and predicts AD dementia, raising the possibility that CVD may be involved in AD pathogenesis (Brickman, 2013). There is therefore considerable interest in understanding the relationship between Aβ and WMHs in cognitively normal elderly, and the extent to which they act separately or together to influence downstream neurodegeneration.

In this chapter, I first describe the longitudinal changes in whole brain, ventricular and total hippocampal volume that were quantified from serial MRI in cognitively normal Insight 46 participants. I then assess whether baseline Aβ deposition and WMHV were related to these changes and, if so, whether their effects were independent or interactive. Finally, I examine the contribution of upstream risk factors, including APOE ε4 carrier status and vascular risk measured at different stages of adulthood.

5.4. Methods

5.4.1. Determining variables

Baseline Aβ status, global Aβ SUVR, WMHV and total intracranial volume (TIV), and longitudinal whole brain, ventricular and total hippocampal volume changes, were quantified as described in section 2.2. Framingham Heart Study Cardiovascular Risk Scores (FHS-CVS) and systolic blood pressure (BP) at ages 36, 53 and 69 were derived as outlined in section 2.4, as was APOE ε4 status, socioeconomic position, presence of diabetes, smoking status, and body mass index around time of baseline scan.

5.4.2. Statistical analysis

Participants were excluded from analyses if they had incomplete longitudinal T1 data or baseline dementia, mild cognitive impairment, or confounding brain disorders, as outlined in Chapter Three. For analyses involving Aβ or WMHV, participants needed Aβ PET or WMHV segmentation data that passed quality control; for APOE ε4 analyses, genotype data also had to be available; and for vascular risk analyses, participants were

required to have FHS-CVS or systolic BP data and complete covariate data at one or more time-point.

Group differences between variables were assessed using t-tests for continuous normally distributed variables, Wilcoxon rank-sum tests for continuous non-normally distributed variables, and χ^2 tests for categorical variables. Spearman's rank correlation was used to test bivariate associations involving continuous non-normally distributed variables.

Linear regression was used to test associations between predictors of interest and rates of change in whole brain, ventricular and total hippocampal volume. Each model included the BSI measure in millilitres as the outcome, scan interval in years as the explanatory variable, and interactions between scan interval and (i) each predictor variable of interest and (ii) each covariate. Interactions between two variables were tested by including a term for the three-way interaction between each predictor and scan interval. No constant term was included since the model estimates mean change over time.

Effects of baseline Aβ and WMHV on each volume change measure were examined in separate models and then together as predictors in a single model, with adjustment for sex, age at baseline scan and TIV. Baseline Aβ was considered in separate models as a binary Aβ status (positive/negative) and using the continuous global Aβ SUVR measure. Semi-partial r^2 values were calculated to assess the relative contribution of Aβ and WMHV, above the explanatory contribution of all other variables in the model. Further models examined whether there was an interaction between Aβ and WMHV and whether there was an interaction between sex and each of Aβ and WMHV.

Separate models were fitted to assess the effects of APOE ε4 (carrier/non-carrier) on each volume change measure. Models were adjusted for sex, age at baseline scan and TIV, before further adjusting for baseline Aβ status or WMHV to assess whether this attenuated their effects. Similar models were used to test the contributions of FHS-CVS and systolic BP at each time-point (ages 36, 53 and 69 years) to each volume change measure. Since FHS-CVS and systolic BP were associated with WMHV but not with Aβ status in previous Insight 46 analyses (Lane *et al.*, 2019, 2020), models were adjusted for sex, age at baseline scan, TIV, baseline Aβ status, APOE ε4 status and adult socioeconomic position, before further adjusting for baseline WMHV to assess whether it might explain any effects. Models with systolic BP as a predictor were also adjusted for smoking status, presence of diabetes and body mass index around the time of baseline scan. Interactions between Aβ status and each of FHS-CVS and systolic BP at age 69 were also tested.

If relationships were detected with rates of hippocampal atrophy, whole brain atrophy rate was added as a covariate to examine whether effects were disproportionate to global brain changes.

Regression assumptions were checked by examination of residual plots. If assumptions were not fully met, bootstrapping (2,000 replications) was used to produce bias-corrected and accelerated 95% confidence intervals. Non-linear associations were assessed using plots of residuals against each predictor and were also formally tested by adding quadratic terms to models.

Sensitivity analyses also examined the effect of: (i) not adjusting for age at baseline scan; and (ii) using the whole cerebellum as a reference region for Aβ SUVRs rather than eroded white matter (see section 2.5.3 for rationale).

5.5. Results

346 participants (mean [SD] age at baseline scan 70.5 [0.6] years; 48% female) had high-quality MRI data from both time-points (mean [SD] scan interval 2.4 [0.2] years) and were free of dementia, MCI, and confounding brain disorders at baseline.

5.5.1. Baseline variables

There was no significant difference in WMHV between Aβ positive and negative participants (Z = -0.667; p=0.50), but there was a weak positive correlation between WMHV and Aβ SUVR (r_s = 0.16; p<0.01). Age at baseline scan was not significantly associated with WMHV (r_s = 0.08; p=0.12), Aβ SUVR (r_s = -0.01; p=0.82) or Aβ status (t(339)=0.7032; p=0.48), and there were no significant sex differences in WMHV (Z = -1.533; p=0.13), Aβ SUVR (Z = 0.637; p=0.52) or Aβ status (χ^2 = 0.5617; p=0.45).

5.5.2. Rates of change in whole brain, ventricular and hippocampal volume

Mean rates of whole brain and hippocampal atrophy were 5.86 ml/year and 0.039 ml/year (equivalent to 0.53% and 0.63% per year respectively) and mean rate of ventricular expansion was 1.24 ml/year (%/year not included as less appropriate for ventricular volume change, where the denominator, baseline ventricular volume, does not reflect

the maximum possible loss). Descriptive statistics for each BSI measure are summarised in Table 5.1 and histograms showing their distributions are provided in Figure 5.1.

Table 5.1. Rates of volume change in cognitively normal participants

	Mean (SD) rates of change in brain volume measures using BSI †					
	All participants (n=346)		Aβ positive (n=57)		Aβ negative (n=284)	
Region	ml/year	%/year	ml/year	%/year	ml/year	%/year
Whole brain	-5.86 (3.19)	-0.53 (0.28)	-6.63 (3.07)	-0.59 (0.26)	-5.65 (3.15)	-0.51 (0.28)
Ventricles	1.24 (0.92)	-	1.55 (0.86)	-	1.16 (0.90)	-
Total hippocampus	-0.039 (0.041)	-0.63 (0.66)	-0.051 (0.046)	-0.83 (0.75)	-0.037 (0.040)	-0.59 (0.63)

Aβ = β-amyloid; BSI = boundary shift integral; † negative values represent atrophy and positive values indicate expansion; N.B. a few participants were missing β-amyloid PET data (n=5)

There were no significant sex differences in rates of change in whole brain, ventricular and hippocampal volume after controlling for TIV, but there were associations with age. Specifically, older age at baseline scan had significant associations with greater rates of ventricular expansion (0.16 ml/year faster expansion per one-year increment in age; 95% CI 0.03, 0.30) and hippocampal atrophy (0.009 ml/year faster atrophy per one-year increment in age; 95% CI 0.002, 0.016), and there was a directionally consistent but non-significant relationship with rate of whole brain atrophy (0.46 ml/year faster atrophy per one-year increment in age; 95% CI -0.04, 0.95).

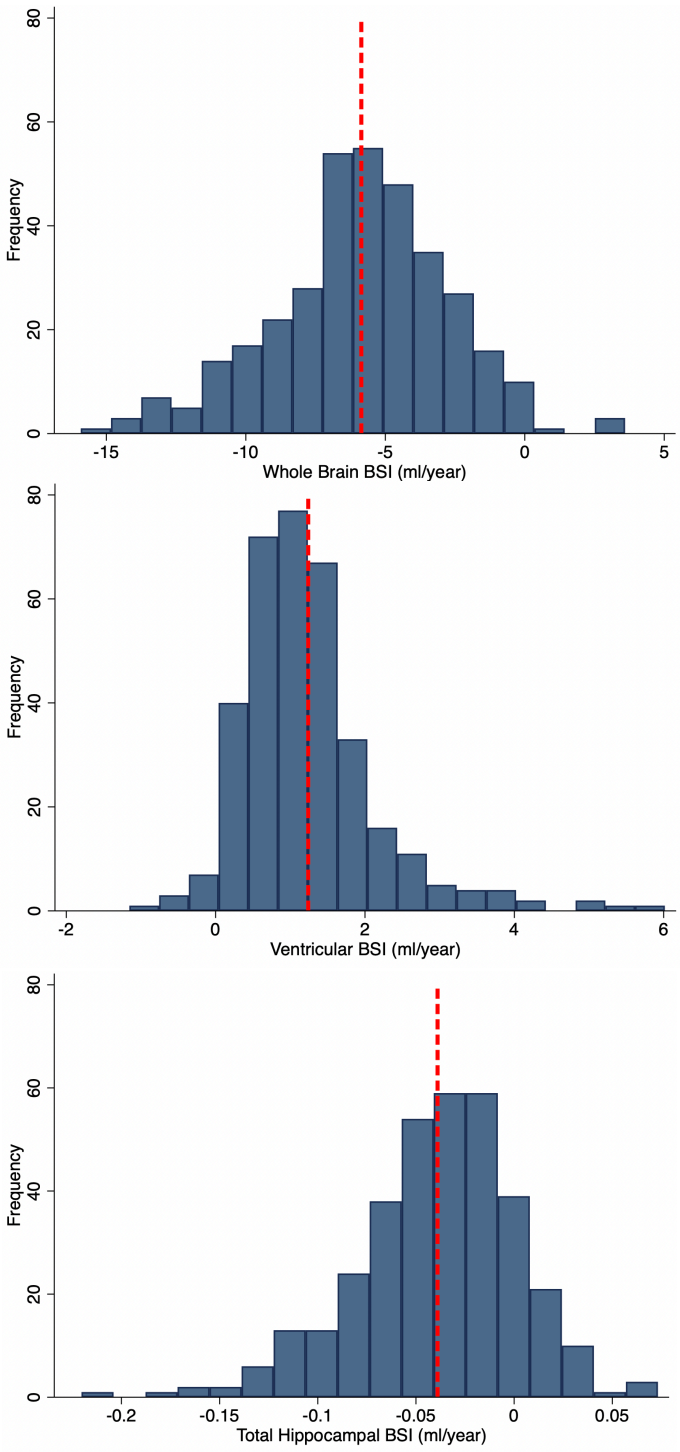

Figure 5.1. Histograms showing distribution and mean (red dashed line) of BSI data

5.5.3. Effects of baseline β-amyloid deposition

Results of analyses testing associations of Aβ (status and SUVR) at age 70 years with rates of change in whole brain, ventricular and hippocampal volume over the next 2.4 years are provided in Figure 5.2 and Figure 5.3.

Being Aβ positive (versus negative) at baseline was associated with significantly greater rates of neurodegeneration: 0.92 ml/year faster whole brain atrophy, 0.40 ml/year greater ventricular expansion and 0.016 ml/year faster hippocampal atrophy. Similar relationships were seen with higher baseline Aβ SUVR, which showed significant associations with faster rates of ventricular expansion (0.20 ml/year per 0.1 increment in SUVR) and hippocampal atrophy (0.009 ml/year per 0.1 increment in SUVR), and a non-significant association with rates of whole brain atrophy (0.39 ml/year per 0.1 increment in SUVR). There was no evidence of non-linear relationships.

There was an interaction between Aβ and sex, whereby Aβ had a greater effect on whole brain atrophy rates in women than men (Table 5.2). Post hoc stratification by sex revealed that being Aβ positive (versus negative) was related to 1.82 ml/year greater whole brain atrophy in females (95% CI 0.64 to 3.00) and 0.31 ml/year faster whole brain atrophy in males (95% CI -0.93 to 1.56), while a 0.1 increment in baseline Aβ SUVR was associated with 0.85 ml/year greater whole brain atrophy in females (95% CI 0.24 to 1.47) and 0.06 ml/year faster whole brain atrophy in males (95% CI -0.62, 0.73).

5.5.4. Effects of baseline vascular burden

Results of analyses testing associations of WMHV at age 70 years with rates of change in of whole brain, ventricular and hippocampal volume over the next 2.4 years are provided in Figure 5.2 and Figure 5.4.

Higher WMHV at baseline was associated with significantly greater rates of neurodegeneration: each 10ml additional WMHV was associated with 1.09 ml/year faster whole brain atrophy, 0.32 ml/year greater ventricular expansion and 0.014 ml/year faster hippocampal atrophy. There was no interaction between WMHV and sex ($p>0.1$, all tests; Table 5.2), and no evidence of non-linear relationships.

5.5.5. Independent and interactive effects of β-amyloid and vascular burden

Effects of Aβ (status or SUVR) and WMHV were similar when they were assessed as predictors in the same model (Figure 5.2). After accounting for WMHV, in addition to age, sex and TIV, Aβ status explained an additional 1.1% of the variance in whole brain atrophy rate, 2.6% of the variance in ventricular expansion rate and 2.1% of the variance in hippocampal atrophy rate. After accounting for Aβ status, in addition to age, sex and TIV, WMHV explained an additional 3.3% of the variance in whole brain atrophy and ventricular expansion rates and 3.1% of the variance in hippocampal atrophy rate. There was no interaction between Aβ and WMHV ($p>0.1$, all tests; Table 5.2).

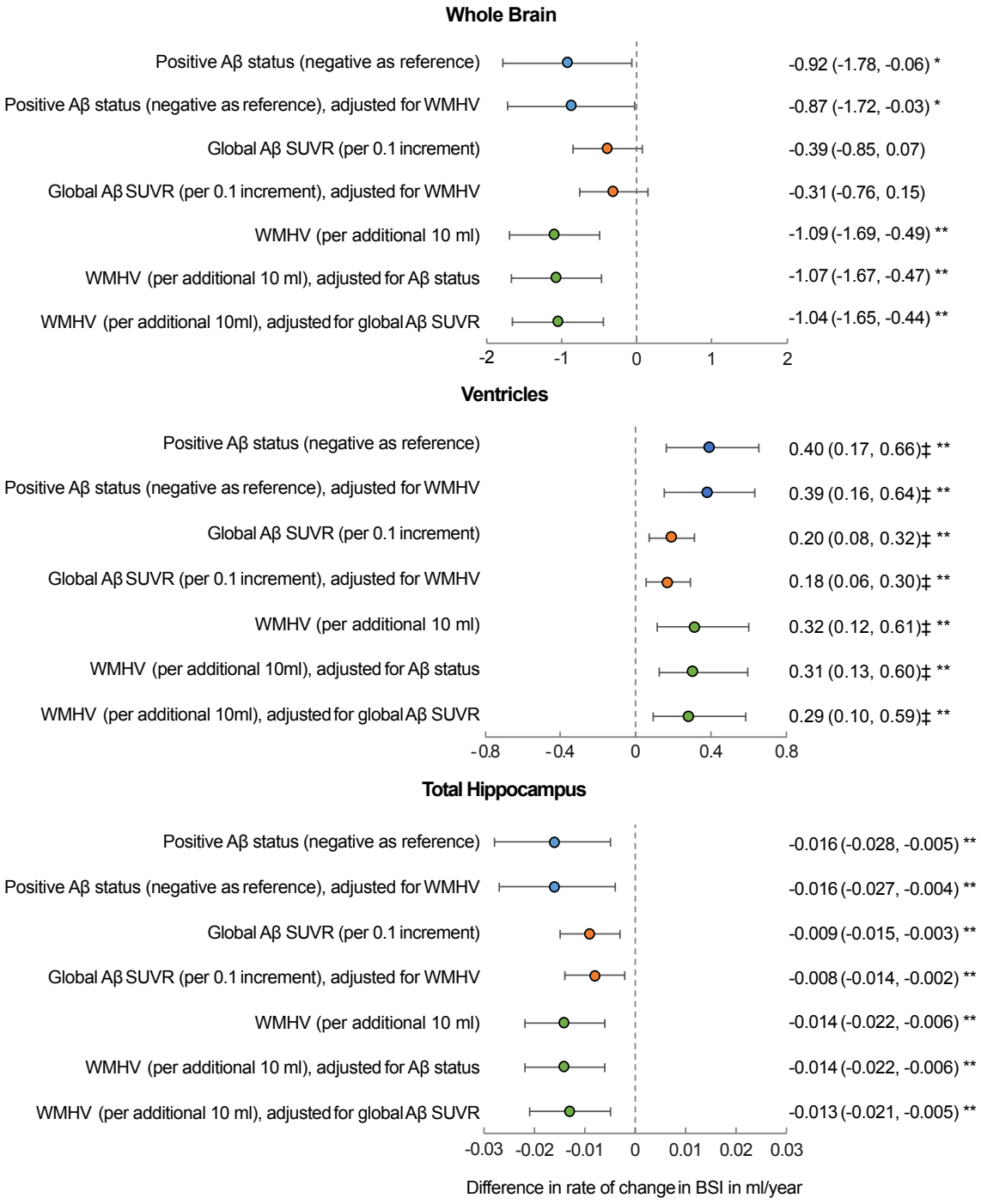

*Aβ = β-amyloid; SUVR = standardised uptake value ratio; WMHV = white matter hyperintensity volume; BSI = boundary shift integral.‡ bias-corrected and accelerated bootstrap 95% CIs; * p ≤0.05; ** p ≤0.01.*

Figure 5.2. Forest plot showing coefficients and 95% confidence intervals for associations of baseline Aβ and WMHV with rates of change in whole brain, ventricular and hippocampal volume in cognitively normal participants.

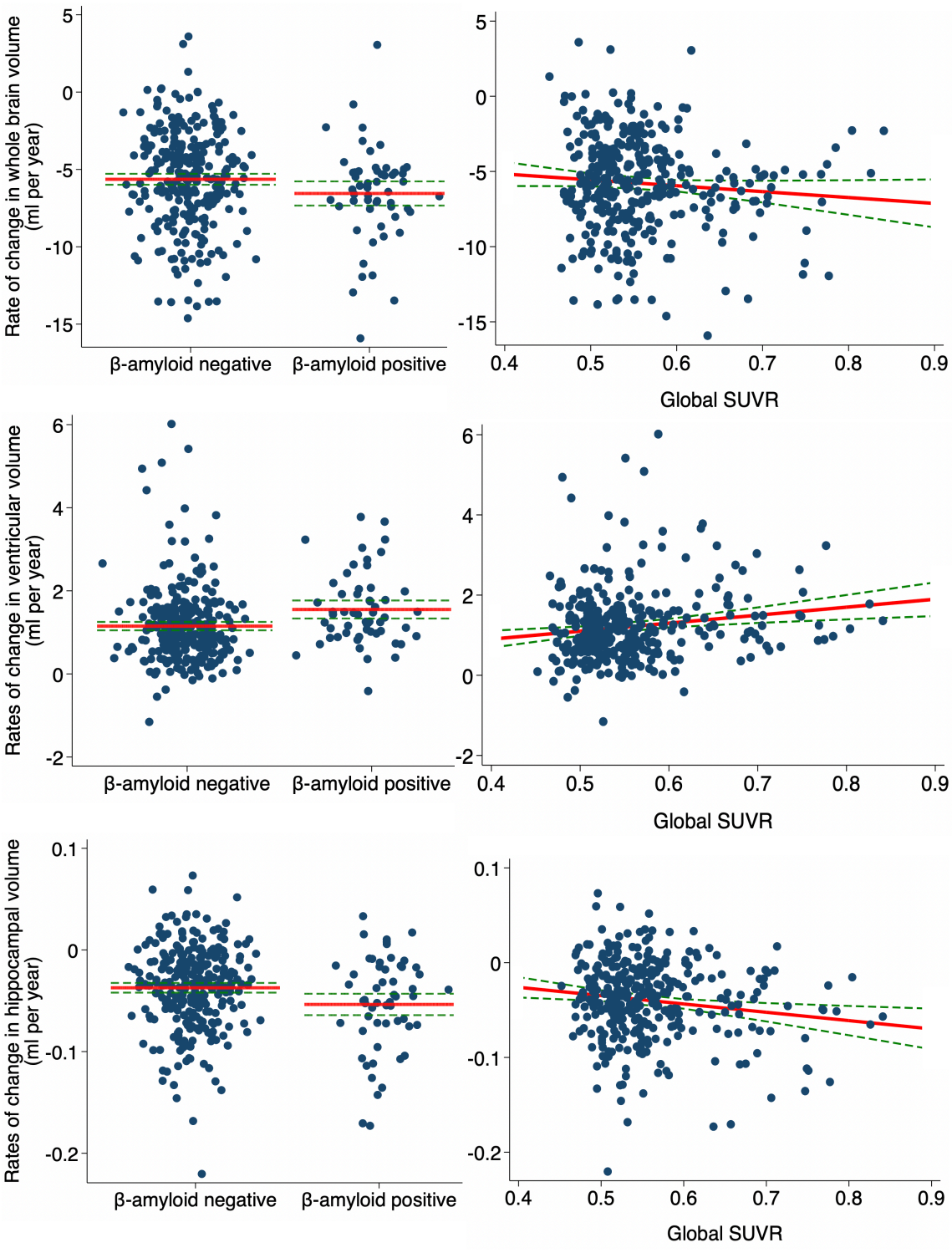

SUVR = standardised uptake value ratio. Scatter plots show the raw data. The solid red line represents the mean or line of best fit from the regression model (adjusted for sex, age at baseline scan and total intracranial volume) and dashed green lines represent the 95% confidence intervals

Figure 5.3. Scatter plots for associations of baseline Aβ (status and SUVR) with rates of change in whole brain, ventricular and hippocampal volume in cognitively normal participants.

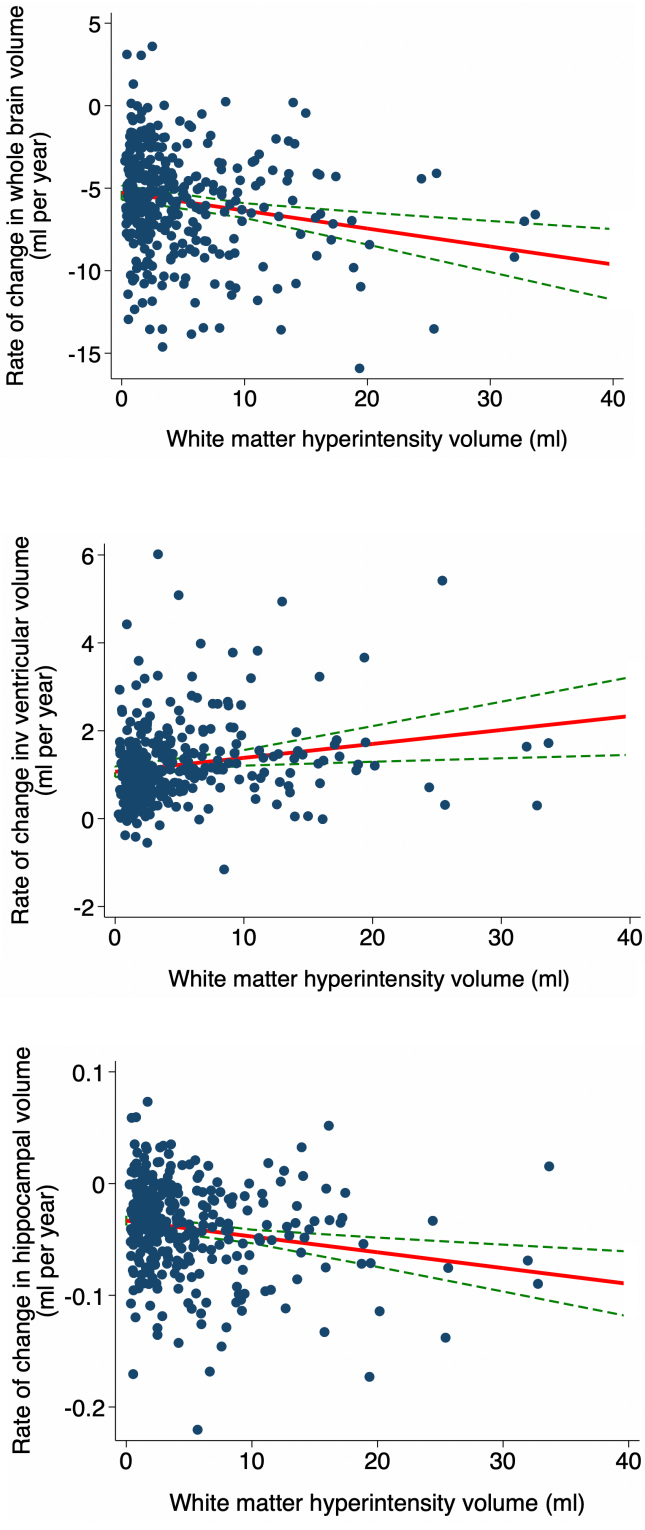

Scatter plots show the raw data. The solid red line represents the line of best fit from the regression model (adjusted for sex, age at baseline scan and total intracranial volume) and dashed green lines represent the 95% confidence intervals

Figure 5.4. Scatter plots for associations of baseline WMHV with rates of change in whole brain, ventricular and hippocampal volume in cognitively normal participants.

Table 5.2. Interactive associations of predictors with rates of change in whole brain, ventricular and total hippocampal volume in cognitively normal participants

Interaction	Difference in rate of change in BSI in ml/year (95% CIs)		
	Whole brain	Ventricles	Total hippocampus
WMHV x Aβ status	-0.17 (-1.68, 1.34)	0.01 (-0.51, 0.62)‡	0.007 (-0.013, 0.027)
WMHV x global Aβ SUVR	0.21 (-0.89, 1.32)	-0.12 (-0.49, 0.26)‡	0.006 (-0.009, 0.021)
Sex x Aβ status	-1.49* (-3.22, 0.25)	0.19 (-0.27, 0.66)‡	-0.013 (-0.037, 0.010)
Sex x global Aβ SUVR	-0.78* (-1.70, 0.15)	0.11 (-0.13, 0.36)‡	-0.006 (-0.018, 0.007)
Sex x WMHV	0.12 (-1.09, 1.33)	0.15 (-0.29, 0.68)‡	0.002 (-0.015, 0.018)
FHS-CVS at age 69 x Aβ status	0.28* (-0.01, 0.58)	-0.07* (-0.15, 0.00)‡	0.006** (0.002, 0.010)
Systolic BP at age 69 x Aβ status	0.27 (-0.26, 0.80)	-0.09 (-0.24, 0.07)‡	0.003 (-0.004, 0.010)

*BSI = boundary shift integral; Aβ = β-amyloid; SUVR = standardised uptake value ratio; WHMV = white matter hyperintensity volume; FHS-CVS = Framingham Heart Study Cardiovascular Risk Score; BP = blood pressure. *p ≤0.1; **p ≤0.01 ‡ bias-corrected and accelerated bootstrap 95% CIs. Interactions represent the following: WMHV x Aβ status is the effect of Aβ positive versus negative per 10ml additional WMHV; WMHV x global Aβ SUVR is the additional effect of 0.1 increment in global Aβ SUVR per 10ml additional WMHV; sex x Aβ status is the difference in effect of Aβ positive versus negative for females versus males; sex x global Aβ SUVR is the difference in effect of 0.1 increment in global Aβ SUVR for females versus males; sex x WMHV is the difference in effect of 10ml additional WMHV for females versus males; FHS-CVS x Aβ status is the effect of Aβ positive versus negative per 5% increment in FHS-CVS; systolic BP x Aβ status is the effect of Aβ positive versus negative per 10mmHg increment in BP.*

5.5.6. Disproportionate hippocampal atrophy

Effects of Aβ and WMHV on hippocampal atrophy rates were attenuated after adjustment for whole brain BSI, such that only the effect of global Aβ SUVR remained significant. Specifically, after adding whole brain BSI as a covariate, each 0.1 increment in baseline global Aβ SUVR was related to 0.006 ml/year faster hippocampal atrophy (95% CI 0.001 to 0.010), while baseline Aβ positivity was related to 0.009 ml/year greater hippocampal

atrophy (95% CI -0.000 to 0.018), and each 10ml increment in baseline WMHV was associated with 0.005 ml/year faster hippocampal atrophy (95% CI -0.001 to 0.012).

5.5.7. Effects of APOE ε4 status

Results of analyses testing associations of APOE ε4 with rates of change in whole brain, ventricular and total hippocampal volume around age 70 are reported in Table 5.3.

APOE ε4 carriers had significantly greater rates of hippocampal atrophy (0.011 ml/year faster than non-carriers) and there were directionally consistent but non-significant relationships with rates of whole brain atrophy (0.67 ml/year higher than non-carriers) and ventricular expansion (0.13 ml/year faster than non-carriers). Effects were attenuated after adjusting for Aβ status and, to a lesser extent, WMHV.

5.5.8. Effects of exposure to vascular risk at ages 36, 53 and 69 years

Results of analyses testing associations of the FHS-CVS and systolic BP at different stages of adulthood with rates of change in whole brain, ventricular and hippocampal volume around age 70 years are reported in Table 5.4 and Table 5.5 respectively.

Higher FHS-CVS and systolic BP at age 53 years were initially found to be associated with faster rates of hippocampal atrophy in later life, but effects were small and no longer significant after exclusion of an influential data-point (identified on review of scatter plot; see Figure 5.4). Otherwise, there were no significant relationships between the FHS-CVS or systolic BP and rates of whole brain, ventricular or hippocampal volume change when assessed across the whole sample, and no evidence of non-linear associations.

Systolic BP at age 69 did not interact with Aβ status, but there were differential effects of FHS-CVS at age 69 by Aβ status (Table 5.2). Specifically, higher FHS-CVS at age 69 was related to greater rates of whole brain atrophy (0.20 ml/year faster per 5% increment in FHS-CVS; 95% CI 0.01, 0.40) and hippocampal atrophy (0.004 ml/year faster per 5% increment in FHS-CVS; 95% CI 0.001, 0.006) in Aβ negative individuals, whereas it had non-significant and directionally opposite effects on rates of whole brain atrophy (0.05 ml/year slower per 5% increment in FHS-CVS; 95% CI -0.32, 0.41) and hippocampal atrophy (0.004 ml/year slower per 5% increment in FHS-CVS; 95% CI -0.001, 0.010) in Aβ positive individuals. There was a substantial difference in sample size between groups, however, with much fewer Aβ positive (n=56) than negative (n=274) participants.

Table 5.3. Associations of APOE ε4 with rates of change in whole brain, ventricular and hippocampal volume in cognitively normal participants

Model	**Difference in rate of change in BSI in ml/year (95% CIs) in APOE ε4 carriers compared to non-carriers**		
	Whole brain	Ventricles	Total hippocampus
1	-0.67 (-1.38, 0.04)	0.13 (-0.06, 0.32)‡	-0.011* (-0.021, -0.002)
2	-0.48 (-1.22, 0.27)	0.02 (-0.16, 0.23)‡	-0.008 (-0.018, 0.002)
3	-0.56 (-1.26, 0.14)	0.09 (-0.10, 0.28)‡	-0.010* (-0.020, -0.001)
4	-0.37 (-1.10, 0.37)	-0.01 (-0.22, 0.19)‡	-0.007 (-0.017, 0.003)

*BSI = boundary shift integral. Model 1 was adjusted for sex, age at baseline scan and total intracranial volume. Model 2 represents Model 1 plus adjustment for baseline β-amyloid status. Model 3 represents Model 1 plus adjustment for baseline white matter hyperintensity volume. Model 4 represents Model 1 plus adjustment for baseline β-amyloid status and white matter hyperintensity volume. *p ≤0.05; ‡ bias-corrected and accelerated bootstrap 95% CIs.*

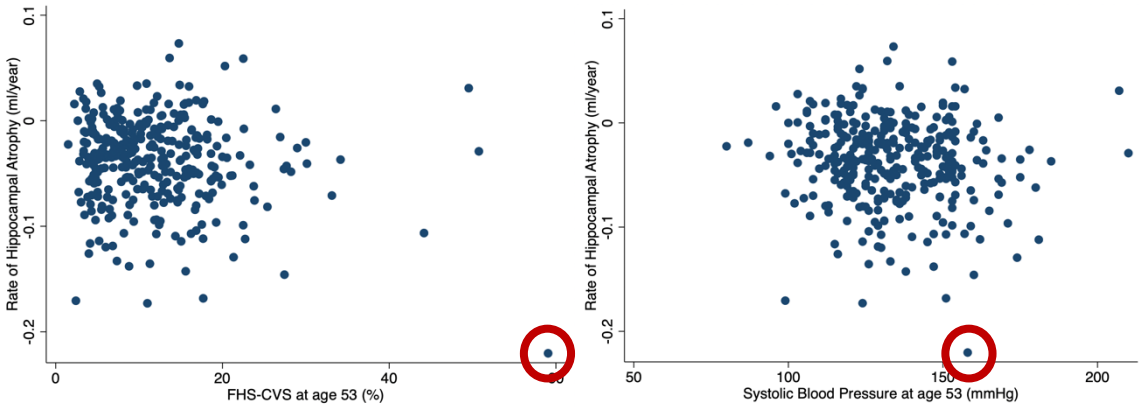

Figure 5.5. Scatter plots highlighting outlier (circled in red) in analyses of effects of FHS-CVS and systolic BP at age 53 on rates of hippocampal atrophy in later life

Table 5.4. Associations of FHS-CVS at ages 36, 53 and 69 with rates of change in whole brain, ventricular and hippocampal volume in cognitively normal participants

Model		**Difference in rate of change in BSI in ml/year (95% CIs) per 5% increment in the FHS-CVS**		
		Whole brain	Ventricles	Total hippocampus
Age 36 (n=301)	1	-0.48 (-1.73, 0.78)	0.12 (-0.25, 0.48)‡	0.004 (-0.013, 0.022)
	2	-0.34 (-1.58, 0.91)	0.08 (-0.28, 0.43)‡	0.006 (-0.011, 0.024)
Age 53 (n=326)	1	-0.10 (-0.39, 0.20)	-0.01 (-0.09, 0.08)‡	-0.002 (-0.006, 0.002)
	2	-0.07 (-0.36, 0.22)	-0.02 (-0.10, 0.06)‡	-0.002 (-0.006, 0.002)
Age 69 (n=330)	1	-0.15 (-0.32, 0.02)	0.05 (-0.00, 0.14)‡	-0.002 (-0.004, 0.001)
	2	-0.11 (-0.28, 0.06)	0.04 (-0.01, 0.12)‡	-0.001 (-0.004, 0.001)

BSI = boundary shift integral; FHS-CVS = Framingham Heart Study Cardiovascular Risk Score. Model 1 was adjusted for sex, age at baseline scan, total intracranial volume, baseline β-amyloid status, APOE ε4 status and adult socioeconomic position. Model 2 was further adjusted for baseline white matter hyperintensity volume. Effects of the FHS-CVS at age 53 refer to results after excluding an outlier (Figure 5.3). ‡ bias-corrected and accelerated bootstrap 95% CIs.

Table 5.5. Effects of systolic BP at ages 36, 53 and 69 on rates of change in whole brain, ventricular and hippocampal volume in cognitively normal participants

Model		Difference in rate of change in BSI in ml/year (95% CIs) per 10mmHg increment in systolic blood pressure		
		Whole brain	Ventricles	Total hippocampus
Age 36 (n=302)	1	-0.07 (-0.33, 0.19)	-0.00 (-0.08, 0.06)‡	-0.001 (-0.004, 0.003)
	2	-0.07 (-0.33, 0.19)	-0.01 (-0.08, 0.06)‡	-0.001 (-0.004, 0.003)
Age 53 (n=325)	1	-0.08 (-0.26, 0.10)	0.03 (-0.02, 0.08)‡	-0.002 (-0.005, 0.000)
	2	-0.05 (-0.22, 0.13)	0.01 (-0.04, 0.06)‡	-0.002 (-0.004, 0.000)
Age 69 (n=333)	1	-0.02 (-0.22, 0.19)	0.05 (-0.01, 0.13)‡	-0.001 (-0.004, 0.002)
	2	0.03 (-0.18, 0.23)	0.03 (-0.03, 0.10)‡	-0.000 (-0.003, 0.003)

BSI = boundary shift integral. BP = blood pressure. Model 1 was adjusted for sex, age at baseline scan, total intracranial volume, baseline β-amyloid status, APOE ε4 status, adult socioeconomic position and smoking status, presence of diabetes and body mass index around time of baseline scan. Model 2 was further adjusted for baseline white matter hyperintensity volume. Effects of systolic blood pressure at age 53 refer to results after excluding an outlier (Figure 5.3). ‡ bias-corrected and accelerated bootstrap 95% CIs.

5.5.9. Sensitivity analyses

Re-running analyses without adjustment for age at baseline did not substantially change the findings (Appendix 2). After re-running analyses using global SUVRs with a whole cerebellum rather than eroded white matter reference region: slightly fewer participants (15.8% versus 16.7%) were Aβ positive (SUVR cut-point for positivity 1.08); associations between baseline Aβ status and rates of volume change were similar, while relationships between baseline global SUVR and rates of volume change were somewhat weaker but directionally the same (Table 5.6); there was a reduced correlation between baseline

global SUVR and WMHV (r_s = 0.02; p=0.75); and the interactions of Aβ and sex and of Aβ and FHS-CVS at age 69 were reduced and non-significant (Table 5.7).

Table 5.6. Sensitivity analyses using SUVR with a whole cerebellum reference: effects of Aβ and WMHV on rates of whole brain, ventricular and hippocampal volume change in cognitively normal participants

a) Effects of Aβ status, global Aβ SUVR and WMHV (assessed in separate models)

Predictor of interest	**Difference in rate of change in BSI in ml/year (95% CIs)**		
	Whole Brain	Ventricles	Total Hippocampus
Positive Aβ status (negative as reference)	-1.08* (-1.95, -0.20)	0.36** (0.16, 0.60)‡	-0.017** (-0.029, -0.005)
Global Aβ SUVR (per 0.1-unit increment)	-0.19 (-0.45, 0.06)	0.07 (-0.01, 0.13)‡	-0.004* (-0.007, -0.000)
WMHV (per 10ml increment)	-1.09** (-1.69, -0.49)	0.32** (0.12, 0.61)‡	-0.014** (-0.022, -0.006)

b) Effects of Aβ status and WMHV (assessed in same model)

Predictor of interest	**Difference in rate of change in BSI in ml/year (95% CIs)**		
	Whole Brain	Ventricles	Total Hippocampus
Positive Aβ status (negative as reference)	-1.12* (-1.97, -0.26)	0.37** (0.17, 0.61)‡	-0.018** (-0.029, -0.006)
WMHV (per 10ml increment)	-1.11** (-1.71, -0.51)	0.32** (0.14, 0.65)‡	-0.014** (-0.023, -0.006)

c) Effects of Aβ SUVR and white matter hyperintensity volume (assessed in same model)

Predictor of interest	**Difference in rate of change in BSI in ml/year (95% CIs)**		
	Whole Brain	Ventricles	Total Hippocampus
Global Aβ SUVR (per 0.1-unit increment)	-0.20 (-0.46, 0.05)	0.07* (0.00, 0.14)‡	-0.004* (-0.007, -0.000)
WMHV (per 10ml increment)	1.10** (-1.70, -0.50)	0.32** (0.12, 0.62)‡	-0.014** (-0.022, -0.006)

*Aβ = β-amyloid; SUVR = standardised uptake value ratio; WMHV = white matter hyperintensity volume; BSI = boundary shift integral. Models were adjusted for sex, age at baseline scan and total intracranial volume. *p ≤0.05; ** p ≤0.01; ‡ bias-corrected accelerated bootstrap 95% CIs.*

Table 5.7. Sensitivity analyses using SUVR with a whole cerebellum reference: interactive associations of predictors with rates of change in whole brain, ventricular and hippocampal volume in cognitively normal participants

Interaction	Difference in rate of change in BSI in ml/year (95% CIs)		
	Whole brain	Ventricles	Total hippocampus
WMHV x Aβ status	0.35 (-1.55, 2.25)	-0.04 (-0.60, 0.78)‡	-0.014 (-0.040, 0.012)
WMHV x global Aβ SUVR	0.37 (-0.16, 0.89)	-0.16 (-0.44, 0.04)‡	0.002 (-0.005, 0.009)
Sex x Aβ status	-0.30 (-2.05, 1.45)	-0.08 (-0.49, 0.41)‡	0.011 (-0.013, 0.035)
Sex x global Aβ SUVR	-0.22 (-0.73, 0.29)	-0.00 (-0.15, 0.14)‡	-0.002 (-0.009, 0.005)
FHS-CVS at age 69 x Aβ status	0.22 (-0.10, 0.53)	-0.04 (-0.13, 0.05)‡	0.000 (-0.004, 0.005)
Systolic BP at age 69 x Aβ status	-0.16 (-0.68, 0.37)	0.06 (-0.09, 0.21)‡	-0.006 (-0.013, 0.001)

Aβ = β-amyloid; BSI = boundary shift integral; WHMV = white matter hyperintensity volume; SUVR = standardised uptake value ratio; FHS-CVS = Framingham Heart Study Cardiovascular Risk Score; BP = blood pressure. ‡ bias-corrected and accelerated bootstrap 95% CIs. Interactions represent the following: WMHV x Aβ status is the effect of Aβ positive versus negative per 10ml additional WMHV; WMHV x global Aβ SUVR is the additional effect of 0.1 increment in global Aβ SUVR per 10ml additional WMHV; sex x Aβ status is the difference in effect of Aβ positive versus negative for females versus males; and sex x global Aβ SUVR is the difference in effect of 0.1 additional global Aβ SUVR for females versus males; FHS-CVS x Aβ status is the effect of Aβ positive versus negative per 5% increment in FHS-CVS; systolic BP x Aβ status is the effect of Aβ positive versus negative per 10mmHg increment in BP.

5.6. Discussion

Key findings of this chapter were that Aβ positivity and higher WMHV were both associated with faster rates of whole brain atrophy, ventricular expansion, and hippocampal atrophy, and that these effects were independent and not interactive.

WMHs have a heterogenous aetiology and underlying pathology, but in older adults they are largely thought to occur as a result of chronic ischaemia due to cerebral small vessel

disease (SVD) (Wardlaw, Smith and Dichgans, 2013). In the current analysis, I found no significant difference in WMHV between Aβ positive and negative participants, but there was a weak positive correlation between WMHV and global Aβ SUVR defined using a white matter reference region. This relationship was no longer observed using SUVRs with a whole cerebellum reference region, however, raising the possibility that quantification of Aβ using a white matter reference region may be influenced by the presence of WMHs or SVD, as has been described previously (Glodzik *et al.*, 2015; Goodheart *et al.*, 2015).

Prior studies investigating the relationship between WMHs and Aβ on PET have reported mixed results, but a recent systematic review concluded that they were mostly independent processes (Roseborough *et al.*, 2017). Some studies have observed increased WMHs in relation to lower Aβ42 in cerebrospinal fluid (Marnane *et al.*, 2016; Pietroboni *et al.*, 2018; Walsh *et al.*, 2020), while others have not or have only found a relationship in AD dementia rather than in mild cognitive impairment or healthy controls (Kalheim *et al.*, 2017; Soldan *et al.*, 2020; Van Waalwijk Van Doorn *et al.*, 2021). There is also evidence that individuals with cerebral amyloid angiopathy – a form of SVD involving deposition of Aβ in blood vessels – have greater WMHs, often with a predilection for posterior brain regions (Gurol *et al.*, 2013; Thanprasertsuk *et al.*, 2014). This may explain some of the variability in findings between studies.

Irrespective of the reference region used to calculate Aβ SUVR in the current analysis, Aβ positivity and greater WMHV were both independently associated with faster rates of whole brain atrophy, ventricular expansion, and hippocampal atrophy. The contribution of WMHV was somewhat greater than Aβ, and there was no evidence that Aβ and WMHV interacted with each other in their effects. While it is worth bearing in mind that

there may not have been sufficient power to detect an interaction between Aβ and WMHV, these findings are supportive of the hypothesis that Aβ and CVD predominantly act via distinct rather than synergistic pathways (Vemuri *et al.*, 2015; Bos *et al.*, 2017), and are consistent with a number of other studies that have shown independent effects in relation to rates of atrophy or cognitive decline (Barnes, Carmichael, *et al.*, 2013; Provenzano *et al.*, 2013; Gordon *et al.*, 2015; Soldan *et al.*, 2020).

Notably, Aβ positive (versus negative) individuals had around 15% faster whole brain atrophy and 50% greater hippocampal atrophy rates, and higher Aβ SUVR was related to disproportionate hippocampal atrophy, despite participants being cognitively normal and years before significant numbers are expected to develop dementia. The effect of WMHV on disproportionate hippocampal atrophy was directionally similar but non-significant. Selective vulnerability of the hippocampus is a characteristic feature of early AD, but it has also been reported in relation to WMHs, including in healthy controls (Fiford *et al.*, 2017). An unbiased voxel-wise analysis of regional volume changes may provide further support for these findings but was beyond the scope of this thesis.

I initially observed an interactive effect of Aβ and sex, whereby higher Aβ deposition at baseline was related to faster rates of whole brain atrophy in women but not in men, suggesting that females are perhaps more susceptible to the consequences of Aβ pathology. Women are known to be at higher risk of AD, which may be partly related to their longer lifespan, but sex differences in relationships between AD pathologies or risk factors and downstream atrophy or cognition have also been reported (Barnes *et al.*, 2005; Altmann *et al.*, 2014; Koran, Wagener and Hohman, 2017). The interaction was reduced and non-significant in sensitivity analyses using SUVRs with a whole cerebellum

reference, however, which could mean that the original finding was a spurious result or that methods of Aβ measurement may be affected by sex differences in some way.

There were no clear associations between the FHS-CVS or systolic BP (at ages 36, 53 and 69) and progressive neurodegeneration in later life when assessed across the whole sample. In previous Insight 46 analyses, we have shown that having a higher FHS-CVS or BP, particularly in early or middle adulthood, was related to smaller brain volumes around age 70 (Lane *et al.*, 2019, 2020). This might reflect that cross-sectional volumes are more indicative of the effects of brain insult(s) prior to the point of brain imaging, and that vascular risk exposure earlier in life is perhaps more detrimental to brain health or associated with greater cumulative risk exposure. I also considered whether differences in findings might be related to a reduction in statistical power, since there were fewer participants with longitudinal imaging data. However, post hoc analyses using the smaller analytical sample of this study showed similar relationships with cross-sectional volumes to those previously reported (data not shown).

There was also no evidence that vascular risk and Aβ acted synergistically, in contrast to findings from other studies that have examined their effects on tau deposition and cognitive decline (Villeneuve *et al.*, 2014; Rabin *et al.*, 2018, 2019). If anything, the results show that elevated vascular risk may be associated with faster rates of neurodegeneration in Aβ negative individuals, as has recently been reported elsewhere (Rosenich *et al.*, 2022), suggesting strategies to reduce vascular risk may be particularly beneficial in this group. Unlike the FHS-CVS, there were no differential effects of systolic BP by Aβ status, perhaps reflecting that the FHS-CVS incorporates data on additional risk factors and that a composite score may increase power to detect associations.

The interpretation of the association between older age (despite the narrow age range of the sample) and faster rates of atrophy/expansion is uncertain. Previous studies suggest that rates of ventricular expansion are stable before the age of 70 years at around one ml/year, but accelerate thereafter, approaching four ml/year towards the age of 80 years (Resnick *et al.*, 2003; Scahill *et al.*, 2003). This suggests that the effect I observed here (0.16 ml/year per one-year increment in age) may be plausible. Alternatively, age effects in Insight 46 might reflect a degree of recruitment bias, in which healthier individuals may have been more likely to attend at the start of the study (as discussed in section 2.5.2).

The findings of this study have implications for the use of MRI-derived volume measures as biomarkers in AD. The AT(N) framework proposes the use of biomarkers of Aβ [A], tau [T] and neurodegeneration [N] to classify individuals on the AD continuum (Jack *et al.*, 2018a). However, neurodegeneration is not specific to AD and this study highlights that CVD – as represented by WMHs – has significant independent effects on expansion and atrophy rates, which are potentially greater in magnitude than those of Aβ. As such, the findings of this study are supportive of the view of others (e.g. Schneider and Viswanathan, 2019), that biomarkers of CVD should be added to the AT(N) framework, something that has already been discussed as a possibility in a recent position paper (Jack *et al.*, 2018). They also highlight the importance of accounting for WMHV in AD trials where MRI-derived volume measures are included as outcomes, since it may confound detection of treatment effects, particularly in the preclinical phase of AD when the relative contribution of CVD may be greater.

The results of this study also have broader relevance to our understanding of the processes leading to dementia. While this is a cognitively normal population, it is

reasonable to infer that increased rates of atrophy or expansion may have subsequent consequences for cognition, given that they are known to be related (Schott *et al.*, 2008; also see Chapter Seven). As such, the findings of this study are supportive of the view that Aβ and CVD predominantly influence risk of cognitive decline through distinct pathways, and that CVD does not contribute to the development of AD pathology *per se* but may lower the threshold for AD dementia. Early interventions and risk management targeting both potential pathways are therefore likely to be important. The attenuation of associations between APOE ε4 and rates of atrophy and expansion after adjusting for Aβ and WMHV suggests that the effects of APOE ε4 were mediated by Aβ and – to a lesser degree – WMHV. This is consistent with APOE ε4 primarily, but not exclusively, influencing risk of dementia via Aβ deposition (Verghese, Castellano and Holtzman, 2011).

Key strengths of this study include the almost identical age of participants and the use of a single scanner and standardised protocol. This is reflected in their mean [SD] atrophy rates (whole brain 5.86 [3.19] ml/year; hippocampal 0.039 [0.041] ml/year), which are considerably less variable (SD/mean ratios around half) compared to those reported in the Alzheimer's Disease Neuroimaging Initiative (ADNI) (whole brain 6.27 [6.15] ml/year; hippocampal 0.052 [0.089] ml/year) and Australian Imaging Biomarker and Lifestyle (AIBL) study (whole brain: 5.46 [7.0] ml/year; hippocampal 0.031 [0.061] ml/year), despite using the same BSI measurement technique (Schott *et al.*, 2010; Andrews *et al.*, 2013).

A significant limitation of this study is that without tau PET data it was not possible to investigate whether tau deposition is more strongly related to neurodegenerative changes than Aβ or whether it interacts with WMHs, as has been reported elsewhere

(Tarawneh *et al.*, 2015; Tosto *et al.*, 2015). There was also insufficient power to assess the impact of other aspects of CVD, such as lacunar infarcts and cerebral microbleeds, which had a much lower frequency in this sample (Lane *et al.*, 2019). Other limitations related to the Insight 46 study more generally are discussed in Chapter Nine.

5.7. Conclusion

In summary, this chapter provides evidence that Aβ and presumed CVD have distinct and additive effects on rates of whole brain atrophy, ventricular expansion, and hippocampal atrophy on MRI in cognitively normal older adults. These findings have implications for the utility of these measures as biomarkers of neurodegeneration in preclinical AD and for understanding the processes that might confer increased risk of dementia in later life.

6. LONGITUDINAL CORTICAL THICKNESS CHANGES

6.1. Publication statement

Work undertaken in this chapter formed part of an oral presentation at the Alzheimer's Association International Conference in 2022: Keuss SE, Coath W, Cash DM, et al., Rates of cortical thinning in Alzheimer's disease signature regions: pathological influences and cognitive consequences in members of the 1946 British birth cohort.

6.2. Statement of contributions

I conceived and designed this study, with advice from Professor Jonathan Schott, Professor Nick Fox, Dr Jo Barnes, and Dr David Cash. Data collection and variable derivation were performed with assistance, as described in section 2.6. I conducted the analyses and interpretation of the results, with statistical support from Dr Jennifer Nicholas.

6.3. Introduction

MRI-derived cortical thickness has also gained significant attention as a potential biomarker of neurodegeneration in AD. Previous studies have identified fairly consistent patterns of reduced cortical thickness in early AD (so-called AD signatures) (Bakkour, Morris and Dickerson, 2009; Dickerson *et al.*, 2009), which predict cognitive decline and AD dementia in cognitively normal older adults (Dickerson *et al.*, 2011; Dickerson and Wolk, 2012). Similar findings have also been detected longitudinally in presymptomatic AD mutation carriers (Weston *et al.*, 2016), suggesting that AD signature cortical

thickness change may be useful as a biomarker for tracking disease progression in the preclinical phase.

Its relationship with Aβ deposition in cognitively normal older adults and the extent to which it is influenced by other brain pathologies, such as CVD, however, remains to be clarified. Two cross-sectional studies – including one based on Insight 46 data – found that lower AD signature cortical thickness in cognitively normal older adults was associated with higher WMHV but not with Aβ status (Wirth, Villeneuve, *et al.*, 2013; Parker *et al.*, 2020). Studies examining the relative contributions of Aβ and WMHs to longitudinal changes in AD signature cortical thickness, however, have been limited.

In this chapter, I first describe the longitudinal changes in AD signature cortical thickness that were quantified from serial MRI in cognitively normal participants. As in the previous chapter, I then aimed to determine the influence of baseline Aβ deposition and WMHV, and of APOE ε4 status and vascular risk at different stages of adulthood. Finally, I assessed whether additional insights into Aβ-related differences could be gained using an unbiased vertex-wise analysis of longitudinal cortical thickness.

6.4. Methods

6.4.1. Determining variables

Baseline Aβ status, global Aβ SUVR and WMHV, and longitudinal cortical thickness, were derived as outlined in section 2.2. Framingham Heart Study Cardiovascular Risk Scores (FHS-CVS) and systolic blood pressure (BP) at ages 36, 53 and 69 were generated as described in section 2.4, as was APOE ε4 status, socioeconomic position,

presence of diabetes, smoking status, and body mass index close to the time of baseline scan.

6.4.2. Statistical analysis

Participants were excluded from analyses if they had incomplete longitudinal T1 data or baseline dementia, mild cognitive impairment, or confounding brain disorders, as outlined in Chapter Three. For analyses involving Aβ or WMHV, participants all had Aβ PET or WMHV segmentation data that passed quality control; for APOE ε4 analyses, genotype data also had to be available; and for vascular risk analyses, participants were required to have FHS-CVS or systolic BP data and complete covariate data at one or more time-point.

Cortical thickness change was summarised in millimetres per year and percentage change from baseline per year, stratified by baseline Aβ status.

Linear regression was used to test associations between predictors of interest and rates of change in cortical thickness. Each model included: change in thickness in millimetres or percentage change from baseline as the outcome; scan interval in years as the explanatory variable; and interactions between scan interval and (i) each predictor of interest and (ii) each covariate. Interactions between two variables were tested by including a term for the three-way interaction between each predictor and scan interval. No constant term was included since the model estimates mean change over time.

Effects of baseline Aβ and WMHV on each cortical thickness change measure were examined in separate models and then together as predictors in a single model, with

adjustment for sex and age at baseline scan. Baseline Aβ was considered in separate models as a binary Aβ status (positive/negative) and using the continuous global Aβ SUVR measure. Further models examined whether there was an interaction between Aβ and WMHV and whether there was an interaction between sex and each of Aβ and WMHV.

Separate models were fitted to assess associations between APOE ε4 (carrier/non-carrier) and each cortical thickness change measure. Models were initially adjusted for sex and age at baseline scan, before further adjusting for baseline Aβ status or WMHV to test whether they mediated any effects. Similar models were fitted to test the effects of FHS-CVS and systolic BP at ages 36, 53 and 69 years to each cortical thickness change measure. Similar to the previous chapter, models were initially adjusted for sex, age at baseline scan, APOE ε4 status, adult socioeconomic position and baseline Aβ status, before further adjusting for baseline WMHV to assess the extent to which it attenuated any effects. Models with systolic BP as a predictor were also adjusted for smoking status, presence of diabetes and body mass index near time of baseline scan. Interactions between Aβ status and each of FHS-CVS and systolic BP at age 69 were also tested.

If relationships were detected with rates of cortical thinning in AD signature regions, models were additionally adjusted for rates of whole cortex thinning in order to examine whether effects were disproportionate to global thickness changes.

Unlike brain volume, cortical thickness is not related to head size, so models were not adjusted for total intracranial volume, in keeping with the consensus in the literature (Fjell *et al.*, 2009; Barnes *et al.*, 2010; Westman *et al.*, 2013).

Regression assumptions were checked by examination of residual plots. Non-linear relationships were assessed by visual inspection of residual versus predictor plots and were also formally tested by adding quadratic terms to models.

As in the previous chapter, sensitivity analyses also examined the effect of: (i) not adjusting for age at baseline scan; and (ii) using the whole cerebellum as a reference region for Aβ SUVRs rather than eroded white matter (see section 2.5.3 for rationale).

A vertex-wise analysis of differences in rates of change in cortical thickness by Aβ status was performed as described in section 2.2.6. A longitudinal two stage model was run in Freesurfer (https://surfer.nmr.mgh.harvard.edu/fswiki/LongitudinalTwoStageModel) with adjustment for sex and age at baseline scan, and a cluster-wise correction for multiple comparisons (1000 permutations; cluster-forming threshold $p<0.05$).

6.5. Results

6.5.1. Rates of change in cortical thickness in AD signature regions

Descriptive statistics for rates of change in cortical thickness in the two AD signature regions are summarised in Table 6.1, stratified by baseline Aβ status. Histograms showing their distribution are provided in Figure 6.1.

Table 6.1. Rates of cortical thickness change in cognitively normal participants

Region	Mean (SD) rate of change in cortical thickness †					
	All participants (n=346)		β-amyloid positive (n=57)		β-amyloid negative (n=284)	
	mm/year	%/year	mm/year	%/year	mm/year	%/year
ADsig Harvard	-0.007 (0.013)	-0.27 (0.52)	-0.005 (0.013)	-0.20 (0.52)	-0.007 (0.013)	-0.28 (0.52)
ADsig Mayo	-0.005 (0.016)	-0.19 (0.58)	-0.005 (0.015)	-0.18 (0.58)	-0.005 (0.015)	-0.18 (0.58)

† Negative values indicate cortical thinning; N.B. a few participants were missing β-amyloid PET data (n=5)

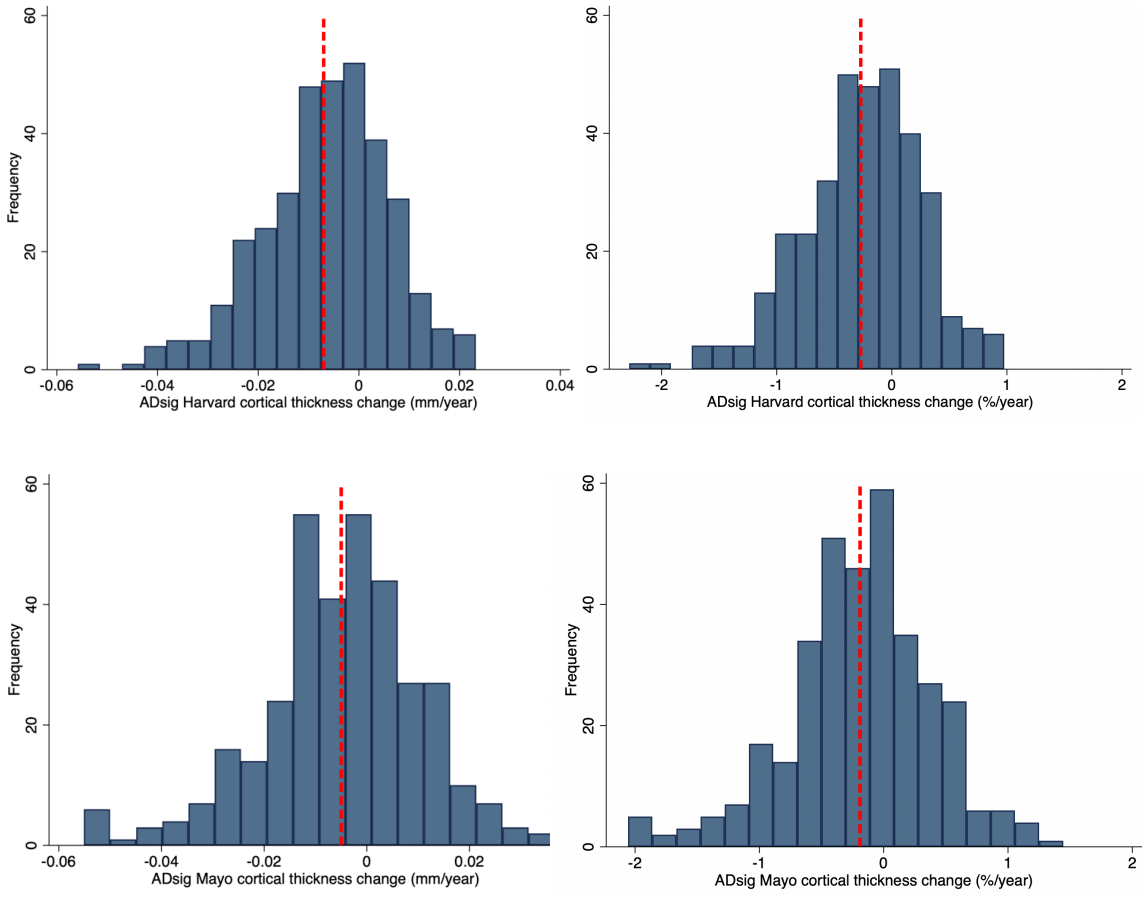

Figure 6.1. Histograms showing distribution and mean (red dashed line) of cortical thickness change values

Older age at baseline scan was related to faster rates of AD signature cortical thinning, with a significant effect detected for the Harvard region. Specifically, a one-year

increment in age was related to a 0.002 mm/year (95% CI 0.000 to 0.004) or 0.09 %/year (95% CI 0.01 to 0.17) faster rate of ADsig Harvard thinning and a 0.002 mm/year (95% CI -0.001 to 0.004) or 0.08 %/year (95% CI -0.02 to 0.17) faster rate of ADsig Mayo thinning. Sex differences were also observed, independent of age at baseline scan, whereby men had 0.003 mm/year (95% CI 0.001 to 0.006) or 0.14 %/year (95% CI 0.03 to 0.25) faster rates of ADsig Harvard thinning than women.

Effects were reduced and non-significant after adjustment for rates of whole cortex thinning, such that a one-year increment in age was related to a 0.000 mm/year (95% CI -0.001 to 0.000) or 0.01 %/year (95% CI -0.01 to 0.03) faster rate of ADsig Harvard thinning and a 0.000 mm/year (95% CI -0.001 to 0.002) or 0.01 %/year (95% CI -0.06 to 0.07) faster rate of ADsig Mayo thinning, and men had 0.001 mm/year (95% CI -0.000 to 0.001) or 0.02 %/year (95% CI -0.01 to 0.05) faster rates of ADsig Harvard thinning than women.

6.5.2. Effects of baseline β-amyloid deposition

Results of analyses testing associations of Aβ at age 70 years with rates of change in ADsig cortical thickness over the next 2.4 years are shown in Figure 6.2 and Figure 6.3.

There were no significant relationships between Aβ (status or global SUVR) and rates of change in cortical thickness in either ADsig region. There was also no evidence of non-linear associations, and no interactions between Aβ and sex (both $p>0.1$, Table 6.2).

6.5.3. Effects of baseline vascular burden

Results of analyses testing associations of WMHV at age 70 years with rates of change in ADsig cortical thickness over the next 2.4 years are given in Figure 6.2 and Figure 6.3.

Higher baseline WMHV was associated with significantly faster rates of cortical thinning in both regions: each 10ml additional WMHV was associated with 0.004 mm/year (95% CI 0.001 to 0.006) or 0.15 %/year (95% CI 0.04, 0.25) faster thinning in the ADsig Harvard region, and 0.004 mm/year (95% CI 0.001 to 0.007) or 0.15 %/year (95% CI 0.03, 0.26) faster thinning in the ADsig Mayo region. There was no evidence of non-linear relationships, and no interactions between WMHV and sex (both $p>0.1$, Table 6.2).

Effects of WMHV were substantially reduced and non-significant after adjustment for rates of whole cortex thinning. Specifically, each 10 ml increment in baseline WMHV was associated with 0.000 mm/year (95% CI 0.000, 0.001) or 0.01 %/year (95% CI -0.02, 0.04) faster thinning in the ADsig Harvard region and 0.001 mm/year (95% CI -0.001, 0.003) or 0.03 %/year (95% CI -0.05, 0.10) faster thinning in the ADsig Mayo region.

6.5.4. Independent and interactive effects of β-amyloid and vascular burden

Relationships of Aβ (status or SUVR) and WMHV with rates of change in ADsig cortical thickness remained similar when they were assessed as predictors in the same model (Figure 6.2), and there were no interactions between Aβ and WMHV (both $p>0.1$; Table 6.2).

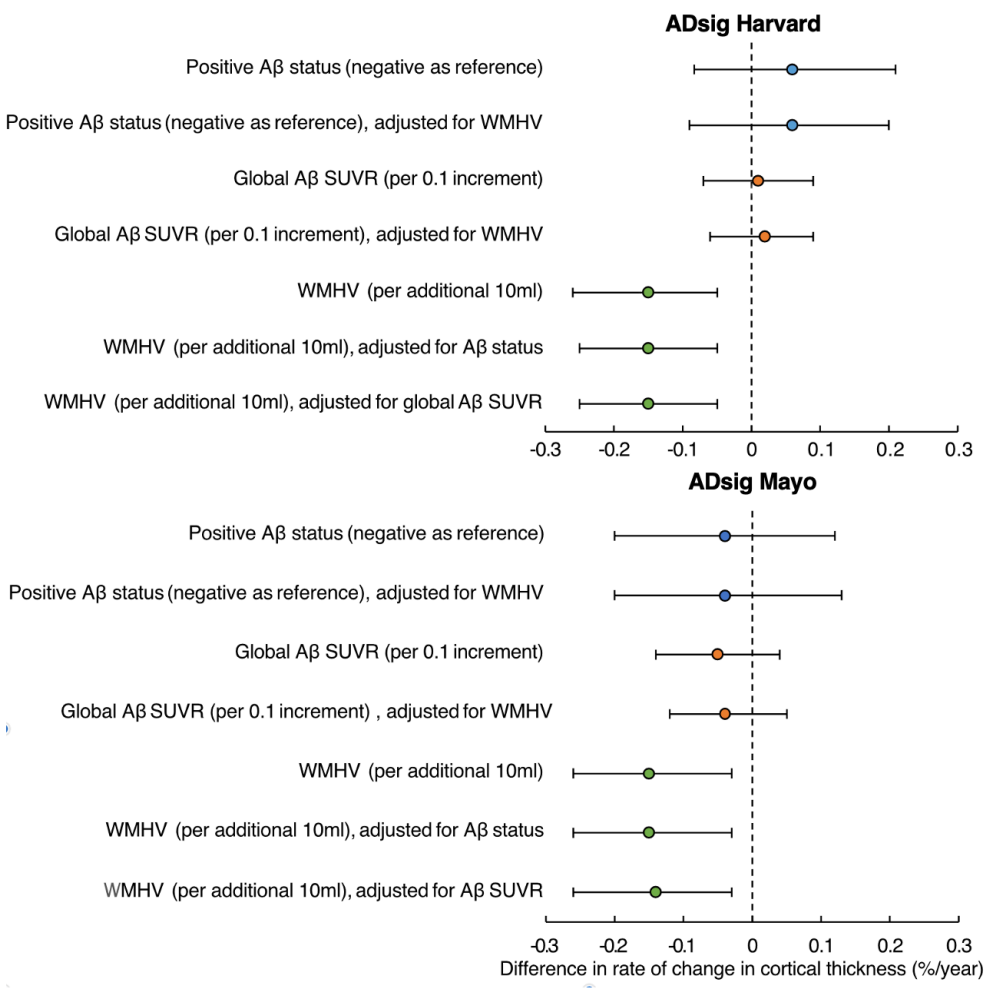

	%/year	mm/year
ADsig Harvard		
Positive Aβ status (negative as reference)	0.06 (-0.09, 0.20)	0.001 (-0.002, 0.005)
Positive Aβ status (negative as reference), adjusted for WMHV	0.06 (-0.08, 0.21)	0.002 (-0.002, 0.005)
Global Aβ SUVR (per 0.1 increment)	0.01 (-0.07, 0.09)	0.000 (-0.002, 0.002)
Global Aβ SUVR (per 0.1 increment), adjusted for WMHV	0.02 (-0.05, 0.10)	0.001 (-0.001, 0.003)
WMHV (per additional 10ml)	-0.15 (-0.25, -0.04) **	-0.004 (-0.006, -0.001)**
WMHV (per additional 10ml), adjusted for Aβ status	-0.15 (-0.25, -0.05) **	-0.004 (-0.006, -0.001)**
WMHV (per additional 10ml), adjusted for global Aβ SUVR	-0.15 (-0.25, -0.05) **	-0.004 (-0.006, -0.001)**
ADsig Mayo		
Positive Aβ status (negative as reference)	-0.04 (-0.20, 0.12)	-0.001 (-0.005, 0.003)
Positive Aβ status (negative as reference), adjusted for WMHV	-0.04 (-0.20, 0.13)	-0.001 (-0.005, 0.003)
Global Aβ SUVR (per 0.1 increment)	-0.05 (-0.14, 0.04)	-0.001 (-0.004, 0.001)
Global Aβ SUVR (per 0.1 increment) , adjusted for WMHV	-0.04 (-0.12, 0.05)	-0.001 (-0.003, 0.001)
WMHV (per additional 10ml)	-0.15 (-0.26, -0.03)*	-0.004 (-0.007, -0.001)*
WMHV (per additional 10ml), adjusted for Aβ status	-0.15 (-0.26, -0.03)*	-0.004 (-0.007, -0.001)*
WMHV (per additional 10ml), adjusted for Aβ SUVR	-0.14 (-0.26, -0.03)*	-0.004 (-0.007, -0.001)*

*Aβ = β-amyloid; SUVR = standard uptake value ratio; WMHV = white matter hyperintensity volume. * p ≤0.05; ** p ≤0.01*

Figure 6.2. Forest plots showing coefficients and 95% confidence intervals for associations of baseline Aβ and WMHV with rates of change in AD signature cortical thickness in cognitively normal participants

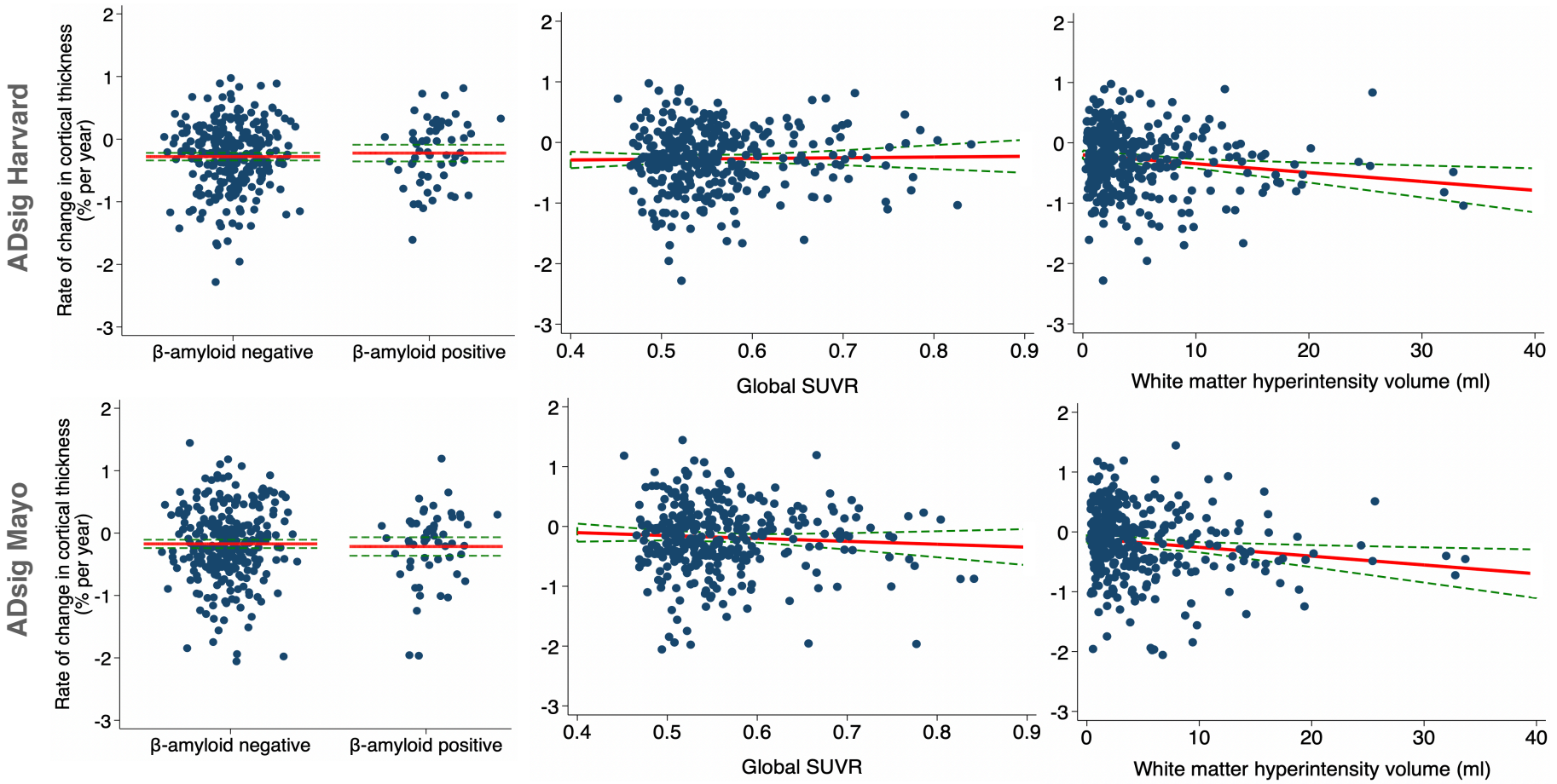

SUVR = standardised uptake value ratio; Scatter plots show the raw data. The solid red line represents the mean or line of best fit from the regression model (adjusted for sex and age at baseline scan) and dashed green lines represent the 95% confidence intervals.

Figure 6.3. Scatter plot showing associations of baseline Aβ and WMHV with rates of change in cortical thickness in ADsig Harvard (top) and ADsig Mayo (bottom) regions in cognitively normal participants

Table 6.2. Interactive associations of predictors with rates of change in cortical thickness in AD signature regions in cognitively normal participants

Interaction	Difference in rate of change in cortical thickness (95% CIs)			
	ADsig Harvard		ADsig Mayo	
	mm/year	%/year	mm/year	%/year
WMHV x Aβ status	-0.002 (-0.008, 0.005)	-0.06 (-0.32, 0.20)	-0.002 (-0.009, 0.006)	-0.06 (-0.35, 0.23)
WMHV x global Aβ SUVR	-0.001 (-0.006, 0.003)	-0.04 (-0.23, 0.14)	-0.001 (-0.007, 0.004)	-0.04 (-0.25, 0.17)
Sex x Aβ status	-0.002 (-0.010, 0.005)	-0.09 (-0.38, 0.21)	0.001 (-0.008, 0.010)	0.05 (-0.28, 0.38)
Sex x global Aβ SUVR	-0.002 (-0.005, 0.002)	-0.06 (-0.22, 0.10)	0.002 (-0.003, 0.007)	0.08 (-0.10, 0.25)
Sex x WMHV	0.001 (-0.004, 0.006)	0.04 (-0.17, 0.25)	0.002 (-0.005, 0.008)	0.06 (-0.17, 0.29)
FHS-CVS at age 69 x Aβ status	0.000 (-0.001, 0.001)	0.00 (-0.05, 0.05)	0.000 (-0.001, 0.002)	0.01 (-0.05, 0.06)
Systolic BP at age 69 x Aβ status	-0.002 (-0.004, 0.001)	-0.06 (-0.15, 0.03)	-0.002 (-0.004, 0.001)	-0.06 (-0.16, 0.04)

WMHV x Aβ status is the effect of Aβ positive versus negative per 10ml additional WMHV; WMHV x global Aβ SUVR is the additional effect of 0.1 increment in global Aβ SUVR per 10ml additional WMHV; sex x Aβ status is the difference in effect of Aβ positive versus negative for females versus males; sex x global Aβ SUVR is the difference in effect of 0.1 increment in global Aβ SUVR for females versus males; and sex x WMHV is the difference in effect of 10ml additional WMHV for females versus males; FHS-CVS x Aβ status is the effect of Aβ positive versus negative per 5% increment in FHS-CVS; systolic BP x Aβ status is the effect of Aβ positive versus negative per 10mmHg increment in BP.

6.5.5. Effects of APOE ε4 status

Results of analyses examining relationships between APOE ε4 status and rates of change in ADsig cortical thickness around age 70 are reported in Table 6.3.

APOE ε4 carriers had 0.003 (95% CI 0.000, 0.006) mm/year or 0.13 (95% CI 0.01, 0.25) %/year faster rates of thinning in the ADsig Harvard region compared to non-carriers.

Effects were similar after adjustment for Aβ status and WMHV, and they were reduced but remained significant after adjustment for rates of whole cortex thinning. There were no significant effects of APOE ε4 on rates of cortical thinning in the ADsig Mayo region.

Table 6.3. Associations of APOE ε4 with rates of change in AD signature cortical thickness in cognitively normal participants

	Difference in rate of change in cortical thickness (95% CIs) in APOE ε4 carriers compared to non-carriers			
	ADsig Harvard		ADsig Mayo	
Model	mm/year	%/year	mm/year	%/year
1	-0.003* (-0.006, -0.000)	-0.13* (-0.25, -0.01)	-0.001 (-0.005, 0.003)	-0.04 (-0.18, 0.09)
2	-0.004* (-0.007, -0.001)	-0.16* (-0.28, -0.03)	-0.001 (-0.005, 0.003)	-0.03 (-0.18, 0.11)
3	-0.004* (-0.007, -0.000)	-0.14* (-0.27, -0.02)	-0.000 (-0.004, 0.003)	-0.02 (-0.16, 0.12)
4	-0.001** (-0.002, -0.000)	-0.05** (-0.08, -0.01)	0.002 (-0.001, 0.004)	0.07 (-0.02, 0.16)

*Model 1 was adjusted for sex and age at baseline scan. Model 2 represents Model 1 plus adjustment for baseline β-amyloid status. Model 3 represents Model 2 plus adjustment for baseline white matter hyperintensity volume. Model 4 represents Model 3 plus adjustment for rates of whole cortex thinning. * p ≤0.05 ** p ≤0.01*

6.5.6. Effects of vascular risk at ages 36, 53 and 69

Results of analyses examining relationships of the FHS-CVS and systolic BP with rates of change in ADsig cortical thickness around age 70 are reported in Table 6.4 and Table 6.5.

There were no significant effects of FHS-CVS or systolic BP at any of the ages examined, and no evidence of non-linear relationships or interactions with Aβ (p>0.1, all tests; Table 6.2).

Table 6.4. Associations of the FHS-CVS at ages 36, 53 and 69 with rates of change in cortical thickness in AD signature regions in cognitively normal participants

Model		Difference in rate of change in cortical thickness (95% CIs) per 5% increment in the FHS-CVS			
		ADsig Harvard		ADsig Mayo	
		mm/year	%/year	mm/year	%/year
Age 36 (n=301)	1	0.003 (-0.003, 0.008)	0.10 (-0.11, 0.32)	-0.000 (-0.007, 0.006)	-0.01 (-0.25, 0.23)
	2	0.003 (-0.002, 0.008)	0.12 (-0.09, 0.33)	0.000 (-0.006, 0.007)	0.01 (-0.23, 0.25)
Age 53 (n=327)	1	-0.000 (-0.001, 0.001)	-0.01 (-0.06, 0.03)	-0.000 (-0.001, 0.001)	-0.00 (-0.05, 0.05)
	2	-0.000 (-0.001, 0.001)	-0.01 (-0.06, 0.04)	0.000 (-0.001, 0.001)	0.00 (-0.05, 0.05)
Age 69 (n=330)	1	-0.000 (-0.001, 0.001)	-0.00 (-0.03, 0.03)	0.000 (-0.000, 0.001)	0.01 (-0.02, 0.05)
	2	0.000 (-0.001, 0.001)	0.00 (-0.03, 0.03)	0.001 (-0.000, 0.001)	0.02 (-0.01, 0.05)

FHS-CVS = Framingham Heart Study Cardiovascular Risk Score. Model 1 was adjusted for sex, age at baseline scan, baseline β-amyloid status, APOE ε4 status and adult socioeconomic position. Model 2 was further adjusted for baseline white matter hyperintensity volume.

Table 6.5. Associations of systolic BP at ages 36, 53 and 69 with rates of change in cortical thickness in AD signature regions in cognitively normal participants

Model		Difference in rate of change in cortical thickness (95% CIs) per 10 mmHg increment in the systolic BP			
		ADsig Harvard		ADsig Mayo	
		mm/year	%/year	mm/year	%/year
Age 36 (n=302)	1	-0.000 (-0.002, 0.001)	-0.02 (-0.06, 0.03)	-0.001 (-0.002, 0.001)	-0.03 (-0.08, 0.02)
	2	-0.000 (-0.002, 0.001)	-0.02 (-0.06, 0.02)	-0.000 (-0.002, 0.001)	-0.03 (-0.08, 0.02)
Age 53 (n=326)	1	-0.001 (-0.001, 0.000)	-0.02 (-0.06, 0.01)	-0.000 (-0.001, 0.001)	-0.01 (-0.05, 0.02)
	2	-0.000 (-0.001, 0.000)	-0.02 (-0.05, 0.01)	-0.000 (-0.001, 0.001)	-0.01 (-0.04, 0.02)
Age 69 (n=333)	1	-0.000 (-0.001, 0.001)	-0.01 (-0.04, 0.03)	-0.000 (-0.002, 0.001)	-0.02 (-0.06, 0.02)
	2	-0.000 (-0.001, 0.001)	-0.00 (-0.04, 0.03)	-0.000 (-0.001, 0.001)	-0.01 (-0.05, 0.03)

BP = blood pressure. Model 1 was adjusted for sex, age at baseline scan, baseline β-amyloid status, APOE ε4 status, adult socioeconomic position, and, smoking status, presence of diabetes and body mass index around time of baseline scan. Model 2 was further adjusted for baseline white matter hyperintensity volume.

6.5.7. An unbiased analysis of β-amyloid-related cortical thickness changes

Results of whole cortex vertex-wise analyses (uncorrected, $p<0.05$) can be visualised in Figure 6.4. Aβ positive (versus negative) participants had greater rates of cortical thinning in two small clusters in the left hemisphere (involving the middle temporal gyrus and the anterior cingulate) and a few small clusters in the right hemisphere (involving the lateral temporal lobe and precuneus). They also had slower rates of cortical thinning (or relatively greater cortical thickening) in several areas across both hemispheres, including

frontal regions, the pre-, para- and post-central gyri, and aspects of the occipital lobe. None of these effects survived correction for multiple comparisons.

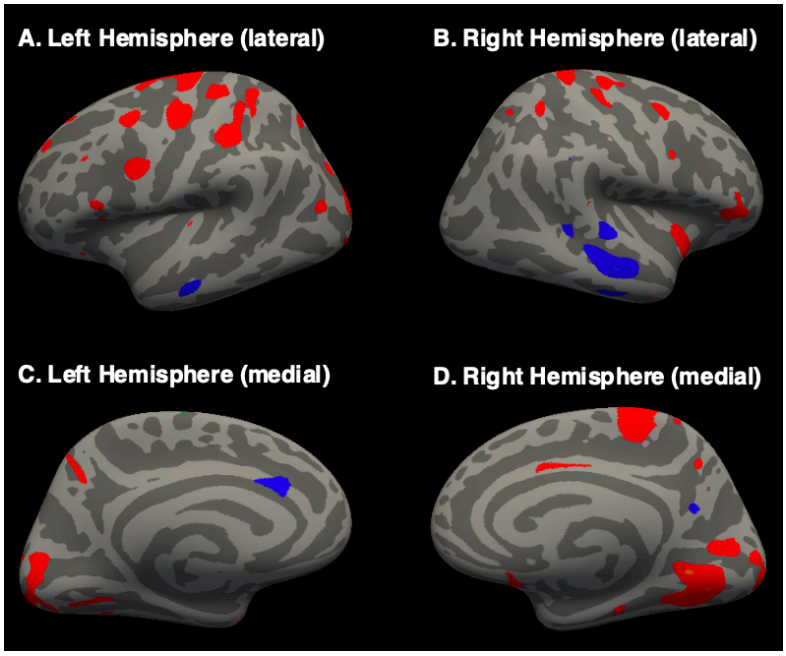

Blue represents faster and red indicates slower rates of cortical thinning in Aβ positive versus negative participants.

Figure 6.4. Vertex-wise analysis of Aβ-related cortical thickness changes

6.5.8. Sensitivity analyses

Re-running analyses without adjustment for age at baseline scan did not meaningfully alter the results (Appendix 3). After re-running analyses using global Aβ SUVRs with a whole cerebellum reference, the main findings remained consistent (Table 6.6), but there were differences in the results of analyses testing interactions (Table 6.7). Specifically, there was an interaction between systolic BP at age 69 and Aβ status, whereby higher systolic BP was related to faster rates of ADsig (Harvard and Mayo) cortical thinning in Aβ positive individuals only. There was also an interaction between sex and Aβ status, such that being Aβ positive was associated with faster rates of cortical thinning in the ADsig Mayo region in males versus females. In post hoc analyses stratified by sex,

however, there were no significant relationships between Aβ status and rates of change in ADsig Mayo thickness.

Table 6.6. Sensitivity analyses using SUVR with a whole cerebellum reference: effects of Aβ and WMHV on rates of change in AD signature cortical thickness in cognitively normal participants

a) Effects of Aβ status, global Aβ SUVR and WMHV (assessed in separate models)

	Difference in rate of change in cortical thickness (95% CIs)			
	ADsig Harvard		ADsig Mayo	
Predictor	mm/year	%/year	mm/year	%/year
Positive Aβ status (negative as reference)	0.002 (-0.001, 0.006)	0.09 (-0.06, 0.24)	0.001 (-0.004, 0.005)	0.02 (-0.15, 0.18)
Global Aβ SUVR (per 0.1-unit increment)	0.001 (-0.000, 0.002)	0.03 (-0.02, 0.07)	-0.000 (-0.002, 0.001)	-0.01 (-0.06, 0.04)
WMHV (per 10ml increment)	-0.004** (-0.006, -0.001)	-0.15** (-0.25, -0.04)	-0.004* (-0.007, -0.001)	-0.15* (-0.26, -0.03)

b) Effects of Aβ status and WMHV (assessed in the same model)

	Difference in rate of change in cortical thickness (95% CIs)			
	ADsig Harvard		ADsig Mayo	
Predictor	mm/year	%/year	mm/year	%/year
Positive Aβ status (negative as reference)	0.002 (-0.001, 0.006)	0.09 (-0.06, 0.23)	0.000 (-0.004, 0.005)	0.01 (-0.15, 0.18)
WMHV (per 10ml increment)	-0.004** (-0.006, -0.001)	-0.15** (-0.25, -0.04)	-0.004* (-0.007, -0.001)	-0.15* (-0.26, -0.03)

c) Effects of global Aβ SUVR and WMHV (assessed in the same model)

	Difference in rate of change in cortical thickness (95% CIs)			
	ADsig Harvard		ADsig Mayo	
Predictor	mm/year	%/year	mm/year	%/year
Global Aβ SUVR (per 0.1-unit increment)	0.001 (-0.000, 0.002)	0.02 (-0.02, 0.07)	-0.000 (-0.002, 0.001)	-0.01 (-0.06, 0.03)
WMHV (per 10ml increment)	-0.004** (-0.006, -0.001)	-0.15** (-0.25, -0.04)	-0.004* (-0.007, -0.001)	-0.15* (-0.26, -0.03)

*Aβ = β-amyloid; SUVR = standardised uptake value ratio; WMHV = white matter hyperintensity volume. * p ≤0.05 ** p ≤0.01*

Table 6.7. Sensitivity analyses using SUVR with a whole cerebellum reference: interactive associations of predictors with rates of change in cortical thickness in AD signature regions in cognitively normal participants

Interaction	Difference in rate of change in cortical thickness (95% CIs)			
	ADsig Harvard		ADsig Mayo	
	mm/year	%/year	mm/year	%/year
WMHV x Aβ status	0.001 (-0.007, 0.009)	0.06 (-0.27, 0.39)	-0.003 (-0.013, 0.007)	-0.11 (-0.48, 0.25)
WMHV x global Aβ SUVR	0.000 (-0.002, 0.002)	0.01 (-0.08, 0.10)	-0.000 (-0.003, 0.002)	-0.01 (-0.11, 0.09)
Sex x Aβ status	0.002 (-0.005, 0.009)	0.09 (-0.21, 0.39)	0.009* (-0.000, 0.017)	0.32* (-0.01, 0.65)
Sex x global Aβ SUVR	-0.001 (-0.003, 0.001)	-0.03 (-0.11, 0.06)	0.002 (-0.001, 0.004)	0.06 (-0.03, 0.16)
FHS-CVS at age 69 x Aβ status	-0.000 (-0.002, 0.001)	-0.03 (-0.07, 0.04)	-0.001 (-0.003 0.001)	-0.04 (-0.10, 0.02)
Systolic BP at age 69 x Aβ status	-0.003** (-0.005, -0.001)	-0.11** (-0.20, -0.02)	-0.003** (-0.006, -0.001)	-0.12** (-0.22, -0.02)

WMHV x Aβ status is the effect of Aβ positive versus negative per 10ml additional WMHV; WMHV x global Aβ SUVR is the additional effect of 0.1 increment in global Aβ SUVR per 10ml additional WMHV; sex x Aβ status is the difference in effect of Aβ positive versus negative for females versus males; sex x global Aβ SUVR is the difference in effect of 0.1 increment in global Aβ SUVR for females versus males; and sex x WMHV is the difference in effect of 10ml additional WMHV for females versus males; FHS-CVS x Aβ status is the effect of Aβ positive versus negative per 5% increment in FHS-CVS; systolic BP x Aβ status is the effect of Aβ positive versus negative per 10mmHg increment in BP.

** p ≤0.1 **≤p 0.05*

6.6. Discussion

Key findings of this chapter were that baseline WMHV was associated with faster subsequent rates of cortical thinning including within so-called AD signature regions, whereas baseline Aβ positivity and global Aβ SUVR were not.

There are several possible explanations for the lack of association between baseline Aβ and subsequent rates of cortical thinning. Compared with the boundary shift integral (BSI), longitudinal cortical thickness is a “noisier” measure, which may make it more difficult to detect subtle Aβ-related differences in cognitively normal individuals. This increased noise might reflect that cortical thickness is computationally more difficult to quantify than volume, and that longitudinal change was assessed indirectly by calculating the difference between time-points, whereas the BSI provides a direct measure of volume change.

Cortical thickness measurement might also be more susceptible to partial volume effects (PVEs), particularly those related to cerebrospinal fluid contamination of grey matter (Koo *et al.*, 2009). Since this phenomenon also affects quantification of Aβ PET data and since the magnitude of PVE increases with greater brain tissue loss (Berlot *et al.*, 2014), this has the potential to confound results of analyses investigating Aβ-related changes in cortical thickness. There remained no association between Aβ (status or global SUVR) and rates of change in AD signature cortical thickness, however, when models were re-run using Aβ PET data processed with partial volume correction (Appendix 4).

Another consideration is that Aβ pathology begins accumulating as early as twenty years prior to dementia (De Strooper and Karran, 2016), whereas neurodegenerative changes are thought to occur later, around five to seven years before dementia (Ridha *et al.*, 2006; Weston *et al.*, 2016). Given the relatively young age of Insight 46 participants, many Aβ positive individuals may still be at an early stage on the AD continuum, potentially years before the development of significant excess neurodegeneration. This might explain why other studies of cognitively normal elderly – often with older age ranges – *have* detected Aβ-related reductions in cortical thickness or faster rates of

cortical thinning (Dickerson *et al.*, 2009; Becker *et al.*, 2011; Doré *et al.*, 2013), whereas Insight 46 analyses – both here and in a previous cross-sectional study (Parker *et al.*, 2020) – have not.

It has also been suggested that, in the early stages of AD, there may be apparent cortical 'thickening' caused by a transient response to Aβ, possibly involving neuronal hypertrophy or inflammation (Fortea *et al.*, 2010, 2011, 2014). Evidence supporting this remains somewhat controversial, since it is largely based on cross-sectional MRI data from studies with small subject numbers and has not been widely replicated. However, if this were the case, it might explain some of the "noise" within the data.

The finding that higher baseline WMHV was associated with greater subsequent rates of cortical thinning is consistent with other studies that have detected relationships between greater WMHV and lower cortical thickness or faster rates of cortical thinning in later life (Wirth, Villeneuve, *et al.*, 2013; Tuladhar *et al.*, 2015; Habes *et al.*, 2016; Lao and Brickman, 2018; Rizvi *et al.*, 2018; Parker *et al.*, 2020). The effects of WMHV on rates of cortical thinning in AD signature regions were reduced to almost zero and non-significant after adjustment for rates of whole cortex thinning, indicating that they were mostly driven by generalised rather than region-specific changes, which perhaps might have been expected if CVD was directly involved in AD pathogenesis.

APOE ε4 carriers had faster rates of cortical thinning in the ADsig Harvard region, but not in the ADsig Mayo region. This might reflect that ADsig Harvard consists of a number of additional frontal and parietal areas. Of note, a previous meta-analysis demonstrated a consistent association between APOE ε4 and frontal lobe hypometabolism in cognitively normal individuals (Liu *et al.*, 2015), and other studies have detected APOE

ε4-related deficits in executive function (Chu *et al.*, 2014; Seo *et al.*, 2016). The effect of APOE ε4 was not attenuated after adjustment for Aβ and WMHV, suggesting it was not mediated via either of these pathologies. It was reduced but remained significant after adjustment for rate of whole cortex thinning, indicating that it was to some extent region-specific.

There were no clear effects of the FHS-CVS or systolic BP (at ages 36, 53 and 69) on rates of change in AD signature cortical thickness in later life when assessed across the whole sample. Previous work has detected relationships between elevated vascular risk and cortical thickness in AD-specific regions (Cardenas *et al.*, 2012; Villeneuve *et al.*, 2014), although both of these studies were cross-sectional in nature. As previously discussed, cross-sectional measures might reflect the effects of prior insults or cumulative neurodegeneration over many years, and it may be difficult to detect the subtle effects of vascular risk on longitudinal changes in brain structure over a relatively short interval.

With the caveat that age effects in Insight 46 might be related to recruitment bias, there was a significant association between older age at baseline scan and faster rates of cortical thinning in the ADsig Harvard region, and a directionally consistent relationship with rates of cortical thinning in the ADsig Mayo region. Cortical thinning has been shown to accelerate with age, with previous work suggesting that the entorhinal cortex may be especially vulnerable (Fjell *et al.*, 2014). There were also significant differences in rates of change in cortical thickness in the ADsig Harvard region by sex, whereby males demonstrated faster rates of thinning than females. Sex differences have been reported elsewhere, with men showing consistently faster rates of cortical thinning than women in multiple brain areas (Thambisetty *et al.*, 2010). Similar to WMHV, the effects of age and

sex were reduced and non-significant after adjustment for rates of whole cortex thinning, indicating that they were related to generalised rather than region-specific changes.

The findings of this study have important implications for the use of longitudinal changes in AD signature cortical thickness as a biomarker of neurodegeneration. First, the absence of significant differences in rates of change in AD signature cortical thickness between Aβ positive and negative participants suggests that it may not be useful as a biomarker of neurodegeneration in the preclinical phase of AD, at least at this early stage and over a short interval. Furthermore, the association with WMHV indicates that, even in so-called AD signature regions, changes in cortical thickness are not specific to AD (assuming, as discussed before, that WMHs primarily develop due to conventional arteriosclerosis-related small vessel disease, rather than secondary to AD pathology).

The results also shed light on the processes that might lead to cognitive decline in later life. In particular, the finding that WMHV was associated with faster rates of cortical thinning in regions known to be vulnerable in AD provides a potential mechanism via which CVD might lower the threshold for AD dementia. Moreover, the observation that APOE ε4 was associated with faster region-specific cortical thinning, independent of Aβ, is consistent with evidence that APOE ε4 might also influence dementia risk via non-Aβ pathways (e.g., direct neurotoxicity) (Yu, Tan and Hardy, 2014; Shi *et al.*, 2017).

As in the previous chapter, some of the results in the current analysis, specifically those related to interactions, varied when analyses were repeated using SUVRs with a whole cerebellum reference. Whether this reflects chance due to the number of interactions tested or confounding related to methods of calculating SUVR is unclear. Importantly,

the main findings – including the lack of significant association between Aβ and rates of change in AD signature cortical thickness – remained consistent.

A limitation of this study is that it was not possible to study the role of tau deposition. As discussed above, one interpretation of the lack of association between Aβ and rates of change in AD signature cortical thickness is that the majority of Aβ positive individuals in this sample may still be at an early stage on the AD continuum. Since tau deposition is thought to develop later (Jack *et al.*, 2010, 2018a), its quantification may have allowed identification of individuals further along the disease process, at a stage when detectable differences in rates of cortical thinning may have been more likely.

Another limitation relates to the measurement of cortical thickness. Unlike the rest of the cortex which is thin and sheet-like, the hippocampal cortex is folded upon itself and appears bulbous (Schwarz *et al.*, 2016). The medial temporal lobe is also one of furthest regions from the coils that detect the MRI signal and is often affected by susceptibility artefacts (Freesurfer FAQ, 2015). For these reasons, it is generally considered too difficult to get reliable thickness estimates from the hippocampus and other medial temporal lobe structures, and Freesurfer excludes them from analyses.

6.7. Conclusion

In conclusion, baseline WMHV – a marker of presumed CVD – was associated with faster subsequent rates of cortical thinning including within so-called AD signature regions, whereas baseline Aβ deposition was not. These findings have implications for the utility of rates of change in AD signature cortical thickness as a biomarker of neurodegeneration in the preclinical phase of AD.

7. ASSOCIATIONS WITH PERFORMANCE ON COGNITIVE TESTING

7.1. Publication statement

Work in this chapter formed part of an oral presentation at the Alzheimer's Association International Conference in 2022: Keuss SE, Coath W, Cash DM, et al., Rates of cortical thinning in Alzheimer's disease signature regions: pathological influences and cognitive consequences in members of the 1946 British birth cohort.

7.2. Statement of contributions

I conceived and designed this study, with advice from Professor Jonathan Schott and Dr Kirsty Lu. Data collection and variable derivation were performed with assistance, as described in section 2.6. I conducted the analyses and interpretation of the results, with statistical support from Dr Jennifer Nicholas.

7.3. Introduction

Structural MRI measures have often been included as outcomes in AD trials, with the expectation that an effective disease-modifying therapy should attenuate rates of change in these measures in treated patients relative to controls. As previously discussed, one advantage of including them as outcomes is that structural MRI changes can be detected before the onset of cognitive decline and continue to be present throughout the disease course (Kaye *et al.*, 2005). Cognitive tests, on the other hand, are more variable in their ability to detect change across different disease severities, often being limited by ceiling and practice effects in early AD and by floor effects in advanced disease.

If structural MRI measures are to be clinically meaningful as outcomes, however, it is important that they are related to changes in cognition or that they at least predict future cognition. While individuals with preclinical AD are cognitively normal, subtle deficits can be detected on neuropsychological measures during this phase. One such measure is the Preclinical Alzheimer Cognitive Composite (PACC), which consists of four tests of global cognition, episodic memory and executive function that were specifically selected due to their sensitivity in early AD (Donohue *et al.*, 2014). Several studies of cognitively normal adults – including one based on cross-sectional Insight 46 data – have detected lower PACC scores or faster PACC decline in Aβ positive versus negative individuals (Donohue *et al.*, 2017; Mormino *et al.*, 2017; Bransby *et al.*, 2019; Lu *et al.*, 2019).

In this chapter, I first summarise the cross-sectional and longitudinal performance of cognitively normal participants on the PACC and its components. I then examine whether cognitive performance at phase two or rates of change in cognitive performance between time-points were related to rates of change in structural MRI measures, and whether these relationships were modified by baseline Aβ status or WMH burden.

7.4. Methods

7.4.1. Determining variables

Baseline Aβ status, WMHV and longitudinal brain volume and cortical thickness changes were derived as outlined in section 2.2. The PACC and its components (mini-mental state examination, MMSE; digit symbol substitution test, DSST; logical memory delayed recall, LMDR; face-name associative memory exam, FNAME) were determined at each time-point as described in section 2.1.4. Childhood cognition, educational attainment,

adult socioeconomic position and APOE ε4 status were assessed as described in section 2.4.

7.4.2. Statistical analysis

Participants were excluded if they had incomplete PACC data or dementia, mild cognitive impairment, or any major brain disorder at baseline, as outlined in Chapter Three. For analyses testing predictors of cognition or rates of cognitive change, complete APOE ε4 data and good quality Aβ PET, WMHV and longitudinal T1 MRI data were required.

To test whether cognitive scores at phase two were significantly different from cognitive scores at phase one, paired t-tests or Wilcoxon signed rank tests were used (depending on whether scores were normally or non-normally distributed).

Linear regression was used to test associations between predictors and rates of change in cognition. Each model included the z-score difference in cognition between time-points as the outcome, visit interval in years as the explanatory variable, and interactions between visit interval and each predictor. No constant term was included since the model estimates mean change over time. Interactions between two variables were tested by including a term for the three-way interaction between each predictor and visit interval.

Linear regression was also used to examine predictors of phase two cognition. Each model included the phase two cognitive z-score as the outcome and each predictor. Interactions were tested by including a term for the two-way interaction between each predictor.

Separate models were fitted to test the effects of each structural MRI measure. Each model also included age at baseline visit, sex, childhood cognition, educational attainment, adult socioeconomic position, APOE ε4 status, baseline Aβ status and baseline WMHV, since they were found to be predictive of cognition at phase one in previous Insight 46 analyses (Lu *et al.*, 2019, 2021). Interaction terms were added in further models to test whether relationships with PACC performance at phase two or rates of change in PACC performance between time-points were modified by baseline Aβ status or WMHV.

Regression assumptions were checked by examination of residual plots. Where those assumptions were not fully met, bootstrapping (2000 replications) was used to produce bias-corrected and accelerated 95% confidence intervals. Sensitivity analyses were also used to examine the effect of not adjusting for age at baseline visit; and of using the whole cerebellum as a reference region for Aβ quantification rather than eroded white matter.

7.5. Results

7.5.1. Cross-sectional and longitudinal cognitive data

The cognitive data of cognitively normal participants are summarised as z-scores in Table 7.1, and histograms showing the distribution of change scores are provided in Figure 7.1. The raw scores for each PACC component are also given in Table 7.2.

Table 7.1. Cognitive performance in cognitively normal participants

Measure	Mean phase one z-score	Mean phase two z-score	Mean change score †	p-value
PACC	0.07	0.04	-0.04	0.08
MMSE[a]	0.05	-0.15	-0.21	≤0.0001
DSST	0.08	-0.10	-0.18	≤0.0001
LMDR	0.08	0.24	+0.16	≤0.0001
FNAME[b]	0.07	0.13	+0.05	0.03

PACC = preclinical Alzheimer cognitive composite; MMSE = mini-mental state examination; DSST = digit symbol substitution test; LMDR = logical memory delayed recall; FNAME = face-name associative memory test. † negative values indicate cognitive decline and positive values indicate improvement; [a]25 participants had missing phase two MMSE data so their PACC scores were based on DSST, FNAME and LMDR scores only; [b]eight participants had missing FNAME data (seven in phase one and one in both phases) so their PACC scores were based on MMSE, DSST and LMDR scores only.

Table 7.2. Raw scores for each PACC component in cognitively normal participants

Measure	Phase one				Phase two			
	Mean	SD	Median	Range	Mean	SD	Median	Range
MMSE[a] (max. 30)	29.3	0.9	30	26-30	29.1	1.02	29	24-30
DSST (max. 93)	48.5	10.1	49	22-82	46.6	10.5	46	21-83
LMDR (max. 25)	11.8	3.6	12	0-23	12.4	3.5	13	0-21
FNAME[b] (max. 96)	66.6	17.4	69	12-95	67.6	18.5	71	3-96

MMSE = mini-mental state examination; DSST = digit symbol substitution test; LMDR = logical memory delayed recall; FNAME = face-name associative memory test. [a]25 participants had missing phase two MMSE data; [b]eight participants had missing FNAME data (seven in phase one and one in both phases).

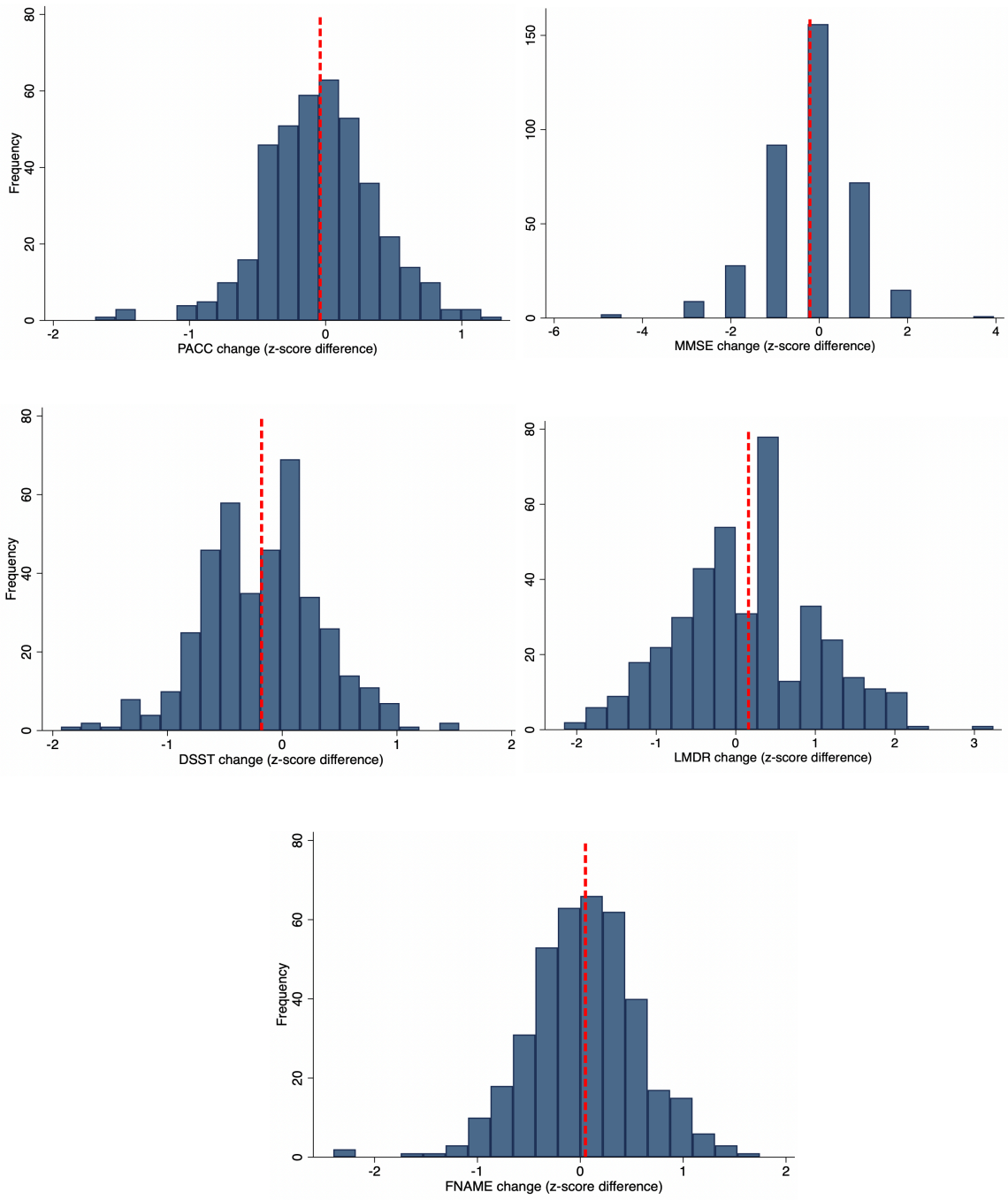

PACC = preclinical Alzheimer cognitive composite; MMSE = mini-mental state examination; DSST = digit symbol substitution test; LMDR = logical memory delayed recall; FNAME = face-name associative memory test.

Figure 7.1. Histograms showing the distribution and mean (red dashed line) of cognitive change scores

7.5.2. Predictors of rates of change in cognition between time-points

Results of analyses examining associations of life-course and pathological predictors and rates of change in structural MRI measures between time-points with rates of change in performance on the PACC and its components are given in Figure 7.2 and Table 7.3.

Females had significantly faster LMDR decline (or less improvement) than males. Higher education was related to marginally slower decline on the FNAME (or relatively greater improvement), as was being an APOE ε4 carrier. There were no significant effects of baseline Aβ or WMHV on subsequent rates of change on the PACC or its components, and no significant interactions between baseline Aβ and WMHV ($p>0.1$, all tests).

Greater rates of whole brain and total hippocampal atrophy were associated with slightly faster concurrent rates of PACC decline (or relatively smaller improvement), and there was a directionally consistent effect of rates of ventricular expansion ($p=0.053$). Examination of the PACC components revealed that the greatest effect was between greater rates of total hippocampal atrophy and faster rates of LMDR decline (or less improvement). There were no significant associations between rates of change in AD signature cortical thickness (Harvard or Mayo) and concurrent rates of change on the PACC or its components when assessed across the whole sample.

There were, however, differential effects by baseline Aβ status, whereby greater rates of whole brain atrophy, ventricular expansion, total hippocampal atrophy, and AD signature cortical thinning (Harvard and Mayo) were associated with significantly faster concurrent rates of PACC decline (or less improvement) in Aβ positive individuals only (Figure 7.3). There was no evidence that baseline WMHV modified associations between rates of

change in structural MRI measures and rates of change in PACC performance (p>0.1, all tests).

A) Life-course and pathological predictors

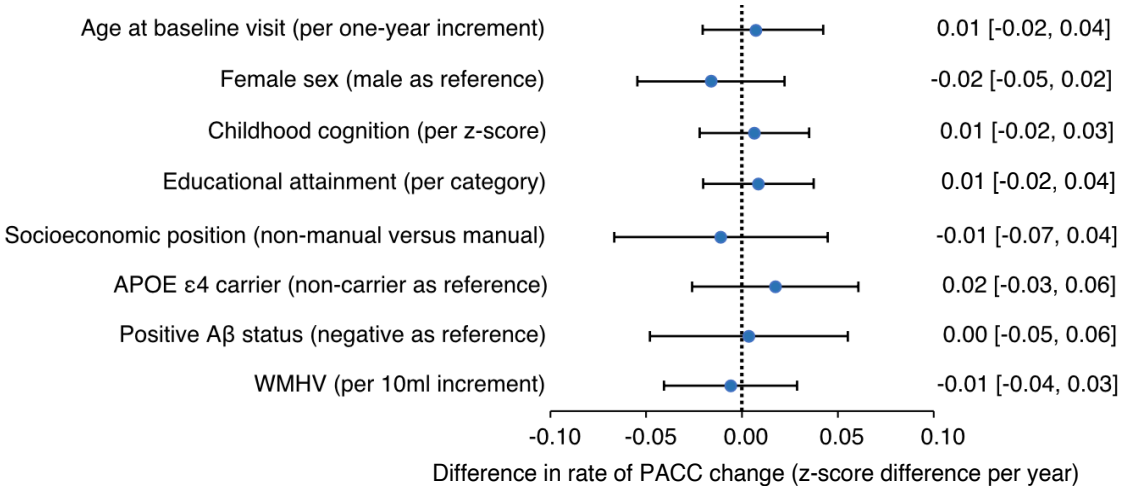

B) Rates of change in structural MRI measures

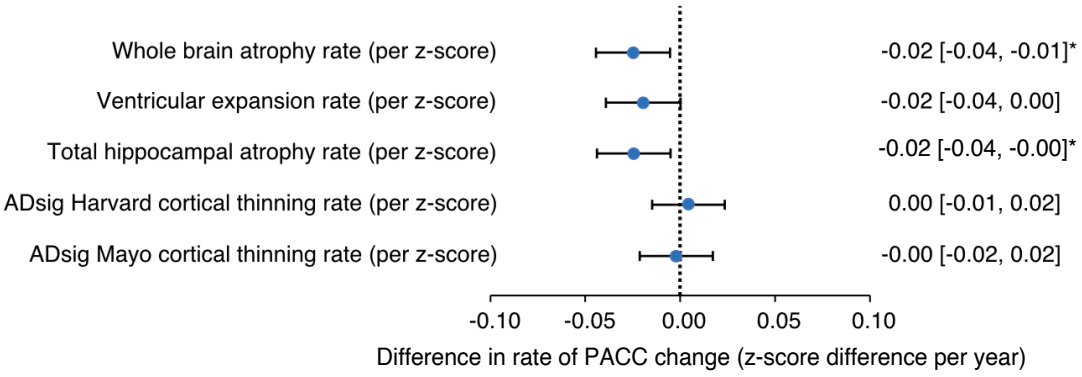

PACC = preclinical Alzheimer cognitive composite; Aβ = β-amyloid; WMHV = white matter hyperintensity volume. Each structural MRI measure was assessed in a separate model, together with all life-course and pathological predictors. The coefficients for age, female sex, childhood cognition, educational attainment, non-manual SEP, APOE ε4 carrier status, *positive Aβ status and WMHV are from the model that included rate of whole brain atrophy.* [a]*there remained no significant effect of positive Aβ status when the model was not adjusted for APOE ε4 carrier status, WMHV and rate of whole brain atrophy. *p≤0.05*

Figure 7.2. Predictors of rates of change in performance on the PACC between time-points in cognitively normal participants

Table 7.3. Predictors of rates of change in performance on the PACC components between time-points in cognitively normal participants

Predictor	z-score difference in cognition per year (95% CIs)			
	MMSE	DSST	LMDR	FNAME
Age at baseline visit (per one-year increment)	0.00 (-0.08, 0.09)‡	-0.03 (-0.06, 0.00)	0.05 (-0.01, 0.11)	0.00 (-0.04, 0.04)
Female sex (male as reference)	0.05 (-0.06, 0.16)‡	-0.01 (-0.05, 0.04)	**-0.10*** (-0.18, -0.02)	-0.01 (-0.06, 0.05)
Childhood cognition (per z-score)	0.06 (-0.01, 0.14)‡	-0.02 (-0.05, 0.02)	0.01 (-0.05, 0.07)	-0.04 (-0.07, 0.00)
Educational attainment (per category)	-0.02 (-0.10, 0.06)‡	-0.00 (-0.04, 0.03)	0.01 (-0.05, 0.07)	**0.04*** (0.01, 0.08)
Non-manual SEP (manual as reference)	-0.01 (-0.20, 0.17)‡	0.06 (-0.01, 0.13)	-0.06 (-0.17, 0.06)	-0.04 (-0.12, 0.03)
APOE ε4 carrier (non-carrier as reference)	-0.03 (-0.15, 0.09)‡	-0.03 (-0.08, 0.03)	0.06 (-0.03, 0.16)	**0.06*** (0.00, 0.12)
Positive Aβ status (negative as reference)[a]	0.12 (-0.01, 0.26)‡	0.01 (-0.05, 0.07)	-0.06 (-0.17, 0.05)	-0.06 (-0.13, 0.01)
WMHV (per 10ml increment)	-0.02 (-0.10, 0.06)‡	-0.01 (-0.05, 0.03)	0.02 (-0.05, 0.09)	-0.01 (-0.06, 0.03)
Rate of whole brain atrophy (per z-score)	-0.04 (-0.10, 0.01)‡	0.01 (-0.02, 0.03)	**-0.04*** (-0.08, -0.00)	-0.02 (-0.04, 0.01)
Rate of ventricular expansion (per z-score)	-0.04 (-0.09, 0.02)‡	0.01 (-0.02, 0.03)	-0.03 (-0.07, 0.01)	-0.02 (-0.04, 0.01)
Rate of total hippocampal atrophy (per z-score)	-0.03 (-0.08, 0.03)‡	0.02 (-0.01, 0.04)	**-0.07**** (-0.11, -0.03)	-0.02 (-0.04, 0.01)
Rate of ADsig Harvard cortical thinning (per z-score)	0.01 (-0.05, 0.06)‡	0.00 (-0.02, 0.03)	-0.00 (-0.04, 0.04)	0.01 (-0.02, 0.04)
Rate of ADsig Mayo cortical thinning (per z-score)	-0.00 (-0.06, 0.05)‡	0.01 (-0.02, 0.03)	-0.02 (-0.06, -0.02)	0.01 (-0.02, 0.03)

MMSE = mini-mental state examination; DSST = digit symbol substitution test; LMDR = logical memory delayed recall; FNAME = face-name associative memory test; SEP = socioeconomic position; Aβ = β-amyloid; WMHV = white matter hyperintensity volume. Each structural MRI measure was assessed in a separate model, together with all other predictors. The coefficients for age, female sex, childhood cognition, educational attainment, non-manual SEP, APOE ε4 carrier status, *positive Aβ status and WMHV are from the model that included rate of whole brain atrophy. [a]there remained no significant effects of Aβ status when models were not adjusted for APOE ε4 carrier status, WMHV and rate of whole brain atrophy. *p≤0.05 **p≤0.001 (highlighted in bold). ‡ bias-corrected and accelerated 95% confidence interval*

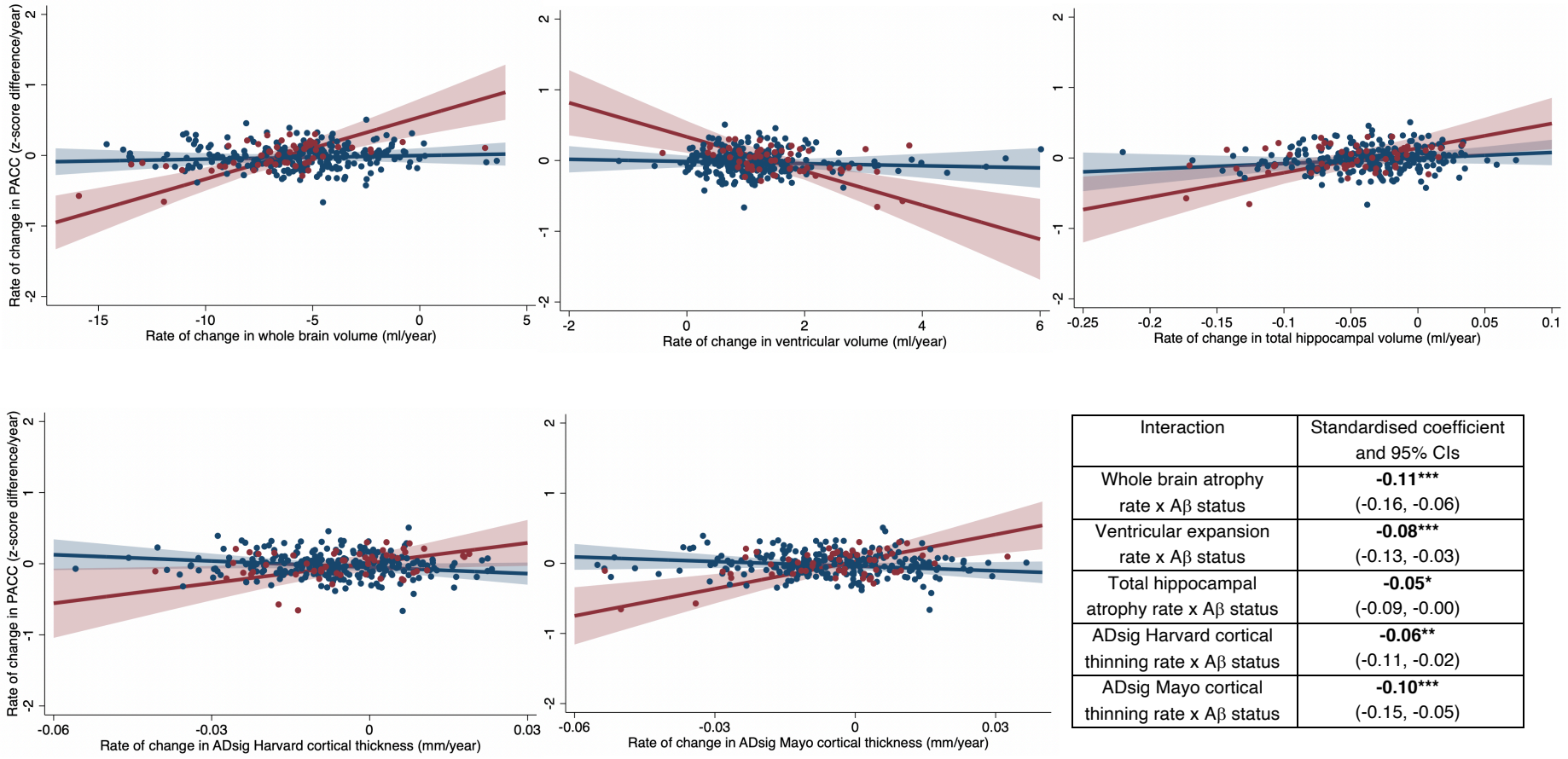

Interaction	Standardised coefficient and 95% CIs
Whole brain atrophy rate x Aβ status	**-0.11*** ** (-0.16, -0.06)
Ventricular expansion rate x Aβ status	**-0.08*** ** (-0.13, -0.03)
Total hippocampal atrophy rate x Aβ status	**-0.05*** (-0.09, -0.00)
ADsig Harvard cortical thinning rate x Aβ status	**-0.06**** (-0.11, -0.02)
ADsig Mayo cortical thinning rate x Aβ status	**-0.10*** ** (-0.15, -0.05)

*PACC = preclinical Alzheimer cognitive composite. *p ≤0.05; **p ≤0.01; ***p ≤0.001* Amyloid-β negative Amyloid-β positive

Figure 7.3. Differential associations between rates of change in structural MRI measures and rates of change in PACC by baseline Aβ status

7.5.3. Predictors of cognitive performance at phase two

Results of analyses examining associations of life-course and pathological predictors and rates of change in structural MRI measures between time-points with performance on the PACC and its components at phase two are provided in Figure 7.4 and Table 7.4.

Higher childhood cognition and educational attainment were related to significantly better performance on the PACC and its components, as was female sex. Non-manual (versus manual) socioeconomic position was related to significantly better DSST scores, and APOE ε4 carriers (versus non-carriers) performed significantly better on LMDR. There were no significant effects of baseline Aβ status or WMHV on the PACC or its components, and no significant interactions between baseline Aβ status and WMHV ($p>0.1$, all tests).

Faster rates of whole brain atrophy, ventricular expansion and total hippocampal atrophy between time-points were related to significantly worse PACC performance at phase two. Examination of the individual PACC components revealed that this was mostly driven by effects on the MMSE and – to a lesser extent – the FNAME. There were no significant associations between rates of change in AD signature cortical thickness (Harvard or Mayo) and the PACC or its components at phase two when assessed across the whole sample.

There were, however, differential effects by baseline Aβ status, whereby faster rates of whole brain atrophy, ventricular expansion, and AD signature cortical thinning (Mayo) were related to poorer phase two PACC scores in Aβ positive versus negative subjects (Figure 7.5). There was no evidence that baseline WMHV modified associations between

rates of change in structural MRI measures and phase two PACC performance (p>0.1, all tests).

A) Life-course and pathological predictors

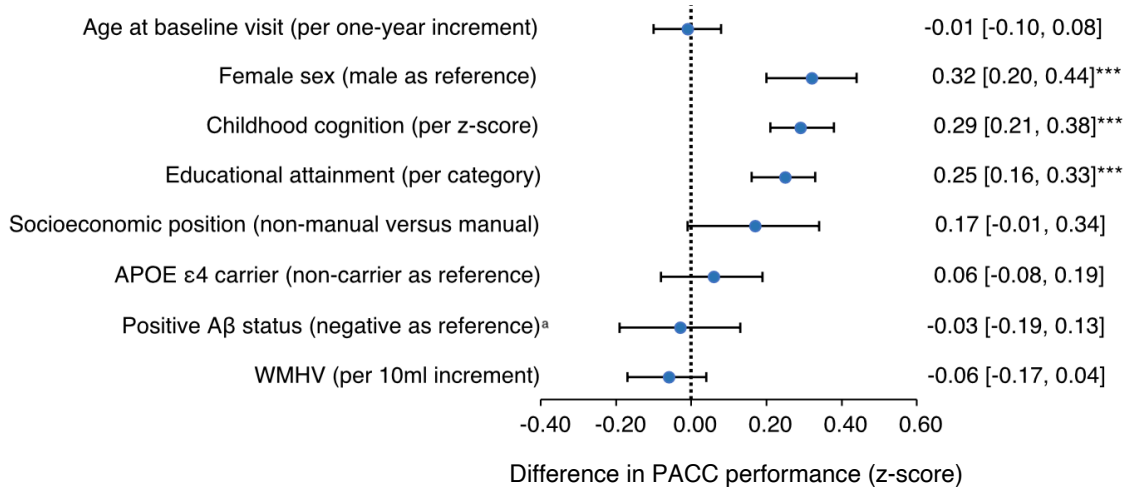

B) Rates of change in structural MRI measures

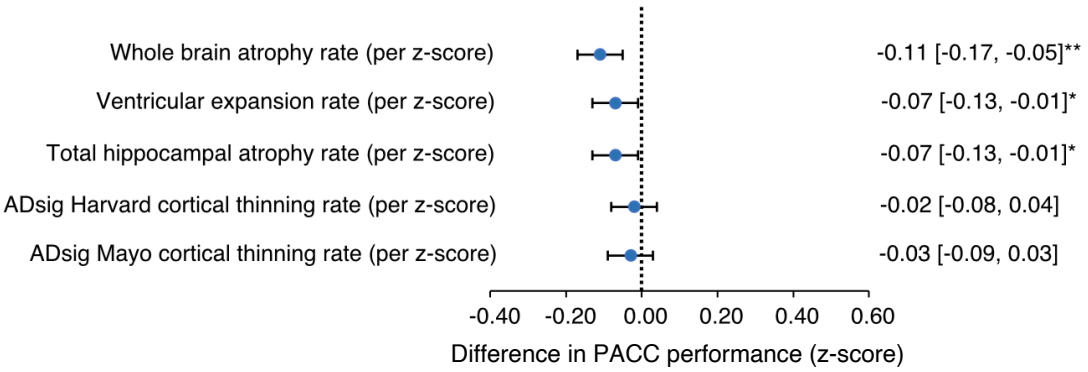

PACC = preclinical Alzheimer cognitive composite; Aβ = β-amyloid; WMHV = white matter hyperintensity volume. Each structural MRI measure was assessed in a separate model, together with all other predictors. The coefficients for age, female sex, childhood cognition, educational attainment, non-manual SEP, APOE ε4 carrier status, *positive Aβ status and WMHV are from the model that included rate of whole brain atrophy.* [a]*there remained no significant effects of Aβ status when models were not adjusted for APOE ε4 carrier status, WMHV and rate of whole brain atrophy.*

**p≤0.05 **p≤0.01 ***p≤0.001.*

Figure 7.4. Predictors of PACC performance at phase two in cognitively normal participants

Table 7.4. Predictors of performance on the PACC components at phase two in cognitively normal participants

Predictor	z-score difference in cognition at phase two (95% CIs)			
	MMSE	DSST	LMDR	FNAME
Age at baseline visit (per one-year increment)	-0.01 (-0.17, 0.15)‡	-0.10 (-0.26, 0.06)	0.13 (-0.02, 0.27)	-0.05 (-0.21, 0.11)
Female sex (male as reference)	**0.31**** (0.10, 0.53)‡	**0.33**** (0.11, 0.54)	**0.29**** (0.10, 0.49)	**0.35***** (0.14, 0.57)
Childhood cognition (per z-score)	**0.30***** (0.13, 0.46)‡	**0.22**** (0.07, 0.38)	**0.33***** (0.18, 0.47)	**0.33***** (0.17, 0.49)
Educational attainment (per category)	**0.19*** (0.01, 0.39)‡	**0.31***** (0.16, 0.47)	**0.20**** (0.05, 0.35)	**0.28***** (0.12, 0.43)
Non-manual SEP (manual as reference)	0.13 (-0.23, 0.55)‡	**0.38*** (0.07, 0.68)	0.00 (-0.29, 0.29)	0.17 (-0.14, 0.48)
APOE ε4 carrier (non-carrier as reference)	-0.05 (-0.29, 0.18)‡	-0.07 (-0.31, 0.17)	**0.25*** (0.03, 0.47)	0.09 (-0.15, 0.33)
Positive Aβ status (negative as reference)[a]	0.15 (-0.10, 0.42)‡	-0.09 (-0.36, 0.21)	-0.18 (-0.44, 0.10)	-0.01 (-0.30, 0.27)
WMHV (per 10ml increment)	0.05 (-0.13, 0.23)‡	-0.16 (-0.36, 0.03)	-0.07 (-0.25, 0.11)	-0.07 (-0.27, 0.12)
Rate of whole brain atrophy (per z-score)	**-0.18***** (-0.29, -0.08)‡	-0.06 (-0.17, 0.04)	-0.06 (-0.16, 0.04)	**-0.12*** (-0.22, -0.01)
Rate of ventricular expansion (per z-score)	**-0.14*** (-0.27, -0.01)‡	-0.05 (-0.16, 0.05)	-0.03 (-0.13, 0.07)	-0.07 (-0.17, 0.04)
Rate of total hippocampal atrophy (per z-score)	**-0.15**** (-0.27, -0.04)‡	0.03 (-0.08, 0.13)	-0.05 (-0.15, 0.05)	-0.10 (-0.20, 0.01)
Rate of ADsig Harvard cortical thinning (per z-score)	-0.04 (-0.14, 0.07)‡	0.00 (-0.10, 0.11)	-0.03 (-0.12, 0.07)	-0.03 (-0.13, 0.08)
Rate of ADsig Mayo cortical thinning (per z-score)	-0.02 (-0.14, 0.11)‡	0.02 (-0.09, 0.12)	-0.05 (-0.15, 0.04)	-0.08 (-0.18, 0.03)

MMSE = mini-mental state examination; DSST = digit symbol substitution test; LMDR = logical memory delayed recall; FNAME = face-name associative memory test; SEP = socioeconomic position; Aβ = β-amyloid; WMHV = white matter hyperintensity volume. Each structural MRI measure was assessed in a separate model, together with all other predictors. The coefficients for age, female sex, childhood cognition, educational attainment, non-manual SEP, APOE ε4 carrier status, *positive Aβ status and WMHV are from the model that included rate of whole brain atrophy. [a]there remained no significant effects of Aβ status when models were not adjusted for APOE ε4 carrier status, WMHV and rate of whole brain atrophy. *p≤0.05 **p≤0.01 ***p≤0.001 (highlighted in bold). ‡ bias-corrected and accelerated 95% confidence intervals.*

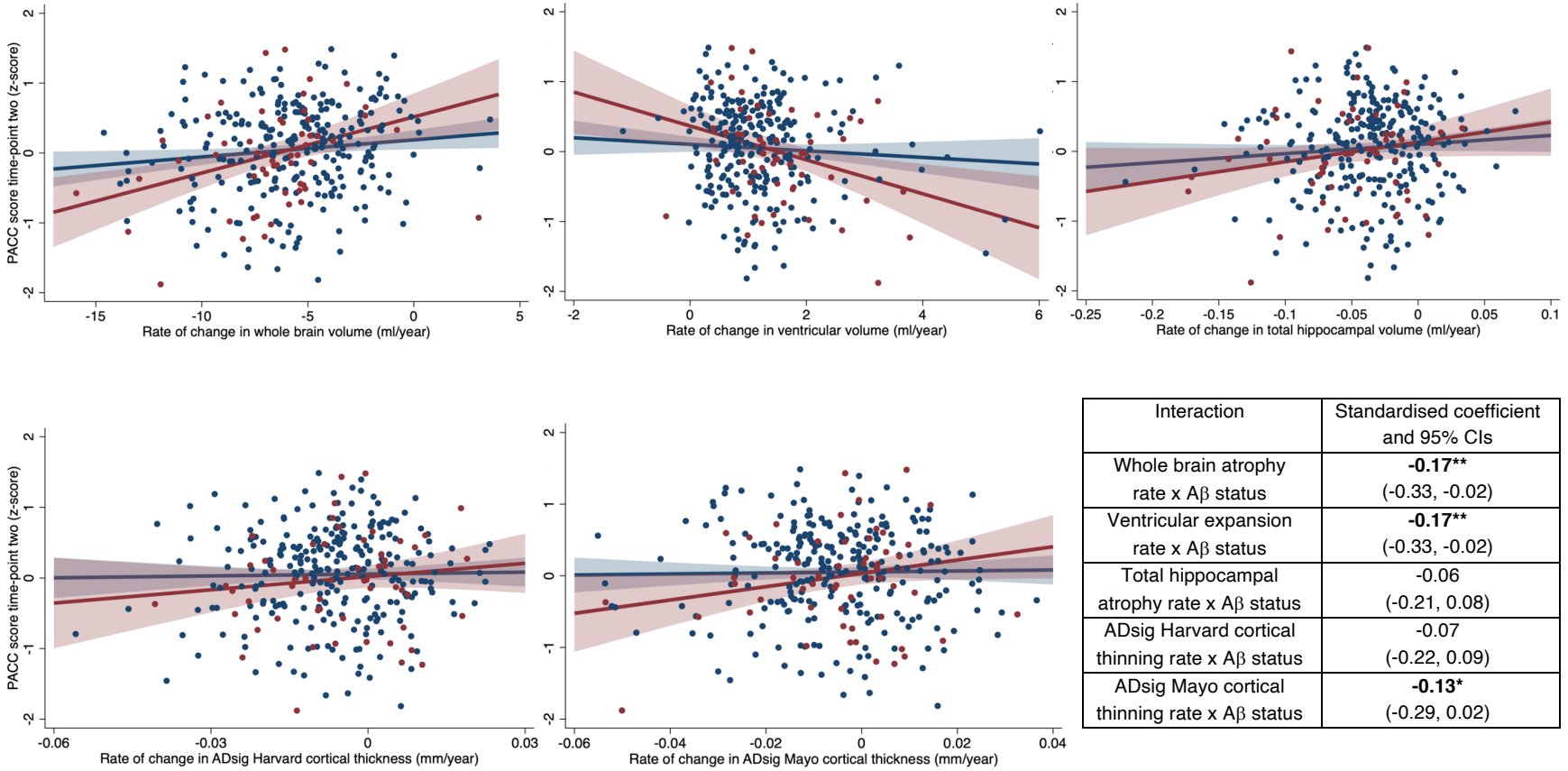

Interaction	Standardised coefficient and 95% CIs
Whole brain atrophy rate x Aβ status	**-0.17**** (-0.33, -0.02)
Ventricular expansion rate x Aβ status	**-0.17**** (-0.33, -0.02)
Total hippocampal atrophy rate x Aβ status	-0.06 (-0.21, 0.08)
ADsig Harvard cortical thinning rate x Aβ status	-0.07 (-0.22, 0.09)
ADsig Mayo cortical thinning rate x Aβ status	**-0.13*** (-0.29, 0.02)

*PACC = preclinical Alzheimer cognitive composite. *p ≤0.1; **p ≤0.05.* Amyloid-β negative Amyloid-β positive

Figure 7.5. Differential associations between rates of change in structural MRI measures and PACC at phase two by baseline Aβ status

7.5.4. Sensitivity analyses

Re-running analyses without adjustment for age at baseline visit did not meaningfully alter the findings (Appendix 5). After re-running analyses using SUVRs with a whole cerebellum reference region: there remained no significant effects of baseline Aβ status or WMHV (Table 7.5), and no significant interactions between baseline Aβ status and WMHV (p>0.1, all tests); and the differential effects of rates of change in structural MRI measures by baseline Aβ status were similar with respect to PACC performance at phase two and were attenuated but directionally consistent with respect to rates of PACC change (Table 7.6).

Table 7.5. Sensitivity analyses using SUVR with a whole cerebellum reference: effects of baseline Aβ and WMHV

Predictor	z-score difference in PACC per year (95% CIs)	z-score difference in PACC at phase two (95% CIs)
Positive Aβ status (negative as reference)	-0.00 (-0.06, 0.05)	0.01 (-0.16, 0.17)
WMHV (per 10ml increment)	-0.01 (-0.04, 0.03)	-0.06 (-0.17, 0.04)

PACC = preclinical Alzheimer cognitive composite; Aβ = β-amyloid; WMHV = white matter hyperintensity volume. Baseline Aβ status and WMHV were assessed together in the same model, with adjustment for sex, childhood cognition, educational attainment, adult socioeconomic position, APOE ε4 carrier status, *and rate of whole brain atrophy.*

Table 7.6. Sensitivity analyses using SUVR with a whole cerebellum reference: differential associations of rates of change in structural MRI measures with rates of change in PACC and PACC performance at phase two by baseline Aβ status

Predictor	z-score difference in PACC per year (95% CIs)	z-score difference in PACC at phase two (95% CIs)
Whole brain atrophy rate x Aβ status	**-0.06*** (-0.12, -0.00)	**-0.22*** (-0.41, -0.04)
Ventricular expansion rate x Aβ status	-0.03 (-0.08, 0.03)	**-0.22**** (-0.39, -0.06)
Total hippocampal atrophy rate x Aβ status	-0.01 (-0.06, 0.05)	-0.08 (-0.25, 0.08)
ADsig Harvard cortical thinning rate x Aβ status	**-0.06*** (-0.12, -0.01)	-0.08 (-0.25, 0.09)
ADsig Mayo cortical thinning rate x Aβ status	**-0.08**** (-0.14, -0.03)	**-0.18*** (-0.35, -0.01)

PACC = preclinical Alzheimer cognitive composite; Aβ = β-amyloid. Each interaction was assessed in a separate model with adjustment for sex, childhood cognition, educational attainment, adult socioeconomic position, APOE ε4 carrier status, *baseline white matter hyperintensity volume and rate of whole brain atrophy. * p≤0.05 **p≤0.01.*

7.6. Discussion

Key findings of this chapter were that rates of change in structural MRI measures were associated with concurrent rates of PACC change and phase two PACC performance, and these effects were driven primarily or entirely by changes in Aβ positive individuals.

On average, there was little change in PACC performance over time, which is perhaps not unexpected in a cognitively normal sample over a period of around two years. Examination of the PACC components, however, revealed a more complex picture, with mean scores improving over time on some measures (LMDR and FNAME) and declining on others (DSST and MMSE). Thus, the small decrease observed in mean PACC

performance between time-points was driven by DSST and MMSE scores. The DSST is known to be highly sensitive to small changes in cognition over time, likely because it assesses speed (Jaeger, 2018), while the MMSE is prone to ceiling effects, meaning individuals with high scores at baseline can only get worse or remain stable (Salthouse, 2019). The LMDR and FNAME, on the other hand, both involve learning and recall of information, which makes them more susceptible to practice effects (Gavett *et al.*, 2016; Samaroo *et al.*, 2020).

Of note, being Aβ positive at baseline was not associated with subsequent rates of change in performance on the PACC or its components. Other studies have detected faster rates of PACC decline in Aβ positive versus negative cognitively normal individuals (Donohue *et al.*, 2017; Mormino *et al.*, 2017), although in one study this was not evident until around three to four years from baseline (Donohue *et al.*, 2017). Thus, as previously discussed, Insight 46 participants could be on average several years before dementia, and it may be that Aβ-related differences in rates of PACC decline will become detectable after a longer interval.

There were also no significant relationships between baseline Aβ status and performance on the PACC or its components at phase two. This contrasts with previously published Insight 46 work which found an association between Aβ positivity and poorer PACC performance at phase one (Lu *et al.*, 2019), and might reflect a reduction in statistical power since there were fewer participants with longitudinal data. Consistent with this possibility, Aβ status was not related to PACC scores at phase one in post-hoc analyses using the smaller analytical sample of the current study (data not shown).

Although there were no significant effects of Aβ itself in the current study, relationships between rates of change in structural MRI measures and concurrent rates of PACC change and PACC performance at phase two were driven either primarily or entirely by changes in Aβ positive individuals. The interpretation of this finding is unclear, but one explanation may be that Aβ positivity is associated with faster progression of structural MRI changes (not necessarily across the whole sample, but in some individuals) and that this, in turn, leads to faster cognitive decline. Another, not mutually exclusive, interpretation is that the presence of Aβ pathology may make the brain more susceptible to the effects of neurodegeneration (or vice versa), as has been suggested elsewhere (Wirth, Madison, *et al.*, 2013; Wirth, Villeneuve, *et al.*, 2013).

The finding that rates of change in structural MRI measures was related to concurrent rates of PACC change and phase two PACC performance in cognitively normal Aβ positive individuals is consistent with other studies that have found associations between structural MRI changes in preclinical AD and cognition or future dementia (Rusinek *et al.*, 2003; Den Heijer *et al.*, 2006; Hua *et al.*, 2008; Henneman *et al.*, 2009; den Heijer *et al.*, 2010; Murphy *et al.*, 2010; Dickerson and Wolk, 2012; Vyhnalek *et al.*, 2014). As such, it adds to a growing body of evidence that suggests that a drug that could slow or stop progression of structural MRI changes in preclinical AD (for example, by targeting Aβ or vascular disease) would be expected to have beneficial, albeit possibly delayed, effects on cognition.

Another notable finding of this chapter was that higher childhood cognition and educational attainment were strong predictors of better cognitive performance at phase two, but they were generally not predictive of rates of change in cognition (except for the FNAME, on which higher education predicted marginally slower decline or greater

improvement). This suggests that higher childhood cognition and educational attainment may make individuals more resilient to dementia, at least in part, because individuals reach older age with a greater level of cognitive function from which to decline (Wilson *et al.*, 2009).

The observation that APOE ε4 carriers (versus non-carriers) had slower decline (or relatively greater improvement) on the FNAME, and better performance on LMDR at phase two is also interesting since it suggests that being an APOE ε4 carrier might confer some memory advantages, despite being a risk factor for AD. This is consistent with previously published Insight 46 analyses which detected superior visual working memory at phase one in APOE ε4 carriers, even in the presence of significant Aβ deposition (Lu *et al.*, 2021), and is in keeping with idea of antagonistic pleiotropy, whereby a gene might have both beneficial and detrimental effects, with the latter presenting later in life when the forces of natural selection decline (Byars and Voskarides, 2020).

Also in keeping with phase one analyses (Lu *et al.*, 2019), females performed better than males on all phase two measures. However, in the current analysis, they also had slightly greater LMDR decline (or relatively less improvement) between time-points. Females are known to be at higher risk of AD dementia, but the underlying mechanisms are not well understood (see Chapter Five). It may be that, despite having better cognition at baseline, females are more susceptible to the effects of neurodegenerative disease.

A key limitation of this study was that analyses were limited to two time-points of data. Since cognitive testing shows considerable variability within individuals, and between examiners, and is subject to practice and ceiling effects, incorporation of data from future time-points after a longer interval may provide greater certainty regarding cognitive

trajectories. Longer-term follow up is also needed to determine clinically relevant outcomes, such as the development of mild cognitive impairment or dementia.

Another limitation was that, due to loss of participants at follow-up, it was difficult to make conclusions about differences observed between the results presented here and phase one analyses (Lu *et al.*, 2019), noting, however, that findings were mostly consistent.

7.7. Conclusion

In summary, rates of change in structural MRI measures were associated with concurrent rates of change in cognition and subsequent cognitive performance in cognitively normal older adults, and this was driven either primarily or entirely by changes in Aβ positive individuals. These findings support the potential utility of structural MRI measures as surrogate endpoints in trials targeting the preclinical phase of AD.

8. SAMPLE SIZE REQUIREMENTS FOR PRECLINICAL TRIALS

8.1. Statement of contributions

I conceived and designed this study, with advice from Professor Jonathan Schott and Dr David Cash. Data collection and variable derivation were performed with assistance, as described in section 2.6. Dr David Cash provided the code for sample size calculations, which I adapted for the purposes of this analysis and ran. I interpreted the results.

8.2. Introduction

Another factor that is helpful in determining the utility of a biomarker as an outcome in trials is the sample size required to detect a treatment effect. An attractive biomarker requires a small sample size over a short time interval, since this is more cost- and time-effective. Several studies have reported sample size requirements for AD trials using structural MRI measures as outcomes (Fox *et al.*, 2000; Hua *et al.*, 2009, 2010; Beckett *et al.*, 2010; Ho *et al.*, 2010; Leung *et al.*, 2010a; Leung *et al.*, 2010b; McEvoy *et al.*, 2010; Holland, McEvoy and Dale, 2012; Cash *et al.*, 2015), including in the preclinical stages (Schott *et al.*, 2010; Andrews *et al.*, 2013), and they consistently provide lower smaller sample size estimates than traditional cognitive and functional endpoints (Jack *et al.*, 2004; Ridha *et al.*, 2008). However, there has been considerable variability in the sample sizes reported for each particular MRI measure, likely due to differences in methods and model assumptions used in their calculation (Ard and Edland, 2011).

A key consideration when estimating sample size requirements for preclinical AD trials using structural MRI measures as outcomes is whether to account for the changes

associated with ageing. If age-related effects are not accounted for in calculations, the treatment effect that can be detected with sufficient statistical power represents the absolute reduction of the rate of change in outcome towards zero (i.e., a 100% effective treatment would stop neurodegeneration completely) (Figure 8.1). If they are accounted for, then the treatment effect that can be detected represents the impact on excess neurodegeneration, above and beyond that experienced with normal ageing (Figure 8.1).

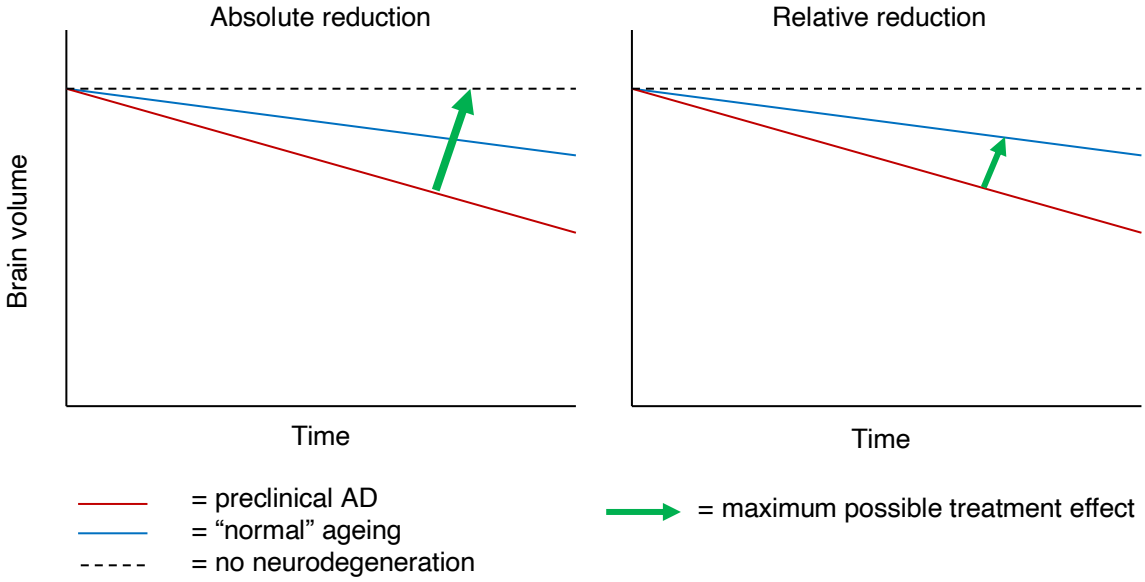

Figure 8.1. Diagram showing the difference between an absolute and relative reduction in rate of outcome change

On the face of it, the latter approach sounds more biologically plausible because it is likely unrealistic to expect a disease modifying therapy for AD to slow down the effects of ageing. However, the definition of normal ageing and its distinction from preclinical AD is not straightforward. In particular, there is no consensus regarding the level at which Aβ deposition is considered abnormal, and individuals with sub-threshold Aβ deposition may still be in the preclinical stages of AD (Mormino *et al.*, 2012; Landau, Horng and Jagust, 2018). Furthermore, comorbidities such as CVD are common in later life, and have significant effects on rates of neurodegeneration, even among apparently normal

individuals (see Chapters Five and Six). Thus, while sample size estimates that do not account for the effects of ageing might be underpowered to detect a change that is clinically relevant, those that do may be too conservative.

With that in mind, in this chapter, I used Insight 46 data to estimate sample sizes for a hypothetical trial of a putative disease-modifying therapy targeting cognitively normal Aβ positive individuals, both with and without adjustment for ageing (represented by changes in Aβ negative individuals). Sample sizes were estimated using structural MRI measures that showed significant differences in rates of change between Aβ positive and negative individuals in previous chapters as outcomes (i.e., whole brain, ventricular and total hippocampal volume rather than AD signature cortical thickness).

8.3. Methods

8.3.1. Determining variables

Baseline Aβ status and longitudinal changes in whole brain, ventricular and total hippocampal volume were determined as described in section 2.2.

8.3.2. Sample size calculations

Participants were excluded if they had incomplete T1 MRI or Aβ PET data or if they had dementia, mild cognitive impairment, or confounding brain disorders, as outlined in Chapter Three.

Sample sizes were estimated for a trial design with two visits, one pre-randomisation and another at the end of follow-up approximately two years later, assuming that a t-test would be used to compare the difference between treatment and placebo groups, and that there would be equal numbers of participants in each group. Estimates were calculated for a range of treatment effects, taking into consideration that a disease-modifying therapy would be expected to produce a smaller absolute than relative reduction. Results can be converted into sample sizes for any other treatment effect since sample sizes are inversely proportional to the square of the treatment effect. It was also assumed that the treatment would reduce the rate of change in the outcome without altering its variability.

To estimate sample sizes for a trial powered to detect a reduction in the rate of outcome change in Aβ positive individuals relative to the rate in Aβ negative individuals (i.e., accounting for the effects of ageing), effect sizes were first determined for each measure:

$$ES = (\mu_1 - \mu_0)/ \sigma_1$$

Where,

ES = effect size

μ_1 = mean annualised rate of change in the MRI measure in Aβ positive participants

μ_0 = mean annualised rate of change in the MRI measure in Aβ negative participants

σ_1 = standard deviation of annualised rate of change in the MRI measure in Aβ positive participants

Effect sizes were then converted into sample size estimates using the formula:

$$n = 2 \times [(u+v)/(TE \times ES)]^2$$

Where,

n = sample size required per treatment arm

u = 0.84 to provide 80% power

v = 1.96 to test at the 5% significance level

TE = treatment effect (e.g., for 10% slowing in rate of outcome change, TE = 0.1)

ES = effect size

These steps were repeated to obtain sample size estimates for a trial powered to detect an absolute reduction in rate of outcome change in Aβ positive individuals (i.e., without adjustment for ageing), except that effect size was calculated as ES = μ_1 / σ_1 instead.

Bias-corrected and accelerated confidence intervals were determined for each sample size estimate using bootstrap resampling methodology (100000 samples) (Efron, 1987). The confidence intervals were calculated on the effect sizes, since their distribution is likely to be more symmetric than that of the estimated sample sizes, and so their confidence intervals are likely to have better coverage properties (Frost *et al.*, 2017).

8.4. Results

Sample size estimates differed considerably depending on whether trials were powered to detect a relative reduction in rate of outcome change (i.e., as a proportion of the difference between Aβ positive and negative individuals; Table 8.1) or an absolute reduction in rate of outcome change (Table 8.2). Overall, measures of global volume change provided lower sample size estimates than hippocampal volume change, although it was not possible to calculate accurate estimates for a trial powered to detect a relative reduction in rate of whole brain atrophy because multiple samples produced

annualised rates of change that were not significantly different between Aβ positive and negative individuals.

Table 8.1. Sample sizes for a relative reduction in rate of change in the outcome

Treatment effect	Sample size required per treatment arm (95% bias corrected and accelerated confidence intervals)		
	Whole brain	Ventricles	Total hippocampus
20%	3881 (1146, ∞)	1856 (776, 12927)	4211 (1240, 349314)
40%	970 (286, ∞)	464 (194, 3232)	1053 (310, 87328)
60%	431 (127, ∞)	206 (86, 1436)	468 (138, 38813)
80%	243 (72, ∞)	116 (48, 808)	263 (78, 21832)
100%	155 (46, ∞)	74 (31, 517)	168 (50, 13973)

∞ = indicates that the confidence interval for the effect size crossed zero

Table 8.2. Sample sizes for an absolute reduction in rate of change in the outcome

Treatment effect*	Sample size required per treatment arm (95% bias corrected and accelerated confidence intervals)		
	Whole brain	Ventricles	Total hippocampus
10%	336 (212, 688)	479 (346, 758)	1284 (859, 2148)
20%	84 (53, 172)	120 (87, 189)	321 (215, 537)
30%	37 (24, 76)	53 (38, 84)	143 (95, 239)
40%	21 (13, 43)	30 (22, 47)	80 (54, 134)
50%	13 (8, 28)	19 (14, 30)	51 (34, 86)

*a disease-modifying therapy would be expected to produce a smaller absolute than relative reduction

8.5. Discussion

Key findings of this chapter were that measures of global volume change provided lower sample size estimates than hippocampal volume change, and that, as expected, sample size estimates differed considerably depending on whether a trial was powered to detect an absolute or relative reduction in rate of outcome change.

Calculations based on absolute reductions in rate of outcome change provided the lowest sample size estimates and tightest confidence intervals. This approach has been used in multiple other studies (Nestor *et al.*, 2008; Hua *et al.*, 2009; Beckett *et al.*, 2010; Cummings, 2010; Ho *et al.*, 2010; Vemuri *et al.*, 2010), including several from the Alzheimer's Disease Neuroimaging Initiative (ADNI). Whether it is realistic to estimate sample sizes in this way depends on whether a drug is expected to act solely on AD-related neurodegeneration or whether it might also influence changes related to ageing and other pathologies. In trials of Aβ-targeted therapies, the former is more likely.

Calculations based on relative reductions in rate of outcome change (assuming that the maximum possible treatment effect would be to reduce the rate to that observed in Aβ negative individuals) produced much larger sample size estimates with wider confidence intervals. For reasons discussed above, these estimates may be more plausible. However, it has been argued that this approach to adjustment for normal ageing is unfair (Barnes, Bartlett, *et al.*, 2013), since it assumes that Aβ negative individuals do not have biologically meaningful Aβ deposition and are free of other neurodegenerative diseases, which is usually not the case. Consequently, some researchers have proposed that sample sizes intermediate between the two approaches might be more appropriate (Ard and Edland, 2011).

It is also helpful to consider what a relative reduction equates to absolute terms. For example, if one assumes that an Aβ-lowering therapy given early enough in the disease course might reasonably lead to a 100% relative reduction in rate of outcome change (i.e., a slowing to the rate observed in Aβ negative individuals), this is equivalent to a 15%, 25% and 27% absolute reduction in rates of whole brain atrophy, ventricular expansion, and hippocampal atrophy, which would require 149, 77, and 176 participants per treatment arm. To put this into context, the A4 study – the first secondary prevention trial for sporadic AD – aims to recruit 1000 cognitively normal Aβ positive participants (500 per treatment arm), suggesting that it would be well powered to detect an attenuation in rates of atrophy even if the effect was considerably less than a complete reduction to "normal" ageing.

Notably, global volume changes such as ventricular expansion provided the lowest sample size estimates. This likely reflects the precision with which they can be measured, since sample sizes are critically dependent on the variability of the outcome. The ventricles have a central position in the brain, which makes them close to the isocentre of the scanner, meaning they are less susceptible to the effects of field inhomogeneities compared to regions that are further away (Schott *et al.*, 2005). Moreover, the high contrast between the cerebrospinal fluid in the ventricles and the surrounding brain tissue makes it easier to delineate their boundary, which facilitates automated segmentation (Nestor *et al.*, 2008). Despite being a more specific marker of AD-related neurodegeneration, hippocampal volume loss was the least efficient outcome, possibly because the location of the hippocampi and their less well-defined boundary make quantifying volume changes in this region more challenging, particularly in the early stages of disease when atrophy is mild.

Potential drawbacks of using ventricular expansion as an outcome include that it may be more susceptible to non-neurodegenerative factors, including dehydration, alcohol, drugs, and hydrocephalus (Zipursky, Lim and Pfefferbaum, 1989; Kempton *et al.*, 2009; Damasceno, 2015). Furthermore, it is possible that disease-modifying therapies might influence ventricular expansion to a different degree than other MRI measures, as observed in the AN1792 vaccination trial in patients with AD dementia (Fox *et al.*, 2005). Paradoxically, this trial detected increased rates of whole brain atrophy and ventricular expansion in antibody responders versus placebo patients, possibly due to Aβ removal and associated cerebral fluid shift. Similar findings have been detected in a number of other studies, as discussed elsewhere (Cash *et al.*, 2014). Whether this phenomenon also occurs in preclinical AD, the target group in the current analysis, is unknown.

An important limitation of the work in this chapter is that, given that only two time-points were available, calculations were limited to a trial analysis that would be performed using a simple t-test on rates of change between a scan at the beginning and end of a trial. Observational studies with more than two time-points available allow implementation of linear mixed effects models that can divide the variance of the outcome into two components: the between subject variability, representing the heterogeneity in the population, and the within subject variability, effectively representing the measurement error. The overall variance used in the effect size, and thus sample size, formula is now dependent on time, which provides an understanding of how extending trial duration might impact sample size estimates (Frost *et al.*, 2017). Future work incorporating data from additional time-points might therefore be informative; a phase three of Insight 46 is currently underway. A real trial analysis would also likely involve adjustment for covariates, which might reduce the variance of the outcome further (Schott *et al.*, 2010).

Another limitation relates to the generalisability of the findings. While a closely age-matched population-based sample imaged on a single scanner might represent the ideal scenario for a trial, it may not reflect reality. In practice, trials recruit participants of varying ages across multiple centres with different scanners and those targeting the preclinical phase might be biased towards individuals with subjective cognitive concerns or a family history of dementia. This might explain why rates of atrophy are higher, and also more variable, in the ADNI cohort compared to Insight 46 (Andrews *et al.*, 2013).

8.6. Conclusion

In conclusion, the findings in this chapter suggest that atrophy rates derived from MRI are plausible outcomes for preclinical AD trials, with the caveat that Insight 46 data and the assumptions made in this analysis may not fully emulate a real trial scenario.

9. GENERAL DISCUSSION

9.1. Overview

This thesis describes analyses based on Insight 46 data that were undertaken with the primary goal of investigating the determinants and consequences of longitudinal changes in brain structure quantified from MRI in cognitively normal older adults, as well as examining the feasibility and practicalities of recruiting a large representative elderly cohort to a longitudinal MRI study. The work was motivated by the recent shift towards secondary prevention of dementia, which requires better understanding of the processes that occur in the preclinical phase of AD, and the identification of sensitive biomarkers for assessing disease progression and response to therapies in trials. In this chapter, I summarise the key findings of this thesis and their implications. I then discuss the strengths and limitations of analyses, and potential directions for future research.

9.2. Summary of key findings

In the first data chapter (Chapter Three), I provide a detailed overview of the recruitment of a large elderly cohort to a longitudinal MRI study, including information about attrition between time-points and incomplete MRI data. The results highlight that the participants recruited to Insight 46 had lower rates of dementia and stroke than population estimates, and those who completed an MRI scan at both time-points had a lower WMH burden and body mass index on average that those who did not. Importantly, however, rates of Aβ positivity and APOE ε4 carriers were consistent with expected prevalences.

In Chapter Four, I consider an important logistical and ethical issue related to the use of MRI in research: how to deal with incidental findings. The results demonstrate the feasibility of implementing a pre-specified standardised protocol for detecting and managing incidental findings, and show that potentially serious or treatable abnormalities were identified on brain MRI in almost 5% of scanned participants. Cerebral aneurysms were the single most common abnormality, affecting around 1% of participants, and most findings were managed with observation, although a few participants went on to have surgical intervention.

In the subsequent two chapters (Chapters Five and Six), I address one of my main objectives, which was to better understand the factors that influence progression of structural brain changes on MRI in cognitively normal older adults. One of the key findings was that being Aβ positive and having greater WMHV at baseline were both related to faster subsequent rates of global and hippocampal volume loss, and these effects were independent and not interactive. Notably, Aβ positive participants had around 15% faster whole brain atrophy rates and 50% greater hippocampal atrophy rates than Aβ negative participants, and higher Aβ burden at baseline was related to disproportionate progressive hippocampal atrophy, despite participants being years before significant numbers are expected to develop dementia. Interestingly, however, rates of cortical thinning in regions known to be vulnerable in early AD (so-called AD signatures) were associated with greater WMHV at baseline, but not with baseline Aβ status or burden. Moreover, using an unbiased vertex-wise analysis, I show that there were no significant Aβ-related differences in rates of change in cortical thickness elsewhere in the brain.

In Chapter Seven, I assess the cognitive consequences of longitudinal changes in brain structure quantified from MRI. The results demonstrate that progression of structural MRI changes was related to concurrent rates of change in cognition and subsequent cognitive performance in cognitively normal older adults, and this was driven either primarily or entirely by changes in Aβ positive individuals.

In the final data chapter (Chapter Eight), I provide data on sample size requirements for hypothetical preclinical AD trials using structural MRI measures as outcomes, both with and without adjustment for ageing. Of note, I found that MRI measures of global volume loss may allow smaller sample sizes than MRI measures of hippocampal volume loss.

9.3. Implications

9.3.1. Pathophysiological processes underlying progression to dementia

The finding that Aβ positivity and greater Aβ burden were related to faster subsequent rates of global and hippocampal volume loss is supportive of the view that the presence of Aβ pathology in cognitively normal older adults is not a benign state and that it may represent an early stage of AD development. Longitudinal follow-up is needed to confirm whether Aβ positive individuals will eventually go on to develop dementia, but it is noteworthy that Aβ deposition was associated with disproportionate progressive hippocampal atrophy, since the hippocampi are known to be affected early in AD.

The lack of association between Aβ and rates of change in AD signature cortical thickness might seem to contradict this hypothesis. However, as discussed in Chapter Six, there are several questions that need to be addressed before this apparent

discrepancy can be resolved. One possibility may be that changes in cortical thickness do not become detectable on MRI until further along the AD continuum, perhaps because cortical thickness is more difficult to quantify or because it is not affected until later in the disease. Existing data from studies of presymptomatic AD mutation carriers suggest that this may not be the case (Ridha *et al.*, 2006; Weston *et al.*, 2016), but whether these findings can be translated to the more common sporadic form of AD is unclear.

Another consideration is the role of tau, which is thought to accumulate downstream of Aβ. Deposition of tau is initially limited to the temporal lobe, before becoming more diffusely spread throughout the cortex in the more advanced stages of AD (Braak *et al.*, 2006). While it was not possible to study its effects in this thesis, several lines of evidence from other studies suggest that tau is more closely related to neurodegeneration than Aβ (Arriagada *et al.*, 1992; Gómez-Isla *et al.*, 1997; Tarawneh *et al.*, 2015; La Joie *et al.*, 2020). Thus, it could be that Aβ does not contribute directly to neurodegeneration; rather, its effects may be mediated via tau pathology or related processes.

With regards to WMHs, the findings in this thesis suggest that they influence progression of neurodegeneration in brain areas that are vulnerable in AD, but that they do not interact with Aβ to increase neurodegeneration beyond their additive effect. As previously discussed, WMHs are presumed to occur as a result of hypertension-related arteriosclerosis (i.e., conventional CVD), although they can also develop in the context of cerebral amyloid angiopathy (CAA) and possibly Wallerian degeneration secondary to AD (McAleese *et al.*, 2017; Ferrer and Vidal, 2018). In previous Insight 46 analyses, greater WMHV was predicted by elevated blood pressure and cardiovascular risk scores (Lane *et al.*, 2019, 2020), whereas it had a weak relationship, if any at all, with Aβ burden (see Chapter Five). This suggests that the dominant mechanism underlying WMHs in

Insight 46 is conventional CVD, perhaps reflecting that CAA is uncommon or not very advanced in the Insight 46 sample. Consistent with this possibility, very few participants had cerebral microbleeds on MRI at baseline (n=10; unreported data).

Overall, the findings in this thesis, and in previous Insight 46 analyses (Lane *et al.*, 2019, 2020), suggest that Aβ and CVD predominantly act via distinct processes, and that early interventions targeting both potential pathways are likely to be important.

Lastly, while not a major focus of this thesis, the findings regarding APOE ε4 merit further discussion. There was a higher proportion of APOE ε4 carriers among Aβ positive than negative individuals, and relationships between APOE ε4 and faster atrophy rates were attenuated after accounting for Aβ status and – to a lesser degree – WMHV. These results are consistent with the well-reported association between APOE ε4 and Aβ deposition, which is thought to be due to the role of APOE ε4 in Aβ clearance from the brain (Yu, Tan and Hardy, 2014). APOE ε4 carriers also had faster rates of cortical thinning in the AD signature Mayo region, independent of Aβ status and WMHV, indicating that APOE ε4 may influence neurodegeneration via additional pathways, as has been shown elsewhere (Shi *et al.*, 2017). Verification of these results in larger samples is required. Nonetheless, these observations provide important insights into potential mechanisms underlying the relationship between APOE ε4 and dementia.

9.3.2. Trials targeting the preclinical phase of Alzheimer's disease

Knowledge regarding the recruitment of elderly cohort to a longitudinal MRI study should be relevant to future studies involving MRI, including prevention trials for AD. Information regarding rates of attrition and incomplete MRI data is useful because it can inform

decisions regarding the number of participants needed for a particular trial duration. This is important given than inadequate trial recruitment and retention has often been cited as a reason for the early termination or failure of previous AD trials (Gauthier *et al.*, 2016). An understanding of the nature and expected prevalence of incidental findings is also helpful since it should allow researchers to counsel participants regarding their likelihood and possible consequences as part of the consent process.

The analyses in this thesis also contribute important data regarding the utility of structural MRI measures as biomarkers for assessing treatment efficacy in preclinical AD. First, since one of the key requirements of a biomarker is that it is clearly different between individuals with and without disease, the results suggest that rates of global and hippocampal volume loss quantified using the boundary shift integral may be more useful than rates of AD signature cortical thinning quantified using Freesurfer. Furthermore, estimated sample sizes for preclinical AD trials, based on the effect size of the difference in biomarker between Aβ positive and negative individuals, highlight that global volume changes such as ventricular expansion may be more efficient as outcomes than hippocampal volume change, with the caveat that ventricular expansion may occur for reasons other than AD and may be influenced to a different extent by treatments.

The effects of WMHV on longitudinal changes in brain structure indicate that the presence of CVD may well confound detection of treatment effects in AD trials using structural MRI measures as outcomes, particularly in the preclinical phase of disease when the relative contribution of WMHV may be greater. This suggests that more efficient trial designs might be achieved by accounting for CVD, either by stratification of participants by CVD burden or enrolment of participants without significant CVD – not

ideal since it limits the generalisability of the trial findings and the number of eligible participants – or by adjusting for CVD burden in statistical analyses.

Lastly, the finding that progression of structural MRI changes was related to concurrent rates of change in cognition and subsequent cognitive performance in cognitively normal Aβ positive individuals is important, since it suggests that an AD therapy that modifies (slows or halts) MRI changes may have clinically relevant consequences.

Taken together, these findings support the potential utility of structural MRI measures as biomarkers for assessing treatment efficacy in trials targeting the preclinical phase of AD, particularly those that provide direct measures of volume change.

9.4. Strengths and limitations

A key strength of the Insight 46 study is the population-based nature of its sample, which means that findings detected in this thesis may be more generalisable than many other studies of preclinical AD, which often involve convenience samples and exclusion of participants with significant CVD (Weiner *et al.*, 2010). Insight 46 members were also almost identical in age and underwent imaging on a single scanner according to a standardised protocol, virtually eliminating these factors as potential confounders. These strengths are particularly advantageous when studying disease mechanisms but – as discussed in Chapter Eight – may not be representative of a typical clinical trial.

A significant limitation of the Insight 46 study was that all participants were white, reflecting the general population in post-war Britain, and so their findings may not be translatable to more ethnically or culturally diverse populations. They also had higher

socioeconomic position, educational attainment and self-rated health than the wider NSHD cohort (James *et al.*, 2018), and those with incomplete longitudinal MRI data were slightly older and had marginally higher body mass index and WMHV at baseline. This suggests that individuals with poorer health may have been underrepresented in the analyses, raising the possibility that effects may have been underestimated.

Another limitation is that without tau PET it was not possible to assess the contribution of tau pathology, nor was it possible to fully characterise participants according to the latest diagnostic criteria for preclinical AD, which require evidence of both Aβ and tau (Dubois *et al.*, 2016; Jack *et al.*, 2018a). However, for reasons previously discussed, many studies continue to draw conclusions about changes in preclinical AD from differences detected in cognitively normal Aβ positive individuals, and they are increasingly recognised as an important target population for secondary prevention trials (Sperling *et al.*, 2014).

9.5. Directions for future research

Work in this thesis was restricted to two commonly used techniques for quantifying longitudinal changes in brain structure from MRI, but it would be interesting to apply other approaches (such as the fluid registration method described in 1.3.3.3) to assess whether the effects detected in Chapter Five were driven by loss of grey or white matter volume and whether regions other than the hippocampus were disproportionately affected.

Use of advanced diffusion MRI approaches such as neurite orientation dispersion and density imaging would also be an exciting avenue for future research (Zhang *et al.*,

2012), since it would allow examination of longitudinal changes at the microstructural level, which may be a more sensitive marker of neurodegeneration (Parker *et al.*, 2018). Furthermore, assessment of longitudinal changes in hippocampal subfield volume might be informative (Iglesias *et al.*, 2016), since there is some evidence – mostly from cross-sectional studies – that the subfields are differentially influenced in AD and CVD (Wu *et al.*, 2008; Apostolova *et al.*, 2010; Carlesimo *et al.*, 2015; Parker *et al.*, 2019).

Once phase two Aβ and WMHV data are available, it will be important to extend the analyses in this thesis to assess how longitudinal changes in Aβ and WMHV relate to rates of neurodegeneration on MRI, which may provide further support for the independence of these processes. Comparing the effects of regional Aβ and WMHV (e.g., frontal versus parietal) or WMH subtypes (e.g., periventricular versus deep) might also be useful, since this could help to distinguish between different aetiologies (e.g., conventional SVD versus CAA), and might produce different results (Tosto *et al.*, 2015; Pålhaugen *et al.*, 2021).

Ultimately, it will be helpful to directly visualise these pathologies at post-mortem (almost 40% of participants have agreed to donate their brain to research) so that their underlying aetiology can be better determined. In the meantime, phase three of data collection has recently got started, which will enable assessment of whether the relationships examined in thesis change over time as some participants get closer to, or start to develop signs of, cognitive impairment or dementia. A sub-sample of participants will also undergo tau PET imaging, and several cardiovascular measures have been added to the battery of assessments performed, which may provide further mechanistic insights.

9.6. Concluding statement

In summary, the findings in this thesis provide valuable insight into the processes that might underlie progression to dementia in later life and contribute important data relevant to the utility of structural MRI measures as biomarkers of neurodegeneration in the preclinical phase of AD. Collectively, it is hoped that the work undertaken may help to inform future therapeutic strategies and trials aimed at preventing or delaying dementia, as well as highlighting several avenues for further research.

Acknowledgements

I am very grateful to the 1946 British birth cohort members, both for taking part in Insight 46 and for their commitments to research over the last eight decades. I would like to thank my supervisors – Jonathan Schott, Nick Fox, and David Cash – for their excellent guidance and support. I am especially grateful to my primary supervisor Jonathan Schott who has been incredibly encouraging throughout this experience and has helped make it a positive one, even amid a global pandemic. It has been an immense privilege to be a part of the Insight 46 team; without their dedication and hard work, this work would not have been possible. Will Coath, in particular, has provided endless advice and support regarding all things imaging-related and kept me sane when I encountered any hurdles. I am also very grateful to colleagues at the Dementia Research Centre, many of whom have become friends. Last, but not least, I would like to thank my family for their love and encouragement, especially my parents, my husband Matt, and daughter Violet.

Declaration Form 1

Referencing doctoral candidate's own published work(s) in thesis

1. **For a research manuscript that has already been published**
    a. **Where was the work published?**
    BMJ Open
    b. **Who published the work?**
    BMJ Publishing Group Ltd
    c. **When was the work published?**
    2019
    d. **Was the work subject to academic peer review?**
    YES
    e. **Have you retained the copyright for the work?**

2. **For multi-authored work, please give a statement of contribution covering all authors**

    Sarah Keuss conceived, designed, and conducted the analyses, with advice from Jonathan Schott. Sarah Keuss, Thomas Parker, Christopher Lane, Ashvini Keshavan, Sarah Buchanan, Sarah-Naomi James, Kirsty Lu and Jessica Collins contributed to data collection. Chandrashekar Hoskote and Sachit Shah reviewed the MRI scans for incidental findings. David Cash, Ian Malone, David Thomas, Anna Barnes, and Daniel Beasley developed or managed the imaging protocols and pipelines. Heidi Murray-Smith and Andrew Wong are study managers. Marcus Richards, Nick Fox, and Jonathan Schott are co-principal study investigators. Sarah Keuss drafted the initial manuscript. All authors critically revised the manuscript.

    For further description of contributions, see section 2.6. of this thesis.

3. **In which chapter(s) of your thesis can this material be found?**
    Chapter Four

4. **Candidate's e-signature:**
    Date: 01/04/2022

5. **Supervisor/senior author(s) e-signature:**
    Date: 01/04/2022

Declaration Form 2

Referencing doctoral candidate's own published work(s) in thesis

1. **For a research manuscript that has already been published**
    a. **Where was the work published?**
    Neurology
    b. **Who published the work?**
    Wolters Kluwer
    c. **When was the work published?**
    2022
    d. **Was the work subject to academic peer review?**
    YES
    e. **Have you retained the copyright for the work?**

2. **For multi-authored work, please give a statement of contribution covering all authors**

    Sarah Keuss conceived, designed, and conducted the analyses, with advice from Jonathan Schott, Nick Fox, and Josephine Barnes, and statistical support from Jennifer Nicholas and Teresa Poole. Sarah Keuss, Thomas Parker, Christopher Lane, Ashvini Keshavan, Sarah Buchanan, Aaron Wagen, Mathew Storey, Matthew Harris, Sarah-Naomi James, Kirsty Lu, and Rebecca Street contributed to data collection and variable derivation. William Coath performed image quality control and analysis. David Cash, Ian Malone, David Thomas, Josephine Barnes, Carole Sudre and John Dickson developed or managed the imaging protocols and pipelines. Heidi Murray-Smith and Andrew Wong are study managers. Tamar Freiberger coordinated study visits. Marcus Richards, Nick Fox, and Jonathan Schott are co-principal study investigators. Sarah Keuss drafted the initial manuscript. All authors critically revised the manuscript.

    For further description of contributions, see section 2.6. of this thesis.

3. **In which chapter(s) of your thesis can this material be found?**
    Chapter Five

4. **Candidate's e-signature:**
    Date: 27/04/2022

5. **Supervisor/senior author(s) e-signature:**
    Date: 27/04/2022

Publications

Publications arising directly from work in this thesis

Papers

Keuss SE, Parker TD, Lane CA, et al. Incidental findings on brain imaging and blood tests: results from the first phase of Insight 46, a prospective observational substudy of the 1946 British birth cohort. BMJ Open 2019;9:e029502. doi: 10.1136/bmjopen-2019-029502.

Keuss SE, Coath W, Nicholas JM, et al. Associations of β-amyloid and vascular burden with rates of neurodegeneration in cognitively normal members of the 1946 British birth cohort. Neurology 2022;99(2):e129-e141. doi: https://doi.org/10.1212/WNL.0000000000200524.

Abstracts

Keuss SE, Parker TD, Lane CA, et al., Incidental Findings on Brain Magnetic Resonance Imaging. Neurology 2020;94(15).

Keuss SE, Poole T, Cash DM, et al., Cerebral amyloid and white matter hyperintensity volume are independently associated with rates of cerebral atrophy in Insight 46, a sub-study of the 1946 British birth cohort. Alzheimer's and dementia 2020;16(S4). doi.org/10.1002/alz.044924.

Other publications contributed to during this thesis

Papers based on Insight 46 data

Wagen AZ, Coath W, Keshavan A, James, S-N, Parker TD, Lane CA, Buchanan SM, **Keuss SE**, Storey M, Lu K, Macdougall A, Murray-Smith H, Freiberger T, Cash DM, Malone IB, Barnes J, Sudre CH, Wong A, Pavisic I, Street R, Crutch SJ, Escott-Price V, Leonenko G, Zetterberg H, Wellington H, Heslegrave A, Barkhof F, Richards M, Fox NC, Cole JH, Schott JM. Life course, genetic, and neuropathological associations with brain age in the 1946 British Birth Cohort: a population-based study. Lancet Healthy Longev. 2022. doi: 10.1016/S2666-7568(22)00167-2

Dissociable effects of *APOE*-ε4 and β-amyloid pathology on visual working memory. Lu K, Nicholas JM, Pertzov Y, Grogan J, Husain M, Pavisic IM, James SN, Parker TD, Lane CA, Keshavan A, **Keuss SE**, Buchanan SM, Murray-Smith H, Cash DM, Malone IB, Sudre CH, Coath W, Wong A, Henley SMD, Fox NC, Richards M, Schott JM, Crutch SJ. Nat Aging. 2021;1(11):1002-1009. doi: 10.1038/s43587-021-00117-4.

Pavisic IM, Lu K, **Keuss SE**, James SN, Lane CA, Parker TD, Keshavan A, Buchanan SM, Murray-Smith H, Cash DM, Coath W, Wong A, Fox NC, Crutch SJ, Richards M, Schott JM. Subjective cognitive complaints at age 70: associations with amyloid and mental health. J Neurol Neurosurg Psychiatry. 2021;92(11):1215-1221. doi: 10.1136/jnnp-2020-325620.

Lane CA, Barnes J, Nicholas JM, Baker JW, Sudre CH, Cash DM, Parker TD, Malone IB, Lu K, James SN, Keshavan A, Buchanan S, **Keuss S**, Murray-Smith H, Wong A,

Gordon E, Coath W, Modat M, Thomas D, Hardy R, Richards M, Fox NC, Schott JM. Investigating the relationship between BMI across adulthood and late life brain pathologies. Alzheimers Res Ther. 2021;13(1):91. doi: 10.1186/s13195-021-00830-7.

James SN, Nicholas JM, Lane CA, Parker TD, Lu K, Keshavan A, Buchanan SM, **Keuss SE**, Murray-Smith H, Wong A, Cash DM, Malone IB, Barnes J, Sudre CH, Coath W, Prosser L, Ourselin S, Modat M, Thomas DL, Cardoso J, Heslegrave A, Zetterberg H, Crutch SJ, Schott JM, Richards M, Fox NC. A population-based study of head injury, cognitive function and pathological markers. Ann Clin Transl Neurol. 2021 Apr;8(4):842-856. doi: 10.1002/acn3.51331.

Lu K, Nicholas JM, Weston PSJ, Stout JC, O'Regan AM, James SN, Buchanan SM, Lane CA, Parker TD, **Keuss SE**, Keshavan A, Murray-Smith H, Cash DM, Sudre CH, Malone IB, Coath W, Wong A, Richards M, Henley SMD, Fox NC, Schott JM, Crutch SJ. Visuomotor integration deficits are common to familial and sporadic preclinical Alzheimer's disease. Brain Commun. 2021;3(1):fcab003. doi: 10.1093/braincomms/fcab003.

Keshavan A, Wellington H, Chen Z, Khatun A, Chapman M, Hart M, Cash DM, Coath W, Parker TD, Buchanan SM, **Keuss SE**, Harris MJ, Murray-Smith H, Heslegrave A, Fox NC, Zetterberg H, Schott JM. Concordance of CSF measures of Alzheimer's pathology with amyloid PET status in a preclinical cohort: A comparison of Lumipulse and established immunoassays. Alzheimers Dement (Amst). 2021;13(1):e12131. doi: 10.1002/dad2.12131.

Keshavan A, Pannee J, Karikari TK, Rodriguez JL, Ashton NJ, Nicholas JM, Cash DM, Coath W, Lane CA, Parker TD, Lu K, Buchanan SM, **Keuss SE**, James SN, Murray-Smith H, Wong A, Barnes A, Dickson JC, Heslegrave A, Portelius E, Richards M, Fox NC, Zetterberg H, Blennow K, Schott JM. Population-based blood screening for preclinical Alzheimer's disease in a British birth cohort at age 70. Brain. 2021;144(2):434-449. doi: 10.1093/brain/awaa403.

Lu K, Nicholas JM, James SN, Lane CA, Parker TD, Keshavan A, **Keuss SE**, Buchanan SM, Murray-Smith H, Cash DM, Sudre CH, Malone IB, Coath W, Wong A, Henley SMD, Fox NC, Richards M, Schott JM, Crutch SJ. Increased variability in reaction time is associated with amyloid beta pathology at age 70. Alzheimers Dement (Amst). 2020;12(1):e12076. doi: 10.1002/dad2.12076.

Buchanan SM, Parker TD, Lane CA, Keshavan A, **Keuss SE**, Lu K, James SN, Murray-Smith H, Wong A, Nicholas J, Cash DM, Malone IB, Coath W, Thomas DL, Sudre C, Fox NC, Richards M, Schott JM. Olfactory testing does not predict β-amyloid, MRI measures of neurodegeneration or vascular pathology in the British 1946 birth cohort. J Neurol. 2020;267(11):3329-3336. doi: 10.1007/s00415-020-10004-4.

Parker TD, Cash DM, Lane CA, Lu K, Malone IB, Nicholas JM, James SN, Keshavan A, Murray-Smith H, Wong A, Buchanan SM, **Keuss SE**, Sudre CH, Thomas DL, Crutch SJ, Fox NC, Richards M, Schott JM. Amyloid β influences the relationship between cortical thickness and vascular load. Alzheimers Dement (Amst). 2020;12(1):e12022. doi: 10.1002/dad2.12022.

Parker T, Cash DM, Lane C, Lu K, Malone IB, Nicholas JM, James S, Keshavan A, Murray-Smith H, Wong A, Buchannan S, **Keuss S**, Sudre CH, Thomas D, Crutch S, Bamiou DE, Warren JD, Fox NC, Richards M, Schott JM. Pure tone audiometry and cerebral pathology in healthy older adults. J Neurol Neurosurg Psychiatry. 2020; 91(2):172-176. doi: 10.1136/jnnp-2019-321897.

Lane CA, Barnes J, Nicholas JM, Sudre CH, Cash DM, Malone IB, Parker TD, Keshavan A, Buchanan SM, **Keuss SE**, James SN, Lu K, Murray-Smith H, Wong A, Gordon E, Coath W, Modat M, Thomas D, Richards M, Fox NC, Schott JM. Associations Between Vascular Risk Across Adulthood and Brain Pathology in Late Life: Evidence From a British Birth Cohort. JAMA Neurol. 2020;77(2):175-183. doi: 10.1001/jamaneurol.2019.3774.

Lu K, Nicholas JM, Collins JD, James SN, Parker TD, Lane CA, Keshavan A, **Keuss SE**, Buchanan SM, Murray-Smith H, Cash DM, Sudre CH, Malone IB, Coath W, Wong A, Henley SMD, Crutch SJ, Fox NC, Richards M, Schott JM. Cognition at age 70: Life course predictors and associations with brain pathologies. Neurology. 2019;93(23):e2144-e2156. doi: 10.1212/WNL.0000000000008534.

Parker TD, Cash DM, Lane CAS, Lu K, Malone IB, Nicholas JM, James SN, Keshavan A, Murray-Smith H, Wong A, Buchanan SM, **Keuss SE**, Sudre CH, Modat M, Thomas DL, Crutch SJ, Richards M, Fox NC, Schott JM. Hippocampal subfield volumes and pre-clinical Alzheimer's disease in 408 cognitively normal adults born in 1946. PLoS One. 2019;14(10):e0224030. doi: 10.1371/journal.pone.0224030.

Lane CA, Barnes J, Nicholas JM, Sudre CH, Cash DM, Parker TD, Malone IB, Lu K, James SN, Keshavan A, Murray-Smith H, Wong A, Buchanan SM, **Keuss SE**, Gordon E, Coath W, Barnes A, Dickson J, Modat M, Thomas D, Crutch SJ, Hardy R, Richards M, Fox NC, Schott JM. Associations between blood pressure across adulthood and late-life brain structure and pathology in the neuroscience substudy of the 1946 British birth cohort (Insight 46): an epidemiological study. Lancet Neurol. 2019;18(10):942-952. doi: 10.1016/S1474-4422(19)30228-5.

James SN, Lane CA, Parker TD, Lu K, Collins JD, Murray-Smith H, Byford M, Wong A, Keshavan A, Buchanan S, **Keuss SE**, Kuh D, Fox NC, Schott JM, Richards M. Using a birth cohort to study brain health and preclinical dementia: recruitment and participation rates in Insight 46. BMC Res Notes. 2018;11(1):885. doi: 10.1186/s13104-018-3995-0

Other work

Keuss SE, Bowen J, Schott JM. Looking beyond the eyes: visual impairment in posterior cortical atrophy. Lancet. 2019;394(10203):1055. doi: 10.1016/S0140-6736(19)31818-5.

References

Aisen, P. S., Cummings, J. and Schneider, L. S. (2012) 'Symptomatic and nonamyloid/tau based pharmacologic treatment for Alzheimer disease.', *Cold Spring Harbor perspectives in medicine*, 2(3), p. a006395. doi: 10.1101/cshperspect.a006395.

Alawode, D. O. T. *et al.* (2021) 'Transitioning from cerebrospinal fluid to blood tests to facilitate diagnosis and disease monitoring in Alzheimer's disease', *Journal of Internal Medicine*, 290(3), pp. 583–601. doi: 10.1111/joim.13332.

Althouse, A. D. (2016) 'Adjust for Multiple Comparisons? It's Not That Simple', *Ann Thorac Surg*, 101, pp. 1644–45. doi: 10.1016/j.athoracsur.2015.11.024.

Altmann, A. *et al.* (2014) 'Sex modifies the APOE -related risk of developing Alzheimer disease', *Annals of Neurology*, 75(4), pp. 563–573. doi: 10.1002/ana.24135.

Andrews, K. A. *et al.* (2013) 'Atrophy Rates in Asymptomatic Amyloidosis: Implications for Alzheimer Prevention Trials', *PLoS ONE*, 8(3). doi: 10.1371/journal.pone.0058816.

Apostolova, L. G. *et al.* (2010) 'Subregional hippocampal atrophy predicts Alzheimer's dementia in the cognitively normal', *Neurobiology of Aging*, 31(7), pp. 1077–1088. doi: 10.1016/j.neurobiolaging.2008.08.008.

Ard, M. C. and Edland, S. D. (2011) 'Power Calculations for Clinical Trials in Alzheimer's Disease', *Journal of Alzheimer's Disease*. Edited by J. W. Ashford et al., 26(s3), pp. 369–377. doi: 10.3233/JAD-2011-0062.

Armstrong, N. M. *et al.* (2019) 'Sex differences in the association between amyloid and longitudinal brain volume change in cognitively normal older adults', *NeuroImage: Clinical*, 22. doi: 10.1016/j.nicl.2019.101769.

Aron, A. R. *et al.* (2004) 'A componential analysis of task-switching deficits associated with lesions of left and right frontal cortex', *Brain*, 127(7), pp. 1561–1573. doi: 10.1093/brain/awh169.

Arriagada, P. V. *et al.* (1992) 'Neurofibrillary tangles but not senile plaques parallel duration and severity of Alzheimer's disease', *Neurology*, 42(3), pp. 631–631. doi: 10.1212/WNL.42.3.631.

Ashburner, J. *et al.* (2003) 'Computer-assisted imaging to assess brain structure in healthy and diseased brains.', *The Lancet Neurology*, 2(2), pp. 79–88. doi: 10.1016/S1474-4422(03)00304-1.

Attems, J. and Jellinger, K. A. (2014) 'The overlap between vascular disease and Alzheimer's disease - lessons from pathology', *BMC Medicine*, 12(1), p. 206. doi: 10.1186/s12916-014-0206-2.

Bacioglu, M. *et al.* (2016) 'Neurofilament Light Chain in Blood and CSF as Marker of Disease Progression in Mouse Models and in Neurodegenerative Diseases', *Neuron*, 91(1), pp. 56–66. doi: 10.1016/j.neuron.2016.05.018.

Bakkour, A., Morris, J. C. and Dickerson, B. C. (2009) 'The cortical signature of prodromal AD: Regional thinning predicts mild AD dementia', *Neurology*, 72(12), pp. 1048–1055. doi: 10.1212/01.wnl.0000340981.97664.2f.

Barnes, J. *et al.* (2010) 'Head size, age and gender adjustment in MRI studies: A necessary nuisance?', *NeuroImage*, 53(4), pp. 1244–1255. doi: 10.1016/j.neuroimage.2010.06.025.

Barnes, J., Bartlett, J. W., *et al.* (2013) 'Targeted Recruitment Using Cerebrospinal Fluid Biomarkers: Implications for Alzheimer's Disease Therapeutic Trials', *Journal of*

Alzheimer's Disease, 34(2), pp. 431–437. doi: 10.3233/JAD-121936.

Barnes, J., Carmichael, O. T., *et al.* (2013) 'Vascular and Alzheimer's disease markers independently predict brain atrophy rate in Alzheimer's Disease Neuroimaging Initiative controls', *Neurobiology of Aging*, 34(8), pp. 1996–2002. doi: 10.1016/j.neurobiolaging.2013.02.003.

Barnes, L. *et al.* (2005) 'Sex differences in the clinical manifestations of Alzheimer disease pathology', *Archives of general psychiatry*, 62(6). doi: 10.1001/ARCHPSYC.62.6.685.

Bateman, R. J. *et al.* (2011) 'Autosomal-dominant Alzheimer's disease: a review and proposal for the prevention of Alzheimer's disease.', *Alzheimer's research & therapy*, 3(1), p. 1. doi: 10.1186/alzrt59.

Becker, J. A. *et al.* (2011) 'Amyloid-β associated cortical thinning in clinically normal elderly', *Annals of Neurology*. Ann Neurol, 69(6), pp. 1032–1042. doi: 10.1002/ana.22333.

Beckett, L. A. *et al.* (2010) 'The Alzheimer's Disease Neuroimaging Initiative: Annual change in biomarkers and clinical outcomes', *Alzheimer's & Dementia*, 6(3), pp. 257–264. doi: 10.1016/j.jalz.2010.03.002.

Benzinger, T. L. S. *et al.* (2013) 'Regional variability of imaging biomarkers in autosomal dominant Alzheimer's disease', *Proceedings of the National Academy of Sciences*, 110(47). doi: 10.1073/pnas.1317918110.

Berg, L. *et al.* (1998) 'Clinicopathologic Studies in Cognitively Healthy Aging and Alzheimer Disease', *Archives of Neurology*, 55(3), p. 326. doi: 10.1001/archneur.55.3.326.

Berlot, R. *et al.* (2014) 'CSF contamination contributes to apparent microstructural alterations in mild cognitive impairment', *NeuroImage*, 92, pp. 27–35. doi: 10.1016/j.neuroimage.2014.01.031.

Bertheau, R. C. *et al.* (2016) 'Management of Incidental Findings in the German National Cohort', in *Incidental radiological findings*, pp. 57–70. doi: 10.1007/174_2016_63.

Bertram, L. *et al.* (2008) 'Genome-wide Association Analysis Reveals Putative Alzheimer's Disease Susceptibility Loci in Addition to APOE', *The American Journal of Human Genetics*, 83(5), pp. 623–632. doi: 10.1016/j.ajhg.2008.10.008.

Bitar, R. *et al.* (2006) 'MR Pulse Sequences: What Every Radiologist Wants to Know but Is Afraid to Ask', *RadioGraphics*, 26(2), pp. 513–537. doi: 10.1148/rg.262055063.

Bobinski, M. *et al.* (1999) 'The histological validation of post mortem magnetic resonance imaging-determined hippocampal volume in Alzheimer's disease', *Neuroscience*, 95(3), pp. 721–725. doi: 10.1016/S0306-4522(99)00476-5.

de Boer, A. W. *et al.* (2018) 'Incidental findings in research: A focus group study about the perspective of the research participant', *Journal of Magnetic Resonance Imaging*, 47(1), pp. 230–237. doi: 10.1002/jmri.25739.

Booth, T. C. *et al.* (2012) 'Management of incidental findings during imaging research in "healthy" volunteers: Current UK practice', *British Journal of Radiology*, 85(1009), pp. 11–21. doi: 10.1259/bjr/73283917.

Bos, D. *et al.* (2016) 'Prevalence, clinical management, and natural course of incidental findings on brain MR images: The population-based Rotterdam scan study', *Radiology*, pp. 507–515. doi: 10.1148/radiol.2016160218.

Bos, I. *et al.* (2017) 'Cerebrovascular and amyloid pathology in predementia stages: The relationship with neurodegeneration and cognitive decline', *Alzheimer's Research and Therapy*, 9(1). doi: 10.1186/s13195-017-0328-9.

Bourgeat, P. *et al.* (2010) 'β-Amyloid burden in the temporal neocortex is related to hippocampal atrophy in elderly subjects without dementia', *Neurology*, 74(2), pp. 121–127. doi: 10.1212/WNL.0b013e3181c918b5.

Braak, H. *et al.* (2006) 'Staging of Alzheimer disease-associated neurofibrillary pathology using paraffin sections and immunocytochemistry', *Acta Neuropathologica*, 112(4), pp. 389–404. doi: 10.1007/s00401-006-0127-z.

Braak, H. and Braak, E. (1991) 'Neuropathological stageing of Alzheimer-related changes', *Acta Neuropathologica*, 82(4), pp. 239–259. doi: 10.1007/BF00308809.

Bransby, L. *et al.* (2019) 'Sensitivity of a Preclinical Alzheimer's Cognitive Composite (PACC) to amyloid β load in preclinical Alzheimer's disease', *Journal of Clinical and Experimental Neuropsychology*, 41(6), pp. 591–600. doi: 10.1080/13803395.2019.1593949.

Brendel, M. *et al.* (2015) 'Improved longitudinal [18F]-AV45 amyloid PET by white matter reference and VOI-based partial volume effect correction', *NeuroImage*, 108, pp. 450–459. doi: 10.1016/j.neuroimage.2014.11.055.

Brickman, A. M. (2013) 'Contemplating Alzheimer's disease and the contribution of white matter hyperintensities', *Current Neurology and Neuroscience Reports*, 13(12). doi: 10.1007/s11910-013-0415-7.

Brilleman, S. L., Pachana, N. A. and Dobson, A. J. (2010) 'The impact of attrition on the representativeness of cohort studies of older people', *BMC Medical Research*

Methodology, 10(1), p. 71. doi: 10.1186/1471-2288-10-71.

Brodaty, H. *et al.* (2014) 'Influence of population versus convenience sampling on sample characteristics in studies of cognitive aging', *Annals of Epidemiology*, 24(1), pp. 63–71. doi: 10.1016/j.annepidem.2013.10.005.

Buchman, A. S. *et al.* (2005) 'Change in body mass index and risk of incident Alzheimer disease', *Neurology*, 65(6), pp. 892–897. doi: 10.1212/01.wnl.0000176061.33817.90.

Burgos, N. *et al.* (2014) 'Attenuation correction synthesis for hybrid PET-MR scanners: Application to brain studies', *IEEE Transactions on Medical Imaging*, 33(12), pp. 2332–2341. doi: 10.1109/TMI.2014.2340135.

Burgos, N. *et al.* (2015) 'CT synthesis in the head & neck region for PET/MR attenuation correction: an iterative multi-atlas approach', *EJNMMI Physics*. Springer Nature, 2(S1). doi: 10.1186/2197-7364-2-s1-a31.

Byars, S. G. and Voskarides, K. (2020) 'Antagonistic Pleiotropy in Human Disease', *Journal of Molecular Evolution*, 88(1), pp. 12–25. doi: 10.1007/s00239-019-09923-2.

Byrum, C. E. *et al.* (1996) 'Accuracy and reproducibility of brain and tissue volumes using a magnetic resonance segmentation method', *Psychiatry Research - Neuroimaging*, 67(3), pp. 215–234. doi: 10.1016/0925-4927(96)02790-4.

Calderon-Garcidueñas, A. L. and Duyckaerts, C. (2018) 'Alzheimer disease', *Handbook of Clinical Neurology*, 145, pp. 325–337. doi: 10.1016/B978-0-12-802395-2.00023-7.

Calsolaro, V. and Edison, P. (2016) 'Neuroinflammation in Alzheimer's disease: Current evidence and future directions', *Alzheimer's & Dementia*, 12(6), pp. 719–732.

doi: 10.1016/j.jalz.2016.02.010.

Cano, S. J. *et al.* (2010) 'The ADAS-cog in Alzheimer's disease clinical trials: psychometric evaluation of the sum and its parts.', *Journal of neurology, neurosurgery, and psychiatry*, 81(12), pp. 1363–8. doi: 10.1136/jnnp.2009.204008.

Cardenas, V. A. *et al.* (2012) 'Associations Among Vascular Risk Factors, Carotid Atherosclerosis, and Cortical Volume and Thickness in Older Adults', *Stroke*, 43(11), pp. 2865–2870. doi: 10.1161/STROKEAHA.112.659722.

Cardoso, M. J. *et al.* (2013) 'STEPS: Similarity and Truth Estimation for Propagated Segmentations and its application to hippocampal segmentation and brain parcelation', *Medical Image Analysis*, 17(6), pp. 671–684. doi: 10.1016/j.media.2013.02.006.

Cardoso, M. J. *et al.* (2015) 'Geodesic Information Flows: Spatially-Variant Graphs and Their Application to Segmentation and Fusion', *IEEE Transactions on Medical Imaging*, 34(9), pp. 1976–1988. doi: 10.1109/TMI.2015.2418298.

Carlesimo, G. A. *et al.* (2015) 'Atrophy of presubiculum and subiculum is the earliest hippocampal anatomical marker of Alzheimer's disease', *Alzheimer's & Dementia: Diagnosis, Assessment & Disease Monitoring*, 1(1), pp. 24–32. doi: 10.1016/j.dadm.2014.12.001.

Carmona, S., Hardy, J. and Guerreiro, R. (2018) 'The genetic landscape of Alzheimer disease', in *Handbook of Clinical Neurology*, pp. 395–408. doi: 10.1016/B978-0-444-64076-5.00026-0.

Carrillo, M. C. *et al.* (2013) 'Global standardization measurement of cerebral spinal fluid for Alzheimer's disease: An update from the Alzheimer's Association Global Biomarkers Consortium', *Alzheimer's & Dementia*, 9(2), pp. 137–140. doi:

10.1016/j.jalz.2012.11.003.

Cash, D. M. *et al.* (2013) 'The pattern of atrophy in familial alzheimer disease: Volumetric MRI results from the DIAN study', *Neurology*, 81(16), pp. 1425–1433. doi: 10.1212/WNL.0b013e3182a841c6.

Cash, D. M. *et al.* (2014) 'Imaging endpoints for clinical trials in Alzheimer's disease.', *Alzheimer's research & therapy*, 6(9), p. 87. doi: 10.1186/s13195-014-0087-9.

Cash, D. M. *et al.* (2015) 'Assessing atrophy measurement techniques in dementia: Results from the MIRIAD atrophy challenge', *NeuroImage*, 123, pp. 149–164. doi: 10.1016/j.neuroimage.2015.07.087.

Castellano, J. M. *et al.* (2011) 'Human apoE isoforms differentially regulate brain amyloid-β peptide clearance.', *Science translational medicine*, 3(89), p. 89ra57. doi: 10.1126/scitranslmed.3002156.

Chatfield, M. D., Brayne, C. E. and Matthews, F. E. (2005) 'A systematic literature review of attrition between waves in longitudinal studies in the elderly shows a consistent pattern of dropout between differing studies', *Journal of Clinical Epidemiology*, 58(1), pp. 13–19. doi: 10.1016/j.jclinepi.2004.05.006.

Chen, K. *et al.* (2015) 'Improved power for characterizing longitudinal amyloid-βPET changes and evaluating amyloid-modifying treatments with a cerebral white matter reference region', *Journal of Nuclear Medicine*, 56(4), pp. 560–566. doi: 10.2967/jnumed.114.149732.

Chen, M. (2015) 'The Maze of APP Processing in Alzheimerâ€™s Disease: Where Did We Go Wrong in Reasoning?', *Frontiers in Cellular Neuroscience*, 9. doi: 10.3389/fncel.2015.00186.

Cherbuin, N. *et al.* (2010) 'Mild cognitive disorders are associated with different patterns of brain asymmetry than normal aging: The PATH through life study', *Frontiers in Psychiatry*, 1(MAY). doi: 10.3389/fpsyt.2010.00011.

Chételat, G. *et al.* (2010) 'Larger temporal volume in elderly with high versus low beta-amyloid deposition', *Brain*, 133(11), pp. 3349–3358. doi: 10.1093/brain/awq187.

Chételat, G. *et al.* (2012) 'Accelerated cortical atrophy in cognitively normal elderly with high β-amyloid deposition', *Neurology*, 78(7), pp. 477–484. doi: 10.1212/WNL.0b013e318246d67a.

Chu, C.-S. *et al.* (2014) 'APOE ε4 polymorphism and cognitive deficit among the very old Chinese veteran men without dementia', *Neuroscience Letters*, 576, pp. 17–21. doi: 10.1016/j.neulet.2014.05.046.

Chui, H. C. *et al.* (2011) 'Vascular risk factors and Alzheimer's disease: are these risk factors for plaques and tangles or for concomitant vascular pathology that increases the likelihood of dementia? An evidence-based review', *Alzheimer's Research & Therapy*, 3(6), p. 36. doi: 10.1186/alzrt98.

Coughlan, A. and Hollows, S. (1985) *The adult memory and information processing battery: test manual*. Psychology Dept, St James' Hospital.

Crum, W. R., Scahill, R. I. and Fox, N. C. (2001) 'Automated hippocampal segmentation by regional fluid registration of serial MRI: Validation and application in Alzheimer's disease', *NeuroImage*, 13(5), pp. 847–855. doi: 10.1006/nimg.2001.0744.

Crutch, S. J. *et al.* (2012) 'Posterior cortical atrophy.', *The Lancet. Neurology*, 11(2), pp. 170–8. doi: 10.1016/S1474-4422(11)70289-7.

Cummings, J. L. (2010) 'Integrating ADNI results into Alzheimer's disease drug development programs', *Neurobiology of Aging*, 31(8), pp. 1481–1492. doi: 10.1016/j.neurobiolaging.2010.03.016.

Currie, S. *et al.* (2013) 'Understanding MRI: basic MR physics for physicians', *Postgraduate Medical Journal*, 89(1050), pp. 209–223. doi: 10.1136/postgradmedj-2012-131342.

D'Agostino, R. B. *et al.* (2008) 'General cardiovascular risk profile for use in primary care: The Framingham heart study', *Circulation*, 117(6), pp. 743–753. doi: 10.1161/CIRCULATIONAHA.107.699579.

Dale, A. M., Fischl, B. and Sereno, M. I. (1999) 'Cortical Surface-Based Analysis: I. Segmentation and Surface Reconstruction', *NeuroImage*, 9(2), pp. 179–194. doi: 10.1006/NIMG.1998.0395.

Damasceno, B. P. (2015) 'Neuroimaging in normal pressure hydrocephalus', *Dementia & Neuropsychologia*, 9(4), pp. 350–355. doi: 10.1590/1980-57642015DN94000350.

Desikan, R. S. *et al.* (2006) 'An automated labeling system for subdividing the human cerebral cortex on MRI scans into gyral based regions of interest', *NeuroImage*, 31(3), pp. 968–980. doi: 10.1016/j.neuroimage.2006.01.021.

Deture, M. A. and Dickson, D. W. (2019) 'The neuropathological diagnosis of Alzheimer's disease', *Molecular Neurodegeneration*, pp. 1–18. doi: 10.1186/s13024-019-0333-5.

Devenney, E. and Hodges, J. R. (2017) 'The Mini-Mental State Examination: pitfalls and limitations.', *Practical neurology*, 17(1), pp. 79–80. doi: 10.1136/practneurol-2016-001520.

Dewey, M., Schink, T. and Dewey, C. F. (2007) 'Claustrophobia during magnetic resonance imaging: Cohort study in over 55,000 patients', *Journal of Magnetic Resonance Imaging*, 26(5), pp. 1322–1327. doi: 10.1002/jmri.21147.

Dickerson, B. C. *et al.* (2009) 'The cortical signature of Alzheimer's disease: Regionally specific cortical thinning relates to symptom severity in very mild to mild AD dementia and is detectable in asymptomatic amyloid-positive individuals', *Cerebral Cortex*, 19(3), pp. 497–510. doi: 10.1093/cercor/bhn113.

Dickerson, B. C. *et al.* (2011) 'Alzheimer-signature MRI biomarker predicts AD dementia in cognitively normal adults', *Neurology*, 76(16), pp. 1395–1402. doi: 10.1212/WNL.0b013e3182166e96.

Dickerson, B. C. and Wolk, D. A. (2012) 'MRI cortical thickness biomarker predicts AD-like CSF and cognitive decline in normal adults', *Neurology*, 78(2), pp. 84–90. doi: 10.1212/WNL.0b013e31823efc6c.

Donohue, M. C. *et al.* (2014) 'The Preclinical Alzheimer Cognitive Composite', *JAMA Neurology*, 71(8), p. 961. doi: 10.1001/jamaneurol.2014.803.

Donohue, M. C. *et al.* (2017) 'Association between elevated brain amyloid and subsequent cognitive decline among cognitively normal persons', *JAMA - Journal of the American Medical Association*, 317(22), pp. 2305–2316. doi: 10.1001/jama.2017.6669.

Doraiswamy, P. M. *et al.* (2001) 'The Alzheimer's Disease Assessment Scale: evaluation of psychometric properties and patterns of cognitive decline in multicenter clinical trials of mild to moderate Alzheimer's disease.', *Alzheimer disease and associated disorders*, 15(4), pp. 174–83. Available at:

http://www.ncbi.nlm.nih.gov/pubmed/11723368 (Accessed: 2 April 2019).

Doré, V. *et al.* (2013) 'Cross-sectional and longitudinal analysis of the relationship between aβ deposition, cortical thickness, and memory in cognitively unimpaired individuals and in alzheimer disease', *JAMA Neurology*, 70(7), pp. 903–911. doi: 10.1001/jamaneurol.2013.1062.

Driscoll, I. *et al.* (2011) 'Lack of association between 11C-PiB and longitudinal brain atrophy in non-demented older individuals', *Neurobiology of Aging*, 32(12), pp. 2123–2130. doi: 10.1016/j.neurobiolaging.2009.12.008.

Du, A. T. *et al.* (2003) 'Atrophy rates of entorhinal cortex in AD and normal aging', *Neurology*, 60(3), pp. 481–486. doi: 10.1212/01.WNL.0000044400.11317.EC.

Du, A. T. *et al.* (2006) 'Age effects on atrophy rates of entorhinal cortex and hippocampus', *Neurobiology of Aging*, 27(5), pp. 733–740. doi: 10.1016/j.neurobiolaging.2005.03.021.

Dubois, B. *et al.* (2007) 'Research criteria for the diagnosis of Alzheimer's disease: revising the NINCDS–ADRDA criteria', *The Lancet Neurology*, 6(8), pp. 734–746. doi: 10.1016/S1474-4422(07)70178-3.

Dubois, B. *et al.* (2014) 'Advancing research diagnostic criteria for Alzheimer's disease: the IWG-2 criteria', *The Lancet Neurology*, 13(6), pp. 614–629. doi: 10.1016/S1474-4422(14)70090-0.

Dubois, B. *et al.* (2016) 'Preclinical Alzheimer's disease: Definition, natural history, and diagnostic criteria', *Alzheimer's & Dementia*, 12, pp. 292–323. doi: 10.1016/j.jalz.2016.02.002.

Duyckaerts, C., Delatour, B. and Potier, M.-C. (2009) 'Classification and basic pathology of Alzheimer disease', *Acta Neuropathologica*, 118(1), pp. 5–36. doi: 10.1007/s00401-009-0532-1.

Efron, B. (1987) 'Better Bootstrap Confidence Intervals', *Journal of the American Statistical Association*, 82(397), pp. 171–185. doi: 10.1080/01621459.1987.10478410.

Erlandsson, K. *et al.* (2012) 'A review of partial volume correction techniques for emission tomography and their applications in neurology, cardiology and oncology', *Physics in Medicine and Biology*. doi: 10.1088/0031-9155/57/21/R119.

Evans, D. A. *et al.* (1989) 'Prevalence of Alzheimer's Disease in a Community Population of Older Persons: Higher Than Previously Reported', *JAMA: The Journal of the American Medical Association*, 262(18), pp. 2551–2556. doi: 10.1001/jama.1989.03430180093036.

Ewers, M. *et al.* (2012) 'CSF biomarker and PIB-PET-derived beta-amyloid signature predicts metabolic, gray matter, and cognitive changes in nondemented subjects', *Cerebral Cortex*, 22(9), pp. 1993–2004. doi: 10.1093/cercor/bhr271.

Fagan, A. M. *et al.* (2009) 'Decreased cerebrospinal fluid Aβ 42 correlates with brain atrophy in cognitively normal elderly', *Annals of Neurology*, 65(2), pp. 176–183. doi: 10.1002/ana.21559.

Fantoni, E. R. *et al.* (2018) 'A Systematic Review and Aggregated Analysis on the Impact of Amyloid PET Brain Imaging on the Diagnosis, Diagnostic Confidence, and Management of Patients being Evaluated for Alzheimer's Disease', *Journal of Alzheimer's Disease*, 63(2), pp. 783–796. doi: 10.3233/JAD-171093.

Ferrer, I. and Vidal, N. (2018) 'Neuropathology of cerebrovascular diseases', in

Handbook of Clinical Neurology, pp. 79–114. doi: 10.1016/B978-0-12-802395-2.00007-9.

Fiford, C. M. *et al.* (2017) 'White matter hyperintensities are associated with disproportionate progressive hippocampal atrophy', *Hippocampus*, 27(3), pp. 249–262. doi: 10.1002/hipo.22690.

Fischl, B. and Dale, A. M. (2000) 'Measuring the thickness of the human cerebral cortex from magnetic resonance images', *Proceedings of the National Academy of Sciences*, 97(20), pp. 11050–11055. doi: 10.1073/pnas.200033797.

Fischl, B., Liu, A. and Dale, A. M. (2001) 'Automated manifold surgery: constructing geometrically accurate and topologically correct models of the human cerebral cortex', *IEEE Transactions on Medical Imaging*, 20(1), pp. 70–80. doi: 10.1109/42.906426.

Fischl, B., Sereno, M. I. and Dale, A. M. (1999) 'Cortical Surface-Based Analysis: II: Inflation, Flattening, and a Surface-Based Coordinate System', *NeuroImage*, 9(2), pp. 195–207. doi: 10.1006/NIMG.1998.0396.

Fjell, A. M. *et al.* (2009) 'High consistency of regional cortical thinning in aging across multiple samples', *Cerebral Cortex*, 19(9), pp. 2001–2012. doi: 10.1093/cercor/bhn232.

Fjell, A. M. *et al.* (2014) 'Accelerating Cortical Thinning: Unique to Dementia or Universal in Aging?', *Cerebral Cortex*, 24(4), pp. 919–934. doi: 10.1093/cercor/bhs379.

Van Der Flier, W. M. and Scheltens, P. (2005) 'Epidemiology and risk factors of dementia', *J Neurol Neurosurg Psychiatry*, 76, pp. 2–7. doi: 10.1136/jnnp.2005.082867.

Folstein, M. F., Folstein, S. E. and McHugh, P. R. (1975) 'Mini-mental state examination: A practical method for grading the cognitive state of patients for the

clinician.', *Journal of psychiatric research*, 12(3), pp. 189–98. Available at: http://www.ncbi.nlm.nih.gov/pubmed/1202204 (Accessed: 28 March 2019).

Forster, S. and Lavie, N. (2011) 'Entirely irrelevant distractors can capture and captivate attention', *Psychonomic Bulletin and Review*, 18(6), pp. 1064–1070. doi: 10.3758/s13423-011-0172-z.

Fortea, J. *et al.* (2010) 'Increased cortical thickness and caudate volume precede atrophy in psen1 mutation carriers', *Journal of Alzheimer's Disease*, 22(3), pp. 909–922. doi: 10.3233/JAD-2010-100678.

Fortea, J. *et al.* (2011) 'Cognitively preserved subjects with transitional cerebrospinal fluid ß-amyloid 1-42 values have thicker cortex in Alzheimer's disease vulnerable areas', *Biological Psychiatry*, 70(2), pp. 183–190. doi: 10.1016/j.biopsych.2011.02.017.

Fortea, J. *et al.* (2014) 'Cerebrospinal fluid β-amyloid and phospho-tau biomarker interactions affecting brain structure in preclinical Alzheimer disease', *Annals of Neurology*, 76(2), pp. 223–230. doi: 10.1002/ana.24186.

Fox, N. C. *et al.* (1996) 'Presymptomatic hippocampal atrophy in Alzheimer's disease', *Brain*, 119(6), pp. 2001–2007. doi: 10.1093/brain/119.6.2001.

Fox, N. C. *et al.* (1999) 'Correlation between rates of brain atrophy and cognitive decline in AD', *Neurology*, 52(8), pp. 1687–1689. doi: 10.1212/wnl.52.8.1687.

Fox, N. C. *et al.* (2000) 'Using Serial Registered Brain Magnetic Resonance Imaging to Measure Disease Progression in Alzheimer Disease', *Archives of Neurology*, 57(3), p. 339. doi: 10.1001/archneur.57.3.339.

Fox, N. C. *et al.* (2001) 'Imaging of onset and progression of Alzheimer's disease with

voxel-compression mapping of serial magnetic resonance images', *Lancet*, 358(9277), pp. 201–205. doi: 10.1016/S0140-6736(01)05408-3.

Fox, N. C. *et al.* (2005) 'Effects of A immunization (AN1792) on MRI measures of cerebral volume in Alzheimer disease', *Neurology*, 64(9), pp. 1563–1572. doi: 10.1212/01.WNL.0000159743.08996.99.

Fraser, M. A., Shaw, M. E. and Cherbuin, N. (2015) 'A systematic review and meta-analysis of longitudinal hippocampal atrophy in healthy human ageing', *NeuroImage*, pp. 364–374. doi: 10.1016/j.neuroimage.2015.03.035.

Freeborough, P. A. and Fox, N. C. (1997) 'The boundary shift integral: an accurate and robust measure of cerebral volume changes from registered repeat MRI', *IEEE Transactions on Medical Imaging*, 16(5), pp. 623–629. doi: 10.1109/42.640753.

Freeborough, P. A. and Fox, N. C. (1998) 'Modeling brain deformations in alzheimer disease by fluid registration of serial 3d MR images', *Journal of Computer Assisted Tomography*, 22(5), pp. 838–843. doi: 10.1097/00004728-199809000-00031.

Freeborough, P. A., Fox, N. C. and Kitney, R. I. (1997) 'Interactive algorithms for the segmentation and quantitation of 3-D MRI brain scans', *Computer Methods and Programs in Biomedicine*, 53(1), pp. 15–25. doi: 10.1016/S0169-2607(97)01803-8.

Freesurfer (2015) *Frequently Asked Questions*. Available at: https://surfer.nmr.mgh.harvard.edu/fswiki/UserContributions/FAQ#Q.Thesurfacesneartthemedialwall.2Chippocampus.2Candamygdalaaren.27taccuratelyfollowingthestructuresthere.HowcanIfixthis.3F (Accessed: 4 May 2022).

Friston, K. J. *et al.* (1991) 'Comparing functional (PET) images: The assessment of significant change', *Journal of Cerebral Blood Flow and Metabolism*, 11(4), pp. 690–

699. doi: 10.1038/jcbfm.1991.122.

Frost, C. *et al.* (2017) 'Design optimization for clinical trials in early-stage manifest Huntington's disease', *Movement Disorders*, 32(11), pp. 1610–1619. doi: 10.1002/mds.27122.

Galvin, J. E. *et al.* (2005) 'The AD8: A brief informant interview to detect dementia', *Neurology*, 65(4), pp. 559–564. doi: 10.1212/01.wnl.0000172958.95282.2a.

Gauthier, S. *et al.* (2016) 'Why has therapy development for dementia failed in the last two decades?', *Alzheimer's & Dementia*, 12(1), pp. 60–64. doi: 10.1016/j.jalz.2015.12.003.

Gavett, B. E. *et al.* (2016) 'Practice Effects on Story Memory and List Learning Tests in the Neuropsychological Assessment of Older Adults', *PLOS ONE*. Edited by E. Ito, 11(10), p. e0164492. doi: 10.1371/journal.pone.0164492.

Giannakopoulos, P. *et al.* (2003) 'Tangle and neuron numbers, but not amyloid load, predict cognitive status in Alzheimer's disease.', *Neurology*, 60(9), pp. 1495–500. Available at: http://www.ncbi.nlm.nih.gov/pubmed/12743238 (Accessed: 1 March 2019).

Gibson, Lorna M., Littlejohns, T. J., *et al.* (2018) 'Impact of detecting potentially serious incidental findings during multi-modal imaging [version 3; referees: 2 approved, 1 approved with reservations]', *Wellcome Open Research*, 2. doi: 10.12688/wellcomeopenres.13181.3.

Gibson, Lorna M *et al.* (2018) 'Potentially serious incidental findings on brain and body magnetic resonance imaging of apparently asymptomatic adults: systematic review and meta-analysis.', *BMJ (Clinical research ed.)*, 363, p. k4577. doi: 10.1136/bmj.k4577.

Gibson, Lorna M., Paul, L., *et al.* (2018) 'Potentially serious incidental findings on brain and body magnetic resonance imaging of apparently asymptomatic adults: Systematic review and meta-analysis', *BMJ (Online)*. BMJ Publishing Group, 363. doi: 10.1136/bmj.k4577.

Giedd, J. N. *et al.* (1995) 'Reliability of cerebral measures in repeated examinations with magnetic resonance imaging', *Psychiatry Research: Neuroimaging*, 61(2), pp. 113–119. doi: 10.1016/0925-4927(95)02593-M.

Glodzik, L. *et al.* (2015) 'Reduced retention of Pittsburgh compound B in white matter lesions', *European Journal of Nuclear Medicine and Molecular Imaging*, 42(1), pp. 97–102. doi: 10.1007/s00259-014-2897-1.

Goetz, C. G. *et al.* (2008) 'Movement Disorder Society-Sponsored Revision of the Unified Parkinson's Disease Rating Scale (MDS-UPDRS): Scale presentation and clinimetric testing results', *Movement Disorders*, 23(15), pp. 2129–2170. doi: 10.1002/mds.22340.

Gómez-Isla, T. *et al.* (1997) 'Neuronal loss correlates with but exceeds neurofibrillary tangles in Alzheimer's disease', *Annals of Neurology*, 41(1), pp. 17–24. doi: 10.1002/ana.410410106.

Goodheart, A. E. *et al.* (2015) 'Reduced binding of Pittsburgh Compound-B in areas of white matter hyperintensities', *NeuroImage: Clinical*, 9, pp. 479–483. doi: 10.1016/j.nicl.2015.09.009.

Gordon, B. A. *et al.* (2015) 'The effects of white matter hyperintensities and amyloid deposition on Alzheimer dementia', *NeuroImage: Clinical*, 8, pp. 246–252. doi: 10.1016/j.nicl.2015.04.017.

Gottesman, R. F. *et al.* (2010) 'Blood pressure and white-matter disease progression in a biethnic cohort: Atherosclerosis risk in communities (ARIC) study', *Stroke*, 41(1), pp. 3–8. doi: 10.1161/STROKEAHA.109.566992.

Guerreiro, R. *et al.* (2013) 'TREM2 Variants in Alzheimer's Disease', *New England Journal of Medicine*, 368(2), pp. 117–127. doi: 10.1056/NEJMoa1211851.

Gurol, M. E. *et al.* (2013) 'Cerebral amyloid angiopathy burden associated with leukoaraiosis: A positron emission tomography/magnetic resonance imaging study', *Annals of Neurology*, 73(4), pp. 529–536. doi: 10.1002/ana.23830.

Habes, M. *et al.* (2016) 'White matter hyperintensities and imaging patterns of brain ageing in the general population', *Brain*, 139(4), pp. 1164–1179. doi: 10.1093/brain/aww008.

Hamelin, L. *et al.* (2016) 'Early and protective microglial activation in Alzheimer's disease: a prospective study using ^{18}F-DPA-714 PET imaging', *Brain*, 139(4), pp. 1252–1264. doi: 10.1093/brain/aww017.

Hampel, H. *et al.* (2010) 'Biomarkers for alzheimer's disease: Academic, industry and regulatory perspectives', *Nature Reviews Drug Discovery*, pp. 560–574. doi: 10.1038/nrd3115.

Hampel, H. *et al.* (2018) 'Blood-based biomarkers for Alzheimer disease: mapping the road to the clinic', *Nature Reviews Neurology*, pp. 639–652. doi: 10.1038/s41582-018-0079-7.

Hardy, J. A. and Higgins, G. A. (1992) 'Alzheimer's disease: the amyloid cascade hypothesis.', *Science*, 256(5054), pp. 184–5. Available at: http://www.ncbi.nlm.nih.gov/pubmed/1566067 (Accessed: 1 March 2019).

Hardy, J. and De Strooper, B. (2017) ‘Alzheimer’s disease: where next for anti-amyloid therapies?’, *Brain*, 140(4), pp. 853–855. doi: 10.1093/brain/awx059.

Harold, D. *et al.* (2009) ‘Genome-wide association study identifies variants at CLU and PICALM associated with Alzheimer’s disease’, *Nature Genetics*, 41(10), pp. 1088–1093. doi: 10.1038/ng.440.

Hegedüs, P. *et al.* (2019) ‘How to report incidental findings from population whole-body MRI: view of participants of the German National Cohort’, *European Radiology*, 29(11), pp. 5873–5878. doi: 10.1007/s00330-019-06077-z.

Hegenscheid, K. *et al.* (2013) ‘Potentially relevant incidental findings on research whole-body MRI in the general adult population: Frequencies and management’, *European Radiology*, 23(3), pp. 816–826. doi: 10.1007/s00330-012-2636-6.

den Heijer, T. *et al.* (2010) ‘A 10-year follow-up of hippocampal volume on magnetic resonance imaging in early dementia and cognitive decline’, *Brain*, 133(4), pp. 1163–1172. doi: 10.1093/brain/awq048.

Den Heijer, T. *et al.* (2006) ‘Use of hippocampal and amygdalar volumes on magnetic resonance imaging to predict dementia in cognitively intact elderly people’, *Archives of General Psychiatry*, 63(1), pp. 57–62. doi: 10.1001/archpsyc.63.1.57.

Henneman, W. J. P. *et al.* (2009) ‘Hippocampal atrophy rates in Alzheimer disease: Added value over whole brain volume measures’, *Neurology*, 72(11), pp. 999–1007. doi: 10.1212/01.wnl.0000344568.09360.31.

Ho, A. J. *et al.* (2010) ‘Comparing 3 T and 1.5 T MRI for tracking Alzheimer’s disease progression with tensor-based morphometry’, *Human Brain Mapping*, 31(4), pp. 499–514. doi: 10.1002/hbm.20882.

Hobart, J. *et al.* (2013) 'Putting the Alzheimer's cognitive test to the test I: Traditional psychometric methods', *Alzheimer's & Dementia*, 9(1), pp. S4–S9. doi: 10.1016/j.jalz.2012.08.005.

Holland, D., McEvoy, L. K. and Dale, A. M. (2012) 'Unbiased comparison of sample size estimates from longitudinal structural measures in ADNI', *Human Brain Mapping*, 33(11), pp. 2586–2602. doi: 10.1002/hbm.21386.

Hollingworth, P. *et al.* (2011) 'Common variants at ABCA7, MS4A6A/MS4A4E, EPHA1, CD33 and CD2AP are associated with Alzheimer's disease', *Nature Genetics*, 43(5), pp. 429–435. doi: 10.1038/ng.803.

Hopperton, K. E. *et al.* (2018) 'Markers of microglia in post-mortem brain samples from patients with Alzheimer's disease: a systematic review.', *Molecular psychiatry*, 23(2), pp. 177–198. doi: 10.1038/mp.2017.246.

Hua, X. *et al.* (2008) 'Tensor-based morphometry as a neuroimaging biomarker for Alzheimer's disease: An MRI study of 676 AD, MCI, and normal subjects', *NeuroImage*, 43(3), pp. 458–469. doi: 10.1016/j.neuroimage.2008.07.013.

Hua, X. *et al.* (2009) 'Optimizing power to track brain degeneration in Alzheimer's disease and mild cognitive impairment with tensor-based morphometry: An ADNI study of 515 subjects', *NeuroImage*, 48(4), pp. 668–681. doi: 10.1016/j.neuroimage.2009.07.011.

Hua, X. *et al.* (2010) 'Mapping Alzheimer's disease progression in 1309 MRI scans: Power estimates for different inter-scan intervals', *NeuroImage*, 51(1), pp. 63–75. doi: 10.1016/j.neuroimage.2010.01.104.

Iglesias, J. E. *et al.* (2016) 'Bayesian longitudinal segmentation of hippocampal

substructures in brain MRI using subject-specific atlases', *NeuroImage*, 141, pp. 542–555. doi: 10.1016/j.neuroimage.2016.07.020.

Illes, J. *et al.* (2004) 'Discovery and disclosure of incidental findings in neuroimaging research', *Journal of Magnetic Resonance Imaging*. J Magn Reson Imaging, 20(5), pp. 743–747. doi: 10.1002/jmri.20180.

Ingelsson, M. *et al.* (2004) 'Early Abeta accumulation and progressive synaptic loss, gliosis, and tangle formation in AD brain.', *Neurology*, 62(6), pp. 925–31. Available at: http://www.ncbi.nlm.nih.gov/pubmed/15037694 (Accessed: 1 March 2019).

Jack, C. R. *et al.* (2004) 'Comparison of different MRI brain athrophy rate measures with clinical disease progression in AD', *Neurology*, 62(4), pp. 591–600. doi: 10.1212/01.WNL.0000110315.26026.EF.

Jack, C. R. *et al.* (2009) 'Serial PIB and MRI in normal, mild cognitive impairment and Alzheimer's disease: implications for sequence of pathological events in Alzheimer's disease', *Brain*, 132(5), pp. 1355–1365. doi: 10.1093/brain/awp062.

Jack, C. R. *et al.* (2010) 'Hypothetical model of dynamic biomarkers of the Alzheimer's pathological cascade.', *The Lancet. Neurology*, 9(1), pp. 119–28. doi: 10.1016/S1474-4422(09)70299-6.

Jack, C. R. *et al.* (2015) 'Different definitions of neurodegeneration produce similar amyloid/neurodegeneration biomarker group findings', *Brain*, 138(12), pp. 3747–3759. doi: 10.1093/brain/awv283.

Jack, C. R. *et al.* (2018a) 'NIA-AA Research Framework: Toward a biological definition of Alzheimer's disease', *Alzheimer's and Dementia*, 14(4), pp. 535–562. doi: 10.1016/j.jalz.2018.02.018.

Jack, C. R. *et al.* (2018b) 'NIA-AA Research Framework: Toward a biological definition of Alzheimer's disease', *Alzheimer's and Dementia*, 14(4), pp. 535–562. doi: 10.1016/j.jalz.2018.02.018.

Jaeger, J. (2018) 'Digit Symbol Substitution Test', *Journal of Clinical Psychopharmacology*, 38(5), pp. 513–519. doi: 10.1097/JCP.0000000000000941.

James, B. D. *et al.* (2016) 'TDP-43 stage, mixed pathologies, and clinical Alzheimer's-type dementia', *Brain*, 139(11), pp. 2983–2993. doi: 10.1093/brain/aww224.

James, S. N. *et al.* (2018) 'Using a birth cohort to study brain health and preclinical dementia: Recruitment and participation rates in Insight 46', *BMC Research Notes*, 11(1), p. 885. doi: 10.1186/s13104-018-3995-0.

Jansen, W. J. *et al.* (2015) 'Prevalence of cerebral amyloid pathology in persons without dementia: A meta-analysis', *JAMA - Journal of the American Medical Association*, 313(19), pp. 1924–1938. doi: 10.1001/jama.2015.4668.

Jarrett, J. T., Berger, E. P. and Lansbury, P. T. (1993) 'The Carboxy Terminus of the β Amyloid Protein Is Critical for the Seeding of Amyloid Formation: Implications for the Pathogenesis of Alzheimer's Disease', *Biochemistry*, 32(18), pp. 4693–4697. doi: 10.1021/bi00069a001.

Jessen, F. *et al.* (2014) 'A conceptual framework for research on subjective cognitive decline in preclinical Alzheimer's disease.', *Alzheimer's & dementia : the journal of the Alzheimer's Association*, 10(6), pp. 844–52. doi: 10.1016/j.jalz.2014.01.001.

Jessen, F. *et al.* (2020) 'The characterisation of subjective cognitive decline', *The Lancet Neurology*, 19(3), pp. 271–278. doi: 10.1016/S1474-4422(19)30368-0.

La Joie, R. *et al.* (2020) 'Prospective longitudinal atrophy in Alzheimer's disease correlates with the intensity and topography of baseline tau-PET', *Science Translational Medicine*, 12(524). doi: 10.1126/scitranslmed.aau5732.

Jonsson, T. *et al.* (2012) 'A mutation in APP protects against Alzheimer's disease and age-related cognitive decline', *Nature*, 488(7409), pp. 96–99. doi: 10.1038/nature11283.

Josephs, K. A. *et al.* (2008) 'β-amyloid burden is not associated with rates of brain atrophy', *Annals of Neurology*, 63(2), pp. 204–212. doi: 10.1002/ana.21223.

Jovicich, J. *et al.* (2006) 'Reliability in multi-site structural MRI studies: Effects of gradient non-linearity correction on phantom and human data', *NeuroImage*, 30(2), pp. 436–443. doi: 10.1016/j.neuroimage.2005.09.046.

Kalheim, L. F. *et al.* (2017) 'White matter hyperintensity microstructure in amyloid dysmetabolism', *Journal of Cerebral Blood Flow and Metabolism*, 37(1), pp. 356–365. doi: 10.1177/0271678X15627465.

Kapasi, A., DeCarli, C. and Schneider, J. A. (2017) 'Impact of multiple pathologies on the threshold for clinically overt dementia', *Acta Neuropathologica*, pp. 171–186. doi: 10.1007/s00401-017-1717-7.

Karch, C. M. and Goate, A. M. (2015) 'Alzheimer's Disease Risk Genes and Mechanisms of Disease Pathogenesis', *Biological Psychiatry*, 77(1), pp. 43–51. doi: 10.1016/j.biopsych.2014.05.006.

Kaye, J. *et al.* (1997) 'Volume loss of the hippocampus and temporal lobe in healthy elderly persons destined to develop dementia.', *Neurology*, 48(5), pp. 1297–304. Available at: http://www.ncbi.nlm.nih.gov/pubmed/9153461 (Accessed: 26 December

2019).

Kaye, J. A. *et al.* (2005) 'Asynchronous regional brain volume losses in presymptomatic to moderate AD', *Journal of Alzheimer's Disease*, 8(1), pp. 51–56. doi: 10.3233/JAD-2005-8106.

Kempton, M. J. *et al.* (2009) 'Effects of acute dehydration on brain morphology in healthy humans', *Human Brain Mapping*, 30(1), pp. 291–298. doi: 10.1002/hbm.20500.

Keshavan, A. *et al.* (2017) 'Blood Biomarkers for Alzheimer's Disease: Much Promise, Cautious Progress', *Molecular Diagnosis and Therapy*, 21(1), pp. 13–22. doi: 10.1007/s40291-016-0241-0.

Klunk, W. E. *et al.* (2015) 'The Centiloid project: Standardizing quantitative amyloid plaque estimation by PET', *Alzheimer's and Dementia*, 11(1), pp. 1-15.e4. doi: 10.1016/j.jalz.2014.07.003.

Knight, W. D. *et al.* (2011) 'Acceleration of cortical thinning in familial Alzheimer's disease', *Neurobiology of Aging*, 32(10), pp. 1765–1773. doi: 10.1016/j.neurobiolaging.2009.11.013.

Knopman, D. S. *et al.* (2003) *Neuropathology of Cognitively Normal Elderly*, *Journal of Neuropathology and Experimental Neurology*. Available at: https://academic.oup.com/jnen/article-abstract/62/11/1087/2916328 (Accessed: 1 March 2019).

Knopman, D. S. *et al.* (2007) 'Incident dementia in women is preceded by weight loss by at least a decade', *Neurology*, 69(8), pp. 739–746. doi: 10.1212/01.wnl.0000267661.65586.33.

Koedam, E. L. G. E. *et al.* (2010) 'Early-Versus Late-Onset Alzheimer's Disease: More than Age Alone', *Journal of Alzheimer's Disease*, 19, pp. 1401–1408. doi: 10.3233/JAD-2010-1337.

Koo, B. *et al.* (2009) 'A framework to analyze partial volume effect on gray matter mean diffusivity measurements', *NeuroImage*, 44(1), pp. 136–144. doi: 10.1016/j.neuroimage.2008.07.064.

Koran, M. E. I., Wagener, M. and Hohman, T. J. (2017) 'Sex differences in the association between AD biomarkers and cognitive decline', *Brain Imaging and Behavior*. Springer New York LLC, 11(1), pp. 205–213. doi: 10.1007/s11682-016-9523-8.

Kruggel, F., Turner, J. and Muftuler, L. T. (2010) 'Impact of scanner hardware and imaging protocol on image quality and compartment volume precision in the ADNI cohort', *NeuroImage*, 49(3), pp. 2123–2133. doi: 10.1016/j.neuroimage.2009.11.006.

Kuh, D. *et al.* (2011) 'Cohort Profile: Updating the cohort profile for the MRC National Survey of Health and Development: a new clinic-based data collection for ageing research The MRC National Survey of Health and Development: how did the latest NSHD data collection come about', *International Journal of Epidemiology*, 40, pp. 1–9. doi: 10.1093/ije/dyq231.

Kuh, D. *et al.* (2016) 'The MRC National Survey of Health and Development reaches age 70: maintaining participation at older ages in a birth cohort study', *European Journal of Epidemiology*, 31(11), pp. 1135–1147. doi: 10.1007/s10654-016-0217-8.

Kuhlmann, J. *et al.* (2017) 'CSF Aβ 1–42 – an excellent but complicated Alzheimer's biomarker – a route to standardisation', *Clinica Chimica Acta*, 467, pp. 27–33. doi:

10.1016/j.cca.2016.05.014.

de la Torre, J. C. (2004) ‘Is Alzheimer’s disease a neurodegenerative or a vascular disorder? Data, dogma, and dialectics’, *The Lancet Neurology*, 3(3), pp. 184–190. doi: 10.1016/S1474-4422(04)00683-0.

Lalli, G. *et al.* (2021) ‘Aducanumab: a new phase in therapeutic development for Alzheimer’s disease?’, *EMBO Molecular Medicine*, 13(8). doi: 10.15252/emmm.202114781.

Lambert, J.-C. *et al.* (2009) ‘Genome-wide association study identifies variants at CLU and CR1 associated with Alzheimer’s disease.’, *Nature genetics*, 41(10), pp. 1094–9. doi: 10.1038/ng.439.

Lambert, J.-C. *et al.* (2013) ‘Meta-analysis of 74,046 individuals identifies 11 new susceptibility loci for Alzheimer’s disease’, *Nature Genetics*, 45(12), pp. 1452–1458. doi: 10.1038/ng.2802.

Landau, S. M. *et al.* (2013) ‘Amyloid-β imaging with Pittsburgh compound B and florbetapir: Comparing radiotracers and quantification methods’, *Journal of Nuclear Medicine*, 54(1), pp. 70–77. doi: 10.2967/jnumed.112.109009.

Landau, S. M. *et al.* (2015) ‘Measurement of longitudinal β-amyloid change with 18F-florbetapir PET and standardized uptake value ratios’, *Journal of Nuclear Medicine*, 56(4), pp. 567–574. doi: 10.2967/jnumed.114.148981.

Landau, S. M., Horng, A. and Jagust, W. J. (2018) ‘Memory decline accompanies subthreshold amyloid accumulation’, *Neurology*, 90(17), pp. e1452–e1460. doi: 10.1212/WNL.0000000000005354.

Lane, C. A. *et al.* (2017) 'Study protocol: Insight 46 - a neuroscience sub-study of the MRC National Survey of Health and Development', *BMC Neurology*, 17(1). doi: 10.1186/s12883-017-0846-x.

Lane, C. A. *et al.* (2019) 'Associations between blood pressure across adulthood and late-life brain structure and pathology in the neuroscience substudy of the 1946 British birth cohort (Insight 46): an epidemiological study', *The Lancet Neurology*, 18(10), pp. 942–952. doi: 10.1016/S1474-4422(19)30228-5.

Lane, C. A. *et al.* (2020) 'Associations between Vascular Risk Across Adulthood and Brain Pathology in Late Life: Evidence from a British Birth Cohort', *JAMA Neurology*, 77(2), pp. 175–183. doi: 10.1001/jamaneurol.2019.3774.

Lane, C. A. *et al.* (2021) 'Investigating the relationship between BMI across adulthood and late life brain pathologies', *Alzheimer's Research & Therapy*, 13(1), p. 91. doi: 10.1186/s13195-021-00830-7.

Lao, P. J. and Brickman, A. M. (2018) 'Multimodal neuroimaging study of cerebrovascular disease, amyloid deposition, and neurodegeneration in Alzheimer's disease progression', *Alzheimer's & Dementia: Diagnosis, Assessment & Disease Monitoring*, 10(1), pp. 638–646. doi: 10.1016/j.dadm.2018.08.007.

de Leeuw, F. -E. *et al.* (2002) 'Hypertension and cerebral white matter lesions in a prospective cohort study', *Brain*, 125(4), pp. 765–772. doi: 10.1093/brain/awf077.

De Leeuw, F. E. *et al.* (2001) 'Prevalence of cerebral white matter lesions in elderly people: A population based magnetic resonance imaging study. The Rotterdam Scan Study', *Journal of Neurology Neurosurgery and Psychiatry*, 70(1), pp. 9–14. doi: 10.1136/jnnp.70.1.9.

Leung, Kelvin K *et al.* (2010) 'Automated cross-sectional and longitudinal hippocampal volume measurement in mild cognitive impairment and Alzheimer's disease', *NeuroImage*, 51(4), pp. 1345–1359. doi: 10.1016/j.neuroimage.2010.03.018.

Leung, Kelvin K. *et al.* (2010) 'Robust atrophy rate measurement in Alzheimer's disease using multi-site serial MRI: Tissue-specific intensity normalization and parameter selection', *NeuroImage*, 50(2), pp. 516–523. doi: 10.1016/j.neuroimage.2009.12.059.

Leung, K. K. *et al.* (2011) 'Brain MAPS: An automated, accurate and robust brain extraction technique using a template library', *NeuroImage*, 55(3), pp. 1091–1108. doi: 10.1016/j.neuroimage.2010.12.067.

Liu, C. C. *et al.* (2013) 'Apolipoprotein e and Alzheimer disease: Risk, mechanisms and therapy', *Nature Reviews Neurology*, pp. 106–118. doi: 10.1038/nrneurol.2012.263.

Liu, Y. *et al.* (2015) 'APOE genotype and neuroimaging markers of Alzheimer's disease: systematic review and meta-analysis', *Journal of Neurology, Neurosurgery & Psychiatry*, 86(2), pp. 127–134. doi: 10.1136/jnnp-2014-307719.

Livingston, G. *et al.* (2020) 'Dementia prevention, intervention, and care: 2020 report of the Lancet Commission', *The Lancet*, pp. 413–446. doi: 10.1016/S0140-6736(20)30367-6.

Lobo, A. *et al.* (2000) 'Prevalence of dementia and major subtypes in Europe: A collaborative study of population-based cohorts. Neurologic Diseases in the Elderly Research Group.', *Neurology*, 54(11 Suppl 5), pp. S4-9. Available at: http://www.ncbi.nlm.nih.gov/pubmed/10854354 (Accessed: 30 September 2018).

Love, S. (2005) 'Neuropathological investigation of dementia: a guide for neurologists.',

Journal of neurology, neurosurgery, and psychiatry, 76 Suppl 5(suppl 5), pp. v8-14. doi: 10.1136/jnnp.2005.080754.

Lowe, V. J. *et al.* (2018) 'White matter reference region in PET studies of 11C-Pittsburgh compound B uptake: Effects of age and amyloid-β deposition', *Journal of Nuclear Medicine*. Society of Nuclear Medicine Inc., 59(10), pp. 1583–1589. doi: 10.2967/jnumed.117.204271.

Lu, K. *et al.* (2019) 'Cognition at age 70: Life course predictors and associations with brain pathologies', *Neurology*, 93(23), pp. E2144–E2156. doi: 10.1212/WNL.0000000000008534.

Lu, K. *et al.* (2021) 'Dissociable effects of APOE ε4 and β-amyloid pathology on visual working memory', *Nature Aging*, 1(11), pp. 1002–1009. doi: 10.1038/s43587-021-00117-4.

Malone, I. B. *et al.* (2015) 'Accurate automatic estimation of total intracranial volume: a nuisance variable with less nuisance.', *NeuroImage*, 104, pp. 366–72. doi: 10.1016/j.neuroimage.2014.09.034.

Marnane, M. *et al.* (2016) 'Periventricular hyperintensities are associated with elevated cerebral amyloid', *Neurology*, 86(6), pp. 535–543. doi: 10.1212/WNL.0000000000002352.

Marshall, C. R. *et al.* (2018) 'Primary progressive aphasia: a clinical approach', *Journal of Neurology*, 265(6), pp. 1474–1490. doi: 10.1007/s00415-018-8762-6.

Martin, S. B. *et al.* (2010) 'Evidence that volume of anterior medial temporal lobe is reduced in seniors destined for mild cognitive impairment', *Neurobiology of Aging*, 31(7), pp. 1099–1106. doi: 10.1016/j.neurobiolaging.2008.08.010.

Mattsson, N. *et al.* (2014) 'Emerging β-amyloid pathology and accelerated cortical atrophy', *JAMA Neurology*, 71(6), pp. 725–734. doi: 10.1001/jamaneurol.2014.446.

Mattsson, N. *et al.* (2015) 'Brain structure and function as mediators of the effects of amyloid on memory', *Neurology*, 84(11), pp. 1136–1144. doi: 10.1212/WNL.0000000000001375.

Mayeux, R. and Stern, Y. (2012) 'Epidemiology of Alzheimer disease', *Cold Spring Harbor Perspectives in Medicine*, 2(8). doi: 10.1101/cshperspect.a006239.

McAleese, K. E. *et al.* (2017) 'Parietal white matter lesions in Alzheimer's disease are associated with cortical neurodegenerative pathology, but not with small vessel disease', *Acta Neuropathologica*, 134(3), pp. 459–473. doi: 10.1007/s00401-017-1738-2.

McEvoy, L. K. *et al.* (2010) 'Neuroimaging enrichment strategy for secondary prevention trials in Alzheimer disease.', *Alzheimer disease and associated disorders*, 24(3), pp. 269–77. doi: 10.1097/WAD.0b013e3181d1b814.

McGeer, P. L. and McGeer, E. G. (2001) 'Inflammation, autotoxicity and Alzheimer disease.', *Neurobiology of aging*, 22(6), pp. 799–809. Available at: http://www.ncbi.nlm.nih.gov/pubmed/11754986 (Accessed: 5 March 2019).

Medical Research Council, T. W. T. (2014) *Framework on the feedback of health-related findings in research*. Available at: https://mrc.ukri.org/documents/pdf/mrc-wellcome-trust-framework-on-the-feedback-of-health-related-findings-in-researchpdf/ (Accessed: 8 January 2020).

Mendez, M. F. (2019) 'Early-onset Alzheimer Disease and Its Variants', *CONTINUUM: Lifelong Learning in Neurology*, 25(1), pp. 34–51. doi:

10.1212/CON.0000000000000687.

Miller, D. H. *et al.* (2002) 'Measurement of atrophy in multiple sclerosis: pathological basis, methodological aspects and clinical relevance', *Brain*, 125(8), pp. 1676–1695. doi: 10.1093/brain/awf177.

Mioshi, E. *et al.* (2006) 'The Addenbrooke's Cognitive Examination Revised (ACE-R): a brief cognitive test battery for dementia screening', *International Journal of Geriatric Psychiatry*, 21(11), pp. 1078–1085. doi: 10.1002/gps.1610.

Mormino, E. C. *et al.* (2012) 'Not quite PIB-positive, not quite PIB-negative: Slight PIB elevations in elderly normal control subjects are biologically relevant', *NeuroImage*, 59(2), pp. 1152–1160. doi: 10.1016/j.neuroimage.2011.07.098.

Mormino, E. C. *et al.* (2017) 'Early and late change on the preclinical Alzheimer's cognitive composite in clinically normal older individuals with elevated amyloid β', *Alzheimer's & Dementia*, 13(9), pp. 1004–1012. doi: 10.1016/j.jalz.2017.01.018.

Mueller, E. A. *et al.* (1998) 'Brain volume preserved in healthy elderly through the eleventh decade', *Neurology*, 51(6), pp. 1555–1562. doi: 10.1212/WNL.51.6.1555.

Murphy, E. A. *et al.* (2010) 'Six-month atrophy in MTL structures is associated with subsequent memory decline in elderly controls', *NeuroImage*, 53(4), pp. 1310–1317. doi: 10.1016/j.neuroimage.2010.07.016.

Naj, A. C. *et al.* (2011) 'Common variants at MS4A4/MS4A6E, CD2AP, CD33 and EPHA1 are associated with late-onset Alzheimer's disease', *Nature Genetics*, 43(5), pp. 436–441. doi: 10.1038/ng.801.

Nasreddine, Z. S. *et al.* (2005) 'The Montreal Cognitive Assessment, MoCA: A Brief

Screening Tool For Mild Cognitive Impairment', *Journal of the American Geriatrics Society*, 53(4), pp. 695–699. doi: 10.1111/j.1532-5415.2005.53221.x.

Nelson, P. T. *et al.* (2012) 'Correlation of Alzheimer disease neuropathologic changes with cognitive status: a review of the literature.', *Journal of neuropathology and experimental neurology*, 71(5), pp. 362–81. doi: 10.1097/NEN.0b013e31825018f7.

Nestor, S. M. *et al.* (2008) 'Ventricular enlargement as a possible measure of Alzheimer's disease progression validated using the Alzheimer's disease neuroimaging initiative database', *Brain*, 131(9), pp. 2443–2454. doi: 10.1093/brain/awn146.

NICE (2018) 'Recommendations | Dementia: assessment, management and support for people living with dementia and their carers | Guidance | NICE'. NICE. Available at: https://www.nice.org.uk/guidance/ng97/chapter/Recommendations#diagnosis (Accessed: 28 March 2019).

Noyce, A. J. *et al.* (2014) 'Bradykinesia-akinesia incoordination test: Validating an online keyboard test of upper limb function', *PLoS ONE*, 9(4). doi: 10.1371/journal.pone.0096260.

O'Sullivan, J. W. *et al.* (2018) 'Prevalence and outcomes of incidental imaging findings: umbrella review.', *BMJ (Clinical research ed.)*, 361, p. k2387. doi: 10.1136/bmj.k2387.

Olsson, B. *et al.* (2016) 'CSF and blood biomarkers for the diagnosis of Alzheimer's disease: a systematic review and meta-analysis', *The Lancet Neurology*, 15(7), pp. 673–684. doi: 10.1016/S1474-4422(16)00070-3.

Ossenkoppele, R. *et al.* (2015) 'The behavioural/dysexecutive variant of Alzheimer's disease: clinical, neuroimaging and pathological features', *Brain*, 138(9), p. 2732. doi: 10.1093/BRAIN/AWV191.

Pålhaugen, L. *et al.* (2021) 'Brain amyloid and vascular risk are related to distinct white matter hyperintensity patterns', *Journal of Cerebral Blood Flow & Metabolism*, 41(5), pp. 1162–1174. doi: 10.1177/0271678X20957604.

Papp, K. V. *et al.* (2014) 'Development of a psychometrically equivalent short form of the face-name associative memory exam for use along the early alzheimers disease trajectory', *Clinical Neuropsychologist*, 28(5), pp. 771–785. doi: 10.1080/13854046.2014.911351.

Parker, T. D. *et al.* (2018) 'Cortical microstructure in young onset Alzheimer's disease using neurite orientation dispersion and density imaging', *Human Brain Mapping*, 39(7), pp. 3005–3017. doi: 10.1002/hbm.24056.

Parker, T. D. *et al.* (2019) 'Hippocampal subfield volumes and pre-clinical Alzheimer's disease in 408 cognitively normal adults born in 1946', *PLOS ONE*. Edited by Y. Huo, 14(10), p. e0224030. doi: 10.1371/journal.pone.0224030.

Parker, T. D. *et al.* (2020) 'Amyloid β influences the relationship between cortical thickness and vascular load', *Alzheimer's & Dementia: Diagnosis, Assessment & Disease Monitoring*. Wiley, 12(1). doi: 10.1002/dad2.12022.

Parnetti, L. *et al.* (2019) 'Prevalence and risk of progression of preclinical Alzheimer's disease stages: a systematic review and meta-analysis', *Alzheimer's Research & Therapy*, 11(1), p. 7. doi: 10.1186/s13195-018-0459-7.

Perneger, T. V. (1998) 'What's wrong with Bonferroni adjustments', *British Medical Journal*, pp. 1236–1238. doi: 10.1136/bmj.316.7139.1236.

Pertzov, Y. *et al.* (2012) 'Forgetting What Was Where: The Fragility of Object-Location Binding', *PLoS ONE*, 7(10). doi: 10.1371/journal.pone.0048214.

Petersen, R. C. (2011) ‘Mild Cognitive Impairment’, *New England Journal of Medicine*. Massachusetts Medical Society , 364(23), pp. 2227–2234. doi: 10.1056/NEJMcp0910237.

Petersen, R. C. *et al.* (2016) ‘Association of elevated amyloid levels with cognition and biomarkers in cognitively normal people from the community’, *JAMA Neurology*, 73(1), pp. 85–92. doi: 10.1001/jamaneurol.2015.3098.

Pietroboni, A. M. *et al.* (2018) ‘CSF β-amyloid and white matter damage: A new perspective on Alzheimer’s disease’, *Journal of Neurology, Neurosurgery and Psychiatry*, 89(4), pp. 352–357. doi: 10.1136/jnnp-2017-316603.

Pooley, R. A. (2005) ‘Fundamental Physics of MR Imaging’, *RadioGraphics*, 25(4), pp. 1087–1099. doi: 10.1148/rg.254055027.

Prince, M., Knapp, M., *et al.* (2014) *Dementia UK: Update*. Available at: https://www.alzheimers.org.uk/sites/default/files/migrate/downloads/dementia_uk_update.pdf (Accessed: 30 September 2018).

Prince, M., Albanese, E., *et al.* (2014) *World Alzheimer Report 2014: Dementia and risk reduction: an analysis of protective and modifiable factors*, *Alzheimer’s Disease International*. Available at: https://www.alzint.org/u/WorldAlzheimerReport2014.pdf (Accessed: 4 May 2022).

Provenzano, F. A. *et al.* (2013) ‘White matter hyperintensities and cerebral amyloidosis: Necessary and sufficient for clinical expression of Alzheimer disease?’, *JAMA Neurology*, 70(4), pp. 455–461. doi: 10.1001/jamaneurol.2013.1321.

Rabin, J. S. *et al.* (2018) ‘Interactive associations of vascular risk and β-amyloid burden with cognitive decline in clinically normal elderly individuals findings from the Harvard

Aging Brain Study', *JAMA Neurology*, 75(9), pp. 1124–1131. doi: 10.1001/jamaneurol.2018.1123.

Rabin, J. S. *et al.* (2019) 'Vascular Risk and β -Amyloid Are Synergistically Associated with Cortical Tau', *Annals of Neurology*, 85(2), pp. 272–279. doi: 10.1002/ana.25399.

Rabin, L. A., Smart, C. M. and Amariglio, R. E. (2017) 'Subjective Cognitive Decline in Preclinical Alzheimer's Disease', *Annual Review of Clinical Psychology*, 13(1), pp. 369–396. doi: 10.1146/annurev-clinpsy-032816-045136.

Rabinovici, G. D. (2019) 'Late-onset Alzheimer Disease', *CONTINUUM: Lifelong Learning in Neurology*, 25(1), pp. 14–33. doi: 10.1212/CON.0000000000000700.

Rami, L. *et al.* (2014) 'The subjective cognitive decline questionnaire (SCD-Q): A validation study', *Journal of Alzheimer's Disease*, 41(2), pp. 453–466. doi: 10.3233/JAD-132027.

Rawle, M. J. *et al.* (2018) 'Apolipoprotein-E (Apoe) ε4 and cognitive decline over the adult life course', *Translational Psychiatry*, 8(1), p. 18. doi: 10.1038/s41398-017-0064-8.

Resnick, S. M. *et al.* (2003) 'Longitudinal magnetic resonance imaging studies of older adults: A shrinking brain', *Journal of Neuroscience*, 23(8), pp. 3295–3301. doi: 10.1523/jneurosci.23-08-03295.2003.

Reuter, M. *et al.* (2012) 'Within-subject template estimation for unbiased longitudinal image analysis.', *NeuroImage*, 61(4), pp. 1402–18. doi: 10.1016/j.neuroimage.2012.02.084.

Reuter, M. and Fischl, B. (2011) 'Avoiding asymmetry-induced bias in longitudinal

image processing', *NeuroImage*, pp. 19–21. doi: 10.1016/j.neuroimage.2011.02.076.

Reuter, M., Rosas, H. D. and Fischl, B. (2010) 'Highly accurate inverse consistent registration: A robust approach', *NeuroImage*, 53(4), pp. 1181–1196. doi: 10.1016/j.neuroimage.2010.07.020.

Ridha, B. H. *et al.* (2006) 'Tracking atrophy progression in familial Alzheimer's disease: a serial MRI study', *Lancet Neurology*, 5(10), pp. 828–834. doi: 10.1016/S1474-4422(06)70550-6.

Ridha, B. H. *et al.* (2008) 'Volumetric MRI and cognitive measures in Alzheimer disease: Comparison of markers of progression', *Journal of Neurology*, 255(4), pp. 567–574. doi: 10.1007/s00415-008-0750-9.

Rizvi, B. *et al.* (2018) 'The effect of white matter hyperintensities on cognition is mediated by cortical atrophy', *Neurobiology of Aging*, 64, pp. 25–32. doi: 10.1016/j.neurobiolaging.2017.12.006.

Roseborough, A. *et al.* (2017) 'Associations between amyloid β and white matter hyperintensities: A systematic review', *Alzheimer's & Dementia*, 13(10), pp. 1154–1167. doi: 10.1016/j.jalz.2017.01.026.

Rosenich, E. *et al.* (2022) 'Differential Effects of APOE and Modifiable Risk Factors on Hippocampal Volume Loss and Memory Decline in Aβ− and Aβ+ Older Adults', *Neurology*, 98(17), pp. e1704–e1715. doi: 10.1212/WNL.0000000000200118.

Rowe, C. C. and Villemagne, V. L. (2013) 'Brain amyloid imaging', *Journal of Nuclear Medicine Technology*, 41(1), pp. 11–18. doi: 10.2967/jnumed.110.076315.

Rusinek, H. *et al.* (2003) 'Regional Brain Atrophy Rate Predicts Future Cognitive

Decline: 6-year Longitudinal MR Imaging Study of Normal Aging', *Radiology*, 229(3), pp. 691–696. doi: 10.1148/radiol.2293021299.

Ryan, N. S. *et al.* (2013) 'Magnetic resonance imaging evidence for presymptomatic change in thalamus and caudate in familial Alzheimer's disease', *Brain*, 136(5), pp. 1399–1414. doi: 10.1093/brain/awt065.

Salthouse, T. A. (2019) 'Trajectories of normal cognitive aging.', *Psychology and Aging*, 34(1), pp. 17–24. doi: 10.1037/pag0000288.

Samaroo, A. *et al.* (2020) 'Diminished Learning Over Repeated Exposures (LORE) in preclinical Alzheimer's disease', *Alzheimer's & Dementia: Diagnosis, Assessment & Disease Monitoring*, 12(1). doi: 10.1002/dad2.12132.

Sandeman, E. M. *et al.* (2013) 'Incidental Findings on Brain MR Imaging in Older Community-Dwelling Subjects Are Common but Serious Medical Consequences Are Rare: A Cohort Study', *PLoS ONE*, 8(8), p. e71467. doi: 10.1371/journal.pone.0071467.

Sarji, S. A. *et al.* (1998) 'Failed magnetic resonance imaging examinations due to claustrophobia', *Australasian Radiology*, 42(4), pp. 293–295. doi: 10.1111/j.1440-1673.1998.tb00525.x.

Say, M. J. *et al.* (2011) 'Visuomotor integration deficits precede clinical onset in Huntington's disease', *Neuropsychologia*, 49(2), pp. 264–270. doi: 10.1016/j.neuropsychologia.2010.11.016.

Scahill, R. I. *et al.* (2003) 'A longitudinal study of brain volume changes in normal aging using serial registered magnetic resonance imaging', *Archives of Neurology*, 60(7), pp. 989–994. doi: 10.1001/archneur.60.7.989.

Scheffer, S. *et al.* (2021) 'Vascular Hypothesis of Alzheimer Disease', *Arteriosclerosis, Thrombosis, and Vascular Biology*, 41(4), pp. 1265–1283. doi: 10.1161/ATVBAHA.120.311911.

Scheuner, D. *et al.* (1996) 'Secreted amyloid beta-protein similar to that in the senile plaques of Alzheimer's disease is increased in vivo by the presenilin 1 and 2 and APP mutations linked to familial Alzheimer's disease.', *Nature medicine*, 2(8), pp. 864–70. Available at: http://www.ncbi.nlm.nih.gov/pubmed/8705854 (Accessed: 5 March 2019).

Schmidt, C. O. *et al.* (2013) 'Psychosocial consequences and severity of disclosed incidental findings from whole-body MRI in a general population study', *European Radiology*, 23(5), pp. 1343–1351. doi: 10.1007/s00330-012-2723-8.

Schneider, J. A. and Viswanathan, A. (2019) 'The time for multiple biomarkers in studies of cognitive aging and dementia is now', *Neurology*, pp. 551–552. doi: 10.1212/WNL.0000000000007120.

Schott, J. M. *et al.* (2003) 'Assessing the onset of structural change in familial Alzheimer's disease', *Annals of Neurology*, 53(2), pp. 181–188. doi: 10.1002/ana.10424.

Schott, J. M. *et al.* (2005) 'Measuring atrophy in Alzheimer disease: a serial MRI study over 6 and 12 months.', *Neurology*, 65(1), pp. 119–24. doi: 10.1212/01.wnl.0000167542.89697.0f.

Schott, J. M. *et al.* (2008) 'Neuropsychological correlates of whole brain atrophy in Alzheimer's disease', *Neuropsychologia*, 46(6), pp. 1732–1737. doi: 10.1016/J.NEUROPSYCHOLOGIA.2008.02.015.

Schott, J.M. *et al.* (2010) 'Increased brain atrophy rates in cognitively normal older

adults with low cerebrospinal fluid Aβ1-42', *Annals of Neurology*, 68(6), pp. 825–834. doi: 10.1002/ana.22315.

Schott, J M *et al.* (2010) 'Reduced sample sizes for atrophy outcomes in Alzheimer's disease trials: baseline adjustment.', *Neurobiology of aging*, 31(8), pp. 1452–62, 1462.e1–2. doi: 10.1016/j.neurobiolaging.2010.04.011.

Schott, J. M. (2017) 'The neurology of ageing: what is normal?', *Practical Neurology*, 17(3), pp. 172–182. doi: 10.1136/practneurol-2016-001566.

Schretlen, D. *et al.* (2000) 'Elucidating the contributions of processing speed, executive ability, and frontal lobe volume to normal age-related differences in fluid intelligence', *Journal of the International Neuropsychological Society*, 6(1), pp. 52–61. doi: 10.1017/S1355617700611062.

Schwarz, C. G. *et al.* (2016) 'A large-scale comparison of cortical thickness and volume methods for measuring Alzheimer's disease severity', *NeuroImage: Clinical*, 11, pp. 802–812. doi: 10.1016/j.nicl.2016.05.017.

Selkoe, D. J. (2001) 'Alzheimer's disease: genes, proteins, and therapy.', *Physiological reviews*, 81(2), pp. 741–66. doi: 10.1152/physrev.2001.81.2.741.

Selkoe, D. J. and Hardy, J. (2016) 'The amyloid hypothesis of Alzheimer's disease at 25 years.', *EMBO molecular medicine*, 8(6), pp. 595–608. doi: 10.15252/emmm.201606210.

Seo, E. H. *et al.* (2016) 'Independent and Interactive Influences of the APOE Genotype and Beta-Amyloid Burden on Cognitive Function in Mild Cognitive Impairment', *Journal of Korean Medical Science*, 31(2), p. 286. doi: 10.3346/jkms.2016.31.2.286.

Seshadri, S. *et al.* (2006) 'The Lifetime Risk of Stroke', *Stroke*, 37(2), pp. 345–350. doi: 10.1161/01.STR.0000199613.38911.b2.

Shi, Y. *et al.* (2017) 'ApoE4 markedly exacerbates tau-mediated neurodegeneration in a mouse model of tauopathy', *Nature*, 549(7673), pp. 523–527. doi: 10.1038/nature24016.

Smith, C. D. *et al.* (2007) 'Brain structural alterations before mild cognitive impairment', *Neurology*, 68(16), pp. 1268–1273. doi: 10.1212/01.wnl.0000259542.54830.34.

Snowdon, D. A. *et al.* (1997) 'Brain Infarction and the Clinical Expression of Alzheimer Disease: The Nun Study', *JAMA*, 277(10), pp. 813–817. doi: 10.1001/jama.1997.03540340047031.

Soldan, A. *et al.* (2020) 'White matter hyperintensities and CSF Alzheimer disease biomarkers in preclinical Alzheimer disease', *Neurology*, 94(9), pp. e950–e960. doi: 10.1212/WNL.0000000000008864.

Sperling, R. A. *et al.* (2014) 'The A4 Study: Stopping AD Before Symptoms Begin?', *Science Translational Medicine*, 6(228), pp. 228fs13-228fs13. doi: 10.1126/scitranslmed.3007941.

Sperling, R., Mormino, E. and Johnson, K. (2014) 'The evolution of preclinical Alzheimer's disease: Implications for prevention trials', *Neuron*, pp. 608–622. doi: 10.1016/j.neuron.2014.10.038.

Spielberger, C. D. *et al.* (1983) 'Manual for the State-Trait Anxiety Inventory', *Consulting Psychologists Press*.

Stafford, M. *et al.* (2013) 'Using a birth cohort to study ageing: Representativeness and

response rates in the National Survey of Health and Development', *European Journal of Ageing*, 10(2), pp. 145–157. doi: 10.1007/s10433-013-0258-8.

Stang, A. *et al.* (2006) 'Algorithms for converting random-zero to automated oscillometric blood pressure values, and vice versa', *American Journal of Epidemiology*, 164(1), pp. 85–94. doi: 10.1093/aje/kwj160.

Stern, Y. and Barulli, D. (2019) 'Cognitive reserve', in *Handbook of Clinical Neurology*. Elsevier B.V., pp. 181–190. doi: 10.1016/B978-0-12-804766-8.00011-X.

Storandt, M. *et al.* (2009) 'Cognitive decline and brain volume loss as signatures of cerebral amyloid-β peptide deposition identified with Pittsburgh compound B: Cognitive decline associated with Aβ deposition', *Archives of Neurology*, 66(12), pp. 1476–1481. doi: 10.1001/archneurol.2009.272.

De Strooper, B. and Karran, E. (2016) 'The Cellular Phase of Alzheimer's Disease', *Cell*, pp. 603–615. doi: 10.1016/j.cell.2015.12.056.

Sudre, C. H. *et al.* (2015) 'Bayesian model selection for pathological neuroimaging data applied to white matter lesion segmentation.', *IEEE transactions on medical imaging*, 34(10), pp. 2079–102. doi: 10.1109/TMI.2015.2419072.

Tarawneh, R. *et al.* (2015) 'Cerebrospinal Fluid Markers of Neurodegeneration and Rates of Brain Atrophy in Early Alzheimer Disease', *JAMA Neurology*, 72(6), p. 656. doi: 10.1001/jamaneurol.2015.0202.

Taylor, A. M., Pattie, A. and Deary, I. J. (2018) 'Cohort profile update: The Lothian birth cohorts of 1921 and 1936', *International Journal of Epidemiology*, pp. 1042–1060. doi: 10.1093/ije/dyy022.

Thal, D. R. *et al.* (2002) 'Phases of Aβ-deposition in the human brain and its relevance for the development of AD', *Neurology*, 58(12), pp. 1791–1800. doi: 10.1212/WNL.58.12.1791.

Thal, D. R., Attems, J. and Ewers, M. (2014) 'Spreading of Amyloid, Tau, and Microvascular Pathology in Alzheimer's Disease: Findings from Neuropathological and Neuroimaging Studies', *Journal of Alzheimer's Disease*, 42(s4), pp. S421–S429. doi: 10.3233/JAD-141461.

Thambisetty, M. *et al.* (2010) 'Longitudinal changes in cortical thickness associated with normal aging', *NeuroImage*, 52(4), pp. 1215–1223. doi: 10.1016/j.neuroimage.2010.04.258.

Thanprasertsuk, S. *et al.* (2014) 'Posterior white matter disease distribution as a predictor of amyloid angiopathy', *Neurology*, 83(9), pp. 794–800. doi: 10.1212/WNL.0000000000000732.

Tondelli, M. *et al.* (2012) 'Structural MRI changes detectable up to ten years before clinical Alzheimer's disease', *Neurobiology of Aging*, 33(4), pp. 825.e25-825.e36. doi: 10.1016/J.NEUROBIOLAGING.2011.05.018.

Tosto, G. *et al.* (2015) 'The effect of white matter hyperintensities on neurodegeneration in mild cognitive impairment', *Alzheimer's & Dementia*, 11(12), pp. 1510–1519. doi: 10.1016/j.jalz.2015.05.014.

Trembath, L., Newell, M. and Devous, M. D. (2015) 'Technical Considerations in Brain Amyloid PET Imaging with 18F-Florbetapir', *Journal of Nuclear Medicine Technology*, 43(3), pp. 175–184. doi: 10.2967/jnmt.115.156679.

Tripathi, Madhavi *et al.* (2014) 'Differential Diagnosis of Neurodegenerative Dementias

Using Metabolic Phenotypes on F-18 FDG PET/CT', *The Neuroradiology Journal*, 27(1), pp. 13–21. doi: 10.15274/NRJ-2014-10002.

Tuladhar, A. M. *et al.* (2015) 'Relationship Between White Matter Hyperintensities, Cortical Thickness, and Cognition', *Stroke*, 46(2), pp. 425–432. doi: 10.1161/STROKEAHA.114.007146.

Tustison, N. J. *et al.* (2010) 'N4ITK: Improved N3 bias correction', *IEEE Transactions on Medical Imaging*, 29(6), pp. 1310–1320. doi: 10.1109/TMI.2010.2046908.

Valenzuela, M. J. (2008) 'Brain reserve and the prevention of dementia', *Current Opinion in Psychiatry*. Curr Opin Psychiatry, pp. 296–302. doi: 10.1097/YCO.0b013e3282f97b1f.

Vemuri, P. *et al.* (2010) 'Serial MRI and CSF biomarkers in normal aging, MCI, and AD', *Neurology*, 75(2), pp. 143–151. doi: 10.1212/WNL.0b013e3181e7ca82.

Vemuri, P. *et al.* (2015) 'Vascular and amyloid pathologies are independent predictors of cognitive decline in normal elderly', *Brain*, 138(3), pp. 761–771. doi: 10.1093/brain/awu393.

Vemuri, P. and Jack, C. R. (2010) 'Role of structural MRI in Alzheimer's disease', *Alzheimer's Research & Therapy*, 2(4), p. 23. doi: 10.1186/alzrt47.

Verghese, P. B., Castellano, J. M. and Holtzman, D. M. (2011) 'Apolipoprotein E in Alzheimer's disease and other neurological disorders', *The Lancet Neurology*, 10(3), pp. 241–252. doi: 10.1016/S1474-4422(10)70325-2.

Verhaaren, B. F. J. *et al.* (2013) 'High blood pressure and cerebral white matter lesion progression in the general population', *Hypertension*, 61(6), pp. 1354–1359. doi:

10.1161/HYPERTENSIONAHA.111.00430.

Villeneuve, S. *et al.* (2014) 'Vascular risk and A interact to reduce cortical thickness in AD vulnerable brain regions', *Neurology*, 83(1), pp. 40–47. doi: 10.1212/WNL.0000000000000550.

Vinters, H. V and Gilbert, J. J. (1983) 'Cerebral amyloid angiopathy: incidence and complications in the aging brain. II. The distribution of amyloid vascular changes.', *Stroke*, 14(6), pp. 924–928. doi: 10.1161/01.STR.14.6.924.

Vipin, A. *et al.* (2018) 'Regional white matter hyperintensity influences grey matter atrophy in mild cognitive impairment', *Journal of Alzheimer's Disease*, 66(2), pp. 533–549. doi: 10.3233/JAD-180280.

Vizza, P. *et al.* (2013) 'Methodologies for the analysis and classification of PET neuroimages', *Network Modeling Analysis in Health Informatics and Bioinformatics*, 2(4), pp. 191–208. doi: 10.1007/s13721-013-0035-9.

Vos, S. J. B. *et al.* (2013) 'Preclinical Alzheimer's disease and its outcome: A longitudinal cohort study', *The Lancet Neurology*, 12(10), pp. 957–965. doi: 10.1016/S1474-4422(13)70194-7.

Vyhnalek, M. *et al.* (2014) 'Neuropsychological correlates of hippocampal atrophy in memory testing in nondemented older adults', in *Journal of Alzheimer's Disease*, pp. S81–S90. doi: 10.3233/JAD-132642.

Van Waalwijk Van Doorn, L. J. C. *et al.* (2021) 'White Matter Hyperintensities Are No Major Confounder for Alzheimer's Disease Cerebrospinal Fluid Biomarkers', *Journal of Alzheimer's Disease*, 79(1), pp. 163–175. doi: 10.3233/JAD-200496.

Wadsworth, M. (2010) 'The origins and innovatory nature of the 1946 British national birth cohort study', *Longitudinal and Life Course Studies*, 1(2), pp. 121–136. doi: 10.14301/llcs.v1i2.64.

Wagen, A. Z. *et al.* (2022) 'Life course, genetic, and neuropathological associations with brain age in the 1946 British Birth Cohort: a population-based study', *The Lancet Healthy Longevity*. doi: 10.1016/S2666-7568(22)00167-2.

Walsh, P. *et al.* (2020) 'CSF amyloid is a consistent predictor of white matter hyperintensities across the disease course from aging to Alzheimer's disease', *Neurobiology of Aging*, 91, pp. 5–14. doi: 10.1016/j.neurobiolaging.2020.03.008.

Wardlaw, J. M. *et al.* (2013) 'Neuroimaging standards for research into small vessel disease and its contribution to ageing and neurodegeneration', *The Lancet Neurology*, pp. 822–838. doi: 10.1016/S1474-4422(13)70124-8.

Wardlaw, J. M., Smith, C. and Dichgans, M. (2013) 'Mechanisms of sporadic cerebral small vessel disease: Insights from neuroimaging', *The Lancet Neurology*, pp. 483–497. doi: 10.1016/S1474-4422(13)70060-7.

Wechsler, D. (1987) 'Wechsler memory scale-revised', *Psychological Corporation*.

Wechsler, D. (2011) 'Wechsler abbreviated scale of intelligence', *Psychological Corporation*.

Wechsler, D. and De Lemos, M. M. (1981) 'Wechsler adult intelligence scale-revised', *Harcourt Brace Jovanovich*.

Weiner, M. W. *et al.* (2010) 'The Alzheimer's Disease Neuroimaging Initiative: Progress report and future plans', *Alzheimer's & Dementia*, 6(3), p. 202. doi:

10.1016/j.jalz.2010.03.007.

Westman, E. *et al.* (2013) 'Regional magnetic resonance imaging measures for multivariate analysis in Alzheimer's disease and mild cognitive impairment', *Brain Topography*, 26(1), pp. 9–23. doi: 10.1007/s10548-012-0246-x.

Weston, P. S. J. *et al.* (2016) 'Presymptomatic cortical thinning in familial Alzheimer disease', *Neurology*, 87(19), pp. 2050–2057. doi: 10.1212/WNL.0000000000003322.

Whitwell, J. L. *et al.* (2012) 'Comparison of imaging biomarkers in the Alzheimer Disease Neuroimaging Initiative and the Mayo Clinic Study of Aging', *Archives of Neurology*, 69(5), pp. 614–622. doi: 10.1001/archneurol.2011.3029.

Whitwell, J. L. *et al.* (2013) 'Does amyloid deposition produce a specific atrophic signature in cognitively normal subjects?', *NeuroImage: Clinical*, 2(1), pp. 249–257. doi: 10.1016/j.nicl.2013.01.006.

Wilcock, G. K. (2003) 'Memantine for the treatment of dementia', *The Lancet Neurology*, 2(8), pp. 503–505. doi: 10.1016/S1474-4422(03)00486-1.

Wilson, R. S. *et al.* (2009) 'Educational attainment and cognitive decline in old age', *Neurology*, 72(5), pp. 460–465. doi: 10.1212/01.wnl.0000341782.71418.6c.

Wirth, M., Madison, C. M., *et al.* (2013) 'Alzheimer's disease neurodegenerative biomarkers are associated with decreased cognitive function but not-amyloid in cognitively normal older individuals', *Journal of Neuroscience*, 33(13), pp. 5553–5563. doi: 10.1523/JNEUROSCI.4409-12.2013.

Wirth, M., Villeneuve, S., *et al.* (2013) 'Associations between Alzheimer disease biomarkers, neurodegeneration, and cognition in cognitively normal older people',

JAMA Neurology, 70(12), pp. 1512–1519. doi: 10.1001/jamaneurol.2013.4013.

Wiseman, F. K. *et al.* (2015) 'A genetic cause of Alzheimer disease: mechanistic insights from Down syndrome.', *Nature reviews. Neuroscience*, 16(9), pp. 564–74. doi: 10.1038/nrn3983.

Wolf, S. M. *et al.* (2008) 'Managing incidental findings in human subjects research: Analysis and recommendations', in *Journal of Law, Medicine and Ethics*, pp. 219–248. doi: 10.1111/j.1748-720X.2008.00266.x.

Wu, W. *et al.* (2008) 'The brain in the age of old: The hippocampal formation is targeted differentially by diseases of late life', *Annals of Neurology*, 64(6), pp. 698–706. doi: 10.1002/ana.21557.

Yang, J. *et al.* (1996) 'Investigation of partial volume correction methods for brain fdg pet studies', *IEEE Transactions on Nuclear Science*, 43(6 PART 2), pp. 3322–3327. doi: 10.1109/23.552745.

Yu, J.-T., Tan, L. and Hardy, J. (2014) 'Apolipoprotein E in Alzheimer's Disease: An Update', *Annual Review of Neuroscience*, 37(1), pp. 79–100. doi: 10.1146/annurev-neuro-071013-014300.

Zetterberg, H. (2019) 'Blood-based biomarkers for Alzheimer's disease—An update', *Journal of Neuroscience Methods*, pp. 2–6. doi: 10.1016/j.jneumeth.2018.10.025.

Zeydan, B. *et al.* (2019) 'Investigation of white matter PiB uptake as a marker of white matter integrity', *Annals of Clinical and Translational Neurology*, 6(4), pp. 678–688. doi: 10.1002/acn3.741.

Zhang, H. *et al.* (2012) 'NODDI: Practical in vivo neurite orientation dispersion and

density imaging of the human brain', *NeuroImage*, 61(4), pp. 1000–1016. doi: 10.1016/j.neuroimage.2012.03.072.

Zipursky, R. B., Lim, K. O. and Pfefferbaum, A. (1989) 'MRI Study of Brain Changes with Short-Term Abstinence from Alcohol', *Alcoholism: Clinical and Experimental Research*, 13(5), pp. 664–667. doi: 10.1111/j.1530-0277.1989.tb00401.x.

Zlokovic, B. V. (2011) 'Neurovascular pathways to neurodegeneration in Alzheimer's disease and other disorders', *Nature Reviews Neuroscience*, p. 723. doi: 10.1038/nrn3114.

Appendix 1

MRC National Survey of Health and Development Neuroimaging sub-study
Participant Consent Form
Electronic Version 3.2:09-Jul-2020

PLEASE INITIAL BOXES – where you agree

1. I confirm that I have read and understand the information booklet for this follow-up of the MRC National Survey of Health and Development (version 3.1 dated 15 November 2017) and the remote testing information sheet (version 1.0 dated 09 July 2020). I have had the opportunity to consider the information, ask questions about the study and have had these answered satisfactorily. ☐
2. I understand that certain assessments will be audio and video recorded. ☐
3. I understand that relevant sections of any of my medical notes and data collected during the study may be looked at by responsible individuals from the MRC National Survey of Health and Development, from regulatory authorities or from the NHS Trust where it is relevant to my taking part in this research. I give permission for these individuals to have access to my records. ☐
4. I agree to have my research data electronically linked to other databases including those from primary care, Hospital Episode Statistics, NHS Health and Social Care Information Centre, research, clinical and administrative registries. To do this, I understand that my name, postcode, date of birth and NHS number will be shared with the NHS Health and Social Care Information Centre. ☐
5. I understand that the blood and urine samples will be used for research purposes only, and that no information found in the DNA or RNA will be given to me. ☐
6. I agree to the information and samples being used for health research carried out by the study team, and by scientists with research projects approved by the study's Data Sharing Committee. I understand that all analysis will be carried out and published using data only in numeric and anonymised form. ☐
7. I agree to the information and samples being held by UCL as the Data Controller. UCL is responsible for ensuring all data are securely stored, handled and used in accordance with the Data Protection Act. ☐
8. I agree that the results of the tests and measures listed in the GP letter will be sent to my GP. ☐
9. I agree to take part in the above study. ☐

_____	_____	_____
Name of study member	Date	Signature
_____	_____	_____
Name of person taking consent	Date	Signature

Thank you for agreeing to participate in the MRC NSHD Neuroimaging sub-study

When completed, 1 for study member, 1 for Institute of Neurology, and original for MRC NSHD

MRC Unit for Lifelong Health and Ageing at UCL 33 Bedford Place London WC1B 5JU
Telephone: 020 7670 5700 www.nshd.mrc.ac.uk

Appendix 2

Chapter Five: Sensitivity analyses without adjustment for age at baseline scan

1. *a) Effects of Aβ status, global Aβ SUVR and WMHV (assessed in separate models)*

Predictor of interest	Difference in rate of change in BSI in ml/year (95% CIs)		
	Whole Brain	Ventricles	Total Hippocampus
Positive Aβ status (negative as reference)	-0.89* (-1.75, -0.03)	0.39** (0.17, 0.65)‡	-0.016** (-0.027, -0.004)
Global Aβ SUVR (per 0.1-unit increment)	-0.39 (-0.85, 0.07)	0.20** (0.08, 0.32)‡	-0.009** (-0.015, -0.002)
WMHV (per 10ml increment)	-1.10** (-1.70, -0.50)	0.32** (0.12, 0.62)‡	-0.014** (-0.023, -0.006)

1. *b) Effects of Aβ status and WMHV (assessed in same model)*

Predictor of interest	Difference in rate of change in BSI in ml/year (95% CIs)		
	Whole Brain	Ventricles	Total Hippocampus
Positive Aβ status (negative as reference)	-0.84* (-1.69, 0.00)	0.38** (0.15, 0.64)‡	-0.015** (-0.027, -0.004)
WMHV (per 10ml increment)	-1.08** (-1.69, -0.48)	0.32** (0.13, 0.60)‡	-0.014** (-0.022, -0.006)

1. *c) Effects of Aβ SUVR and WMHV (assessed in same model)*

Predictor of interest	Difference in rate of change in BSI in ml/year (95% CIs)		
	Whole Brain	Ventricles	Total Hippocampus
Global Aβ SUVR (per 0.1-unit increment)	-0.30 (-0.76, 0.15)	0.17** (0.05, 0.30)‡	-0.008* (-0.014, -0.001)
WMHV (per 10ml increment)	-1.06** (-1.66, -0.45)	0.30** (0.10, 0.59)‡	-0.013** (-0.022, -0.005)

*Aβ = β-amyloid; SUVR = standardised uptake value ratio; WMHV = white matter hyperintensity volume; BSI = boundary shift integral. All models were adjusted for sex and total intracranial volume. *p ≤0.05; **p ≤0.01; ‡ bias-corrected accelerated bootstrap 95% CIs.*

2. *Effects of APOE ε4 carrier status*

Model	Difference in rate of change in BSI in ml/year (95% CIs) in APOE ε4 carriers compared to non-carriers		
	Whole brain	Ventricles	Total hippocampus
1	-0.61 (-1.32, 0.09)	0.11 (-0.08, 0.30)‡	-0.010* (-0.020, -0.001)
2	-0.42 (-1.17, 0.32)	0.00 (-0.18, 0.22)‡	-0.007 (-0.017, 0.003)
3	-0.51 (-1.20, 0.19)	0.07 (-0.12, 0.27)‡	-0.009 (-0.019, 0.001)
4	-0.32 (-1.05, 0.42)	-0.03 (-0.23, 0.18)‡	-0.005 (-0.015, 0.005)

*BSI = boundary shift integral. Model 1 was adjusted for sex and total intracranial volume. Model 2 represents Model 1 plus adjustment for baseline β-amyloid status. Model 3 represents Model 1 plus adjustment for baseline white matter hyperintensity volume. Model 4 represents Model 1 plus adjustment for baseline β-amyloid status and white matter hyperintensity volume. *p ≤0.05; ‡ bias-corrected and accelerated bootstrap 95% CIs.*

3. Effects of the Framingham Heart Study Cardiovascular Risk Score at ages 36, 53 and 69

		Difference in rate of change in BSI in ml/year (95% CIs) per 5% increment in the FHS-CVS		
		Whole Brain	Ventricles	Total Hippocampus
Age 36 (n=301)	Model 1	-0.41 (-1.67, 0.85)	0.09 (-0.25, 0.47)‡	0.006 (-0.012, 0.024)
	Model 2	-0.27 (-1.52, 0.97)	0.05 (-0.30, 0.42)‡	0.008 (-0.009, 0.026)
Age 53 (n=326)	Model 1	-0.09 (-0.38, 0.21)	-0.01 (-0.10, 0.07)‡	-0.002 (-0.006, 0.002)
	Model 2	-0.06 (-0.35, 0.23)	-0.02 (-0.10, 0.06)‡	-0.002 (-0.005, 0.002)
Age 69 (n=330)	Model 1	-0.15 (-0.32, 0.02)	0.06* (0.00, 0.14)‡	-0.002 (-0.004, 0.000)
	Model 2	-0.12 (-0.29, 0.05)	0.05 (-0.01, 0.12)‡	-0.001 (-0.004, 0.001)

*BSI = boundary shift integral; FHS-CVS = Framingham Heart Study Cardiovascular Risk Score. Model 1 was adjusted for sex, total intracranial volume, APOE ε4 status, adult socioeconomic position and baseline β-amyloid status. Model 2 was further adjusted for baseline white matter hyperintensity volume. Effects at age 53 refer to results after excluding an outlier. *p ≤0.05; ‡ bias-corrected and accelerated bootstrap 95% CIs.*

4. Effects of systolic blood pressure at ages 36, 53 and 69

		Difference in rate of change in BSI in ml/year (95% CIs) per 10mmHg increment in systolic blood pressure		
		Whole Brain	Ventricles	Total Hippocampus
Age 36 (m=301)	Model 1	-0.06 (-0.32, 0.20)	-0.01 (-0.09, 0.06)‡	-0.000 (-0.004, 0.003)
	Model 2	-0.06 (-0.32, 0.20)	-0.01 (-0.08, 0.06)‡	-0.000 (-0.004, 0.003)
Age 53 (n=325)	Model 1	-0.07 (-0.25, 0.11)	0.02 (-0.02, 0.08)‡	-0.002 (-0.005, 0.000)
	Model 2	-0.04 (-0.22, 0.14)	0.01 (-0.04, 0.05)‡	-0.002 (-0.004, 0.001)
Age 69 (n=333)	Model 1	-0.02 (-0.23, 0.19)	0.05 (-0.01, 0.14)‡	-0.001 (-0.004, 0.002)
	Model 2	0.02 (-0.18, 0.23)	0.03 (-0.03, 0.11)‡	-0.000 (-0.003, 0.003)

BSI = boundary shift integral. Model 1 was adjusted for sex, total intracranial volume, APOE ε4 status, adult socioeconomic position, baseline β-amyloid status, and smoking status, presence of diabetes and body mass index around time of baseline scan. Model 2 was further adjusted for baseline white matter hyperintensity volume. Effects at age 53 refer to results after excluding an outlier. ‡ bias-corrected and accelerated bootstrap 95% CIs.

Appendix 3

Chapter Six: Sensitivity analyses without adjustment for age at baseline scan

1. *a) Effects of Aβ status, global Aβ SUVR and WMHV (assessed in separate models)*

Predictor of interest	Difference in rate of change in cortical thickness (95% CIs)			
	ADsig Harvard		ADsig Mayo	
	mm/year	%/year	mm/year	%/year
Positive Aβ status (negative as reference)	0.002 (-0.002, 0.005)	0.06 (-0.08, 0.21)	-0.001 (-0.005, 0.003)	-0.04 (-0.20, 0.13)
Global Aβ SUVR (per 0.1-unit increment)	0.000 (-0.002, 0.002)	0.01 (-0.07, 0.09)	-0.001 (-0.004, 0.001)	-0.05 (-0.13, 0.04)
WMHV (per 10ml increment)	-0.004** (-0.006, -0.001)	-0.15** (-0.25, -0.05)	-0.004* (-0.007,-0.001)	-0.15** (-0.26, -0.04)

1. *b) Effects of Aβ status and WMHV (assessed in same model)*

Predictor of interest	Difference in rate of change in cortical thickness (95% CIs)			
	ADsig Harvard		ADsig Mayo	
	mm/year	%/year	mm/year	%/year
Positive Aβ status (negative as reference)	0.002 (-0.002, 0.005)	0.07 (-0.08, 0.21)	-0.001 (-0.005, 0.004)	-0.03 (-0.19, 0.13)
WMHV (per 10ml increment)	-0.004** (-0.006, -0.001)	-0.15** (-0.25, -0.05)	-0.004* (-0.007,-0.001)	-0.15* (-0.26, -0.04)

1. *c) Effects of Aβ SUVR and WMHV (assessed in same model)*

Predictor of interest	Difference in rate of change in cortical thickness (95% CIs)			
	ADsig Harvard		ADsig Mayo	
	mm/year	%/year	mm/year	%/year
Global Aβ SUVR (per 0.1-unit increment)	0.001 (-0.001, 0.003)	0.03 (-0.05, 0.10)	-0.000 (-0.003, 0.001)	-0.04 (-0.12, 0.05)
WMHV (per 10ml increment)	-0.004** (-0.006, -0.001)	-0.15** (-0.26, -0.05)	-0.004* (-0.007,-0.001)	-0.15* (-0.26, -0.03)

Aβ = β-amyloid; SUVR = standardised uptake value ratio; WMHV = white matter hyperintensity volume.

*All models were adjusted for sex. . * p ≤0.05 ** p ≤0.01*

2. *Effects of APOE ε4 carrier status*

Model	Difference in rate of change in cortical thickness (95% CIs) in APOE ε4 carriers compared to non-carriers			
	ADsig Harvard		ADsig Mayo	
	mm/year	%/year	mm/year	%/year
1	-0.003 (-0.006, 0.000)	-0.12 (-0.24, 0.00)	-0.001 (-0.004, 0.003)	-0.03 (-0.17, 0.10)
2	-0.004* (-0.007, -0.001)	-0.15* (-0.27, -0.02)	-0.001 (-0.004, 0.003)	-0.03 (-0.17, 0.11)
3	-0.003* (-0.006, -0.000)	-0.13* (-0.26, -0.01)	-0.000 (-0.004, 0.004)	-0.01 (-0.15, 0.13)
4	-0.001** (-0.002, -0.000)	-0.05** (-0.08, -0.01)	0.002 (-0.001, 0.004)	0.07 (-0.02, 0.16)

*Model 1 was adjusted for sex. Model 2 represents Model 1 plus adjustment for baseline β-amyloid status. Model 3 represents Model 2 plus adjustment for baseline white matter hyperintensity volume. Model 4 represents Model 3 plus adjustment for rates of whole cortex thinning. *p ≤0.05 **p ≤0.01*

3. Effects of the Framingham Heart Study Cardiovascular Risk Score at ages 36, 53 and

Model		Difference in rate of change in cortical thickness (95% CIs) per 5% increment in the FHS-CVS			
		ADsig Harvard		ADsig Mayo	
		mm/year	%/year	mm/year	%/year
Age 36 (n=301)	1	0.003 (-0.002, 0.008)	0.11 (-0.10, 0.33)	-0.000 (-0.007, 0.006)	-0.01 (-0.25, 0.23)
	2	0.003 (-0.002, 0.008)	0.13 (-0.08, 0.34)	0.000 (-0.006, 0.007)	0.01 (-0.23, 0.25)
Age 53 (n=327)	1	-0.000 (-0.001, 0.001)	-0.01 (-0.06, 0.03)	-0.000 (-0.001, 0.001)	-0.00 (-0.05, 0.05)
	2	-0.000 (-0.001, 0.001)	-0.01 (-0.06, 0.04)	0.000 (-0.001, 0.001)	0.00 (-0.05, 0.05)
Age 69 (n=330)	1	-0.000 (-0.001, 0.001)	-0.00 (-0.03, 0.02)	0.000 (-0.001, 0.001)	0.01 (-0.02, 0.04)
	2	0.000 (-0.001, 0.001)	0.00 (-0.03, 0.03)	0.001 (-0.000, 0.001)	0.02 (-0.01, 0.05)

FHS-CVS = Framingham Heart Study Cardiovascular Risk Score. Model 1 was adjusted for sex, baseline β-amyloid status, APOE ε4 status and adult socioeconomic position. Model 2 was further adjusted for baseline white matter hyperintensity volume.

4. Effects of systolic blood pressure at ages 36, 53 and 69

Model		Difference in rate of change in cortical thickness (95% CIs) per 10 mmHg increment in the systolic BP			
		ADsig Harvard		ADsig Mayo	
		mm/year	%/year	mm/year	%/year
Age 36 (n=302)	1	-0.000 (-0.002, 0.001)	-0.02 (-0.06, 0.03)	-0.001 (-0.002, 0.001)	0.03 (-0.08, 0.02)
	2	-0.000 (-0.002, 0.001)	-0.02 (-0.06, 0.03)	-0.001 (-0.002, 0.001)	0.03 (-0.08, 0.02)
Age 53 (n=326)	1	-0.001 (-0.001, 0.000)	-0.02 (-0.05, 0.01)	-0.000 (-0.001, 0.001)	-0.01 (-0.05, 0.02)
	2	-0.000 (-0.001, 0.000)	-0.02 (-0.05, 0.01)	-0.000 (-0.001, 0.001)	-0.01 (-0.04, 0.02)
Age 69 (n=333)	1	-0.000 (-0.001, 0.001)	-0.01 (-0.04, 0.03)	-0.000 (-0.002, 0.001)	-0.01 (-0.06, 0.02)
	2	-0.000 (-0.001, 0.001)	-0.00 (-0.04, 0.03)	-0.000 (-0.001, 0.001)	-0.01 (-0.05, 0.03)

BP = blood pressure. Model 1 was adjusted for sex, baseline β-amyloid status, APOE ε4 status, adult socioeconomic position, and, smoking status, presence of diabetes and body mass index around time of baseline scan. Model 2 was further adjusted for baseline white matter hyperintensity volume.

Appendix 4

Chapter Six: Sensitivity analyses using Aβ data with partial volume correction

Predictor of interest	Difference in rate of change in cortical thickness (95% CIs)			
	ADsig Harvard		ADsig Mayo	
	mm/year	%/year	mm/year	%/year
Positive Aβ status (negative as reference)	0.001 (-0.003, 0.005)	0.04 (-0.11, 0.19)	-0.002 (-0.006, 0.003)	-0.06 (-0.22, 0.10)
Global Aβ SUVR (per 0.1-unit increment)	-0.000 (-0.001, 0.001)	-0.00 (-0.04, 0.04)	-0.001 (-0.002, 0.000)	-0.03 (-0.07, 0.01)

Aβ = β-amyloid; SUVR = standardised uptake value ratio. All models were adjusted for sex.

Appendix 5

Chapter Seven: Sensitivity analyses without adjustment for age at baseline scan

1. Predictors of rates of change in cognitive performance

Predictor	z-score difference in cognition per year (95% CIs)				
	PACC	MMSE	DSST	LMDR	FNAME
Female sex (male as reference)	-0.02 (-0.05, 0.02)	0.05 (-0.06, 0.16)‡	-0.01 (-0.06, 0.04)	**-0.10*** (-0.18, -0.02)	-0.01 (-0.06, 0.05)
Childhood cognition (per z-score)	0.01 (-0.02, 0.03)	0.06 (-0.02, 0.14)‡	-0.02 (-0.05, 0.02)	0.01 (-0.05, 0.07)	-0.04 (-0.07, 0.00)
Educational attainment (per category)	0.01 (-0.02, 0.04)	-0.02 (-0.10, 0.06)‡	-0.00 (-0.04, 0.03)	0.01 (-0.05, 0.07)	**0.04*** (0.01, 0.08)
Non-manual SEP (manual as reference)	-0.01 (-0.07, 0.04)	-0.01 (-0.20, 0.17)‡	0.06 (-0.00, 0.13)	-0.06 (-0.18, 0.06)	-0.04 (-0.12, 0.03)
APOE ε4 carrier (non-carrier as reference)	0.02 (-0.03, 0.06)	-0.03 (-0.15, 0.09)‡	-0.02 (-0.08, 0.03)	0.06 (-0.03, 0.15)	**0.06*** (0.00, 0.12)
Positive Aβ status (negative as reference)[a]	0.00 (-0.05, 0.05)	0.12 (-0.01, 0.26)‡	0.01 (-0.05, 0.07)	-0.06 (-0.17, 0.05)	-0.06 (-0.13, 0.01)
WMHV (per 10ml increment)	-0.01 (-0.04, 0.03)	-0.02 (-0.10, 0.06)‡	-0.01 (-0.05, 0.03)	0.02 (-0.05, 0.09)	-0.01 (-0.06, 0.03)
Rate of whole brain atrophy (per z-score)	**-0.02*** (-0.04, -0.00)	-0.04 (-0.10, 0.01)‡	0.00 (-0.02, 0.03)	-0.04 (-0.08, 0.00)	-0.02 (-0.04, 0.01)
Rate of ventricular expansion (per z-score)	-0.02 (-0.04, 0.00)	-0.04 (-0.09, 0.02)‡	0.00 (-0.02, 0.03)	-0.03 (-0.07, 0.01)	-0.02 (-0.04, 0.01)
Rate of total hippocampal atrophy (per z-score)	**-0.02*** (-0.04, -0.00)	-0.02 (-0.08, 0.03)‡	0.01 (-0.01, 0.04)	**-0.06**** (-0.10, -0.02)	-0.02 (-0.04, 0.01)

continued over

Predictor	z-score difference in cognition per year (95% CIs)				
	PACC	MMSE	DSST	LMDR	FNAME
Rate of ADsig Harvard cortical thinning (per z-score)	0.00 (-0.01, 0.02)	0.01 (-0.05, 0.06)‡	0.00 (-0.02, 0.03)	-0.00 (-0.04, 0.04)	0.01 (-0.01, 0.04)
Rate of ADsig Mayo cortical thinning (per z-score)	-0.00 (-0.02, 0.02)	-0.00 (-0.06, 0.05)‡	0.01 (-0.02, 0.03)	-0.02 (-0.06, 0.02)	0.01 (-0.02, 0.03)

*PACC = preclinical Alzheimer cognitive composite; MMSE = mini-mental state examination; DSST = digit symbol substitution test; LMDR = logical memory delayed recall; FNAME = face-name associative memory test; SEP = socioeconomic position; Aβ = β-amyloid; WMHV = white matter hyperintensity volume. Each structural MRI measure was assessed in a separate model, together with all other predictors. *p≤0.05. **p≤0.01.* ‡ bias-corrected and accelerated bootstrap 95% CIs.

2. Predictors of cognitive performance at phase two

Predictor	z-score difference in cognition at phase two (95% CIs)				
	PACC	MMSE	DSST	LMDR	FNAME
Female sex (male as reference)	**0.32*** ** (0.20, 0.44)	**0.31** ** (0.10, 0.52)‡	**0.32** ** (0.11, 0.53)	**0.30** ** (0.11, 0.50)	**0.35*** ** (0.14, 0.56)
Childhood cognition (per z-score)	**0.29*** ** (0.21, 0.38)	**0.30*** ** (0.13, 0.46)‡	**0.22** ** (0.07, 0.38)	**0.33*** ** (0.18, 0.47)	**0.33*** ** (0.17, 0.49)
Educational attainment (per category)	**0.24*** ** (0.16, 0.33)	**0.19*** (0.00, 0.39)‡	**0.31*** ** (0.15, 0.47)	**0.21** ** (0.06, 0.36)	**0.27*** ** (0.12, 0.43)
Non-manual SEP (manual as reference)	0.17 (-0.01, 0.34)	0.13 (-0.22, 0.56)‡	**0.38*** (0.07, 0.69)	-0.00 (-0.29, 0.28)	0.17 (-0.13, 0.48)
APOE ε4 carrier (non-carrier as reference)	0.06 (-0.08, 0.19)	-0.05 (-0.30, 0.18)‡	-0.05 (-0.29, 0.19)	**0.23*** (0.01, 0.46)	0.10 (-0.14, 0.34)

continued over

Predictor	z-score difference in cognition at phase two (95% CIs)				
	PACC	MMSE	DSST	LMDR	FNAME
Positive Aβ status (negative as reference)[a]	-0.03 (-0.19, 0.13)	0.15 (-0.11, 0.42)‡	-0.08 (-0.37, 0.21)	-0.18, (-0.44, 0.09)	-0.01 (-0.30, 0.27)
WMHV (per 10ml increment)	-0.07 (-0.17, 0.04)	0.05 (-0.13, 0.23)‡	-0.17 (-0.36, 0.03)	-0.07 (-0.25, 0.11)	-0.08 (-0.27, 0.12)
Rate of whole brain atrophy (per z-score)	**-0.11*** ** (-0.17, -0.05)	**-0.18*** ** (-0.29, -0.08)‡	-0.07 (-0.18, 0.04)	-0.06 (-0.16, 0.04)	**-0.12*** (-0.23, -0.01)
Rate of ventricular expansion (per z-score)	**-0.07*** (-0.13, -0.01)	**-0.14*** (-0.27, -0.01)‡	-0.06 (-0.17, 0.05)	-0.02 (-0.12, 0.08)	-0.07 (-0.18, 0.04)
Rate of total hippocampal atrophy (per z-score)	**-0.07*** (-0.13, -0.01)	**-0.15**** (-0.27, -0.04)‡	0.02 (-0.09, 0.12)	-0.04 (-0.14, 0.06)	-0.10 (-0.21, 0.00)
Rate of ADsig Harvard cortical thinning (per z-score)	-0.02 (-0.08, 0.04)	-0.04 (-0.14, 0.07)‡	-0.00 (-0.11, 0.10)	-0.02 (-0.12, 0.08)	-0.03 (-0.14, 0.07)
Rate of ADsig Mayo cortical thinning (per z-score)	-0.03 (-0.09, 0.03)	-0.02 (-0.15, 0.11)‡	0.01 (-0.09, 0.12)	-0.05 (-0.15, 0.05)	-0.08 (-0.18, 0.03)

*PACC = preclinical Alzheimer cognitive composite; MMSE = mini-mental state examination; DSST = digit symbol substitution test; LMDR = logical memory delayed recall; FNAME = face-name associative memory test; SEP = socioeconomic position; Aβ = β-amyloid; WMHV = white matter hyperintensity volume. Each structural MRI measure was assessed in a separate model, together with all other predictors. *p≤0.05. **p≤0.01. ***p≤0.001.* ‡ bias-corrected and accelerated bootstrap 95% CIs.